Journal of Applied Mechanics

(Contributions of the ASME Applied Mechanics Division)

Momentum and Mass Transfer in a Submerged Water Jet . . . *Wallace Forstall and E. W. Gaylord* 161

Prediction of Creep-Deflection and Stress Distribution in Beams From Creep in Tension . . . . *W. N. Findley and J. J. Poczatek* 165

Fracture of Specimens Iron Under Biaxial Stresses . . . . . *L. Cornet and R. C. Grassi* 172

The Formation of a Conical Crater in a Thin Plastic Sheet . . . . . *W. T. Thomson* 175

Thermal Stresses on a Circular Surface of Exposure of an Elastic Half Space . . *M. A. Sadowsky* 177

On the General Three-Dimensional Photoelastic Problem . . . . . *Max M. Frocht and Roscoe Guernsey, Jr.* 183

Determination of Thermal Stresses in Three-Ply Laminates . . . *A. J. Durelli and C. H. Tsao* 190

Stress-Concentration Factors in Shafts With Transverse Holes as Found by the Electroplating Method . . . . . *H. Okubo and S. Sato* 193

Laminar-Diffusion Boundary Layer—A Review . . . . . *Kurt Berman* 197

Application of Saint Venant's Principle in Dynamical Problems . . . . . *B. A. Boley* 204

Frictional Vibrations . . . . . *David Sinclair* 207

A Kinematic Notation for Lower-Pair Mechanisms Based on Matrices . . . . . *J. Denavit and R. S. Hartenberg* 215

Acceleration in Mechanisms . . . . . *R. T. Hinkle, C. Ip, and J. S. Frame* 222

The Effect of a Surrounding Fluid on Pressure Waves in a Fluid-Filled Elastic Tube . . . . . *M. C. Junger* 227

Shell Discontinuities at the Intersection of Several Coaxial Axisymmetric Shells . . . *H. Becher* 232

Solving Highly Complex Elastic Structures in Easy Stages . . . . . *Gabriel Kron* 235

On a Nonlinear Differential Equation for Beam Deflection . . . . . *E. J. Scott and D. R. Carver* 245

Problems of Plane Elasticity for Reinforced Boundaries . . . . . *J. R. M. Radok* 249

Stress Distribution in a Uniformly Rotating Equilateral Triangular Shaft . . . *H. T. Johnson* 255

Further Problems in Orthotropic Plane Stress . . . . . *H. D. Conway* 260

Stresses Due to Biaxial Forces on a Circular Disk With an Eccentric Hole . *A. M. Sen Gupta* 263

Bending of Orthogonally Stiffened Plates . . . . . *W. H. Hoppmann, 2nd* 267

Buckling of Continuous Columns . . . . . *H. C. Pérès* 272

Brief Notes:

Representation of Three-Dimensional Stress Distributions by Mohr Circles . *G. A. Zizicas* 273

Analysis of Some Circular Plates on Elastic Foundations and the Flexural Vibration of Some Circular Plates . . . . . *H. D. Conway* 275

Discussion on previously published papers by *R. Plunkett, H. H. Uhlig, T. K. Caughey, and J. M. Gray* 277

Book Reviews 284

JUNE, 1955

VOL. 22, NO. 2

Transactions of The American Society of Mechanical Engineers

Journal of Applied Mechanics

Papers Contributed to the Transactions by the ASME Applied Mechanics Division

EXECUTIVE COMMITTEE OF THE APPLIED MECHANICS DIVISION

E. J. Hoxie, *Chairman*

R. D. Mindlin, *Secretary*

John M. Lessells, *Technical Editor*

Published Quarterly by

The American Society of Mechanical Engineers

Publication Office, 20th and Northampton Streets, Easton, Pa.
Editorial Department at the Headquarters of the Society, 29 West Thirty-Ninth Street, New York 18, N. Y.

OFFICERS OF THE SOCIETY

David W. L. Moodie, *President*

C. E. Davies, *Secretary*

James L. Kopp, *Treasurer*

E. J. Kates, *Assistant Treasurer*

PUBLICATIONS COMMITTEE

George A. Stetson, *Editor*

K. W. Cammerhino, *Mgr. Editor*

By-Law: The Society shall not be responsible for statements or opinions advanced in papers or . . . printed in its publications (B13, Par. 4).

Published quarterly by The American Society of Mechanical Engineers. Publication office at 20th and Northampton Streets, Easton, Pa. The editorial department is located at the headquarters of the Society, 29 West Thirty-Ninth Street, New York 18, N. Y. Cable address, "Dynamic," New York. Price $1.25 a copy, $5.00 a year; to members $1.00. Add 25c for postage to all countries outside the United States. Changes of address must be received at Society headquarters seven weeks before they are to be effective on the mailing list. Manuscript and correspondence should be addressed to the Editorial Department. Statements and opinions advanced in papers or . . . printed in [illegible] By-Law: The Society shall not be responsible for statements or opinions advanced in papers or . . . printed in its publications (B13, Par. 4). Entered as second-class matter March 14, 1933, at the Post Office at Easton, Pa., under the act of August 24, 1912, . . . Acceptance for mailing at special rate of postage provided for in paragraph (d-2) section 34.40, P. L. and R. of 1948. Authorized August 1, 1950.

Copyright 1951 by The American Society of Mechanical Engineers. Reprints from this publication may be made on condition that full credit be given the JOURNAL OF APPLIED MECHANICS, the author, and date of publication be stated.

Momentum and Mass Transfer in a Submerged Water Jet[1]

By WALTON FORSTALL,[2] AND E. W. GAYLORD,[3] PITTSBURGH, PA.

For a round water jet issuing into stationary water, momentum and material diffusion were measured, the latter by means of a sodium chloride tracer technique. It was found that (*a*) the behavior of the water jet was the same as that found by others for an air jet issuing into air, and hence constants obtained from measurements in air can be applied to water; (*b*) the turbulent Schmidt number for water is approximately the same as the turbulent Schmidt number for air and about equal to the turbulent Prandtl number for air jets; and (*c*) the error curve serves as a useful and satisfactory representation of diffusion profiles for water just as it does for air.

Nomenclature

The following nomenclature is used in the paper:

c_p = specific heat at constant pressure
C_u, C_ξ = empirical constants
D = jet diameter at $x = 0$
D_t = turbulent material diffusion coefficient
k_t = turbulent thermal conductivity
r = radial distance from jet axis
r_{mu} = value of r for which $u = u_c/2$
$r_{m\xi}$ = value of r for which $\xi = \xi_c/2$
S = turbulent Schmidt number
u = axial component of velocity
v = radial component of velocity
x = distance from jet exit measured parallel to jet axis
θ_c = difference between temperature at $r = 0$ and temperature of secondary fluid
θ_0 = difference between temperature at $x = 0$, $r = 0$, and temperature of secondary fluid
ν_t = turbulent velocity diffusion coefficient
ξ = concentration of a tracer material, per unit volume
ρ = density

Subscripts

c = value at $r = 0$
0 = value at $x = 0$, $r = 0$
u = referring to velocity diffusion
ξ = referring to material diffusion

[1] This paper is based in part on a thesis by the junior author in partial fulfillment of the requirements for the degree of Doctor of Philosophy at Carnegie Institute of Technology.

[2] Associate Professor, Mechanical Engineering, Carnegie Institute of Technology. Mem. ASME.

[3] Assistant Professor, Mechanical Engineering, Carnegie Institute of Technology. Assoc. Mem. ASME.

Cosponsored by the Hydraulics Division and Applied Mechanics Division and presented at the Annual Meeting, New York, N. Y., November 28–December 3, 1954, of The American Society of Mechanical Engineers.

Discussion of this paper should be addressed to the Secretary, ASME, 29 West 39th Street, New York, N. Y., and will be accepted until July 11, 1955, for publication at a later date. Discussion received after the closing date will be returned.

Note: Statements and opinions advanced in papers are to be understood as individual expressions of their authors and not those of the Society. Manuscript received by ASME Applied Mechanics Division, February 3, 1954. Paper No. 54—A-38.

Turbulent Diffusion

In the turbulent flow of a fluid, irregularities of local velocity have the effect of transporting fluid in all directions throughout the body of fluid considered moving in some pattern of average flow. In this manner properties associated with the fluid are also transported. Whereas molecular diffusion is a characteristic of the fluid involved, turbulent diffusion (that is, diffusion due to the effect of turbulence alone) is determined by the nature of the turbulence and for the same turbulence is independent of the fluid. Molecular diffusivity can be measured and tabulated for each one of numerous fluids. In contrast, the relating of turbulent diffusion to various flow patterns is still a formidable problem. Yet in many technologically important flow patterns the molecular diffusion is negligible so that turbulent diffusion controls the process.

The attack on this problem is being made by several different methods. Corrsin and his fellow workers are probing the nature of turbulence itself. v. Krzywoblocki is developing a theory in which turbulence is an extension of the spectrum of molecular motion. In the meantime, many investigators have measured turbulent diffusion in simple geometries of flow and correlated the results by empirical formulations. It seems reasonable that the turbulent-diffusion problem ultimately will be solved by an understanding of turbulence itself, but in the interim, measurements of mean values and their corresponding empiricisms provide much useful information.

The Jet Problem

Jets form an important part of the study of the effect of turbulence on mean flow. A paper by Forstall and Shapiro (1)[4] augmented by two discussions (2) contains an extensive compilation of references. Also an extremely comprehensive bibliography on jets is to be found in a doctoral thesis by Nottage (8).

Of primary interest in the jet-diffusion problem are the transport of material, temperature, and momentum. Of these three, material has been the most neglected. Furthermore, because of difficulties inherent in the use of liquids, most of the experimental work has been done with gases.

This paper reports the results of measurements of material and momentum diffusion in a submerged water jet. The jet (primary stream) is of circular cross section and when entering a stationary body of water (secondary) provides the familiar mixing pattern shown schematically in Fig. 1. There were several reasons for carrying out this investigation:

1 It was the test of an instrument for measuring turbulent diffusion in water. It is planned to publish in a later paper a complete description of this instrument, which employs sodium chloride tracer and a specially designed electric conductivity cell.

2 Turbulent diffusion of water is of considerable technological interest. An important paper by Rouse, et al. (3) developed a convenient means for predicting the spread of a fluid jet, which presumably was applicable to a water jet. Rouse determined his empirical values using air. It was the authors' purpose to con-

[4] Numbers in parentheses refer to the Bibliography at the end of the paper.

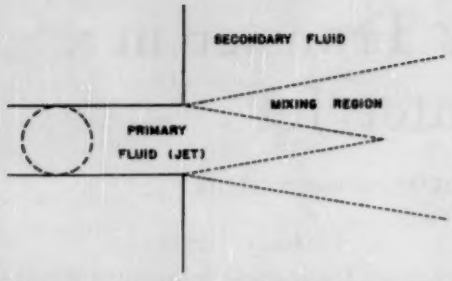

FIG. 1 MIXING PATTERN OF ROUND JET ENTERING STATIONARY FLUID OF SAME DENSITY

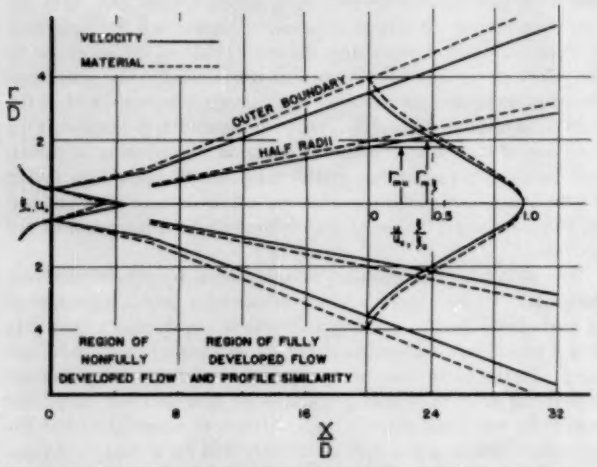

FIG. 2 SKETCH ILLUSTRATING NOMENCLATURE AND INDICATING SIMILARITY OF PROFILES FOR BOTH MATERIAL AND MOMENTUM DIFFUSION

firm the reasonable assumption that these values were independent of the fluid used and would serve to predict the spread of a submerged water jet.

3 It has been well established from measurements with turbulent-air jets that material and temperature diffuse at about the same speed, a rate which is more rapid than momentum diffusion. The relative rate of turbulent-momentum diffusion compared with turbulent-temperature diffusion can be expressed as a "turbulent Prandtl number." The corresponding value for material diffusion and momentum diffusion is the "turbulent Schmidt number." Almost no data exist on turbulent Schmidt numbers for water.

TURBULENT SCHMIDT NUMBER

Consider the steady, axially symmetric flow of a turbulent, incompressible, inviscid, circular jet containing a tracer. Assume pressure constant everywhere and neglect the gradients, assumed small, of certain fluctuation products in the axial direction. Define two turbulent-diffusion coefficients by the equations

$$\overline{u'v'} = -\nu_t \frac{\partial \bar{u}}{\partial r} \quad [1]$$

$$\overline{\xi'v'} = -D_t \frac{\partial \bar{\xi}}{\partial r} \quad [2]$$

where u' and v' are the fluctuations of axial and radial velocity, ξ' is the fluctuation of concentration of tracer material, ν_t is the coefficient of turbulent diffusion of momentum, D_t is the coefficient of turbulent diffusion of material, and the bars denote time averages.

Total diffusion is, of course, the sum of molecular and turbulent effects. Thus the total coefficient of momentum diffusion is $\nu + \nu_t$, where ν is the kinematic viscosity. But in contrast to ν, which is a property of the fluid, ν_t is a mere empiricism and is not a property of the fluid, being dependent instead upon the nature of the turbulence present. In many practical cases of turbulent mixing, including the ones for which measurement are reported here, ν is so small compared to ν_t that it may be ignored.

If the definitions for ν_t and D_t given in Equations [1] and [2] are substituted into the equations for the turbulent diffusion of the mean value of momentum and material, respectively, these equations become identical with the equations for molecular diffusion in nonturbulent flow, except for the bars used to indicate time averages. In what follows bars will not be used but, since we are dealing with turbulent flow, time averages are to be understood.

If it is further assumed that the velocity and concentration profiles are all similar, it may be shown (4, 5) that

$$\frac{\nu_t}{D_t} \frac{d\left(\frac{u}{u_c}\right)}{\frac{u}{u_c}} = \frac{d\left(\frac{\xi}{\xi_c}\right)}{\frac{\xi}{\xi_c}} \quad [3]$$

where u_c is the time average axial velocity and ξ_c is the time average concentration of tracer material on the jet axis. If we define the turbulent Schmidt number S as

$$S = \frac{\nu_t}{D_t}$$

and assume it to be constant, Equation [3] integrates to

$$\frac{\xi}{\xi_c} = \left(\frac{u}{u_c}\right)^S \quad [4]$$

The normal probability or error curve is suitable for describing the profile of a circular jet. This has been shown by many investigators and is confirmed once more by the results of this work. As will be indicated, the error curve presents a special convenience in the evaluation of turbulent Schmidt number from diffusion measurements. Velocity and concentration profiles in terms of the error curve are

$$\frac{u}{u_c} = \exp\left[-0.694\left(\frac{r}{r_{mu}}\right)^2\right] \quad [5]$$

$$\frac{\xi}{\xi_c} = \exp\left[-0.694\left(\frac{r}{r_{m\xi}}\right)^2\right] \quad [6]$$

where r_{mu} and $r_{m\xi}$ are the values of r where the respective values of u/u_c and ξ/ξ_c reach 1/2. This leads to

$$S = \left(\frac{r_{mu}}{r_{m\xi}}\right)^2 \quad [7]$$

EXPERIMENTAL APPARATUS

The apparatus shown in Fig. 3 produced a round water jet issuing from a wall into water which was nearly stationary. The tank is 3 ft in diam and 4 ft high. The jet issues vertically from either a 1/4 or 3/8-in-diam nozzle centered in the bottom. An amount of water equal to that supplied by the jet overflows the rim of the tank while the remainder of the entrained water returns downward outside the jet-mixing region. The tank is so large compared to the jet-mixing region that velocities in the return flow are negligible compared to velocities in the mixing region.

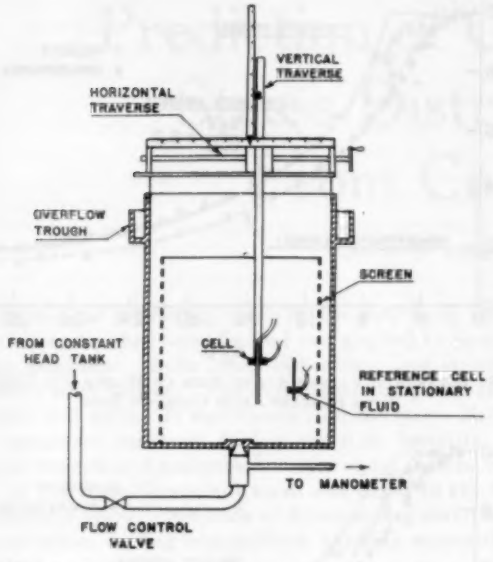

FIG. 3 SCHEMATIC DIAGRAM OF JET-MIXING TANK

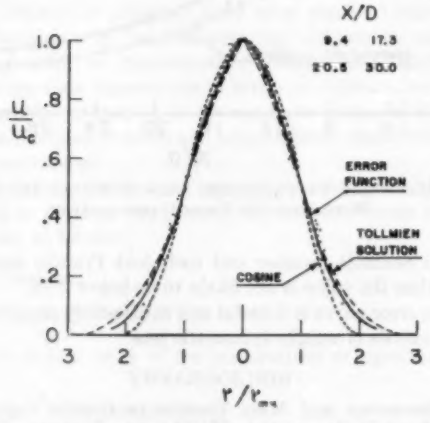

FIG. 4 MEASURED POINTS OF VELOCITY PROFILE COMPARED WITH CERTAIN STANDARD CURVES

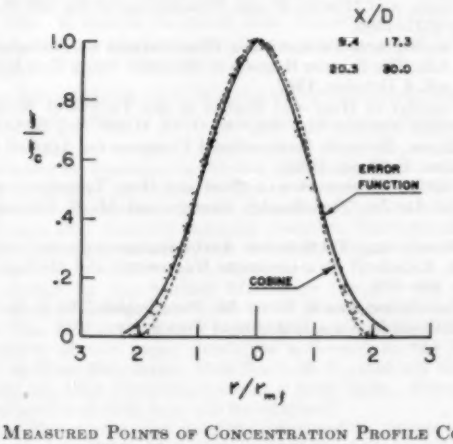

FIG. 5 MEASURED POINTS OF CONCENTRATION PROFILE COMPARED WITH TWO STANDARD CURVES

The tank is 192 and 128 nozzle diameters high, depending on the nozzle used; and below 38 nozzle diameters, where the measurements were made, there was no evidence of any disturbance caused by the water surface at the top of the tank. A traversing impact tube $^1/_{16}$ in. OD was used to measure velocities and take samples for conductivity analysis.

For material diffusion measurements the jet was fresh water and the fluid in the tank was a 1 per cent solution of sodium chloride. Continuous sampling through two electrical conductivity cells compared the salinity of any point in the mixing region to the salinity existing in the stationary water in the tank. This comparison method does not require the salt concentration in the receiving medium to be known or to be constant, so long as the change occurs relatively slowly, as is the case here.

RESULTS

Similarity. Profile similarity in terms of half-radii is shown to be satisfied for both velocity and concentration by Figs. 4 and 5.

Rate of Spreading. If u/u_c and ξ/ξ_c are to be functions of r/x only, the jet should spread along straight lines, and the loci of

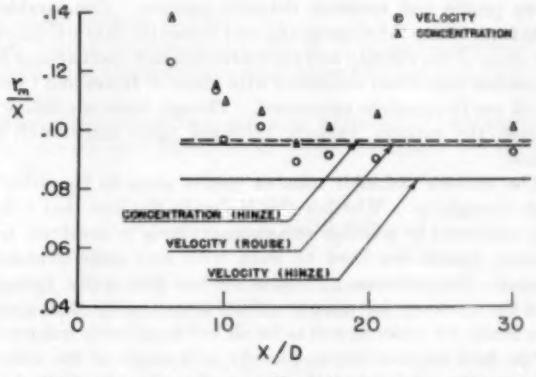

FIG. 6 MEASURED VALUES OF HALF-RADIUS OF A WATER JET COMPARED WITH RESULTS FROM GASEOUS JETS

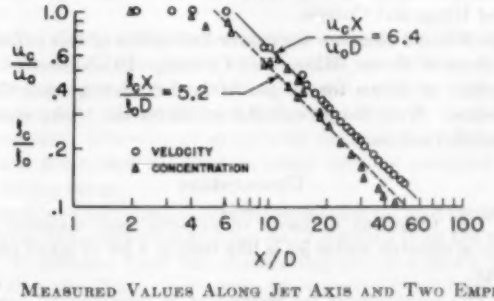

FIG. 7 MEASURED VALUES ALONG JET AXIS AND TWO EMPIRICAL CURVES

half-radii should be a straight line. Fig. 6 shows that this requirement is reasonably well met between 15 and 30 jet diameters.

Center-Line Values. Similarity and conservation of momentum and material flux result in equations for the center-line values having the form

$$\frac{u_c}{u_0} = \frac{C_u D}{x} \quad \text{and} \quad \frac{\xi_c}{\xi_0} = \frac{C_\xi D}{x}$$

when $x = 0$ represents a common point source for the momentum and material flux; u_0 and ξ_0 are values at $x = 0$, $r = 0$; C_u and C_ξ are constants. Fig. 7 compares the data with values of

TABLE 1 MEASURED VALUES

	$\frac{x}{D}$	Half-Radii $\frac{r_{m u}}{x}$	Half-Radii $\frac{r_{m \xi}}{x}$	Half-Radii $\frac{r_{m \theta}}{x}$	Turbulent Schmidt number $\frac{\nu_t}{D_t}$	Turbulent Prandtl number $\frac{\nu_t}{k_t/c_p \rho}$
1/4-in. nozzle	9.45	0.113	0.115		0.965	
	12.6	0.101	0.106		0.903	
	17.3	0.091	0.101		0.810	
	20.5	0.090	0.105		0.750	
	30.0	0.092	0.101		0.827	
1/8-in. nozzle	10.0	0.097	0.110		0.792	
	15.0	0.089	0.096		0.855	
Hinze (5)		0.083	0.096		0.770 (0.750)[a]	
Corrsin (6)		0.083		0.099		0.701 (0.705)[a]
Rouse (3)		0.095				

[a] Computed by authors from reference data using error curve and constant S.

$C_u = 6.4$ and $C_\xi = 5.2$. Rouse (3) obtained the values 6.2 for his results with air. The difference between 6.4 and 6.2 is within the range of experimental error.

Comparison With Other Investigators. Table 1 shows various measured values for velocity and concentration half-radii, and Schmidt number computed from the assumption of an error curve profile and constant Schmidt number. Comparable results from Hinze (5), Corrsin (6), and Rouse (3) also are shown.

Values of the velocity and concentration half-radii appear to be somewhat high when compared with those of Hinze and Corrsin, which are in complete agreement. Though there is considerable scatter, the authors' velocity half-radii agree rather well with Rouse.

The authors' Schmidt number results seem to be rather too high throughout. Whether this is due to the fact that a liquid was employed or whether experimental error is involved, is not known; liquids are hard to work with and more evidence is needed. Nevertheless, all values are less than unity, indicating that the tendency for mass to diffuse more rapidly than momentum is true for water as well as for air and is probably independent of the fluid medium employed. As an example of the utility of the error curve it is interesting to note the values for the turbulent Schmidt number and the turbulent Prandtl number which the authors have computed by applying an error-curve profile to the data of Hinze and Corrsin.

Figs. 8 and 9 compare the center-line values of this experiment with those of Rouse, Hinze, and Corrsin. In all cases excellent agreement is shown for all points farther downstream than 10 diameters. Near the jet exit the points for the 1/4-in. nozzle are of doubtful accuracy.

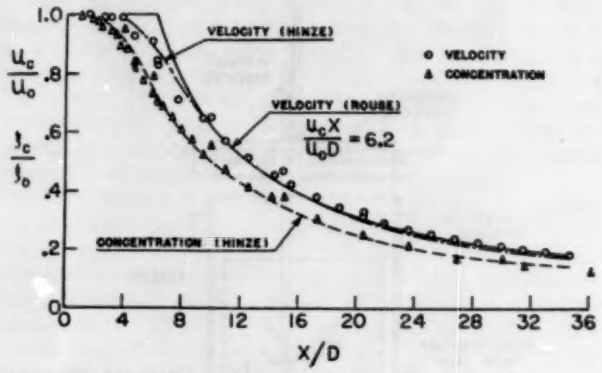

FIG. 8 MEASURED VALUES ALONG AXIS OF WATER JET COMPARED WITH RESULTS FROM GASEOUS JETS

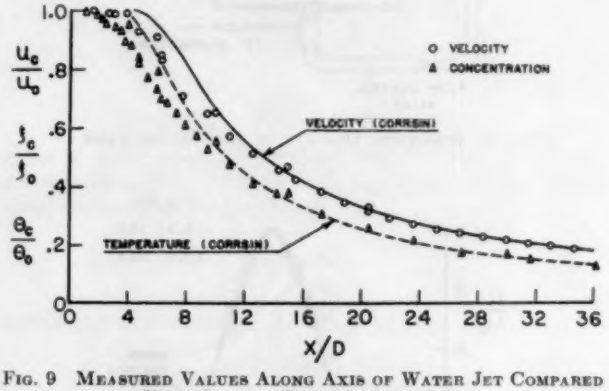

FIG. 9 MEASURED VALUES ALONG AXIS OF WATER JET COMPARED WITH RESULTS FROM GASEOUS JETS

CONCLUSIONS

1 The turbulent diffusion of velocity and material in an axially symmetric water jet is like that in a jet of air of constant density.

2 The employment for water jets of experimental constants determined in air as proposed by Rouse (3) is justified experimentally.

3 The turbulent diffusion of material in water behaves like the turbulent diffusion of temperature in air of nearly constant density.

4 The results of this investigation indicate a turbulent Schmidt number for water in the range of 0.75 to 0.85. Forstall and Shapiro (1) suggested a value of 0.70 ± 10 per cent for the turbulent Schmidt number and turbulent Prandtl number. It appears that the value is not likely to be below 0.70.

5 The error curve is a useful and satisfactory empirical profile for the analysis of axially symmetric jets.

BIBLIOGRAPHY

1 "Momentum and Mass Transfer in Coaxial Gas Jets," by Walton Forstall, Jr., and A. H. Shapiro, JOURNAL OF APPLIED MECHANICS, Trans. ASME, vol. 72, 1950, pp. 399–408.

2 Discussion of reference (1), JOURNAL OF APPLIED MECHANICS, Trans. ASME, vol. 73, 1951, pp. 219–220.

3 "Diffusion of Submerged Jets," by M. L. Albertson, Y. B. Dai, R. A. Jenson, and Hunter Rouse, Proceedings of the ASCE, vol. 74, 1948, pp. 1571–1596.

4 "Velocity and Temperature Distributions in Turbulent Jets," by C. C. Lin, The Science Reports of National Tsing Hua University, series A, vol. 4, October, 1947.

5 "Transfer of Heat and Matter in the Turbulent Mixing Zone of an Axially Symmetrical Jet," by J. O. Hinze and B. G. van der Hegge Zijnen, Seventh International Congress for Applied Mechanics, London, England, 1948.

6 "Further Experiments on Flow and Heat Transfer in a Heated Turbulent Air Jet," by Stanley Corrsin and M. S. Uberoi, NACA TN 1865.

7 "Berechnung Turbulenter Ausbreitungsvorgänge," by Walter Tollmien, *Zeitschrift für angewandte Mathematik und Mechanik*, vol. 6, 1926, pp. 468–478.

8 "Ventilation Jets in Room Air Distribution," by F. B. Nottage, Doctoral thesis for Case Institute of Technology, 1951.

Prediction of Creep-Deflection and Stress Distribution in Beams From Creep in Tension

By W. N. FINDLEY[1] and J. J. POCZATEK[2]

A method of predicting creep in bending from data on creep in tension has been derived and applied to creep of a canvas laminate. Both creep deflections and stress distribution were derived. The deflections compared favorably with test data. It was shown that the stress distribution remained constant during creep in bending when creep in tension and compression were equal and the coefficient of the time-dependent term was equal to the time-independent term. Methods of determining creep deflections of beams having nonuniform bending moments are described.

Status of the Problem

NUMEROUS attempts have been made to express creep behavior by a mathematical expression either empirically or theoretically. Many investigators have assumed the time dependence of creep at constant load to be a linear function of time (1 to 4)[3] and have examined the rate of creep as a function of stress and temperature—usually only stress has been considered.

Tensile Creep. Some of the types of equations which have been employed to describe the relationship between creep rate v and stress σ are as follows

$$v = B\sigma \text{ (viscous)} \quad [1]$$

$$v = B\sigma^a \text{ (power)} \quad [2]$$

$$v = A'e^{B\sigma} \text{ or } \ln v = A + B\sigma \text{ (exponential or logarithmic)} \quad [3]$$

$$v = B \sinh \frac{\sigma}{\sigma_0} \text{ (hyperbolic sine)} \quad [4]$$

where a, A, A', B, and σ_0 are constants.

Of these equations, the hyperbolic sine, Equation [4], has been shown to have fundamental significance in terms of molecular behavior (5). It should be noted that Equations [1] and [3] are approximations of Equation [4] if σ/σ_0 is either small or large, respectively.

Other investigators (6 to 14), observing that creep was usually not a linear function of time, expressed the total strain ϵ, versus time t, relation nonlinearly by equations, such as the following

$$\epsilon = C + D \ln t + Et \quad [5]$$

(see references 7 and 8)

$$\epsilon = C + D(1 - e^{-bt}) + Et \quad [6]$$

(see reference 14)

$$\epsilon = \epsilon_0 + mt^n \quad [7]$$

(see references 6, 9, 11–13)

where b and n are constants and C, D, E, ϵ_0, and m are functions of stress, and ϵ includes both time-dependent and time-independent strain.

When the coefficients ϵ_0 and m in Equation [7] are expressed as hyperbolic sine functions of stress, Equation [7] becomes (13, 15)

$$\epsilon = \epsilon_0' \sinh \frac{\sigma}{\sigma_\epsilon} + m't^n \left(\sinh \frac{\sigma}{\sigma_m}\right) \quad [8]$$

where ϵ_0', m', σ_ϵ, σ_m, and n are constants. From Equation [8] the creep rate v, as obtained by differentiation, is

$$v = m'nt^{n-1} \sinh \frac{\sigma}{\sigma_m} \quad [9]$$

and is a function of time rather than a constant as often assumed.

Bending Creep. The first analysis of creep in bending was reported by MacCullough (16) in 1933. The results of his tests of lead beams were in reasonable agreement with the deflections calculated from observed minimum creep rates in tension and compression. Linearity of strain with distance from the neutral axis was demonstrated; that is, plane sections remained plane even during creep.

Tapsell and Johnson (2) also demonstrated for lead beams that the strain remained a linear function of distance from the neutral axis. It followed from this observation, and was shown by the data, that the strain-time curves at every position (fiber) of the beam have a similar shape.

Creep of beams of aluminum and polystyrene plastic were investigated by Marin and Zwissler (17) and Marin and Cuff (18). The observed minimum creep rates in bending were compared with bending-creep rates computed from tension-creep tests assuming a linear dependence of creep on time and a power relation between creep rate and stress. The theory did not permit computation of deflection. Both the tension- and bending-creep curves depart considerably from the assumed linear dependence on time. In a discussion, Findley (19) presented data on creep of polystyrene which indicated that the power function of stress was not satisfactory for small stresses.

Creep of an imaginary copper beam was examined by Popov (20) using several creep rate versus stress relations. His examination indicated that the stress distribution in a beam changed with

---

[1] Professor of Engineering, Brown University, Providence, R. I.; formerly Research Associate Professor, University of Illinois.

[2] Associate Research Engineer, American Machine and Foundry Co., Chicago, Ill.; formerly Research Assistant, University of Illinois.

[3] Numbers in parentheses refer to the Bibliography at the end of the paper.

Contributed by the Applied Mechanics Division and presented at the Annual Meeting, New York, N. Y., November 28–December 3, 1954, of The American Society of Mechanical Engineers.

Discussion of this paper should be addressed to the Secretary, ASME, 29 West 39th Street, New York, N. Y., and will be accepted until July 11, 1955, for publication at a later date. Discussion received after the closing date will be returned.

Note: Statements and opinions advanced in papers are to be understood as individual expressions of their authors and not those of the Society. Manuscript received by ASME Applied Mechanics Division, August 11, 1953. Paper No. 54—A-5.

time and tended toward a steady-state distribution of a nonlinear shape. An approximate summation procedure was employed to calculate the stress distribution. Deflections were calculated on an assumption of a linear variation of strain with time. Deflections also were calculated using a creep equation of the type of Equation [7] with a linear function of stress for ϵ_0 and an exponential function of stress for m. No experimental verification was reported, however.

In a paper by Marin, Pao, and Cuff (4), a method was described for calculating bending-creep rates and deflections in a beam of material for which the creep behavior is different in tension and compression. The results were compared with data on creep of lucite and plexiglas. Again a linear time function was assumed which was not a close approximation to the observed behavior. Different power functions of stress were employed to describe the elastic strains and creep strains. In the analysis the elastic and creep strains were treated separately. The analysis predicted a different stress distribution and position of the neutral axis for the elastic component of strains than for the creep (time dependent) component of strains in the beam. Since these two stress distributions must exist simultaneously it does not seem possible for them to be different.

In a paper which had just become available at the time this manuscript was prepared, Pao and Marin (14) presented another analysis for bending creep of plexiglas in which a complex equation for creep of the form of Equation [6] was employed. This equation did not describe the initial part of the creep curves much more closely than a linear equation. Identical creep relations in tension and compression were assumed although the authors' previous data on plexiglas showed this to be untrue. The analysis permits the stress distribution to vary with time but neglects the resulting changes in elastic strains. Other simplifications were found necessary in order to solve the problem. The resulting equation predicted a constant creep rate after about 1000 hr which did not agree with the data; these were presented to 11,000 hr, the creep rate decreasing continuously. The paper also described methods for determining creep deflections of beams in which the bending moment varied along the beam.

Derivation for Bending With Equal Creep in Tension and Compression and Equal Time-Dependent and Independent Constants

In previous studies (9, 12, 15) the creep curves obtained from a canvas laminate tested at different constant stresses were found to be closely described by an equation of the form

$$\epsilon = \epsilon_0 + mt^n = (\epsilon_0' + m't^n) \sinh \frac{\sigma}{\sigma_0} \quad [10]$$

where the symbols are the same as described above. The stress dependence in this relation is of the same form as that in the activation-energy theory of creep as advanced by Kauzmann (5). It also has been shown previously (15) that an equation for the stress-strain curve obtained from a constant strain rate-tension test could be derived from Equation [10] and that the resulting equation was in close agreement with the experimental data. It should be noted that the time-independent term $\epsilon_0 = \epsilon'_0 \sinh(\sigma/\sigma_0)$ in Equation [10] expresses the instantaneous strain, i.e., the strain at time zero, and that it does not represent linear elasticity except when σ_0 is large compared to σ.

Fortunately, bending-creep data also were obtained for material of identical composition made by the same manufacturer at about the same time. These data were obtained by Marin (21). While Marin also obtained tension-creep curves on this material which agreed in general with the tension-creep curves in reference (9), they did not have sufficient self-consistency to permit evaluating the constants in Equation [10].

Dr. Marin in a private communication provided compression creep curves of a canvas laminate which show a greater creep for a given stress than the tension-creep data. However, the instantaneous strains also were 50 per cent greater, whereas the stress-strain curves of this material in tension and compression were nearly the same for the stresses involved in the creep tests (12). In view of this observation, the following derivation has been prepared on the assumption that creep in tension and compression was identical for the canvas laminate.

Equation [10] accurately represents the creep data under conditions of constant stress. It probably does not, however, accurately describe creep under varying stress. Thus, if the stress distribution in the beam changed during creep, as described by Popov (20), some inaccuracy might be introduced by the use of this equation unless the material obeys the time-hardening law (22), which probably is not the case.

To determine the bending-creep relation the conditions of equilibrium and geometry must be satisfied. From the geometry of a beam in pure bending, or one in which the distortion due to shear is negligible, the following well-known geometrical relation applies

$$\epsilon = \frac{y}{\rho} \quad [11]$$

where ϵ is the total strain at a distance y measured perpendicularly from the neutral axis and ρ is the radius of curvature of the centroidal axis. This relation is equivalent to assuming that plane sections remain plane—a fact which has been demonstrated for plastically bent beams by Nadai (23) and for creep of lead beams by MacCullough (16). Also, consideration of compatibility of strains in the different "fibers" of a beam of great length, bent by a constant bending moment into the arc of a circle, suggests that plane sections must remain plane at all points along the beam which are remote from the ends.

The conditions of equilibrium for a beam are expressed by the following equations when the accelerations involved in the creep are so small as to be negligible—which is usually the case

$$\int_{c-h}^{c} \sigma y(dA) = M \quad [12]$$

$$\int_{c-h}^{c} \sigma(dA) = 0 \quad [13]$$

where A is the cross-sectional area of the beam, h is the depth of the beam, and c is the distance from the neutral axis to the tension face of the beam.

Substituting Equation [11] for ϵ in Equation [10] and solving for the stress σ the following is obtained

$$\sigma = \sigma_0 \sinh^{-1}\left[\frac{y}{\rho(\epsilon_0' + m't^n)}\right] = \sigma_0 \sinh^{-1}(Ny) \quad [14]$$

where the symbol

$$N = \frac{1}{\rho(\epsilon_0' + m't^n)} \quad [15]$$

has been introduced.

For a beam of rectangular cross section of width b, $(dA) = b(dy)$, in Equations [12] and [13]. Making this substitution and introducing Equation [14] for σ in Equation [13], the following results

$$b\int_{c-h}^{c} \sigma(dy) = b\sigma_0 \int_{c-h}^{c} \sinh^{-1}(Ny)(dy) \quad [16]$$

Upon integration, assuming identical creep relations for tension and compression, Equation [16] shows that $c = h/2$, i.e., the neutral axis is at the center of the beam and does not change position with time under load.

Making the same substitutions in Equation [12] and changing the limits in accordance with the previous paragraph yields

$$M = b\int_{-c}^{c} \sigma y(dy) = b\sigma_0 \int_{-c}^{c} y \sinh^{-1}(Ny)(dy) \ldots [17]$$

After integrating and rearranging terms this becomes

$$\frac{2M}{\sigma_0 bc^2} = (Nc)^{-2}\left\{[2(Nc)^2 + 1]\sinh^{-1}(Nc) - (Nc)\sqrt{1 + (Nc)^2}\right\} \quad \ldots\ldots [18]$$

which for convenience in computations may be written

$$\frac{2M}{\sigma_0 bc^2} = \frac{2\theta \cosh 2\theta - \sinh 2\theta}{\cosh 2\theta - 1}$$

where $\theta = \sinh^{-1} Nc$.

Equation [18] shows that the bending moment M is a function of N for a beam of given size and material. Thus for a constant bending moment M, N must be a constant. Hence, from Equation [15] it is observed that the curvature $1/\rho$ of the beam under a constant bending moment varies with time in accordance with the same time function as strain varies in a tension creep test; that is

$$\frac{1}{\rho} = N(\epsilon_0' + m't^n) \ldots\ldots [19]$$

In this equation N is the function of bending moment M, given by Equation [18]. The most convenient way of determining N from Equation [18] is by means of a diagram of

$$\frac{2M}{\sigma_0 bc^2} \text{ versus } Nc$$

which is easily constructed from the second form of Equation [18] as shown in Fig. 1.

From Equation [14] the stress distribution

$$y = \frac{1}{N}\sinh\frac{\sigma}{\sigma_0} \ldots\ldots [20]$$

is obtained. Since N is a function of the bending moment, size and material of the beam and independent of time (according to Equation [18]), it follows that the stress distribution does not change with time during creep under a constant bending moment.

Application to Creep of Canvas Laminate in Pure Bending

Deflections. Numerical values of the constants in Equation [10] which were determined from tension creep data (9) are as follows

$$\epsilon_0' = m' = 0.001875 \text{ in. per in.}$$
$$n = 0.1183$$
$$\sigma_0 = 4000 \text{ psi}$$

The values differ from the values determined for this laminate in a previous study (15) in which m' was 0.0029 and σ was 5230. The agreement between the tension creep-test data and Equation [10] using the present constants is shown in Fig. 2.

The agreement is excellent except for the highest stresses of 5700 and 6650 psi. Since the specimen at the latter stress fractured at 550 hr, it is possible that the fracturing mechanism may have influenced the creep results at the highest stress. It is also always possible that specimens may have been slightly overstrained during loading, although great care was exercised in this respect. It has been shown (24) that such overstraining alters the shape of the creep curve. The short horizontal lines at the left border of Fig. 2, indicate the first test points for each test.

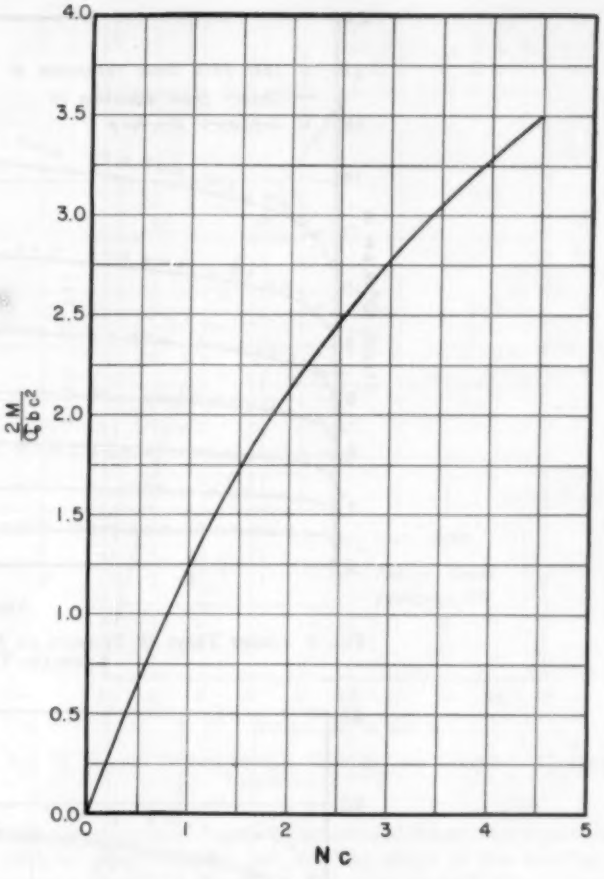

Fig. 1 Nc Versus $\frac{2M}{\sigma_0 bc^2}$ From Equation [18]

To calculate the deflection-time curves for a beam of the dimensions employed by Marin (21), values of N were determined from Fig. 1, corresponding to the desired bending moments. These values were substituted into Equation [19] together with the values of the constants given in the foregoing, and the curvature $1/\rho$ was determined for various values of time t. Then the deflection z at mid-span of a beam of length l subjected to a uniform bending moment was calculated for each curvature from the well-known geometrical relation

$$z = \frac{l^2}{8\rho} \ldots\ldots [21]$$

The resulting theoretical bending-creep curves are shown in Fig. 3, together with the experimental data reported by Marin (21) for a grade C canvas laminate. In Fig. 3, the solid lines show the bending creep predicted by Equation [19], using the constants employed in computing the solid lines shown in Fig. 2. The black dots in Fig. 3 represent the creep that would have been predicted by using the constants previously employed to fit Equation [10] to the data of Fig. 2.

The short horizontal lines at the left border of Fig. 3 indicate

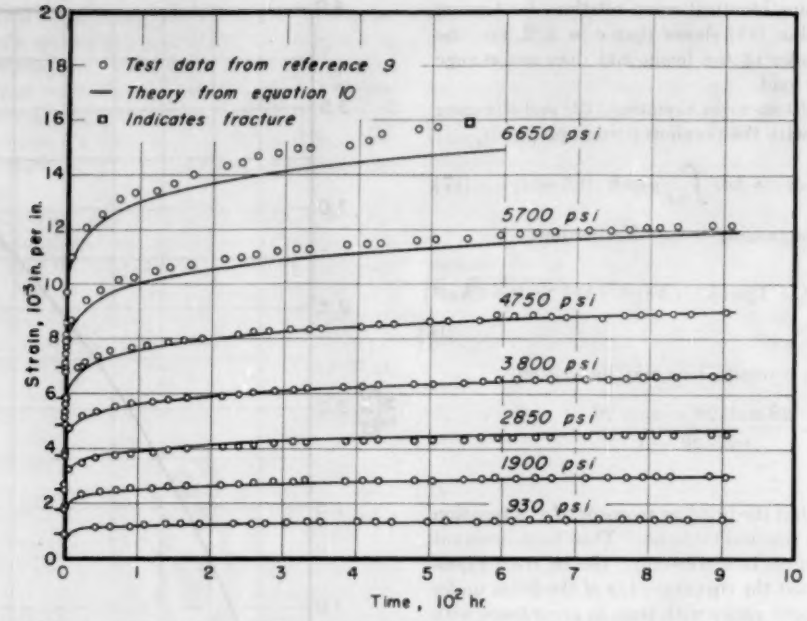

FIG. 2 CREEP TESTS IN TENSION AT DIFFERENT STRESSES FOR GRADE-C CANVAS LAMINATE TESTED AT 77 F

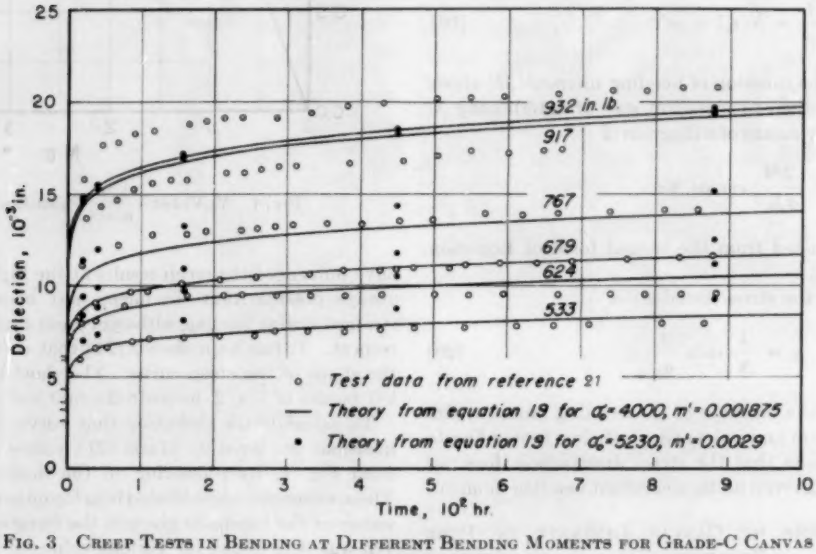

FIG. 3 CREEP TESTS IN BENDING AT DIFFERENT BENDING MOMENTS FOR GRADE-C CANVAS LAMINATE AT 77 F

the deflection predicted at zero time if the load could have been applied instantaneously without shock.

The agreement between the theory given by the solid lines in Fig. 3 and experimental data is reasonably good. Some of the discrepancies which do exist may be explained as follows: For the curve at a bending moment of 624 lb-in. the experimental data indicate a constant deflection between 200 and 900 hr. Since curves for higher and lower moments showed a continuously increasing deflection, it seems likely that experimental difficulties, such as the sticking of a dial, may have been responsible for the constant deflection.

The divergence in the early part of the test at a bending moment of 767 lb-in. may have been caused by overstraining during load application. This possible explanation seems to be supported by the fact that the difference between experimental and theoretical data at this load decreases as the time increases. This trend is in accord with the observations of Everett (24) and MacCullough (16) on the effect of overstraining while loading.

The experimental data for bending moments of 917 lb-in. and 932 lb-in. show a difference that seems too large for the small change in bending moment. There is no way of knowing which of the two curves is more nearly correct.

Stresses. The stress distribution in the beam under a bending moment of 679 lb-in. was computed from Equation [20] and is shown in Fig. 4. The maximum stresses in the beams also were computed for the several beams for which data are reported in Fig. 3. These stresses, in order of increasing bending moments, were 4920, 5640, 6060, 6740, 7940, 8,000 psi, respectively. It was

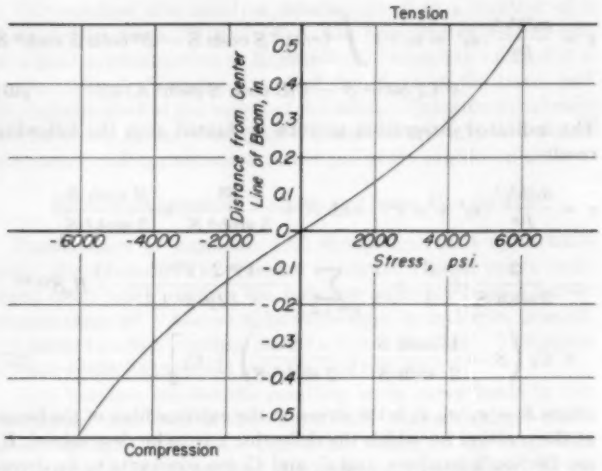

FIG. 4 STRESS DISTRIBUTION IN BEAM DURING CREEP, FOR GRADE-C CANVAS LAMINATE
(Bending moment 679 in-lb.)

observed that the two highest stresses are very near the stress in the tension test, Fig. 5, at which the strain increased rapidly with small increases in stress. This may account in part for the large difference between the creep of the two beams having the highest loads, see Fig. 3.

RELATION TO TENSION TEST OF CANVAS LAMINATE

In a prior paper (15) an equation for the stress-strain relation in a tension test was derived from a creep equation of the form of Equation [10]. The resulting stress-strain equation was

$$\epsilon = \epsilon_0 \sinh \frac{\sigma}{\sigma_0} \left[1 + \left(\frac{\epsilon_0 n}{\dot{\epsilon} t_0} \sinh \frac{\sigma}{\sigma_0} \right)^{\frac{n}{1-n}} \right] \ldots\ldots [22]$$

where $\dot{\epsilon}$ is the strain rate.

Excellent agreement was found between the stress-strain curve computed from the creep data for the canvas laminate used in the foregoing study and the data from a tension test. Since the constants in the creep equation as employed in the present analysis differ from those used in the previous paper, the stress-strain relation has been recomputed from Equation [22] using the new constants. The theoretical and experimental curves are compared in Fig. 5. The agreement is close but not as satisfactory as for the previous set of constants (15).

NONUNIFORM BENDING MOMENT

If the bending moment M in the beam varies with distance x along the beam, then M may be expressed in terms of x as $M = f(x)$. Hence from Equation [18] N is a function of x, $N = g(x)$. If in Equation [19], $g(x)$ is substituted for N, and

$$\frac{1}{\rho} = \frac{\frac{d^2z}{dx^2}}{\left[1 + \left(\frac{dz}{dx}\right)^2\right]^{3/2}} \cong \frac{d^2z}{dx^2} \text{ (for small deflections)} \ldots [23]$$

is substituted for the curvature, the differential equation

$$\frac{d^2z}{dx^2} = g(x)\,(\epsilon_0' + m' t^n) \ldots\ldots [24]$$

is obtained which may be solved for the deflection of the beam.

Example 1. Let $g(x) = Qx$ where Q is a constant. This corresponds to a beam having a bending moment M which varies

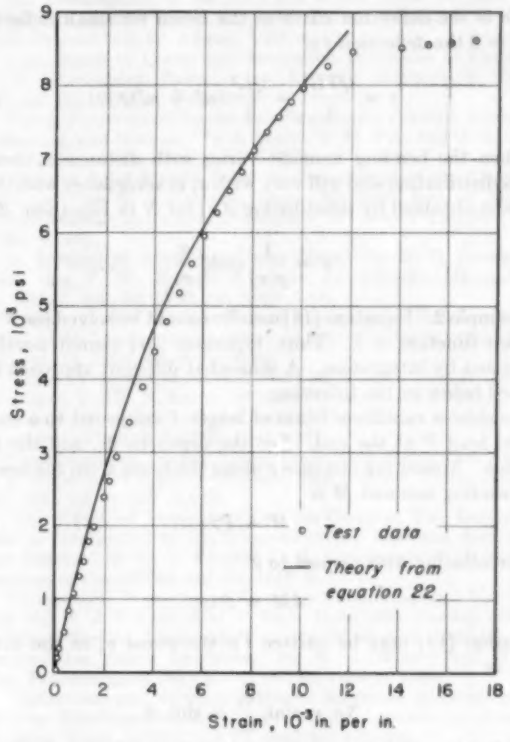

FIG. 5 STATIC STRESS-STRAIN CURVES FOR GRADE-C CANVAS LAMINATE AT 77 F

with distance x according to the equation obtained from Equation [18] by substituting Qx for N. The shape of this bending-moment diagram is the same as the curve shown in Fig. 1, since the ordinate is proportional to the bending moment and the abscissa is proportional to x. Within the range of Nc shown, Fig. 1 has approximately the shape of the bending-moment diagram which would be produced in a cantilever beam loaded with its own weight and having an upward force at the free end. At a given time t_1 the deflection of the beam may be determined in a manner identical to that employed for elastic beams. From Equation [24]

$$\frac{d^2z}{dx^2} = Qx(\epsilon_0' + m' t_1^n) = QTx \ldots\ldots [25]$$

where

$$T = \epsilon_0' + m' t_1^n$$

Integrating once

$$\frac{dz}{dx} = QT\frac{x^2}{2} + C$$

If the beam is rigidly clamped at $x = L$, then

$$\frac{dz}{dx} = 0$$

at $x = L$, and $C = -QT(L^2/2)$. Integrating again

$$z = QT\frac{x^3}{6} - QT\frac{L^2}{2}x + C_1$$

But $z = 0$ at $x = L$ so $C_1 = (QTL^3)/3$, hence

$$z = QTx^3/6 - QTL^2x/2 + QTL^3/3$$

which is the deflection curve of the beam for small deflections. At $x = 0$ the deflection z is

$$z = \frac{QTL^3}{3} = \frac{QL^3}{3}(\epsilon_0' + m'l_1^n) \quad [26]$$

When the bending moment varies with distance x, then the stress distribution also will vary with x, in accordance with the expression obtained by substituting $g(x)$ for N in Equation [20]

$$y = \frac{1}{g(x)} \sinh \frac{\sigma}{\sigma_0} \quad [27]$$

Example 2. Equation [18] usually cannot be solved for N as an explicit function of x. Thus, Equation [24] cannot usually be evaluated by integration. A somewhat different approach is described below in the following.

Consider a cantilever beam of length L subjected to a concentrated load P at the end. Let the depth be $2c$, and the beam width b. Measuring distance x along the beam from the free end, the bending moment M is

$$M = Px \quad [28]$$

Differentiating with respect to x

$$dM = Pdx \quad [29]$$

Equation [14] may be written for the stress σ_1 in the extreme fiber as

$$Nc = \sinh \frac{\sigma_1}{\sigma_0} = \sinh S \quad [30]$$

where $S = \sigma_1/\sigma_0$, and S is a function of x since N is a function of x. Equation [18] can be rewritten as follows by substituting Equation [30] and cancelling terms

$$M = \frac{\sigma_0 bc^2}{2}[S(2 + \operatorname{csch}^2 S) - \coth S] \quad [31]$$

Substituting for M from Equation [28] and differentiating, the following is obtained

$$dx = \frac{\sigma_0 bc^2}{P}(\coth^2 S - S \coth S \operatorname{csch}^2 S)\,dS \quad [32]$$

From Equations [10] and [11], the following may be written for the extreme fiber

$$\frac{1}{\rho} = \frac{\epsilon_1}{c} = \frac{(\epsilon_0' + m't^n)\sinh S}{c} \quad [33]$$

After eliminating $1/\rho$ between Equations [23] and [33], the following integral can be formed in terms of S and x

$$\frac{dz}{dx} = \int \frac{(\epsilon_0' + m't^n)\sinh S}{c}\,dx \quad [34]$$

Substituting dx from Equation [32] into Equation [34] and integrating, an equation for the slope, dz/dx, of the beam is obtained

$$\frac{dz}{dx} = \frac{\sigma_0 bc}{P}(\epsilon_0' + m't^n)(\cosh S + S \operatorname{csch} S + C_1) \quad [35]$$

where C_1 is a constant to be determined from boundary conditions.

The deflection z of the beam may be found by multiplying Equation [35] by dx, substituting for dx from Equation [32] and forming the integral. After expanding and collecting terms, the expression becomes

$$z = \frac{\sigma_0^2 b^2 c^3}{P^2}(\epsilon_0' + m't^n)\int (\coth^2 S \cosh S - S^2 \coth S \operatorname{csch}^2 S + C_1 \coth^2 S - C_1 S \coth S \operatorname{csch}^2 S)\,dS \quad [36]$$

The indicated integration may be evaluated with the following result

$$z = \frac{\sigma_0^2 b^2 c^3}{P^2}(\epsilon_0' + m't^n)\left[\sinh S + \frac{S^2}{3\sinh^2 S} + \frac{S\cosh S}{3\sinh^2 S} - \frac{2}{3\sinh S} + \frac{S}{3} + \frac{1}{3}\sum_{p=1,2\ldots} \frac{(-1)^p\, 2\,(2^{2p-1}-1)}{(2p+1)!} B_p S^{2p+1} + C_1\left(S - \frac{1}{2}\frac{\cosh S}{\sinh S} + \frac{S}{2\sinh^2 S}\right) + C_2\right] \quad [37]$$

where $S = \sigma_1/\sigma_0$, σ_1 is the stress on the extreme fiber of the beam at the position for which the deflection z is to be determined, B_p are Bernoulli numbers, and C_1 and C_2 are constants to be determined from boundary conditions. The series appearing in Equation [37] converges for $S^2 < \pi$.

For the cantilever beam of length L the slope is zero at $x = L$. Thus from Equation [35]

$$C_1 = -\cosh S_L - S_L \operatorname{csch} S_L \quad [38]$$

where S_L is the value of S at the position $x = L$. The value of S_L may be determined from Equation [31] by substituting PL for M and solving for S_L by trial in a numerical example.

Since the deflection of the cantilever beam is zero at $x = L$, the value of C_2 may be determined from Equation [37] by setting $z = 0$ and S equal the same value S_L as in the foregoing.

To obtain the deflection z_x at location x along the beam, substitute the bending moment Px for M in Equation [31] and solve for the corresponding value of S, S_x by trial. Substitute S_x in Equation [37] together with C_1 and C_2 and compute the deflection z_x.

It can be shown by application of L'Hospital's rule to Equation [31] that $S = 0$ when $M = Px = 0$. Thus the deflection z_0, of the free end of the beam may be obtained by substituting $S = 0$ in Equation [37]

$$z_0 = \frac{\sigma_0^2 b^2 c^3}{P^2}(\epsilon_0' + m't^n)\,C_2 \quad [39]$$

The foregoing solutions are valid only when $S^2 < \pi$ as noted previously.

For values of $|S|$ greater than about 5 the hyperbolic functions may be approximated by exponential functions to obtain a solution. Equation [31] then becomes approximately

$$M = \frac{\sigma_0 bc^2}{2}(2S - 1) \quad [40]$$

Differentiating and substituting Equation [29]

$$dM = Pdx = \sigma_0 bc^2 dS \quad [41]$$

Substituting Equation [41] into Equation [34] and integrating; the equation for slope of the beam is obtained

$$\frac{dz}{dx} = \frac{\sigma_0 bc}{2P}(\epsilon_0' + m't^n)(e^S + C_1) \quad [42]$$

The deflection equation is obtained by substituting for dx from Equation [41] into Equation [42] and integrating

$$z = \frac{\sigma_0^2 b^2 c^3}{2P^2}(\epsilon_0' + m't^n)(e^S + C_1 S + C_2) \quad [43]$$

where the symbols are the same as before.

This solution also involves determining S as a function of x through Equations [28] and [40]. The foregoing expression will be a good approximation to Equation [37] when the value of S is greater than 5 throughout most of the depth of the beam and throughout most of the length of the beam. Inaccuracies always will be found in the vicinity of the neutral axis and in a region near zero-bending moment as at the end of the cantilever beam.

Effect of Limiting Values of Creep Constants

Examination of Equation [10] shows that as n approaches unity the creep curve approaches nearer to a linear curve (constant creep rate) which is the behavior expected from a purely viscous material. Also as σ_0 becomes large so that σ/σ_0 is small, the stress function becomes nearer a linear relation. This again is what would be expected from viscous behavior.

As n becomes smaller the resulting creep curve tends to rise sharply and then level off to an apparently constant value—which is not actually constant. For small values of σ_0, such that σ/σ_0 is large, the hyperbolic sine term may be replaced by an exponential one.

It should be pointed out that erroneous results are obtained by substituting σ/σ_0 for $\sinh \sigma/\sigma_0$ in the expressions calculated for bending creep, Equations [14] and [18]. This does not indicate an error in the equations but simply indicates that the simplifying assumption for small stresses cannot be utilized in equations which include a difference of two terms of like magnitude, as the error in making the simplification may be larger than the value of the difference of the two terms.

Conclusions

The form of creep equation employed seems adequate to describe the tension creep of a grade-C canvas laminate. The close agreement between creep in bending predicted by this equation and actual data lends support to the possible usefulness of the equation. Further evidence is provided by the agreement between the stress-strain curve derived from the same creep equation and actual test data.

Acknowledgment

This project was conducted in the Department of Theoretical and Applied Mechanics as part of the work of the Engineering Experiment Station of the University of Illinois, in co-operation with Picatinny Arsenal, Ordnance Corps, Department of the Army. The authors are grateful to P. N. Mathur, H. G. Russel, and E. J. Scott for checking the work and to W. A. Hagemeyer and G. E. Milum for preparing the illustrations.

BIBLIOGRAPHY

1 "Utilization of Creep Test Data in Engineering Design," by R. W. Bailey, Proceedings of The Institution of Mechanical Engineers, vol. 131, 1935, p. 131.

2 "An Investigation of the Nature of Creep Under Stresses Produced by Pure Flexure," by H. J. Tapsell and A. E. Johnson, *Institute of Metals Journal*, vol. 57, August, 1935, p. 121.

3 "Correlation of Creep and Relaxation Properties of Copper," by C. C. Davenport, Journal of Applied Mechanics, Trans. ASME, vol. 60, 1938, pp. A-55–A-60.

4 "Creep Properties of Lucite and Plexiglas for Tension, Compression, Bending, and Torsion," by J. Marin, Y. H. Pao, and G. E. Cuff, Trans. ASME, vol. 73, 1951, pp. 705–719.

5 "Flow of Solid Metals From the Standpoint of the Chemical Rate Theory," by W. Kauzmann, Trans. American Inst. of Mining and Metallurgical Engineering, Institute of Metals Division, vol. 143, 1941, p. 57.

6 "A Method of Analyzing Creep Data," by R. G. Sturm, C. Dumont, and F. M. Howell, Journal of Applied Mechanics, Trans. ASME, vol. 58, 1936, pp. A-62–A-66.

7 "Creep, Elastic Hysteresis, and Damping in Bakelite Under Torsion," by H. Leaderman, Journal of Applied Mechanics, Trans. ASME, vol. 61, 1939, pp. A-79–A-85.

8 "Creep Properties of Molded Phenolic Plastics," by D. Telfair, T. S. Carswell, and H. K. Nason, *Modern Plastics*, vol. 21, 1944, p. 137.

9 "Creep Characteristics of Plastics," by W. N Findley, 1944 Symposium on Plastics, ASTM, 1944, p. 18.

10 "Correlation of Tension Creep Tests With Relaxation Tests," by E. P. Popov, Journal of Applied Mechanics, Trans. ASME, vol. 69, 1947, pp. A-135–A-142.

11 "The Effect of Temperature on the Creep of Two Laminated Plastics as Interpreted by the Hyperbolic-Sine Law and Activation Energy Theory," by W. N. Findley, C. H. Adams, and W. J. Worley, Proceedings of the ASTM, vol. 48, 1948, p. 1217.

12 "Mechanical Properties of Five Laminated Plastics," by W. N. Findley and W. J. Worley, NACA, Tech. Note 1560, August, 1948.

13 "The Effect of Temperature on the Creep and Recovery of a Melamine-Glass Fabric Laminate," by W. J. Worley and W. N. Findley, Proceedings of the ASTM, vol. 50, 1950, p. 1399.

14 "Deflections and Stresses in Beams Subjected to Bending and Creep," by Yoh-Han Pao and Joseph Marin, Journal of Applied Mechanics, Trans. ASME, vol. 74, 1952, pp. 478–484.

15 "Derivation of a Stress-Strain Equation from Creep Data for Plastics," by W. N. Findley, Proceedings of the First U. S. National Congress of Applied Mechanics, June 11–16, 1951, p. 595.

16 "An Experimental and Analytical Investigation of Creep in Bending," by G. H. MacCullough, Journal of Applied Mechanics, Trans. ASME, vol. 55, 1933, paper, APM 55-9-55, pp. 55–60.

17 "Creep of Aluminum Subjected to Bending at Normal Temperatures," by J. Marin and L. E. Zwissler, Proceedings of the ASTM, vol. 40, 1940, p. 937.

18 "Creep-Time Relations for Polystyrene Under Tension, Bending, and Torsion," by J. Marin and G. Cuff, Proceedings of the ASTM, vol. 49, 1949, pp. 1158–1174.

19 "Comments on Creep and Damping Properties of Polystyrene," by W. N. Findley, *Journal of Applied Physics*, vol. 21, 1950, p. 258.

20 "Bending of Beams With Creep," by E. P. Popov, *Journal o Applied Physics*, vol. 20, 1949, pp. 251–256.

21 "Static and Dynamic Creep Properties of Laminated Plastics for Various Types of Stress," by J. Marin, NACA, Tech. Note 1105, February, 1947.

22 "Prediction of Relaxation of Metals From Creep Data," by I. Roberts, Proceedings of the ASTM, vol. 51, 1951, p. 811.

23 "Plasticity," by A. Nadai, The McGraw-Hill Book Co. Inc., New York, N. Y., 1935, p. 121.

24 "Strength of Materials Subjected to Shear at High Temperatures," by Franklin L. Everett, Trans. ASME, vol. 53, paper APM-53—10, 1931, pp. 117–124.

Fracture of Inoculated Iron Under Biaxial Stresses

By I. CORNET[1] and R. C. GRASSI,[2] BERKELEY, CALIF.

Data are presented on the fracture of inoculated-iron thin-wall tubes, investigated under various ratios of axial to tangential stress, ranging from pure tension to pure compression. These data are consistent with published data on gray cast iron. It may be assumed that in cast-iron, plates of friable graphite in an iron matrix, act like solid iron with respect to compressive stresses, but they act as stress-concentrating cavities with respect to tensile stresses. This gives a stress-concentration factor, which is easily determined experimentally. Stress-concentration factors obtained were 3.2–3.3 for gray cast iron, and 2.4–2.5 for inoculated cast iron. A distortion-energy criterion for fracture, modified by this stress-concentration factor, is consistent with the experimental data. It appears that the concentration of the dispersed graphite, and the shape and size of this brittle phase, affect the fracture strength under combined stresses.

Purpose and Scope

MATERIALS of very limited ductility, besides their intrinsic importance, are valuable subjects for the study of fracture laws. The virtual elimination of necking permits greater assurance in determining the state of stress at fracture; it also reduces strain-hardening effects. Brittle materials, such as cast iron, do present problems owing to stress concentrations and residual stresses attributed to microcracks or the presence of a second phase. Also, materials which are brittle in tension may exhibit appreciable ductility in compression or under combined stresses.

The purpose of this investigation was to supplement published studies (1, 2)[3] of the fracture of cast iron under biaxial stresses. New data are reported on the fracture of a calcium-silicide-inoculated cast iron meeting specifications of ASTM Class No. 50 (3). The data obtained represent the result of testing 35 tube specimens and seven solid cylindrical specimens.

Procedure

Tube specimens were machined from cast bars 1.2 in. diam and 22 in. long, all cast bars being from the same foundry heat. Three tube specimens and two solid cylinders were machined from each cast bar, which previously had been given a 1-hr anneal at 1000 F. The tube specimens were drilled, reamed with a carbide reamer to reproduce an internal diameter of 0.500 ± 0.0005 in., and then rough-turned. The blank was then mounted on a mandrel and finish-turned to a diameter of 0.560 ± 0.0005 in.; the specimen was then threaded. A circular radius tool was used for the finish cut, which produced a smooth surface with no discontinuity at the radii. This tubular specimen was mounted in grips sealed with lead gaskets and stressed according to the desired ratio of axial to tangential stress (referred to as "stress ratio") by the proper combination of internal pressure and axial tension or compression. Solid cylindrical specimens, 0.500 in. in height and 0.505 in. diam, were tested in compression only. Details of the specimens and of the grip sections are shown in Figs. 1 and 2.

A modified two-cylinder diesel injection pump was used to produce the internal pressure, which was measured by a calibrated bourdon-type gage accurate to ±½ per cent. The axial loading of the specimen was done on a 200,000-lb Southwark-Emery testing machine, using the 10,000-lb scale with a least division of 10 lb.

Results and Discussion

Results for the tube tests for the inoculated iron are presented graphically in Fig. 3. The seven solid cylinders subjected to pure compression failed at an average stress of 135,000 psi, (not shown in Fig. 3), as compared to an average value of 122,000 psi for the three tube specimens. This difference in averages is reasonable, considering the dissimilarity of the specimens; for the gray iron there also was about 10 per cent difference in compressive strength between the tubular and solid specimens (1). In general, the data for the fracture of inoculated cast iron are consistent in pattern with the data published previously for gray cast iron, but at correspondingly greater stresses.

The results obtained may be approximated by assuming that fracture is governed by a distortion-energy criterion, modified by a concentration of stress due to the notch effect. The procedure used, developed by John C. Fisher (4), is as follows:

It is assumed that fracture cannot occur independently of deformation (5). Now plastic flow in metals is initiated, according to the distortion-energy theory, when

$$(S_1 - S_2)^2 + (S_2 - S_3)^2 + (S_3 - S_1)^2 = 2S_0^2 \qquad [1]$$

where S_1, S_2, S_3 are the principal stresses and S_0 = the yield stress in simple tension.

Cast iron has a heterogeneous polyphase structure. The graphite flakes in this structure are brittle and friable; they can transmit compressive stresses without failure, but are relatively weak in tension. As a first approximation, let it be assumed that the graphite flakes act as ellipsoidal cavities under tension stresses, but as sound, reliable material under compressive stresses. An ellipsoidal cavity will have a stress-concentrating effect, as analyzed by Heinz Neuber (6); experimentally, this stress-concentration factor is simply the ratio of the fracture strength in pure compression to the fracture strength in pure tension. In the tension-tension quadrant the most severe stress state is that for which the largest tensile stress acts in the axial direction rela-

---

[1] Associate Professor of Mechanical Engineering, University of California.

[2] Associate Professor of Mechanical Engineering, University of California. Mem. ASME.

[3] Numbers in parentheses refer to the Bibliography at the end of the paper.

Contributed by the Applied Mechanics Division and presented at the Annual Meeting, New York, N. Y., November 28–December 3, 1954, of The American Society of Mechanical Engineers.

Discussion of this paper should be addressed to the Secretary, ASME, 29 West 39th Street, New York, N. Y., and will be accepted until July 11, 1955, for publication at a later date. Discussion received after the closing date will be returned.

Note: Statements and opinions advanced in papers are to be understood as individual expressions of their authors and not those of the Society. Manuscript received by ASME Applied Mechanics Division, September 16, 1953. Paper No. 54—A-47.

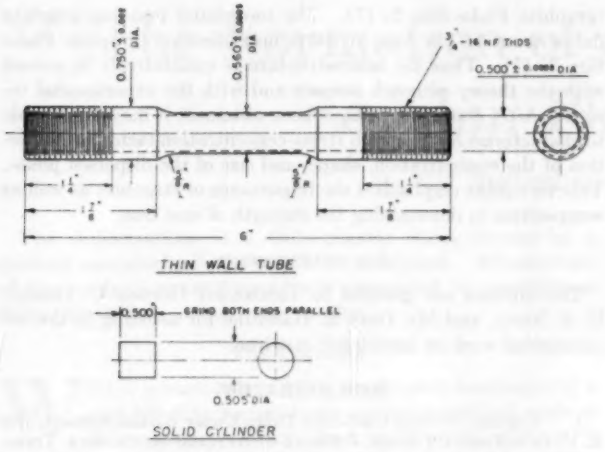

FIG. 1 CAST-IRON FRACTURE SPECIMENS

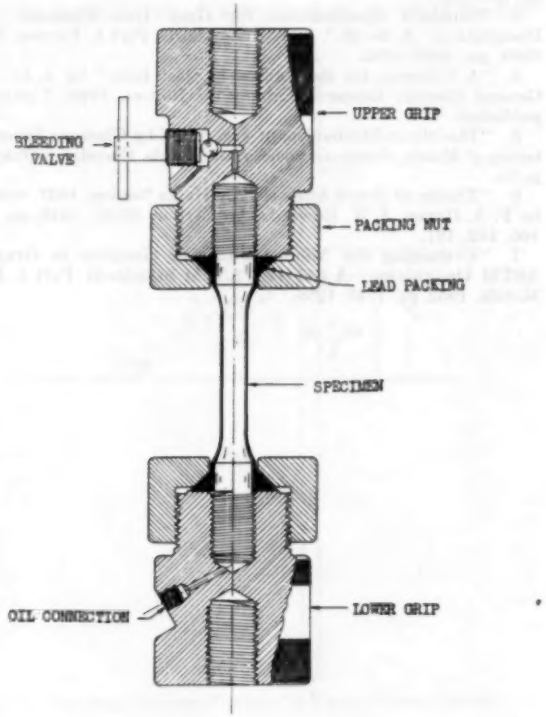

FIG. 2 GRIP SECTIONS FOR STUDY OF FRACTURE OF CAST IRON UNDER BIAXIAL STRESS

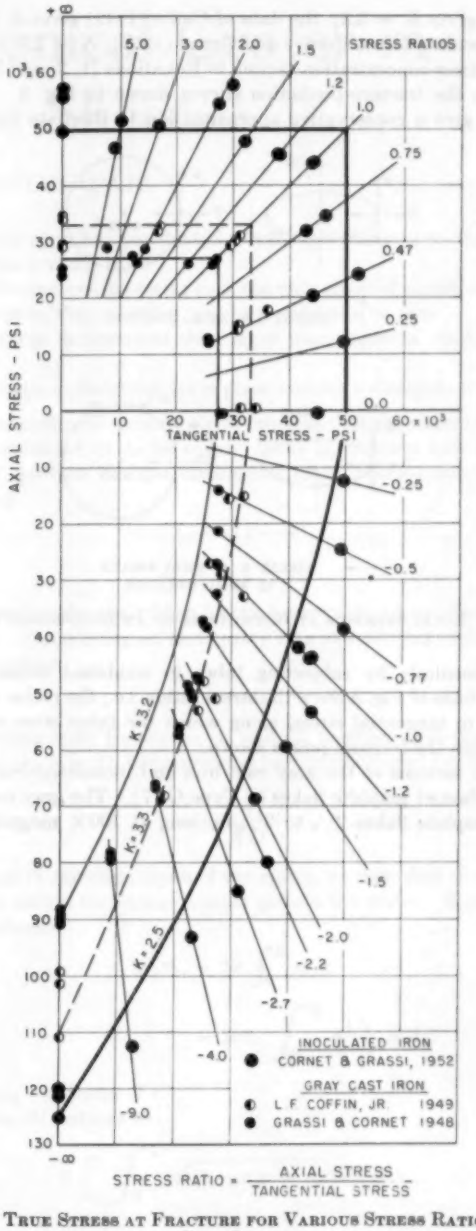

FIG. 3 TRUE STRESS AT FRACTURE FOR VARIOUS STRESS RATIOS FOR CAST IRONS

(The experimental data are fitted by curves calculated from Equations [1, 2, 3]. Compression and tension test data are required to furnish the stress-concentration factor, K, and an anchor point for the curve for the particular cast iron.)

tive to the long axis of the ellipsoidal cavity, as shown in Fig. 4. There is a point at the periphery of the plate where the radial and tangential stresses both are zero, also as shown in Fig. 4. Equation [1] therefore reduces to

$$KS_1 = S_0 \quad \ldots\ldots [2]$$

where S_1 is the maximum tensile stress for the initiation of plastic flow in the cast iron subjected to biaxial tension. Here the distortion-energy criterion coincides with the maximum-stress law.

Consider the case of cast iron subjected to a tensile stress S_1 and a compressive stress S_3, with the intermediate stress S_2 approximately zero. As for the tension-tension quadrant, the most severe stress state is that for tensile stress acting in the axial direction relative to a graphite plate. There is a point at the periphery of the plate where the tangential stress is S_3 and the radial stress is zero. At this point Equation [1] reduces to

$$K^2S_1^2 - KS_1S_3 + S_3^2 = S_0^2 \quad \ldots\ldots [3]$$

Finally, when cast iron is subjected to biaxial compression, Equation [1] is unchanged, for there is no stress concentration.

From tests on tubes in pure compression and in pure tension, one obtains a ratio of the fracture strength in pure compression to the fracture strength in pure tension; this ratio is the stress-concentration factor K. For gray iron the data of Grassi and Cornet

(1948) gives $K = 3.2$; the data of Coffin (1949) gives $K = 3.3$. For inoculated iron, Cornet and Grassi (1952), $K = 2.5$. Using these stress-concentration factors in Equations [1, 2, and 3], one obtains the fracture-prediction curves shown in Fig. 3. These curves give a conservative approximation to the data obtained

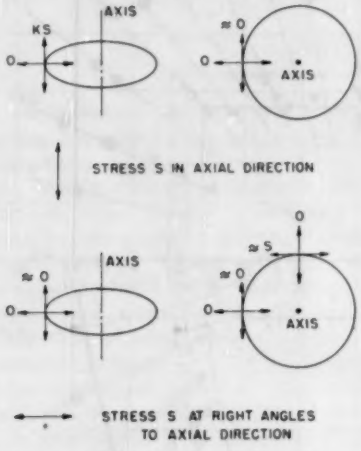

FIG. 4 LOCAL STRESSES AT BOUNDARIES OF AN ELLIPSOIDAL CAVITY

experimentally by subjecting tubes to combined stress. The radial lines of Fig. 3 show the stress ratios, i.e., the ratios of axial stress to tangential stress, along which the tubes were stressed to obtain the fracture points shown.

Test sections of the gray cast iron and inoculated-iron tubes both showed graphite flakes of Type C (7). The gray cast iron has graphite flakes $2^1/_4$ to $2^1/_2$ in. long at 100× magnification (graphite Flake Size 2) (7). The inoculated iron has graphite flakes about $1^1/_2$ in. long at 100× magnification (graphite Flake Size 3) (7). Thus the microstructure is qualitatively in accord with the theory of notch stresses and with the experimental results. After enough data have been obtained, it may be possible to characterize K, the notch stress-concentration factor, as a function of the concentration, shape, and size of the dispersed phase. This viewpoint emphasizes the importance of structure as well as composition in determining the strength of cast iron.

ACKNOWLEDGMENT

The authors are grateful to Lieutenant Gordon C. George, U. S. Navy, and Mr. Oran L. Haseltine for assisting in the experimental work on inoculated cast iron.

BIBLIOGRAPHY

1 "Fracture of Gray Cast-Iron Tubes Under Biaxial Stresses," by R. C. Grassi and I. Cornet, JOURNAL OF APPLIED MECHANICS, Trans. ASME, vol. 71, 1949, pp. 178–182.

2 "The Flow and Fracture of a Brittle Material," by L. F. Coffin, Jr., JOURNAL OF APPLIED MECHANICS, Trans. ASME, vol. 72, 1950, pp. 233–248.

3 "Standard Specifications for Gray Iron Castings, ASTM Designation: A 48–48," ASTM Standards, Part 1, Ferrous Metals, 1949, pp. 1086–1092.

4 "A Criterion for the Failure of Cast Iron," by J. C. Fisher, General Electric Research Laboratory Report, 1949, 7 pages, unpublished.

5 "The Micro-Mechanism of Fracture," by Clarence Zener, *Fracturing of Metals*, American Society for Metals, Cleveland, Ohio, 1948, p. 14.

6 "Theory of Notch Stresses," by Heinz Neuber, 1937, translated by F. A. Raven, J. W. Edwards, Ann Arbor, Mich., 1946, pp. 70–72, 160, 162, 181.

7 "Evaluating the Microstructure of Graphite in Gray Iron, ASTM Designation: A 247–47," ASTM Standards, Part 1, Ferrous Metals, 1952, pp. 1249–1256.

The Formation of a Conical Crater in a Thin Plastic Sheet

By W. T. THOMSON,[1] LOS ANGELES, CALIF.

The deformation of a thin plastic sheet forced by a conical mandrel of any angle is analyzed. Dimensions of the conical crater formed are presented in nondimensional form for various cone angles.

The Problem

WHEN a small hole in a thin plastic plate is enlarged by a mandrel of very small taper the unsymmetrical mode of deformation is a sharp-edged crater whose height is $^3/_4$ times that of the enlarged radius and whose thickness varies as the square root of the distance from the sharp edge.[2]

We will consider here the problem of forcing a conical mandrel of angle 2α partially through a plastic sheet, for which the foregoing conclusions must be obtained as a special case when α approaches zero. Referring to Fig. 1, the following assumptions are made:

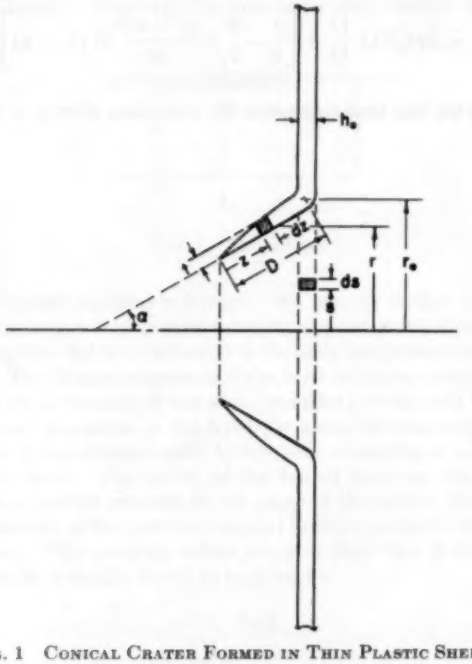

Fig. 1 Conical Crater Formed in Thin Plastic Sheet

1 The cone has penetrated a sufficient distance so that the crater has a sharp edge.

2 Circumferential stress σ_θ is the only stress of significance in the crater so that σ_r and σ_z can be assumed to be zero.

3 Plastic deformation then takes place under a yield stress $\sigma_\theta = Y$.

4 Plastic deformation takes place without a change in volume.

The assumption of uniaxial stress requires that the strains ϵ_r and ϵ_z perpendicular to σ_θ be equal. Thus an element $h_o ds$ in the original position changes dimensions after deformation to the following

$$t = h_o(1 - \epsilon) \quad [1]$$

$$dz = ds(1 - \epsilon) \quad [2]$$

We next make use of the fourth assumption of no change in volume. Considering an elementary ring at s which is deformed into the crater

$$2\pi s h_o ds = 2\pi r t dz \quad [3]$$

Substituting from Equations [1] and [2] together with the relationship $s/z = r_o/D$, the expression for the thickness t becomes

$$t = h_o \sqrt{\frac{r_o}{D}\frac{z}{r}} \quad [4]$$

To find D, the slant depth of the crater, we note that all of the material within the radius r_o must go into the crater. Equating these volumes

$$\pi r_o^2 h_o = 2\pi \int_0^D rt\, dz$$

$$= 2\pi h_o \int_0^D \sqrt{\frac{r_o}{D}}\, zr\, dz \quad [5]$$

Replacing r in terms of z Equation [5] reduces to

$$2\frac{D}{r_o}\int_0^1 \sqrt{(1-a)x + ax^2}\, dx = 1 \quad [6]$$

where

$$x = \frac{z}{D}$$

$$a = \frac{D \sin \alpha}{r_o}$$

On integration, Equation [6] becomes

$$\frac{D}{r_o}\left[\frac{1 + (1-a)^2}{a} - \frac{(1-a)^2}{a\sqrt{a}} \ln \frac{1 + \sqrt{a}}{1 - \sqrt{a}}\right] = 1 \quad [7]$$

which can be solved for D/r_o for any given value of α.

Fig. 2 represents a plot of D/r_o versus α. The special case of $\alpha = 0$ can be obtained directly from Equation [7], by expanding the logarithm in a series and taking the limit as a approaches zero. Fig. 3 is a plot of the thickness t/h_o versus z/r_o for $\alpha = 30$ deg.

---

[1] Professor of Engineering, University of California. Mem. ASME.

[2] "The Formation and Enlargement of a Circular Hole in a Thin Plastic Sheet," by G. I. Taylor, Quarterly of the *Journal of Mechanics and Applied Mathematics*, vol. 1, 1948, pp. 103–124.

Contributed by the Applied Mechanics Division and presented at the Annual Meeting, New York, N. Y., November 28–December 3, 1954, of The American Society of Mechanical Engineers.

Discussion of this paper should be addressed to the Secretary, ASME, 29 West 39th Street, New York, N. Y., and will be accepted until July 11, 1955, for publication at a later date. Discussion received after the closing date will be returned.

Note: Statements and opinions advanced in papers are to be understood as individual expressions of their authors and not those of the Society. Manuscript received by ASME Applied Mechanics Division, April 5, 1954. Paper No. 54—A-36.

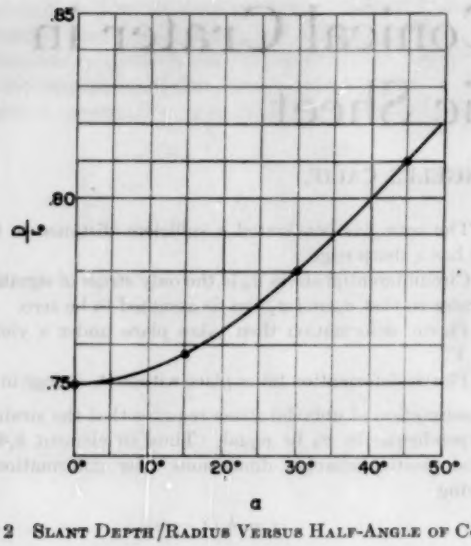

FIG. 2 SLANT DEPTH/RADIUS VERSUS HALF-ANGLE OF CONE

The work required for the plastic deformation is frequently of interest. Since the stress is uniaxial and equal to $\sigma_\theta = Y$, the work required per unit volume for deformation from s to r is

$$Y \int d\epsilon_\theta = Y \int_s^r \frac{ds}{s} = Y \ln \frac{r}{s} \quad \ldots\ldots\ldots\ldots [8]$$

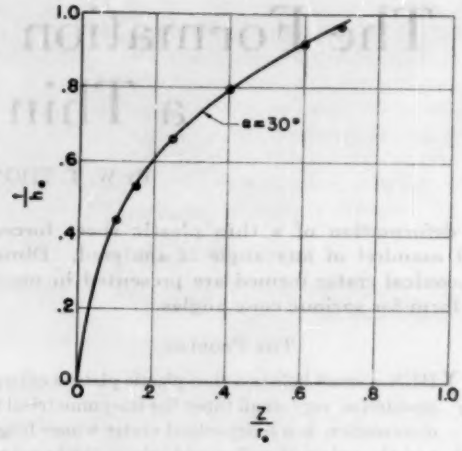

FIG. 3 NONDIMENSIONAL THICKNESS OF CRATER

and the total work done for the plastic deformation becomes

$$W = 2\pi h_0 Y r_0^2 \left\{ \frac{1}{4} + \left[\frac{1}{a} - \frac{3}{2} + \frac{(1-a)^2}{a^2} \ln (1-a) \right] \right\} \quad \ldots [9]$$

where the first term represents the work done when $\alpha = 0$ or $a = 0$.

Thermal Shock on a Circular Surface of Exposure of an Elastic Half Space

By M. A. SADOWSKY,[1] TROY, N. Y.

The paper presents an explicit determination of displacements and stresses in a uniform circular thermal shock. In a generalization to nonuniform shocks on surfaces of arbitrary shape, it is shown that the protrusion arising at any place is proportional to the intensity of the shock at that place.

General Notion of a Thermal-Shock Layer

LET us consider the case in which a part of a plane surface of a body is exposed to a spontaneous radiation causing a finite amount of heat to become absorbed by the exposed part of the surface, Fig. 1. We assume that the duration of exposure is so short that the heat does not penetrate to any appreciable depth. Thus only an extremely thin surface layer of

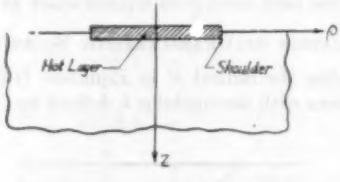

Fig. 1 The Layer

highly heated material is formed. We assume further that the radiation impact is of uniform intensity at every point of exposure, meaning that the layer is heated to the same temperature at every point. The thermal expansion of the layer in its own plane is prevented by a reaction of the curb (shoulder) of the cold bed resisting any expansion of the hot layer along its boundary. The reaction is two-dimensionally hydrostatic, consisting of a normal pressure alone. The action of the heated layer on the elastic body is a uniform pressure in the plane of the surface normal to the boundary of the layer and applied in the expansive (outward) direction. This pressure, whose physical dimension is force per unit length, is readily found to be given by

$$p = \frac{E\alpha Q}{(1-\nu)Acd} \qquad [1]$$

where

E = modulus of elasticity in tension
ν = Poisson's ratio
α = coefficient of linear heat expansion
Q = total heat absorbed by layer
A = area of layer (area exposed to radiation)
c = heat capacity (heat per unit mass per 1 deg)
d = density of the body (mass per unit volume)

The expansion of the layer in the direction z normal to the surface goes uninhibited ($\sigma_z = 0$) and is such that the amount by which the layer thickens is given by

$$\overset{*}{u}_z = \epsilon_z h = \frac{(1+\nu)\alpha Q}{(1-\nu)Acd} \qquad [2]$$

The quantity $\overset{*}{u}_z$ may be interpreted as the normal displacement of exposed surface of the layer relative to its inner (imbedded) surface. We note the following

$$2G\overset{*}{u}_z = -\frac{E\alpha Q}{(1-\nu)Acd} \qquad [3]$$

in which G stands for the modulus of elasticity in shear.

The Special Problem

Let the body be the half space $z \geqslant 0$. Let the circular region $\rho \leqslant b$ on the plane surface $z = 0$ be exposed to uniform thermal shock of total strength Q. According to the layer hypothesis, the body after the shock will be under action of a uniform radial expansive force

$$p = \frac{E\alpha Q}{(1-\nu)\pi b^2 cd} \qquad [4]$$

per unit length of the arc of the circle $\rho = b$, $z = 0$. Since the resultant stress field will be rotationally symmetric about the z-axis, cylindrical co-ordinates ρ, ϕ, z will be used. The cylindrical components of displacements and stress will be independent of ϕ.

Boussinesq stress potentials φ, ϑ, and λ will be used to construct the solution. As functions of ρ, ϕ, z they satisfy the Laplace equation

$$\nabla^2\varphi = \nabla^2\vartheta = \nabla^2\lambda = 0 \qquad [5]$$

They give rise to three basic solutions of the equations of elasticity, in which the displacement vector, $\delta\bar{r}$, is determined as follows

$$\left.\begin{aligned} &\text{First basic solution: } 2G\delta\bar{r} = \text{grad } \varphi \\ &\text{Second basic solution: } 2G\delta\bar{r} = 2\,\text{curl}[0, 0, \vartheta] \\ &\text{Third basic solution: } 2G\delta\bar{r} = z\,\text{grad }\lambda \\ &\qquad\qquad - [0, 0, (3-4\nu)\lambda] \end{aligned}\right\} \qquad [6]$$

The triplet forms a complete system.[2]

---

[1] Professor of Mechanics, Rensselaer Polytechnic Institute. Mem. ASME.

Contributed by the Applied Mechanics Division and presented at the Annual Meeting, New York, N. Y., November 28–December 3, 1954, of The American Society of Mechanical Engineers.

Discussion of this paper should be addressed to the Secretary, ASME, 29 West 39th Street, New York, N. Y., and will be accepted until July 11, 1955, for publication at a later date. Discussion received after the closing date will be returned.

Note: Statements and opinions advanced in papers are to be understood as individual expressions of their authors and not those of the Society. Manuscript received by ASME Applied Mechanics Division, January 25, 1954. Paper No. 54—A-44.

[2] "Stress Concentration Around an Ellipsoidal Cavity in an Infinite Body Under Arbitrary Plane Stress Perpendicular to the Axis of Revolution of Cavity," by E. Sternberg and M. Sadowsky, Journal of Applied Mechanics, Trans. ASME, vol. 69, 1947, p. A-191.

"Stress Concentration Around a Triaxial Ellipsoidal Cavity," by E. Sternberg and M. Sadowsky, Journal of Applied Mechanics, Trans. ASME, vol. 71, 1949, pp. 149–157.

"On the Axisymmetric Problem of the Theory of Elasticity for an Infinite Region Containing Two Spherical Cavities," by E. Sternberg and M. Sadowsky, Trans. ASME, vol. 74, 1952, pp. 19–27.

We will obtain the Boussinesq potentials of our problem by integrating the Boussinesq potentials of the Cerruti solution around the circle $\rho = b$ on $z = 0$. The Cerruti solution, representing the singularity of a concentrated force with components

$$X = 1, \quad Y = 0, \quad Z = 0 \qquad [7]$$

acting at $\rho = z = 0$ tangentially to the free surface $z = 0$ is generated by the Boussinesq potentials

$$\left.\begin{aligned} \varphi &= \frac{1-\nu}{\pi}\,\frac{x}{r+z} \\ \vartheta &= \frac{1}{2\pi}\,\frac{y}{r+z} \\ \lambda &= \frac{-1}{2\pi}\,\frac{x}{r(r+z)} \end{aligned}\right\} \qquad [8]$$

in which $r^2 = x^2 + y^2 + z^2 = \rho^2 + z^2$. Using a second Cerruti solution with a resultant force turned through 90 deg ($Y = 1$) and then locating the point of application at ($b \cos \omega$, $b \sin \omega$, 0) with a Cerruti force $X = \cos \omega$, $Y = \sin \omega$, $Z = 0$ acting at that point, we obtain, by integration from $\omega = 0$ to 2π, for the Bouissinesq potentials of our problem: $\vartheta = 0$, and

$$\left.\begin{aligned} \varphi &= \frac{E\alpha Q}{\pi^2 b^3 cd}\,2b^2 \int_0^\pi \frac{\rho\cos\omega - b}{R+z}\,d\omega \\ \lambda &= -\frac{E\alpha Q}{\pi^2 b^3 cd}\,\frac{b^2}{1-\nu}\int_0^\pi \frac{\rho\cos\omega - b}{R(R+z)}\,d\omega \end{aligned}\right\} \qquad [9]$$

in which R, the irrationality of the elliptic integrals, is given by

$$R = \sqrt{z^2 + \rho^2 + b^2 - 2b\rho\cos\omega} \qquad [10]$$

The result $\vartheta = 0$ is obvious since rotationally symmetric solutions free from twist are formed with the use of φ and λ alone. As for φ and λ, the most expedient procedure of analysis seems to be as follows:

We introduce a characteristic solution, defined by the superposition

Characteristic solution = First Boussinesq solution with

$$\varphi = 2b^2 \int_0^\pi \frac{\rho\cos\omega - b}{R+z}\,d\omega$$

—Third Boussinesq solution with

$$\lambda = \frac{b^2}{1-\nu}\int_0^\pi \frac{\rho\cos\omega - b}{R(R+z)}\,d\omega \qquad [11]$$

We then have:

Solution of present problem equals

$$\frac{E\alpha Q}{\pi^2 b^3 cd} \text{ times the characteristic solution} \qquad [12]$$

The characteristic solution has dimensionless stress components depending on dimensionless co-ordinates ρ/b, z/b only. This makes it best suited for graphical representation. Furthermore, with E held constant, the coefficient

$$\frac{E\alpha Q}{\pi^2 b^3 cd}$$

does not depend on Poisson's ratio ν. In this sense we also obtain information on the ν-dependence of stresses and displacements directly from the characteristic solution.

Identification of a Singularity Due to Mindlin

The singularity of a heat shock concentrated at the point $r = 0$ on the surface could be defined, reasonably, as the limiting case of our present problem with $b \to 0$. The computation leads to the results

$$\left.\begin{aligned} \varphi &= -\frac{E\alpha Q}{\pi cd}\,\frac{1}{r} \\ \lambda &= \frac{E\alpha Q}{2(1-\nu)\pi cd}\,\frac{z}{r^3} \end{aligned}\right\} \qquad [13]$$

The foregoing is the precise limiting form of Equations [9]. The singularity expressed by Equations [13] is identical with the singularity established for the thermal-point shock by Mindlin in a Galerkin-vector form.[3] Mindlin did not start on the surface of the half space; he first obtained the singularity for a point shock at an interior point of the half space and then went through the limit process in which the point of the shock would converge toward a surface point. This procedure is different from ours. The identity of the results testifies positively as to the physical soundness of the limit concept of a point shock at the surface.

Evaluation of Characteristic Solution [11]

To rationalize the radical R in Equation [10] we introduce elliptic functions with the modulus k defined by (Fig. 2)

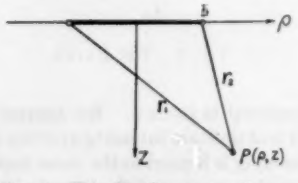

Fig. 2 The Co-Ordinate System

$$k^2 = \frac{4b\rho}{r_1^2} \qquad [14]$$

leading to the conjugate modulus

$$k' = \frac{r_2}{r_1} \qquad [15]$$

in which r_1 and r_2 are bipolar co-ordinates defined by

$$r_1^2 = z^2 + (\rho + b)^2 \qquad [16]$$

$$r_2^2 = z^2 + (\rho - b)^2 \qquad [17]$$

In writing functions with the modulus k we will suppress its mention. Thus K and E will mean $K(k)$ and $E(K, k)$. The modulus k' will be explicitly written whenever it should occur.

Using the notation

$$\psi = \frac{\pi - \omega}{2} \qquad [18]$$

we introduce the argument u of the Jacobian elliptic functions by

$$\left.\begin{aligned} snu &= \sin\psi \\ cnu &= \cos\psi \end{aligned}\right\} \qquad [19]$$

[3] "Force at a Point in the Interior of a Semi-Infinite Solid," by R. D. Mindlin, *Physics*, vol. 7, 1936, pp. 195–202.

from which follows the rationalization of R as

$$R = r_1\, dn\, u \quad \ldots\ldots [20]$$

The integrals in Equations [9] are reducible to complete elliptic integrals of the third kind $\Pi(K, a)$ with

$$\left.\begin{aligned} sn\, a &= \frac{r_1}{\rho + b} \\ cn\, a &= \frac{iz}{\rho + b} \\ dn\, a &= \frac{\rho - b}{\rho + b} \end{aligned}\right\} \quad \ldots\ldots [21]$$

Since $1 \leqslant sn\, a \leqslant 1/k$, we have Legendre's circular case with a complex value of a. For its treatment, we introduce a real parameter β as follows (Fig. 3)

$$a = K - i\beta \qquad 0 \leqslant \beta \leqslant 2K' \quad \ldots\ldots [22]$$

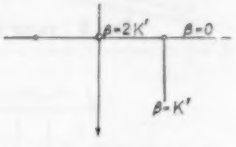

FIG. 3 VALUES OF β

For an equivalent set of real defining equations for β we may use

$$\left.\begin{aligned} sn(\beta, k') &= \frac{z}{r_2} \\ cn(\beta, k') &= \frac{\rho - b}{r_2} \\ dn(\beta, k') &= \frac{\rho + b}{r_1} \end{aligned}\right\} \quad \ldots\ldots [23]$$

The Jacobian Zeta-function involved in $\Pi(K, a)$ is introduced best in the following combination (Fig. 4)

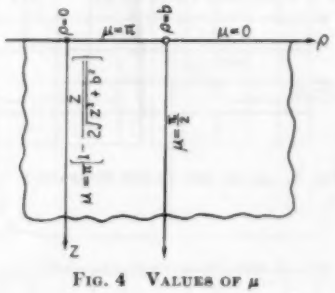

FIG. 4 VALUES OF μ

$$\mu = KZ(\beta, k') + \frac{\pi\beta}{2K'} \quad \ldots\ldots [24]$$

In evaluating $\Pi(K, a)$ attention is to be paid to the fact that a zero of Jacobi's Θ function lies in the interior of the β-range Equation [22] at $\beta = K'$. The locus of $\beta = K'$ is the cylindrical surface $\rho = b$ which lies in the analytically regular interior of the field $z > 0$. The discontinuity of $\Pi(K, a)$ at $\beta = K'$ consequently must be canceled by an opposite equal discontinuity arising from some elementary integral. This actually happens. We cite the pivotal relation involved here

$$2\Pi(K, a) - \frac{\pi}{2}\left[\frac{\rho^2 - b^2}{|\rho^2 - b^2|} - 1\right] = -\frac{z(\rho - b)}{r_1(\rho + b)} K + \mu \ldots [25]$$

The term in the brackets is sectionally constant, having a discontinuity at $\rho = b$.

The final evaluations of the integrals are

$$\int_0^\pi \frac{\rho \cos\omega - b}{R + z}\, d\omega = \frac{\rho^2 - b^2}{br_1} K - \frac{r_1}{b} E + \frac{z\mu}{b} \ldots [26]$$

$$\int_0^\pi \frac{\rho \cos\omega - b}{R(R + z)}\, d\omega = \frac{zK}{br_1} - \frac{\mu}{b} \quad \ldots\ldots [27]$$

Both integrals are potential functions analytic in the interior $z > 0$ of the half space. Their surface values (for $z = 0$) are discontinuous at $\rho = b$.

The computation of the Boussinesq solutions in Equation [11] gives the following table of results for the displacements and stresses in the characteristic solution. The coefficients included in the left members have been introduced to avoid a disturbing accumulation of repetitious factors in the tabulation.

CHARACTERISTIC SOLUTION: TABULATION FOR ENTIRE FIELD

$$\frac{2G(1-\nu)}{b} u_\rho = \frac{(3 - 2\nu)z^2 + (2 - 2\nu)(\rho^2 + b^2)}{\rho r_1} K - \left[\frac{(2 - 2\nu)r_1}{\rho} + \frac{z^2(z^2 + b^2 + \rho^2)}{\rho r_1 r_2^2}\right] E \quad \ldots\ldots [28]$$

$$\frac{2G(1-\nu)}{b} u_z = -\frac{2\nu z K}{r_1} + \frac{z^2 + \rho^2 - b^2}{r_1 r_2^2} zE - (1 - 2\nu)\mu \ldots [29]$$

$$\frac{1-\nu}{b}\sigma_\rho = \left[\frac{2\nu}{r_1} - \frac{(z^2 + \rho^2 - b^2)z^2}{r_1^3 r_2^2} - \frac{(3 - 2\nu)z^2 + (2 - 2\nu)b^2}{\rho^2 r_1}\right] K + \left[\frac{2b^4 + 5b^2z^2 + 3z^4}{\rho^2 r_1 r_2^2} - \frac{2\nu r_1}{\rho^2} - \frac{2b^2}{r_1 r_2^2} - \frac{4z^2[b^4 - (\rho^2 + z^2)^2]}{r_1^3 r_2^4}\right] E \quad \ldots\ldots [30]$$

$$\frac{1-\nu}{b}\sigma_z = \frac{(z^2 + \rho^2 - b^2)z^2}{r_1^3 r_2^2} K + \left[-\frac{z^2}{r_1 r_2^2} + \frac{8b^2z^2(z^2 - \rho^2 + b^2)}{r_1^3 r_2^4}\right] E \quad \ldots\ldots [31]$$

$$\frac{1-\nu}{b}\sigma_\phi = \left[\frac{2\nu}{r_1} + \frac{(3 - 2\nu)z^2 + (2 - 2\nu)(\rho^2 + b^2)}{\rho^2 r_1}\right] K - \left[\frac{(2 - 2\nu)r_1}{\rho^2} + \frac{2\nu(z^2 + \rho^2 - b^2)}{r_1 r_2^2} + \frac{z^2(z^2 + b^2 + \rho^2)}{\rho^2 r_1 r_2^2}\right] E \quad \ldots\ldots [32]$$

$$\frac{1-\nu}{b}\tau_{\rho z} = \left[\frac{1}{\rho r_1} + \frac{(\rho^2 - b^2)^2 + z^2(\rho^2 + b^2)}{\rho r_1^3 r_2^2}\right] zK + \left[\frac{16b^2\rho z^2}{r_1^3 r_2^4} - \frac{z^2 + 2b^2 + 2\rho^2}{\rho r_1 r_2^2}\right] zE \quad \ldots\ldots [33]$$

CHARACTERISTIC SOLUTION: SPECIAL VALUES FOR AXIS OF SYMMETRY $\rho = 0$

$$r_1 = \sqrt{z^2 + b^2} \quad \ldots\ldots [34]$$

$$2Gu_z = -\frac{\pi b}{(1-\nu)r_1^3}[(1 - 2\nu)(r_1^2 - z^2) + 2\nu b^2 z] \ldots [35]$$

$$\sigma_z = \frac{3\pi b^2 z^2}{(1-\nu)r_1^5} \quad \ldots\ldots [36]$$

$$\sigma_\phi = \sigma_\rho = \frac{\pi b^3}{2(1-\nu)r_1^5}[(2 + 2\nu)b^2 - (1 - 2\nu)z^2] \ldots [37]$$

$$u_\rho = \tau_{\rho z} = 0 \quad \ldots\ldots [38]$$

Characteristic Solution: Special Values for Plane Surface $z = 0$

The part of the plane interior of the circle $\rho = b$ will be called the inner disk; the remaining infinite part outside of that circle will be called the outer ring.

The inner disk serves as a bed for the heated layer. The displacement u_z of the bed is constant over ρ and equals

$$-\frac{(1-2\nu)\pi b}{2(1-\nu)G}$$

This value applies to the characteristic solution. For the actual case of thermal shock of strength Q, we have by Equation [12], for the inner disk

$$u_z(\rho, 0) = -\frac{(1-2\nu)(1+\nu)\alpha Q}{(1-\nu)\pi b^2 cd} \quad \ldots\ldots [39]$$

We now add to this $\overset{*}{u}_z$ of Equation [2] which is the additional displacement of the exposed surface of the layer due to the thickening of the layer caused by its heating. The sum

$$u_z(\rho, 0) + \overset{*}{u}_z = -\frac{2(1+\nu)\alpha Q}{\pi b^2 cd} \quad \ldots\ldots [40]$$

is then the true representative of the displacement u_z in the thermal-shock problem for $z = 0$, $0 \leqq \rho < b$.

The following refers to the characteristic solution alone, not including the layer thickening effect on u_z

$$\frac{1-\nu}{b} 2Gu_z = -(1-2\nu)\mu = \begin{cases} 0 \text{ for } \rho > b \\ -(1-2\nu)\pi \text{ for } \rho < b \end{cases} \quad \ldots [41]$$

The following two entries show the correction to $2Gu_z$, caused by the thickening of the heated layer as recomputed in proportion to the scale of the characteristic solution, and, again in the scale of the characteristic solution, the value of $2Gu_z$ corrected according to Equation [43].

Inner Disk (Scale of Characteristic Solution)

$$\text{Correction to } 2Gu_z = -\frac{\pi b}{1-\nu} \quad \ldots\ldots [42]$$

$$\text{Corrected value of } 2Gu_z = -2\pi b \quad \ldots\ldots [43]$$

As $u_z = 0$ on the outer ring ($\rho > b$), we see that u_z is sectionally constant on the plane $z = 0$, Fig. 13.

Discussion of Results

Figs. 5 to 13 show the stress components on the z-axis, on the plane $z = 0$, and on the cylindrical surface $\rho = b$. The dependence of the stresses on Poisson's ratio ν at a constant Young's modulus E is remarkably strong. The result for the displacement u_z on the plane $z = 0$ is peculiar inasmuch as u_z is sectionally constant. This result permits the use of $u_z(\rho, 0)$ as Green's function in the general thermoshock. We generalize in two steps.

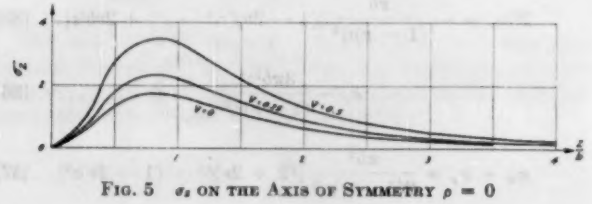

Fig. 5 σ_z on the Axis of Symmetry $\rho = 0$

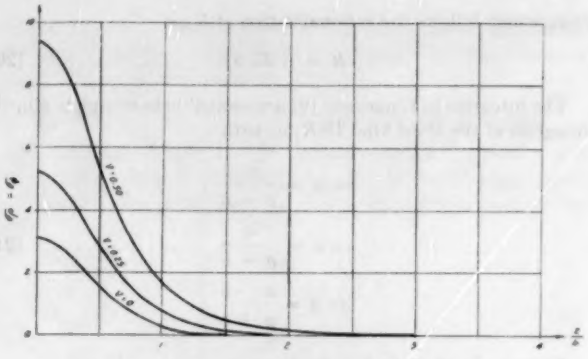

Fig. 6 σ_ρ on the Axis of Symmetry $\rho = 0$

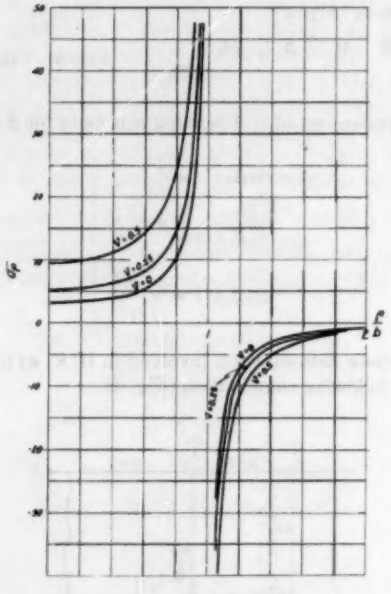

Fig. 7 σ_ρ on the Plane Surface $z = 0$

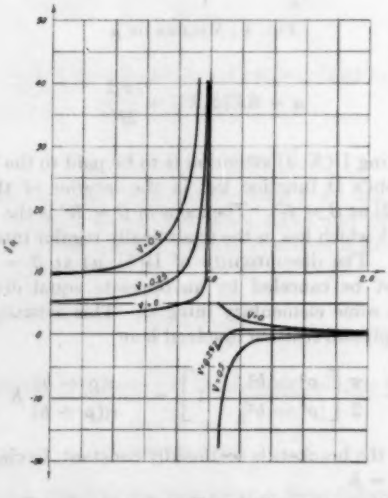

Fig. 8 σ_ϕ on the Plane Surface $z = 0$

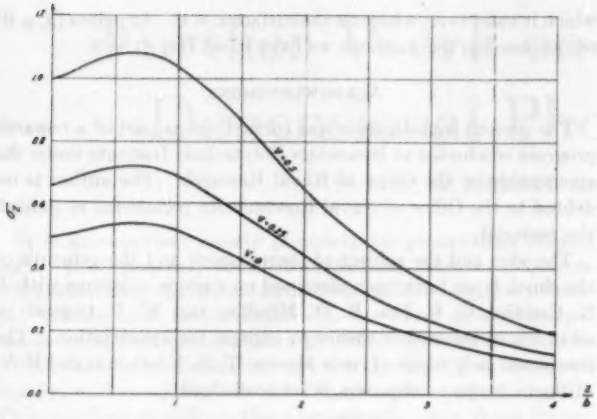

FIG. 9 σ_z ON THE CYLINDER $\rho = b$

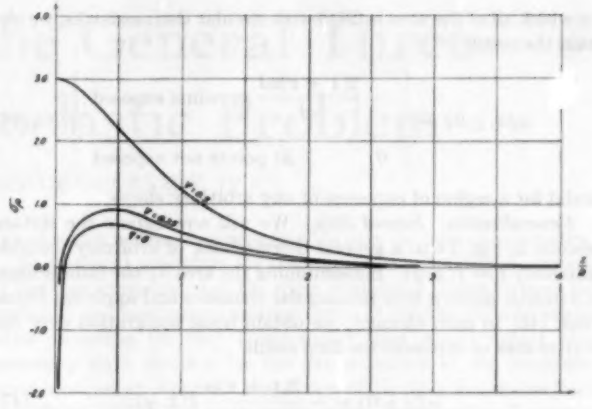

FIG. 10 σ_ρ ON THE CYLINDER $\rho = b$

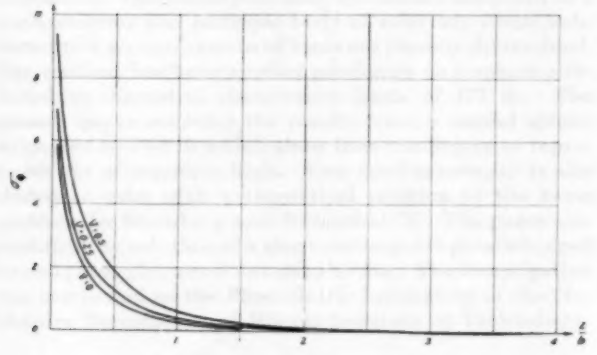

FIG. 11 σ_ϕ ON THE CYLINDER $\rho = b$

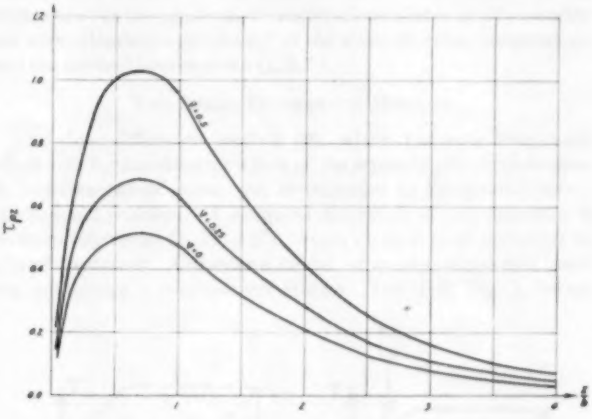

FIG. 12 $\tau_{\rho z}$ ON THE CYLINDER $\rho = b$

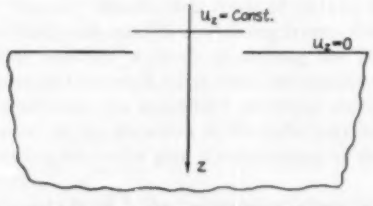

FIG. 13 DISPLACEMENT u_z ON THE PLANE $z = 0$

Generalization: First step. We define the intensity I of a thermoshock as the heat absorbed per unit area of exposure. For a uniform thermoshock

$$I = \frac{Q}{A} \quad \ldots\ldots\ldots\ldots\ldots\ldots\ldots\ldots [44]$$

for a general thermoshock of variable intensity $I(x, y)$

$$Q = \int\int I(x, y)dxdy \quad \ldots\ldots\ldots\ldots\ldots [45]$$

We stay with a thermoshock of uniform intensity I, but will admit an area of exposure of any arbitrary shape. Fig. 14 illustrates such an area. By filling the interior of the area with circular disks in contact the part of the area remaining unfilled can be reduced to an amount as small as we please. Fig. 14 shows the result at an early stage of the filling process. Considering each disk as a thermoshock of constant intensity I and forming the superposition of all thermoshocks represented, and then proceeding to the limit

FIG. 14

in which all of the area is filled with circular thermoshocks, we obtain the result

$$u_z(x, y, 0) = \left\{ \begin{array}{ll} -\dfrac{2(1+\nu)\alpha I}{cd} & \text{at points exposed} \\ 0 & \text{at points not exposed} \end{array} \right\} \quad \ldots [46]$$

valid for a region of exposure of any arbitrary shape.

Generalization: Second Step. We will now expose the surface shown in Fig. 14 to a general thermoshock of arbitrary variable intensity $I = I(x, y)$. Subsectioning the area by the infinitesimal Cartesian pattern into rectangular elements and applying Equation [46] to each element, we obtain upon integration over the entire area of exposure the final result

$$u_z(x, y, 0) = -\frac{2(1+\nu)\alpha}{cd} I(x, y) \ldots\ldots\ldots [47]$$

which is valid everywhere on the surface $z = 0$. At points $(x, y, 0)$ not exposed to thermoshock we have to set $I(x, y) = 0$.

Acknowledgment

The present investigation was carried out as part of a research program conducted at Rensselaer Polytechnic Institute under the sponsorship of the Office of Naval Research. The author is indebted to the Office of Naval Research for permission to publish the material.

The idea and the subject of thermoshock and the principle of the shock layer have been discussed on various occasions with J. N. Goodier, G. H. Lee, R. D. Mindlin, and W. R. Osgood, to all of whom the author wishes to express his appreciation. The competent help received from Messrs. T. N. Edelbaum and R. V. Milligan, project computers, is acknowledged.

Further Work on the General Three-Dimensional Photoelastic Problem

By MAX M. FROCHT[1] and ROSCOE GUERNSEY, JR.[2]

It is known that purely photoelastic procedures cannot solve the general three-dimensional stress problem. Photoelasticity furnishes data from which only the principal shears can be determined, but not the principal stresses. A new, general, and practical method of solution which has been described previously (1, 2)[3] is reviewed briefly, and possible variations in procedure are discussed. This method combines the photoelastic data from frozen stress patterns with a numerical integration of one of the differential equations of equilibrium in Cartesian coordinates. The actual principal stresses at each point of a homogeneous and isotropic body of arbitrary shape subjected to a general system of loads are thereby determined. The method has been applied previously to a sphere subjected to diametral compressive loads of 172 lb. The present paper contains the results from a second sphere subjected to 79.6 lb which show that the degree of reproducibility of results is high. Very good agreement is also shown to exist with a theoretical solution of the same problem by Sternberg and Rosenthal (3) The paper also contains the solution of a short rectangular parallelepiped loaded through a small flat circular die. The investigation was conducted in the Photoelastic Laboratory of the Mechanics Department of Illinois Institute of Technology.

Introduction

It is now well established that elastic stress systems can be fixed or "frozen" into models made of certain diphase plastics, and that such models containing frozen stresses can be sliced into thin sections without disturbing the fixed stresses. The stress patterns from such slices yield information from which the difference between the secondary principal stresses lying in the plane normal to the direction of the light may be computed. The corresponding isoclinics give the directions of the secondary principal stresses.

Photoelastic data furnish five independent stress relations from which only the principal shears can be determined. In order to obtain the principal stresses a sixth relation is needed.

Jessop (4) has developed an extension of the Lamé-Maxwell equations to three dimensions for the determination of the principal stresses along stress trajectories in planes of symmetry. In practice this method becomes feasible only for lines of symmetry.

As a general procedure for the separation of principal stresses it has been proposed that the slices containing frozen stresses be annealed and mechanical measurements of deformations be made after annealing (5, 6). Theoretically, this would supply the necessary sixth relation for the determination of the complete state of stress at a point. Inspection of Hooke's law shows that the strains vanish for an isotropic stress system when Poisson's ratio $\nu = 0.5$. This means that two stress systems differing by an isotropic system cannot be distinguished from one another by this method when $\nu = 0.5$, approximately. Unfortunately, the values of ν for the photoelastic materials available in this country are approximately equal to 0.5 at the stress-freezing temperature and the method breaks down (1, 2, 7).

The Shear-Difference Method

The shear-difference method (8), which has long been used effectively for the determination of the separate principal stresses in two-dimensional cases, can be extended to the general three-dimensional problem. A complete discussion of this extension is given in references (1, 2) or (7). Here we shall limit ourselves to a brief treatment. Consider a model, of general shape and loading, containing a frozen-stress system. Let *A-B*, Fig. 1, be an

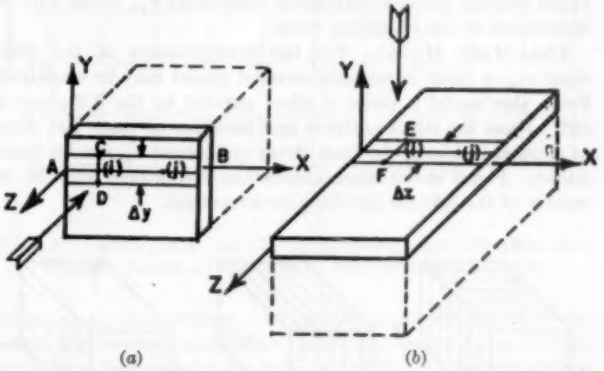

Fig. 1 Sketches Showing Auxiliary Lines in the XY and YZ-Planes for the Shear-Difference Method

arbitrary straight line through any point i, in the interior and let this line be taken as the X-axis. At all points along this line the first partial differential equation of equilibrium, with body forces neglected, is

$$\frac{\partial \sigma_x}{\partial x} + \frac{\partial \tau_{yx}}{\partial y} + \frac{\partial \tau_{zx}}{\partial z} = 0 \quad \ldots\ldots\ldots\ldots [1]$$

from which we obtain the approximate relation

$$(\sigma_x)_j = (\sigma_x)_a - \sum_a^j \frac{\Delta \tau_{yx}}{\Delta y} \Delta x - \sum_a^j \frac{\Delta \tau_{zx}}{\Delta z} \Delta x \ldots\ldots [2]$$

The normal stress $(\sigma_x)_a$ is generally determined from the boundary conditions at the starting point A and the fringe order at that point. This is evidently possible at all free surfaces or

---

[1] Research Professor of Mechanics and Director of Experimental Stress Analysis, Illinois Institute of Technology, Chicago, Ill. Mem. ASME.

[2] Photoelasticity Engineer, General Engineering Laboratory, General Electric Company, Schenectady, N. Y.

[3] Numbers in parentheses refer to the Bibliography at the end of the paper.

Contributed by the Applied Mechanics Division and presented at the Annual Meeting, New York, N. Y., November 28–December 3, 1954, of The American Society of Mechanical Engineers.

Discussion of this paper should be addressed to the Secretary, ASME, 29 West 39th Street, New York, N. Y., and will be accepted until July 11, 1955, for publication at a later date. Discussion received after the closing date will be returned.

Note: Statements and opinions advanced in papers are to be understood as individual expressions of their authors and not those of the Society. Manuscript received by ASME Applied Mechanics Division, November 14, 1952. Paper No. 54—A-11.

surfaces subjected to known tractions. One way to determine the shear difference $\Delta\tau_{yz}$ and $\Delta\tau_{xz}$ is to employ two identically stressed models. From one model, Fig. 1(*a*), a slice is taken parallel to the XY-plane and shears τ_{yz} are determined along the lines through C and D. This is done by means of normal incidence parallel to the Z-axis and the same equations as used in plane problems. The shear difference $(\Delta\tau_{yz})_i$ is then given by

$$(\Delta\tau_{yz})_i = (\tau_{yz})_C - (\tau_{yz})_D$$

We next take a slice from the second model and make the section parallel to the XZ-plane, Fig. 1(*b*). The shears τ_{xz} are then found along the lines through E and F and

$$(\Delta\tau_{xz})_i = (\tau_{xz})_F - (\tau_{xz})_E$$

The summations in Equation [2] can then be evaluated and $(\sigma_x)_j$ determined. We thus have a general procedure for the evaluation of the normal stress σ_x.

The stress components σ_y and σ_z now can be determined from the relationships

$$(\sigma_y)_j = (\sigma_x)_j - (p' - q')_j \cos 2\phi'_j \quad [3a]$$

and

$$(\sigma_z)_j = (\sigma_x)_j - (p'' - q'')_j \cos 2\phi''_j \quad [3b]$$

in which $(p' - q')$ and ϕ' are, respectively, the difference between the secondary principal stresses and their isoclinic parameters in the XY-plane and $(p'' - q'')$ and ϕ'' are similar quantities in the XZ-plane, at normal incidence.

The foregoing quantities can be determined from the same two slices which were used to find $\Delta\tau_{yz}$ and $\Delta\tau_{xz}$, Fig. 1.

In this way five of the six required stress components, i.e., σ_x, σ_y, σ_z, τ_{yz}, and τ_{xz}, can be found at all points of the line A-B. There remains one unknown stress component τ_{yz}, which may be determined in one of several ways.

Three-Model Method. For the determination of the third shear τ_{yz}, a third identically stressed model may be employed. From this model a series of slices parallel to the YZ-plane is cut. From the stress patterns and isoclinics of these last slices at normal incidence the final stress component τ_{yz} can be determined. Fig. 2 shows schematically the slicing plan and the direction of the light for the three-model method.

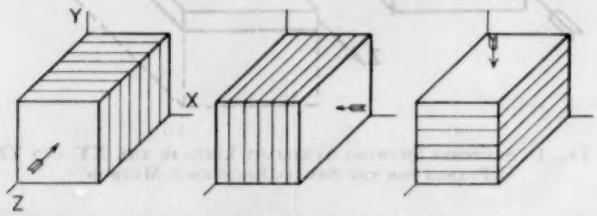

FIG. 2 SKETCHES SHOWING PLAN OF SLICING AND DIRECTIONS OF LIGHT IN THREE-MODEL METHOD

Two-Model Method. The use of a third model may be avoided if oblique incidence is employed. As just outlined, five of the six stress components can be determined from two orthogonal slices taken from two identically stressed models and viewed at normal incidence. Now, let the XY-slice, for example, be rotated about the Y-axis. It can be shown that

$$\tau_{yz} = \frac{\pm F_{\theta_y} n_{\theta_y} \sin 2\phi_{\theta_y} \mp \tau_{yz} \cos \theta_y}{\sin \theta_y} \quad [4]$$

where F_{θ_y} is the fringe value for the actual light path, ϕ_{θ_y} is the isoclinic parameter, and θ_y is the angle of rotation. The choice of signs depends on the direction of rotation (1, 2, 7).

One-Model Method. It is also possible to obtain all the necessary data from a single model. Thus let it be desired to obtain the stress distribution along line A-B, Fig. 3. A slice containing A-B and parallel to the XY-plane is first cut, Fig. 3(*a*). From observations at normal incidence the necessary data in that plane are obtained. From this slice a sub-slice is then cut so that it contains line A-B, Fig. 3(*b*). The necessary data in the XZ-plane

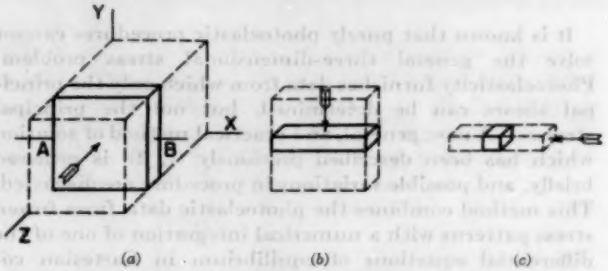

FIG. 3 SKETCHES SHOWING PLAN OF SLICING AND DIRECTIONS OF LIGHT IN ONE-MODEL METHOD

are then obtained from normal incidence on the sub-slice shown. Because the slice, in general, will be thin the auxiliary lines in the XZ-plane cannot be spaced very far apart. Hence, in order to obtain accuracy, it may be necessary to employ the photometric devices which are now being developed (9, 10).

With the data thus obtained five of the six stress components may be computed. The sixth component may be found in one of two ways. Oblique incidence observations may be made on the main slice or on the sub-slice and the shear τ_{yz} computed. Alternatively, the sub-slice may be sliced further into a series of small cubes, Fig. 3(*c*), and each cube observed at normal incidence with the light parallel to the X-axis.

When only one plane of symmetry exists the necessary orthogonal slices can be obtained from one model for all lines except those in the plane of symmetry itself.

Extension to Plastic State. It should be noted that the method described in this paper is not limited to a linear stress-optic law. It is equally valid for a nonlinear stress-optic law. This follows from the fact that the only equations, in addition to the stress-optic law, are the equations of equilibrium which are independent of stress-strain relations. Hence the method is applicable to the plastic state of the model as well as the elastic. However, it should be noted that the plastic stresses in the model are not directly transferable to the prototype (1, 2, 7).

Effect of Poisson's Ratio. It should be noted further that in transferring the results from three-dimensional photoelastic analyses to the prototype the effect of Poisson's ratio has to be considered. It is fortunate, as shown by theoretical solutions obtained to date, that the effect of Poisson's ratio on the numerically greatest stresses is small (11, 12).

APPLICATION TO A SPHERE

The method outlined has been applied previously to the determination of the stress distribution in a sphere subjected to diametral compressive loads of 172 lb (2) and (7). Fig. 4 shows the six lines along which the stresses were determined. The direct determination of all six stress components along line C-C provides a demonstration of the complete generality of the shear-difference method.

The results obtained by the shear-difference method have been checked in six independent ways (2, 7) which will not be repeated here in detail. Briefly, the results were found to satisfy equilibrium, to be independent of the path of integration, to agree with the values obtained from other procedures (oblique incidence,

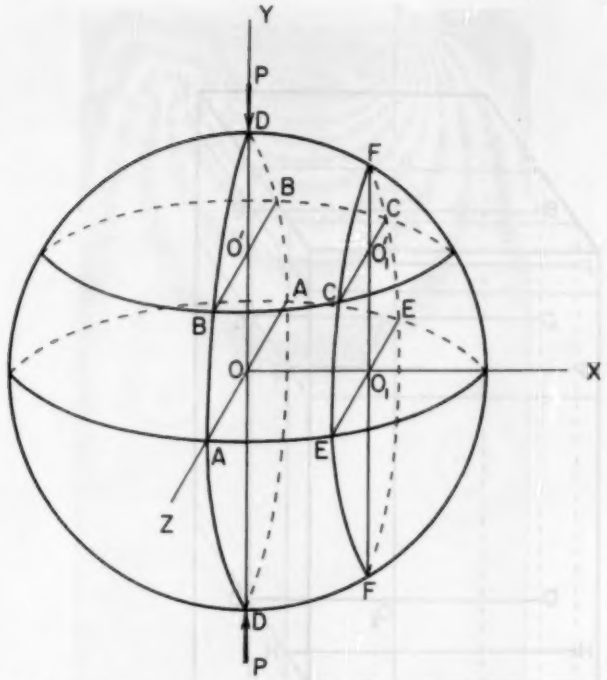

FIG. 4 SKETCH SHOWING LINES ALONG WHICH STRESSES WERE DETERMINED

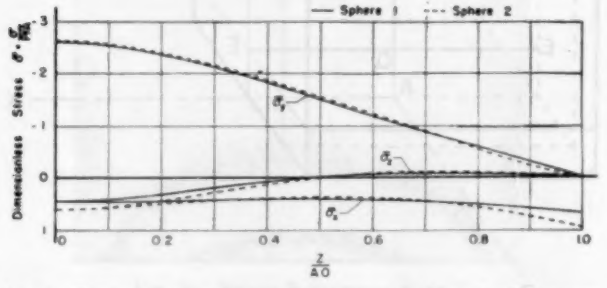

FIG. 5 COMPARISON OF STRESS DISTRIBUTIONS ALONG A DIAMETER IN THE EQUATORIAL PLANES OF TWO SPHERES UNDER DIFFERENT LOADS

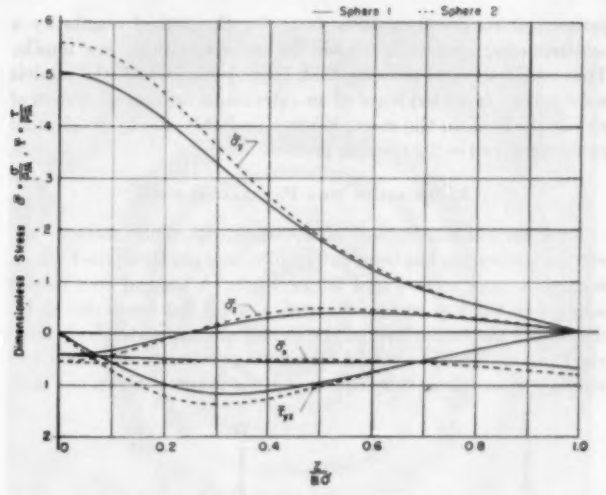

FIG. 6 COMPARISON OF STRESS DISTRIBUTIONS ALONG A DIAMETER IN THE PLANE MIDWAY BETWEEN THE EQUATOR AND THE POLE OF TWO SPHERES UNDER DIFFERENT LOADS

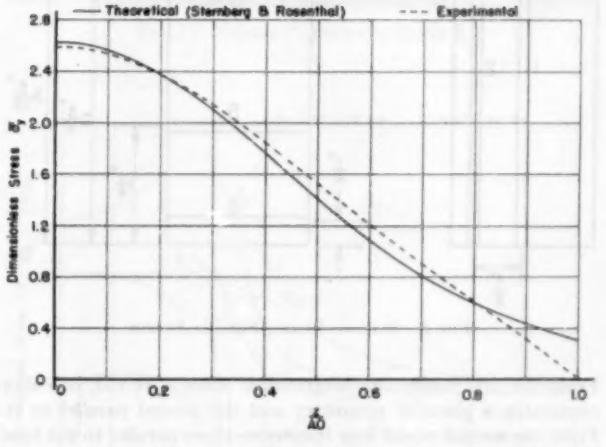

FIG. 7 COMPARISON OF MATHEMATICAL AND PHOTOELASTIC RESULTS ALONG A DIAMETER IN THE EQUATORIAL PLANE

Lamé-Maxwell equations, and stress transformations), and to agree with the theoretical values for contact stresses given by the Hertz theory. In this paper further work is presented bearing on the reliability and accuracy of the shear-difference method.

Reproducibility of Results. The relatively heavy load of 172 lb used on the first sphere produced considerable deformation, mainly in the immediate vicinity of the loads. Therefore the problem was repeated with a load of 79.6 lb. The stress distributions obtained on the equatorial planes are substantially the same for the two spheres, Fig. 5, and they indicate the extent to which the results can be reproduced.

The differences in the stress distributions on line *B-B*, Fig. 6, can be explained by the failure of Saint Venant's principle to be effective on that line which is too close to the load.

Comparison With Results From Theory of Elasticity. The problem of the elastic sphere subjected to diametral loads applied at the end points of a diameter recently has been solved mathematically by Sternberg and Rosenthal (3). Their results for line *A-A*, Fig. 4, for $\nu = 0.48$ are shown by the solid line in Fig. 7. The dotted line indicates the results obtained photoelastically by the shear-difference method. The two solutions agree very well except at the free surface. In particular, at the center of the sphere the theoretical solution yields the value $\delta_y = -2.62$, while the experimental value is $\delta_y = -2.59$. At the free surface the theoretical values are $\delta_x = 0.49$ and $\delta_y = -0.3$, whereas the photoelastically determined values are $\delta_x = 0.8$ (the average for the two spheres, Fig. 5) and $\delta_y = 0$. The difference between the theoretical and photoelastic results on the surface is thus seen to be a plane isotropic tension of the magnitude of $\sigma_x = \sigma_y = 0.3$, approximately.

Measurements with strain gages (13) showed surface stresses of the magnitude predicted by Sternberg and Rosenthal. The small discrepancies between the photoelastic and the theoretical results can be explained by assuming that the thermal cycle used in the freezing process by itself produces a system of self-balancing stresses with tensions on the free surface. Such a state of stress would give rise to isotropic surface tensions which, when added to the theoretical values, would tend to give the values obtained photoelastically.

Inspection of Fig. 7 provides evidence for this hypothesis. Since both curves give stresses which satisfy the laws of equilibrium their differences also satisfy the laws of statics. The ex-

perimental results thus differ from the theoretical results by a self-balancing system in which the surface stresses are tensile. This would seem to indicate that Fosterite, of which the models were made, shows evidence of an extraneous or residual system of stresses, which, in the main, is most probably due to the thermal cycle employed in the freezing process.

Application to a Parallelepiped

As a second illustration of the shear-difference method the stress distribution has been determined in a parallelepiped 1.5 in. square in cross section and 3.5 in. high. A load of 95.3 lb was applied to the top surface through a small flat brass die $\frac{1}{2}$ in. diam, and the entire base of the model was supported by a large rigid plate. The two-model technique previously described was employed, and slices were removed in the manner shown in Fig. 8.

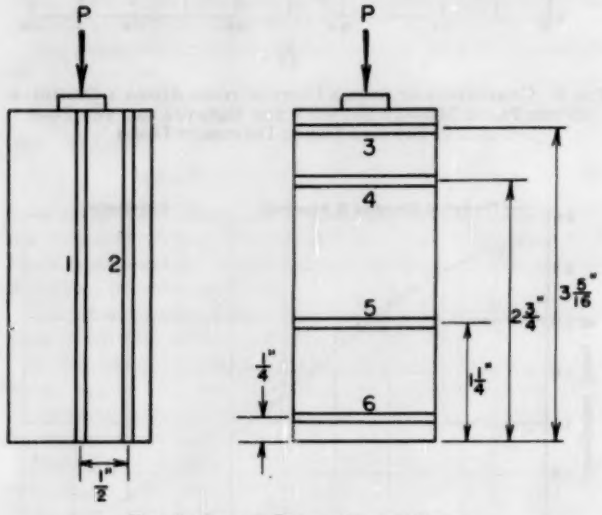

Fig. 8 Slicing Plan—Square Strut

From the first model two longitudinal slices were cut, one slice containing a plane of symmetry and the second parallel to it. From the second model four transverse slices parallel to the base were cut at various positions along the vertical axis as shown.

Scope of Investigation The complete stress distribution was obtained along the nine lines *A-A*, *B-B*, and so on, shown in Fig. 9. The lines *F-F*, *G-G*, and *H-H* are completely general lines; i.e., all six stress components must be determined without the simplifications furnished by symmetry. Fig. 10 shows the stress pattern of slice 1 and Fig. 11 that of slice 3. The results obtained for a few of these lines are given in Figs. 12 through 15.

It should be noted that slice 5 was found to be in pure vertical compression. Therefore the stresses at point O_2 could be used as a starting point for the determination of the stresses along the line *A-A*. On all other lines the starting points were on the free surface and the initial values were zero.

Checks of Stresses. The results obtained from the experimental work were subjected to the following checks: (*a*) static checks, (*b*) cross-checks, i.e., comparison of results at a point obtained from different paths of integration, (*c*) independent calculation of principal stress differences by oblique incidence, (*d*) comparison of the contact stresses with the theoretical values from Sadowsky (14).

Static Checks. Approximate static checks can be obtained on the planes of the transverse slices 3, 4, and 5. With the stresses σ_y determined along lines lying in these planes, and taking advantage of the symmetry present, a reasonably accurate pic-

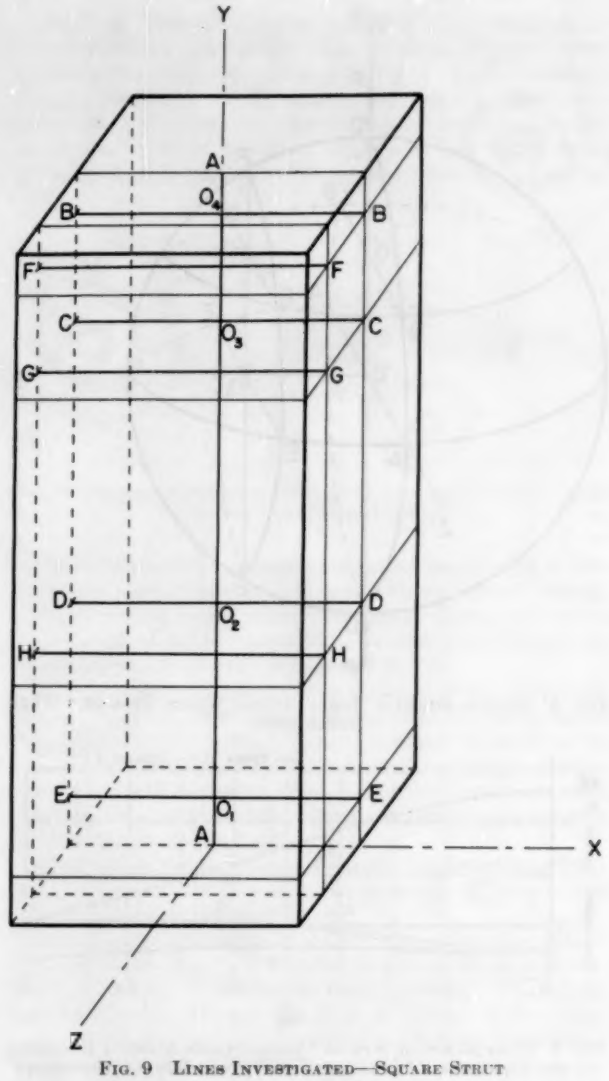

Fig. 9 Lines Investigated—Square Strut

ture of the distribution of stress over each plane can be constructed. From the volume under the surface thus defined the total load on the plane is determined. The load acting on slice 3 was found to be 93 lb, on slice 4, 90 lb, and on slice 5, 100 lb. These are, respectively, 2.2 per cent low, 5.5 per cent low, and 5.5 per cent high compared with the actual load of 95.3 lb.

Cross-Checks. Cross-checks serve to indicate whether the results obtained at a point from different paths of integration agree. Hence they are a measure of the self-consistency of the results. The checks are indicated on the curves showing the results and are summarized in Table 1.

TABLE 1 COMPARATIVE VALUES OF STRESSES FROM DIFFERENT PATHS

Point	Path	$\bar{\sigma}_x$	$\bar{\sigma}_y$	$\bar{\sigma}_z$
O_1	DO_2O_1	—0.32	—1.00	—0.32
	EO_1	—0.30	—0.98	—0.30
O_2	DO_2O_3	0.72	—2.08	0.72
	CO_3	0.66	—2.14	0.66
O_4	DO_2O_4	—4.72	—6.80	—4.72
	BO_4	—4.22	—6.30	—4.22

Oblique Incidence. The method of oblique incidence can be used to determine the differences between the three principal

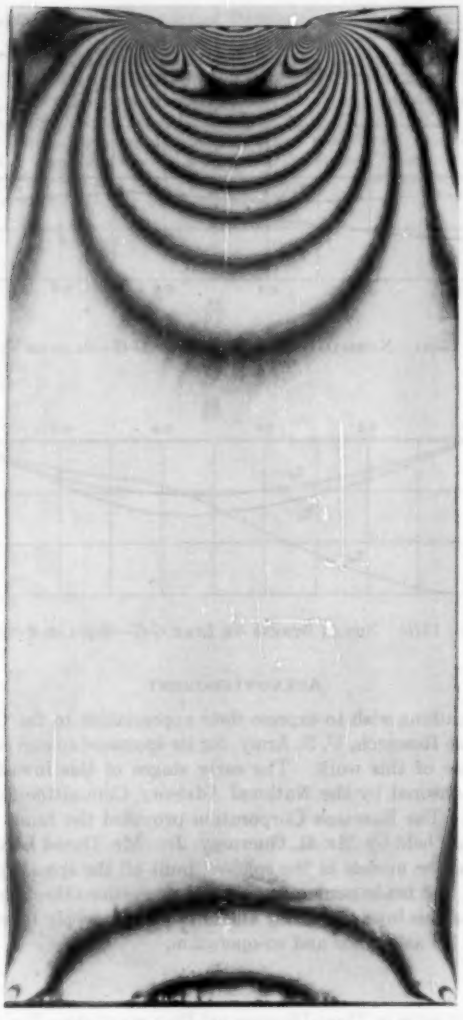

FIG. 10 STRESS PATTERN OF SLICE 1

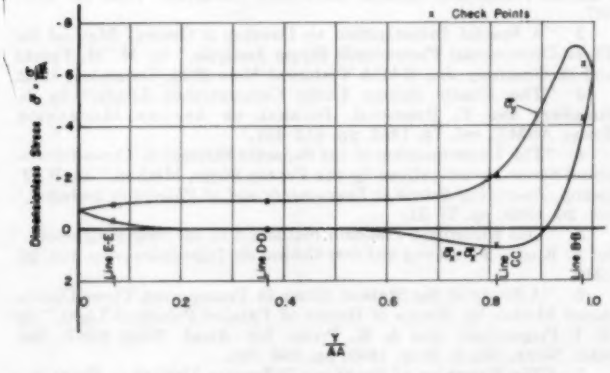

FIG. 12 NORMAL STRESSES ON LINE *A-A*—SQUARE STRUT

stresses for points in the plane of symmetry. This method has been applied to the lines *A-A*, *B-B*, and *C-C*, and with the exception of some parts of line *B-B* the results are in close agreement with values obtained from the shear-difference method. Table 2 gives a few of the comparative values.

The differences along the middle region of line *B-B* are due in

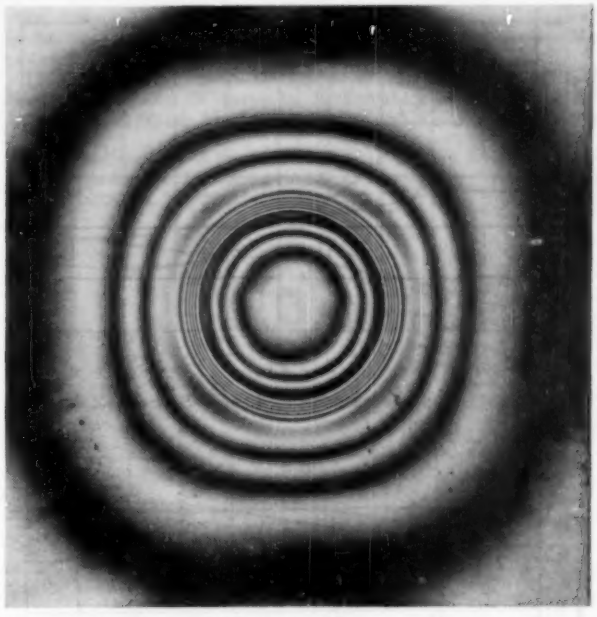

FIG. 11 STRESS PATTERN OF SLICE 3

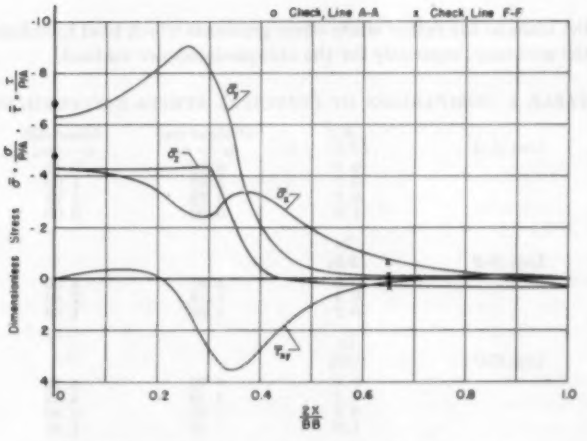

FIG. 13(*a*) STRESSES ON LINE *B-B*—SQUARE STRUT

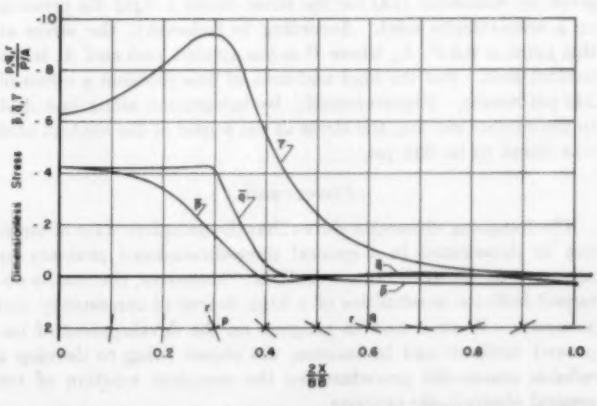

FIG. 13(*b*) PRINCIPAL STRESSES ON LINE *B-B*—SQUARE STRUT

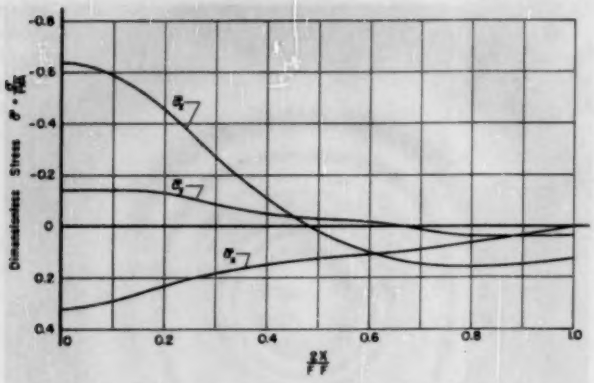

FIG. 14(a) NORMAL STRESSES ON LINE *F-F*—SQUARE STRUT

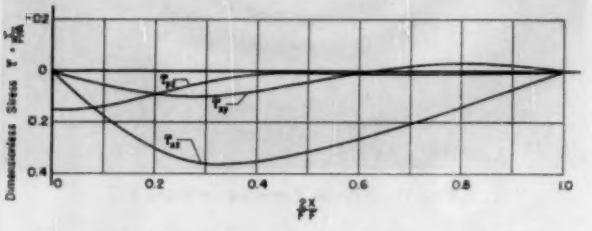

FIG. 14(b) SHEAR STRESS ON LINE *F-F*—SQUARE STRUT

the main to the rather sharp stress gradients which tend to reduce the accuracy, especially for the oblique-incidence method.

TABLE 2 COMPARISON OF PRINCIPAL STRESS DIFFERENCES

	$\frac{y}{(AA)}$	Oblique inc $n_z - n_y$	Shear diff $n_z - n_y$
Line *A-A*	0.0	0.00	0.00
	0.3	1.92	1.90
	0.7	2.78	2.75
	1.0	0.00	0.00
	$\frac{2x}{(BB)}$		
Line *B-B*	0.0	3.57	3.50
	0.3	7.18	7.82
	0.7	1.63	1.36
	$\frac{2x}{(CC)}$		
Line *C-C*	0.0	4.79	4.76
	0.3	4.18	4.33
	0.7	2.84	2.80
	1.0	1.97	1.85

Contact Stresses. The stress on the contact surface directly under the center of the die may be compared with the value given by Sadowsky (14) for the stress under a rigid die pressing on a semi-infinite solid. According to Sadowsky, the stress at this point is $0.5\ P/A_c$, where P is the applied load and A_c is the contact area. For the load and area of this problem a stress of 243 psi results. Experimentally, by integration along line *A-A* to the contact surface, the stress at the center of the contact area was found to be 241 psi.

CONCLUSION

The foregoing discussion shows that the complete state of stress can be determined in a general three-dimensional problem by means of the shear-difference method. Moreover, the results obtained indicate possibilities of a high degree of consistency and accuracy. Work is now in progress on the development of improved methods and techniques, the object being to develop a reliable one-model procedure for the complete solution of the general photoelastic problem.

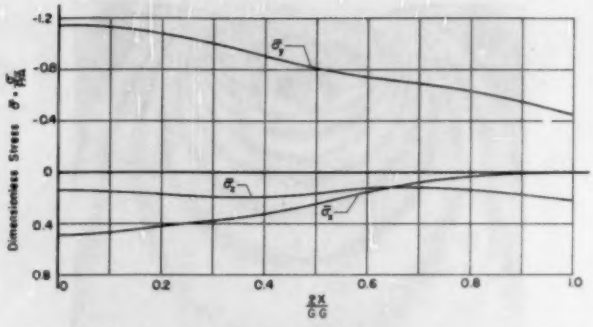

FIG. 15(a) NORMAL STRESSES ON LINE *G-G*—SQUARE STRUT

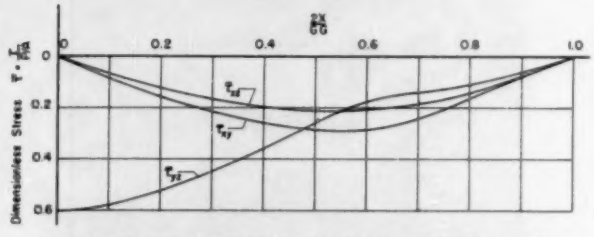

FIG. 15(b) SHEAR STRESS ON LINE *G-G*—SQUARE STRUT

ACKNOWLEDGMENT

The authors wish to express their appreciation to the Office of Ordnance Research, U. S. Army, for its sponsorship and financial assistance of this work. The early stages of this investigation were sponsored by the National Advisory Committee for Aeronautics. The Research Corporation provided the funds for the fellowship held by Mr. R. Guernsey, Jr. Mr. David Landsberg[4] prepared the models of the spheres, built all the special jigs and fixtures, and made numerous valuable suggestions throughout the course of this investigation. The authors feel deeply indebted to him for his assistance and co-operation.

BIBLIOGRAPHY

1 "Studies in Three-Dimensional Photoelasticity—The Application of the Shear Difference Method to the General Space Problem," by M. M. Frocht and R. Guernsey, Jr., Proceedings of the First U. S. National Congress of Applied Mechanics, December, 1952, pp. 301–307.

2 "A Special Investigation to Develop a General Method for Three-Dimensional Photoelastic Stress Analysis," by M. M. Frocht and R. Guernsey, Jr., NACA Technical Note 2822, December, 1952.

3 "The Elastic Sphere Under Concentrated Loads," by E. Sternberg and F. Rosenthal, JOURNAL OF APPLIED MECHANICS, Trans. ASME, vol. 74, 1952, pp. 413–421.

4 "The Determination of the Separate Stresses in Three-Dimensional Stress Investigations by the Frozen Stress Method," by H. T. Jessop, *Journal of Scientific Instruments and of Physics in Industry*," vol. 26, 1949, pp. 27–31.

5 "Das Kunstharz Phenolformaldehyd in der Spannungsoptik," by A. Kuske, *Forschung auf dem Gebiete des Ingenieurwesens*, vol. 20, 1940.

6 "A Study of the State of Stress in Transparent Three-Dimensional Models by Means of Beams of Parallel Polarized Light," by N. I. Prigorovsky and A. K. Preiss, Isv. Akad. Nauk SSSR. Ser tekh. Nauk, No. 5, May, 1949, pp. 686–700.

7 "The Extension of the Shear Difference Method in Photoelasticity to General Space Problems," by R. Guernsey, Jr., doctoral thesis, Illinois Institute of Technology, Chicago, Ill., June, 1952.

8 "Photoelasticity," by M. M. Frocht, vol. 1, John Wiley & Sons, Inc., New York, N. Y., 1941, chapter 8.

9 "Improvements in Photoelastic Technique Obtained by the Use of a Photometric Method," by A. F. C. Brown and V. M. Hick-

[4] Assistant Research Engineer, Photoelasticity Laboratory, Illinois Institute of Technology.

son, *British Journal of Applied Physics*, vol. 1, February, 1950, pp. 39–44.

10 "The Use of Photometric Devices in the Solution of the General Three-Dimensional Photoelastic Problem," by M. M. Frocht, H. Pih, and D. Landsberg, presented at the joint session of the ASME and the SESA, New York, N. Y., Dec. 4, 1953.

11 "Three-Dimensional Solution for the Stress Concentration Around a Circular Hole in a Plate of Arbitrary Thickness," by E. Sternberg and M. A. Sadowsky, JOURNAL OF APPLIED MECHANICS, Trans. ASME, vol. 71, 1949, pp. 27–38.

12 "Stress Concentration Around a Triaxial Ellipsoidal Cavity," by M. A. Sadowsky and E. Sternberg, JOURNAL OF APPLIED MECHANICS, Trans. ASME, vol. 71, 1949, pp. 149–157.

13 "The Elastic Sphere Under Concentrated Loads," by M. M. Frocht: Discussion of paper by E. Sternberg and F. Rosenthal, JOURNAL OF APPLIED MECHANICS, Trans. ASME, vol. 75, 1953, p. 304.

14 "Distribution of Pressure Concentrated on a Small Surface," by M. A. Sadowsky, JOURNAL OF APPLIED MECHANICS, Trans. ASME, vol. 54, 1932, pp. 221–224.

Determination of Thermal Stresses in Three-Ply Laminates

By A. J. DURELLI[1] and C. H. TSAO[2]

The knowledge of the distribution of stresses produced in three-ply laminates when the temperature changes is very important in the design of airplane windshields. This paper gives the result of a photoelastic investigation on the thermal stresses produced in a three-ply laminate consisting of glass, polyvinyl butyral, glass, when the temperature drops slowly from 70 to —20 F. The maximum stress has been found to be about six and one-half times the average longitudinal stress at the mid-section of the glass. Failure characteristics of the laminates check well with these findings. No new methods have been developed in the paper; however, the presently available techniques had to be applied carefully to determine maximum tensile stresses of about 1300 psi on the interface, at a distance of about 0.007 in. from the edge, at low temperature.

Introduction

THREE-ply laminates are often used for windshields in aircraft. The middle layer is made of a material which differs from that of the top and the bottom. When these laminates experience changes in temperature, the middle layer tends to expand or shrink to an amount different from the exterior layers. Stresses therefore are set up which are often large enough to break the bonds between the layers or to produce cracks in the layers themselves. These cracks often occur on the interfaces near the edges of the laminate.

Some contributions can be found in the literature on somewhat similar problems. The determination of the stresses in cemented lap joints was studied by Goland and Reissner.[3] These authors reviewed previous publications on the stresses in welded joints and developed solutions for the two extreme cases of relatively inflexible and relatively very flexible cement layers. In their theoretical analysis these authors assumed that the stresses in the cement layer are constant in the direction of the thickness of the layer.

The distribution of stresses at the end of an adhesive layer of semicircular shape was studied photoelastically by Mylonas.[4]

The shear distribution on the joints of three plies of wood, of the same thickness, was studied experimentally by C. B. Norris and L. A. Ringelstetter.[5] The load was applied, producing compression in the outer and inner plies and shear at the joints.

B. J. Aleck[6] studied the distribution of thermal stresses on the clamped face of a rectangular beam clamped along one side. In his work, Aleck uses the principle of least work. The two-dimensional solution obtained by this author, for Poisson's ratio 0.25, is only approximate. However, it seems to be a good approximation to the solution of the problem of the stresses produced in the outside plies of a laminate by the difference in the coefficients of thermal expansion of the outside and inside plies. The maximum stress found occurs at the corner junction of the free and clamped boundaries, is perpendicular to the clamped edge, and equal to 10.2 times the uniform stress in the beam, far away from the end. The maximum shear on the clamped edge is equal to 2.7 times the uniform stress and takes place at a distance from the corner of about 0.06 of the height of the plate.

To obtain an over-all picture of the stress distribution as well as to verify Aleck's results of the peak stress, two-dimensional photoelasticity was employed in this investigation. The Poisson's ratio of the plastic used varies with temperature from 0.3 to 0.45.

Experimental Technique

The three-ply laminate used in this investigation was made of two identical layers of annealed glass bonded together by a layer of polyvinyl-butyral plastic. Its dimensions are shown in Fig. 1.

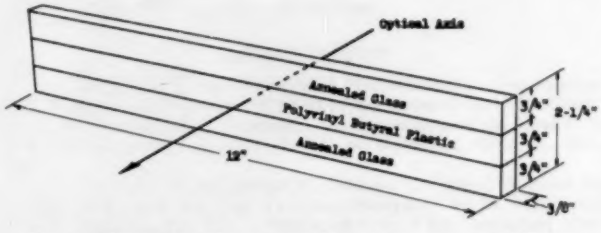

Fig. 1 Three-Ply Laminated Glass Photoelastic Model

The laminate was placed in a cold chamber provided with lucite windows of double panes through which polarized light could pass without appreciable interference. This was obtained by keeping the size of the windows small and by allowing them to shrink freely. The chamber was so arranged that cooled air controlled by a thermostat could be circulated through it to maintain a constant low temperature. Thermal stresses were induced by lowering slowly the temperature of the laminate from room temperature (70 to —20 F).

Standard two-dimensional photoelastic techniques were used to determine the isoclinics and isochromatics except that the image was projected on a ground-glass screen which enlarged it $7^1/_2$

---

[1] Supervisor, Stress Analysis Section, Armour Research Foundation, Chicago, Ill. Assoc. Mem. ASME.

[2] Assistant Professor, University of Southern California, Los Angeles, Calif.

[3] "The Stresses in Cemented Joints," by M. Goland and E. Reissner, Journal of Applied Mechanics, Trans. ASME, vol. 66, 1944, pp. A-17–A-27.

[4] "On the Stress Distribution in Glued Joints," by C. Mylonas, Paper 12, Proceedings of the Seventh International Congress of Applied Mechanics, London, England, vol. 4, September, 1949.

Contributed by the Applied Mechanics Division and presented at the Annual Meeting, New York, N. Y., November 28–December 3, 1954, of The American Society of Mechanical Engineers.

Discussion of this paper should be addressed to the Secretary, ASME, 29 West 39th Street, New York, N. Y., and will be accepted until July 11, 1955, for publication at a later date. Discussion received after the closing date will be returned.

Note: Statements and opinions advanced in papers are to be understood as individual expressions of their authors and not those of the Society. Manuscript received by ASME Applied Mechanics Division, January 7, 1954. Paper No. 54—A-27.

[5] "Shear Stress Distribution Along Glued Line Between Skin and Cap-Strip of an Aircraft Wing," by C. B. Norris and L. A. Ringelstetter, NACA TN 2152, July, 1950.

[6] "Thermal Stresses in a Rectangular Plate Clamped Along an Edge," by B. J. Aleck, Journal of Applied Mechanics, Trans. ASME, vol. 71, 1949, pp. 118–122.

times. This was necessary in order to separate the crowded isoclinics and isochromatics in the region of the peak stress. With the aid of grid lines drawn in ink on the specimen, both isoclinics and isochromatics were sketched directly on the ground glass. Tardy's method of compensation was used for the determination of isochromatics.

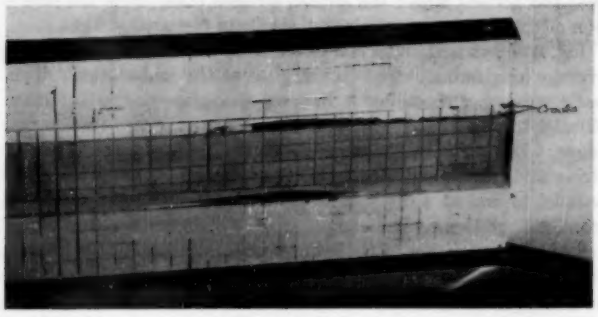

FIG. 2 GLASS-POLYVINYL BUTYRAL-GLASS LAMINATE AFTER FAILING AT —40 F
(Two cracks can be seen at interface, near edge.)

RESULTS

The residual stress at room temperature was found to be negligible. When the temperature of the first two specimens was lowered to —40 F, tiny cracks appeared in the glass near the two edges as shown in Fig. 2. The temperature of the third specimen was lowered only to —20 F. No cracks appeared and the isoclinics and isochromatics were determined for that temperature. These are shown in Fig. 3 and Fig. 4, respectively.

The stress trajectories obtained graphically from the isoclinics are shown in Fig. 5. By integration along these lines, the principal stresses were obtained. The isobars are shown in dimensionless form in Fig. 6 and the stress distribution along the glass-plastic interface is shown in Fig. 7. For the geometry used in the test, the peak stress takes place on the interface at a distance of about 0.007 in. from the edge and its value is about 1300 tensile psi.

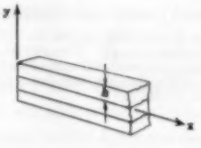

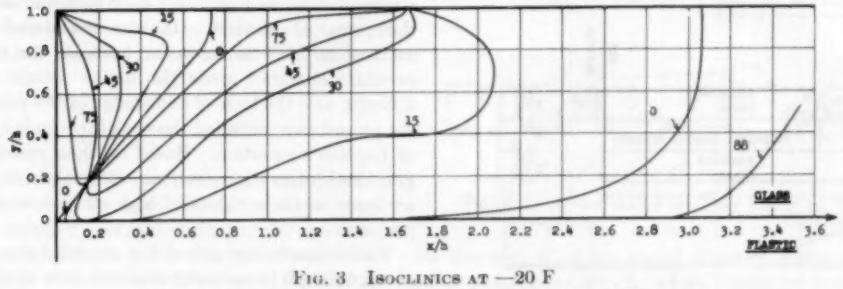

FIG. 3 ISOCLINICS AT —20 F
(Figures shown are in degrees measured in counterclockwise direction.)

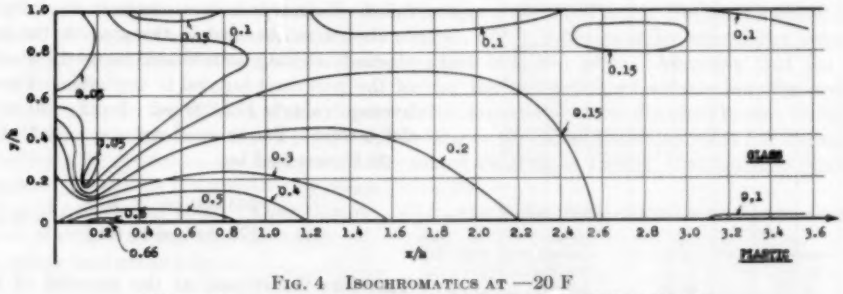

FIG. 4 ISOCHROMATICS AT —20 F
(Figures shown are in fringes. One fringe corresponds to 1560 psi shear.)

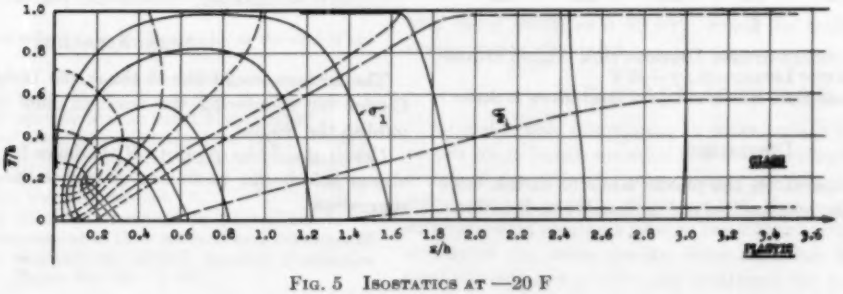

FIG. 5 ISOSTATICS AT —20 F

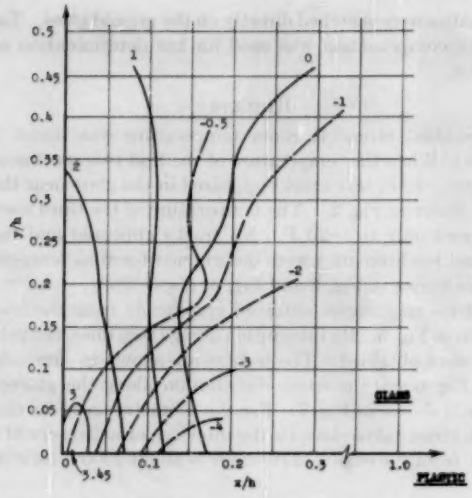

FIG. 6 ISOBARS, IN REGION OF STRESS CONCENTRATION, AT —20 F
(Solid lines are isobars of algebraically larger principal stress σ_1. Dotted lines are isobars of algebraically smaller principal stress σ_3. Figures denote ratios of these principal stresses to σ_m, the average longitudinal compressive stress in the glass at the mid-section. Positive ratios denote tension and negative ratios denote compression.)

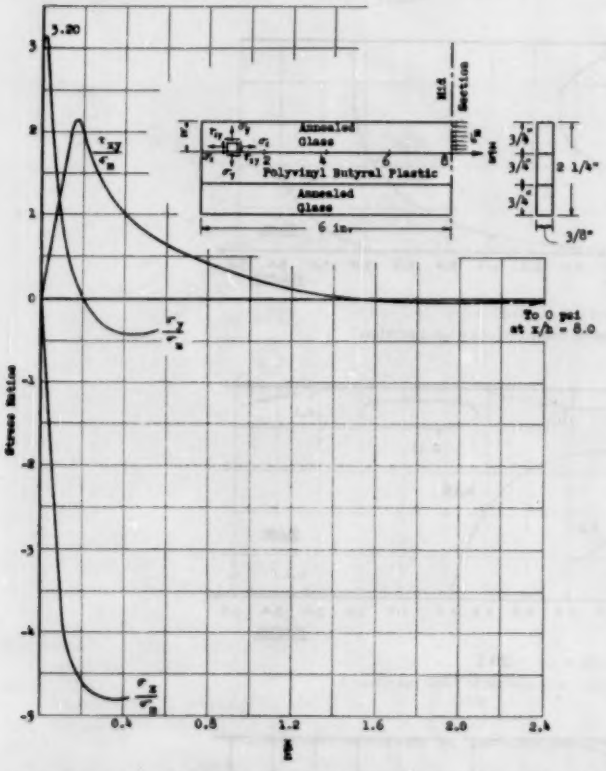

FIG. 7 NORMAL AND SHEAR-STRESS DISTRIBUTION ALONG GLASS-PLASTIC INTERFACE AT —20 F
(Positive stress ratios denote either tension or type of shear shown in sketch.)

DISCUSSION

With a drop in temperature, the plastic tends to shrink more than the glass in both the longitudinal and the transverse directions. The stress distribution is therefore three-dimensional in character; and the results obtained above by two-dimensional photoelasticity represent only a first approximation, since it becomes obvious that near the corners where the largest stresses take place, the direction of the principal stresses changes along the path of light.

Fig. 6 shows that there is a peak stress which is 3.45 times the average longitudinal stress in the glass at the mid-section. This peak stress occurs along a line on the glass-plastic interface parallel to and at a distance of 0.01 h from the two transversal edges, h being the height of either glass lamina. A similar peak stress also can be expected to occur along a line on the interface parallel to and at a distance of probably about 0.01 h from the front or back faces. The highest stress will occur therefore at the points of intersection of these lines of peak stress. This highest stress will be approximately $6^1/_2$ times the average longitudinal stress in the glass at the mid-section. Its inclination to the vertical will be approximately 8 deg. This becomes evident from an enlargement of the bottom-left corner of Fig. 3. The location and direction of the cracks resulting from the temperature drop, Fig. 2, check with the foregoing photoelastic findings.

The values of stress concentrations obtained photoelastically differ from Aleck's values in two respects: (1) The value of the peak stress takes place at the corner instead of being at a distance of 0.01 h from the corner. (2) The value of the peak stress found by Aleck is more than twice the value obtained photoelastically.

The graphical integration of equilibrium equation along isostatics is a tedious and not very accurate method of separating the principal stresses. It was considered the only practical method in this case, however, because the tests in the low-temperature chamber made the use of lateral extensometers very difficult, and the lack of knowledge of the principal stresses on all the boundaries excluded the use of methods based on the solution of Laplace's equation. Based on their previous experience with graphical-integration determinations the authors believe that the accuracy of their values of high stresses is probably about ±10 per cent.

The ultimate strength of the annealed glass used in the tests is about 5500 psi in an undimensional state of stress. At —20 F the photoelastically determined stresses are about $\sigma_1 = +2600$ psi, $\sigma_2 = -200$ psi, and $\sigma_3 = -200$ psi. At —40 F the laminate failed. To compare approximately the failure values of the glass to the stress obtained in the analysis the following modulus of elasticity of the plastic should be used: Above 40 F the modulus of the polyvinyl butyral is negligible. From 40 to —20 F the average value is 172,000 psi. From —20 to —40 F this value is 243,000 psi. The thermal stress at —40 F should be the stress at —20 F increased by

$$\frac{243{,}000 \text{ psi} \times 20 \text{ F}}{172{,}000 \text{ psi} \times 60 \text{ F}} \sigma = 0.473\sigma$$

Therefore the stresses at the moment of failure (—40 F) are approximately

$$\sigma_1 = 3840 \text{ psi}; \quad \sigma_2 = -295 \text{ psi}; \quad \sigma_3 = -295 \text{ psi}$$

ACKNOWLEDGMENT

The authors would like to thank the Wright Air Development Center for sponsoring the research and for allowing them to publish the results.

Credit should be given to R. L. Lake for adapting the photoelastic polariscope to this investigation, and for many valuable suggestions.

Stress-Concentration Factors in Shafts With Transverse Holes as Found by the Electroplating Method

By H. ŌKUBO[1] and S. SATŌ[2]

In this paper the torsion of shafts with transverse holes has been investigated experimentally. Usual methods for stress measurements, such as the method of brittle coatings and the use of sensitive extensometers, are not applied effectively to the present problem because the maximum stress occurs in the bore and does not occur on the outer surface of the shaft. The stress may be measured by the stress-freezing and slicing method but we cannot expect too much from this method for the accurate determination of the stress when the diameter of the hole is comparatively small. In treating the problem theoretically, considerable mathematical difficulties are encountered on account of its axially nonsymmetrical nature. The electroplating method recently developed by one of the authors (1),[3] however, has been proved to be useful in this case, so the maximum stresses in shafts are measured by this method and the stress-concentration factors are found for various diameters of the hole.

Introduction

As is shown in a previous paper, when a specimen plated with copper which contains some impurities is subjected to reversals of a suitable load, the surface of the specimen changes in color owing to the flecks produced by fatigue. The variation in the appearance of flecks, which is due to the change of load, is very sensitive at a proper load, so an accurate determination of the surface stress is feasible by observing the flecks produced. The value of the cyclic load below which these flecks do not appear is characteristic of the plating metal and the impurities contained in the plating solution, if the specimens are plated under the same conditions.

To have the same surface conditions, the surfaces of specimens and bores are polished carefully with fine-mesh emery paper before plating, and the conditions for deposition are kept constant throughout the investigation. Specimens are prepared by treatments in dilute sulphuric acid and caustic alkali. They then receive a preliminary deposit of copper from a cyanide-copper vat.

The conditions for deposition used are as follows:

Solution:	$CuSO_4 \cdot 5H_2O$	250 grams
	H_2SO_4	80 grams
	$ZnSO_4 \cdot 7H_2O$	0.1 gram
	H_2O	1 liter
Current density:	3 amp per sq decimeter	
Temperature:	18 C	

The thickness of plating is always taken to be 0.01 mm, but it has been ascertained that the thickness of plating does not perceptibly affect the results.

Preliminary Test

A preliminary test was made to determine the proper value of cyclic stress within which flecks are not produced by fatigue. Test pieces used are of 0.89 per cent carbon steel, with dimensions as shown in Fig. 1. The use of slightly tapered rods is favorable

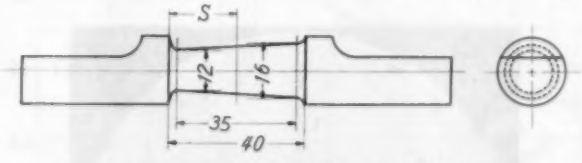

Fig. 1 Dimensions of Test Piece in Millimeters

for this test, since the status of flecks corresponding to a certain range of stress is found by a test. As stated in a previous paper (1) the limiting value of stress, within which flecks are not produced by fatigue, is termed "proper stress" and is denoted by τ_p. The distance S from one end to the point corresponding to the proper stress, Fig. 1, is measured by micrometer, observing carefully the surface of a test piece. Assuming that the stress distribution along the radius follows a linear law, the proper stress is calculated immediately from the usual torsion formula since the torque acting on the rod and its diameter at S is known. The results obtained are given in Table 1, the number of repetitions of the cyclic

TABLE 1 DETERMINATION OF VALUE OF PROPER STRESS

No. of test piece	Torque, kg-m	S, mm	τ_p, kg/mm²	Mean value of τ_p, kg/mm²
1	±3.48	12.0	±7.90	
2	±3.44	11.8	±7.85	±7.88
3	±4.26	19.4	±7.86	
4	±3.48	11.9	±7.92	

load being taken as 5×10^5. From the table we take for the proper stress, the value

$$\tau_p = \pm 7.88 \text{ kg per sq mm}$$

A considerable discrepancy in magnitude is found between the proper stress herein recorded and that previously obtained. The presumed causes for this discrepancy are that conditions for deposition are not exactly the same and that copper-sulphate and sulphuric-acid solutions used in two different experiments are not strictly of the same quality, since materials in the market are used without any preliminary treatment for purification. How-

[1] Professor of Applied Mechanics, Nagoya University, Nagoya, Japan.

[2] Formerly Momma, Research Assistant, Tōhuku University, Sendai, Japan.

[3] Numbers in parentheses refer to the Bibliography at the end of the paper.

Contributed by the Applied Mechanics Division and presented at the Annual Meeting, New York, N. Y., November 28–December 3, 1954, of The American Society of Mechanical Engineers.

Discussion of this paper should be addressed to the Secretary, ASME, 29 West 39th Street, New York, N. Y., and will be accepted until July 11, 1955, for publication at a later date. Discussion received after the closing date will be returned.

Note: Statements and opinions advanced in papers are to be understood as individual expressions of their authors and not those of the Society. Manuscript received by ASME Applied Mechanics Division, March 8, 1954. Paper No. 54—A-88.

ever, the quality of the plating solution is kept constant throughout one experiment since the solution used in that experiment is prepared especially for it. The principal cause of the discrepancy probably is the fact that solutions are not the same for different experiments since it has been ascertained fully that the former has little effect on results.

Fig. 2 (lower) is a test piece partially changed in color owing to the flecks produced by fatigue, and Fig. 3 is a microphotograph of flecks. Their status around the vertical line shows the typical one for the proper stress. Fig. 4 shows a test piece of normal type, generally used in fatigue tests, so that the radius of fillet is taken large enough for usual tests. However, by the electroplating method, the slight stress concentration at the fillet is apparent as is shown in the figure.

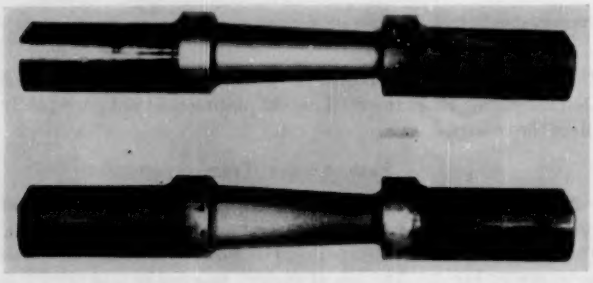

FIG. 2 TEST PIECE PARTIALLY CHANGED IN COLOR—LOWER

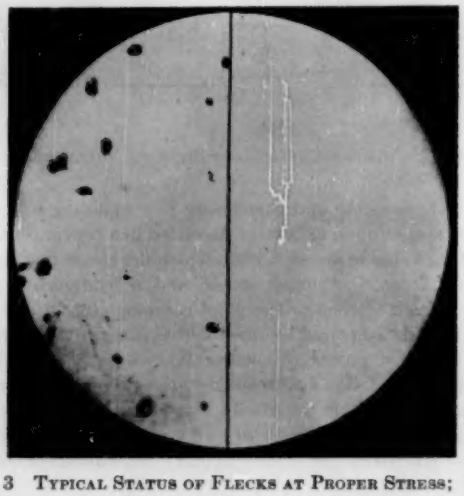

FIG. 3 TYPICAL STATUS OF FLECKS AT PROPER STRESS; ×35

FIG. 4 TEST PIECE USED IN USUAL FATIGUE TESTS

In a shaft with a transverse hole, the locations where the stress concentrates are not presumed precisely from usual knowledge of elasticity. To locate these locations, a test was made for a specimen shown in Fig. 5. This illustration shows color changes in certain places caused by cyclic stress. It shows that on the outer surface of the specimen, the stress concentrates at four points, marked by m in Fig. 6, in the neighborhood of the hole edge. In the bore, however, the stress concentrates at eight points, marked by n in the same figure, at a small distance below the edge of the hole. When the ratio of d/D is comparatively small, the stress

FIG. 5 TEST PIECE WITH TRANSVERSE HOLE, CHANGED IN COLOR IN PLACES WHERE THE STRESS CONCENTRATES

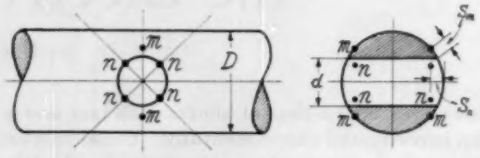

FIG. 6

FIG. 7 FRACTURED SURFACE OF SPECIMEN WITH TRANSVERSE HOLE

at the latter is larger than that at the former, so fatigue cracks always start from the latter. Fig. 7 shows the fractured surface of the specimen. It shows a clear aspect for the stress concentration and also for the crack started from the point n.

ADDITIONAL TESTS CONDUCTED

Having determined the places where the stress concentrates, further tests were carried out to obtain stress-concentration factors for shafts with transverse holes of various diameters. Test pieces used are 20 mm diam with a transverse hole in each, the diameters of which are 2.1, 3.6, and 5.1 mm, respectively.

The torques which produce proper stress at m and n are measured by observing the surfaces of specimens and bores with a microscope. The status of flecks at m or n, corresponding to the proper stress, is assumed to be in such condition that faint flecks appear in some of the cognate points (m or n) but never appear in them for a slightly smaller stress. The torques which produce the proper stress at m and n are denoted by T_m and T_n, respectively, and are shown in Table 2. For an accurate determination of T_n, satisfactory observations in the bore are required. For this purpose, in some instances test pieces are planed through the axis of a hole, according to the requirement in observation.

The stress-concentration factor usually is given by the ratio of the maximum stresses in two shafts of the same diameter, with and without a hole, which are subjected to equal torques. This is equal to the inverse ratio of torques which produce the same maximum stress in either shaft. The torque which produces the proper stress on the surface of the shaft, 20 mm diam and without a hole, is $(\pi/2)\tau_p$, kg-m. Thus we have

$$K = \frac{\pi\tau_p}{2T}$$

where K is the stress-concentration factor. The values of K in the bore (n) and at the hole edge (m), calculated from the foregoing relation, are shown in Table 3, together with S_m and S_n, the roughly found locations of m and n. As is shown in the table, S_m and S_n decrease with the decrease of d/D, and the ratio T_m/T_n is likely to approach almost 1.5 when the diameter of hole becomes infinitely small. This shows that the normal stress at n is 3 times the shearing stress at m, if we take the shearing stress for the

TABLE 2 DETERMINATION OF TORQUE TO PRODUCE FLECKS IN SHAFTS WITH TRANSVERSE HOLES

Diam of hole, mm	Torque, kg-m	Flecks produced at m	Flecks produced at n	T_m, kg-m	T_n, kg-m
5.1	±6.03	Some points	All points	±5.87	
	±5.87	Some points	All points		
	±5.77	No points	All points		
	±5.12	No points	Some points		
	±5.11	No points	Some points		±5.11
	±4.93	No points	No points		
3.6	±6.66	Some points	All points	±6.66	
	+6.44	No points	All points		
	±6.32	No points	All points		
	±5.85	No points	All points		
	±5.75	No points	All points		
	±5.58	No points	Some points		
	±5.46	No points	Some points		
	±5.44	No points	Some points		±5.44
	±5.38	No points	No points		
2.1	±7.62	Some points	All points	±7.62	
	±7.44	No points	All points		
	±7.21	No points	All points		
	±6.79	No points	All points		
	±5.97	No points	All points		
	±5.71	No points	Some points		±5.71
	±5.56	No points	No points		
	±5.40	No points	No points		

TABLE 3 LOCATION OF MAXIMUM STRESS AND VALUE OF STRESS-CONCENTRATION FACTORS

Diam of hole, mm	d/D	S_m, mm	S_n, mm	T_m/T_n	K In bore (n)	K At hole edge (m)
2.1	0.105	0.6	0.4 ~ 0.5	1.33	2.17	1.63
3.6	0.180	1.1	0.5 ~ 0.8	1.22	2.28	1.86
5.1	0.255	1.6	0.8 ~ 1.1	1.15	2.42	2.11

criterion of producing flecks (see Appendix). This result for infinitely small holes agrees with the theoretical one previously derived by Neuber (2). In the range of the diameter of hole treated here, the stress at n is always larger than that at m, but the stress at m also becomes effective when d/D is large enough, since the ratio T_m/T_n decreases with increase of d/D.

The stress-concentration factors in the bore have been derived by Seely and Dolan by means of the plaster-model method (3). From Table 3 the values of K both in the bore and at the hole edge are plotted in Fig. 8, together with their results represented by a dotted line. The latter shows average values for 5 ~ 8 tests, and the deviation of each value from the mean is about 10 per cent for every size of hole. As is shown in the figure, their data for small holes are much smaller in comparison with those obtained here as well as the theoretically presumed values (4). Recent investigations by means of strain gages have been made for similar cases by Thum and Seeger, respectively (5). The results derived by them are considerably larger in comparison with those obtained here. The authors doubt, however, if the stress-concentration factors are not derived in the ratio of the maximum direct stress to the nominal shearing stress. If this difference for the derivation of K be taken into account, their data are much smaller in comparison with those derived here. Their results show that, in a certain range of small d/D, K decreases with the increase of d; namely, the greatest strength for a shaft is obtained by making the diameter of a hole to a suitable size.

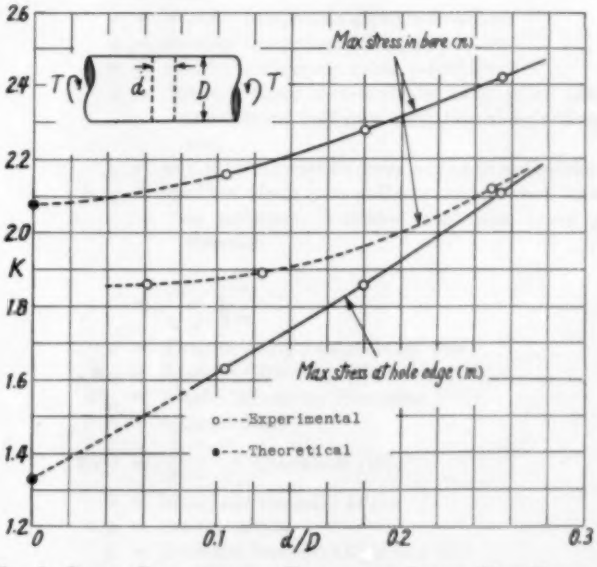

FIG. 8 STRESS-CONCENTRATION FACTORS FOR SHAFTS WITH TRANSVERSE HOLES

CONCLUSION

The same conclusion would be derived from other experimental results obtained previously by various writers for shafts with transverse holes submitted to bending or torsion (6). Such a conclusion, however, is quite contrary to usual practice which tends to make the shaft with the smallest possible size of hole the strongest one. The authors rather incline to conclude that usual methods for stress measurements such as the freezing method and the use of strain gages are not suitable for an accurate measurement of the stress concentration in shafts with small transverse holes.

ACKNOWLEDGMENT

The authors wish to express their thanks to Mr. B. Chiba for his help in this experiment.

BIBLIOGRAPHY

1 "Determination of the Surface Stress by Means of Electroplating," by H. Ōkubo, *Journal of Applied Physics*, vol. 24, 1953, p. 1130.

2 "Kerbspannungslehre," by H. Neuber, Julius Springer, Berlin, Germany, 1937, p. 54.

3 "Stress Concentration at Fillets, Holes and Keyways as Found by the Plaster Model Method," by F. B. Seely and T. J. Dolan, University of Illinois Engineering Experiment Station Bulletin No. 276, 1935.

"Stress and Strength of Manufactured Parts," by C. Lipson, G. C. Noll, and L. S. Clock, McGraw-Hill Book Company, Inc., New York, N. Y., 1950, p. 70.

4 Loc. cit., H. Neuber, p. 136.

5 "Tension, Bending and Torsion of Bars Containing a Transverse Hole and Combinations Thereof," by A. Thum and W. Kirmser, *VDI Forschungsheft*, No. 419, March-April, 1943.

"Stress in Transversely Bored Shafts Subjected to Torsional Loading," by G. Seeger, *Die Technik*, vol. 3, 1948, p. 309; *Engineers Digest*, February, 1949, p. 51.

6 Loc. cit., A. Thum and W. Kirmser.

"Two- and Three-Dimensional Cases of Stress Concentration and Comparison With Fatigue Strength," by R. E. Peterson and A. M. Wahl, JOURNAL OF APPLIED MECHANICS, Trans. ASME, vol. 58, 1936, pp. A-15–A-25.

"Studies in Three-Dimensional Photoelasticity: Stresses in Bent Circular Shafts With Transverse Holes," by M. M. Frocht, JOURNAL OF APPLIED MECHANICS, Trans. ASME, vol. 66, 1944, pp. A-10–A-16.

"Designing by Photoelasticity," by R. B. Heywood, Chapman and Hall, Ltd., London, England, 1952.

Appendix

In the previous discussion, shearing stress was used for the criterion of producing flecks without any experimental evidence. However, the suitability of choosing shearing stress for the criterion was affirmed later by K. Takai, a graduate student at the Nagoya University. The tests were made quite independently of this investigation. The proper stress was determined both in torsion and in bending, using the plating solution prepared for that particular test. The proper stress for the latter was obtained by means of rotary bending tests.

The process of determining the proper stress, however, is quite similar to that employed here. The results are as follows:

In torsion, the averaged value for two tests is $\tau_p = \pm 8.0$ kg per sq mm. In bending, the direct stress averaged for three tests is $\sigma_p = \pm 15.4$ kg per sq mm, and the shearing stress corresponding to the direct stress is $\tau_p = {}^1/_2\sigma_p = \pm 7.7$ kg per sq mm. The proper stresses in shear, measured in two different types of loading, are in rather good agreement. This shows that shearing stress is used, in general, for the criterion of producing flecks without a perceptible error. The substantial effect of direct stress in producing flecks is 8.0/15.4 times that of shearing stress, which is slightly larger than that assumed previously. Consequently, if the maximum direct stress in the bore be 4 times the nominal shearing stress, the stress-concentration factor observed by the present method will be $4 \times 8.0/15.4 = 2.08$, and theoretically the curve of K, in the bore, must pass the point $d = 0$, $K = 2.08$, as is indicated by the dashed curve in Fig. 8. The curve of K, at the hole edge, may be extended to the theoretical value 4/3 at $d = 0$, as is shown in the same figure.

Laminar-Diffusion Boundary Layer—A Review

By KURT BERMAN,[1] SCHENECTADY, N. Y.

Diffusion theory has not assumed as yet the degree of organizational elegance accorded to fluid-flow and heat-transfer theories. In this paper mass-transport phenomena and their nondimensional correlation are summarized. In order that the similarities between energy, momentum, and mass-transport phenomena may be exhibited, the discussion of diffusion is preceded by brief summaries of dynamic and temperature boundary-layer theories.

Nomenclature

The following nomenclature is used in the paper:

$\vec{A}$ = a vector quantity
C_{ij} = coefficient in Equation [12*a*]
c_p = specific heat at constant pressure
$\mathfrak{D}_{12}$ = coefficient of ordinary diffusion
D_T = thermal-diffusion coefficient
$\left.\begin{matrix}\text{div}\,\vec{A}\\ \nabla\vec{A}\end{matrix}\right\}$ = vector operation $= \dfrac{\partial A_x}{\partial x} + \dfrac{\partial A_y}{\partial y} + \dfrac{\partial A_z}{\partial z}$
$f = \dfrac{\psi}{\sqrt{2}\sqrt{\nu x u_0}}$
f = subscript indicates properties evaluated at average condition of boundary layer
$\left.\begin{matrix}\nabla \cdot T\\ \text{grad}\,T\end{matrix}\right\}$ = vector operation $= \dfrac{\partial T}{\partial x} + \dfrac{\partial T}{\partial y} + \dfrac{\partial T}{\partial z}$
h = local heat-transfer coefficient
i = subscript identifying a definite component i
j = subscript identifying a definite component j
ij = subscript identifies gas i diffusing through gas component j
j_h = Colburn function (Equation [44*a*])
j_d = Colburn mass-transfer function (Equation [44*b*])
k = thermal conductivity
$(\dot{m}_i)_x$ = rate of diffusion of component i in x-direction, i.e. $(\dot{m}_1)_x = u_1\rho_1$
M = molecular weight of gas species
N_{Nu} = Nusselt number $= \dfrac{hx}{k}$
N_{Pr} = Prandtl number $= \dfrac{\nu\rho c_p}{k}$
N_{Re} = Reynolds number $= \dfrac{ux}{\nu}$
N_{Sc} = Schmidt number $= \dfrac{\nu}{\mathfrak{D}_{12}}$
N_{Ta} = Taylor number $= \dfrac{\beta x}{\mathfrak{D}_{12}}$
0 = subscript indicates conditions in undisturbed free stream
p = static pressure (subscript 1 or 2 indicates that it represents partial pressure of indicated gas component)
p_t = static pressure of mixture, i.e., $p_t = p_1 + p_2$
$\vec{q}$ = convection velocity of gas molecules
q_y = heat-transfer rate per unit area of plane perpendicular to y-axis
r = distance between molecules
R = universal gas constant
s = subscript indicates conditions at surface of object
T = absolute temperature
t = time
u = velocity component along x-direction
v = velocity component along y-direction
w = velocity component along z-direction
x = distance along x-co-ordinate axis; when used as subscript, indicates conditions along x-direction
X = any external specific force acting in x-direction
y = distance along y-co-ordinate axis; when used as subscript, indicates conditions along y-direction
$z' = \dfrac{y}{\sqrt{2}}\sqrt{\dfrac{u_0}{\nu x}}$
z = distance along z-co-ordinate axis
α_{ij} = pressure diffusivity (Equation [12*b*])
α'_{ij} = weight diffusivity (Equation [17])
λ = reduced mass
$\theta(z') = \dfrac{T - T_s}{T_0 - T_s}$ (Equation [18])
ν = kinematic viscosity of gas
ρ = density of gas
ψ = potential function (Equation [4])
Δ^2 = Laplacian operator $= \dfrac{\partial^2}{\partial x^2} + \dfrac{\partial^2}{\partial y^2} + \dfrac{\partial^2}{\partial z^2}$
$\pi(z') = \dfrac{\rho - \rho_s}{\rho_0 - \rho_s}$
β = mass-transfer coefficient (Equation [33])
δ = effective film thickness of boundary layer
1 = subscript identifies gas component 1
2 = subscript identifies gas component 2
12 = subscript identifies gas 1 diffusing through gas 2
21 = subscript identifies gas 2 diffusing through gas 1
$\phi_1(N_{Re}, N_{Pr})$ = indicates a function of N_{Re} and N_{Pr}
$\phi_2(N_{Re}, N_{Sc})$ = indicates a function of N_{Re} and N_{Sc}

Introduction

As a fluid flows past an immersed body at a high Reynolds number, N_{Re}, the variation of the velocity from zero at the sur-

---

[1] Guided Missiles Department, General Electric Company.

Contributed by the Applied Mechanics Division and presented at the Annual Meeting, New York, N. Y., November 28–December 3, 1954, of The American Society of Mechanical Engineers.

Discussion of this paper should be addressed to the Secretary, ASME, 29 West 39th Street, New York, N. Y., and will be accepted until July 11, 1955, for publication at a later date. Discussion received after the closing date will be returned.

Note: Statements and opinions advanced in papers are to be understood as individual expressions of their authors and not those of the Society. Manuscript received by ASME Applied Mechanics Division, January 21, 1954. Paper No. 54—A-29.

face of the object to the free-stream velocity occurs within a very thin layer, usually called the dynamic boundary layer. In similar fashion, the change of the temperature and constituent concentration fields, which are formed if a temperature and/or diffusion gradient exists between the surface of the body and the free stream, also are concentrated within small layers, usually called the temperature and diffusion boundary layers, respectively. None of these layers or films need be, nor generally is, of equal thickness. However, they are mutually interrelated. Only by making simplifying assumptions, which are too well known to be repeated here, can the phenomena be treated independently of each other. It is on this basis that they will be discussed.

Dynamic Boundary Layer[2]

The characteristics of all three boundary layers are influenced by the existing flow conditions. The flow parallel to an immersed flat plate has been studied extensively and it has been concluded that the boundary layer tends to be laminar as long as the Reynolds number, formed by using the free-stream velocity and the distance from the leading edge as the characteristic length, is less than 84,000 (see reference 6). For values of N_{Re} between 84,000 and 500,000, the flow can be either laminar or turbulent, while for N_{Re} greater than 500,000, it is almost always turbulent.[3] It has been found that this criterion of the nature of the boundary-layer flow is valid not only if the free stream is laminar but also holds true approximately if it is turbulent. Of course, it hardly can be expected in the latter case that there exists a smooth and instantaneous transition from the laminar flow in the boundary layer to the turbulent flow in the main stream.

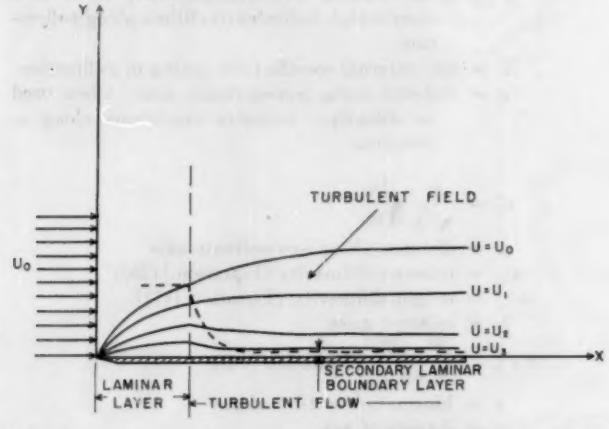

Fig. 1 Simplified Illustration of Boundary-Layer Flow Along a Flat Plate

Fig. 1 shows a schematic diagram of the boundary-layer flow conditions along a flat plate. Several constant-velocity lines have been sketched in. The dotted line indicates the extent of the laminar flow. It can be seen that even in the turbulent-flow region there is a very thin secondary laminar layer.

Prandtl was the first to derive the boundary-layer equations. For steady, incompressible, two-dimensional flow, they are

$$\frac{\partial u}{\partial x} + \frac{\partial v}{\partial y} = 0 \quad \text{(continuity equation)} \ldots\ldots [1]$$

$$u\frac{\partial u}{\partial x} + v\frac{\partial u}{\partial y} = \nu\frac{\partial^2 u}{\partial y^2} - \frac{1}{\rho}\frac{\partial p}{\partial x} \quad \text{(boundary layer)} \ldots [2a]$$

$$\frac{\partial p}{\partial y} = 0 \quad \text{(flow equation)} \ldots\ldots [2b]$$

In these equations the co-ordinate system is chosen in such a manner that the x-axis lies along the surface of the body and the y-axis is perpendicular to it, with the stagnation point chosen as the origin of x. Both the kinematic viscosity ν and the density ρ of the fluid are assumed constant.

The boundary conditions for Equations [1] and [2] are

$$\text{at} \quad \left.\begin{array}{ll} y = 0 & u = v = 0 \\ y = \infty & u = u_0 \end{array}\right\} \ldots\ldots [3]$$

where u_0 is the tangential velocity at the outer limit of the boundary layer. This quantity is usually evaluated by either measuring the pressure distribution along the surface of the body and calculating u_0 from the Bernoulli equation or by assuming it equal to the tangential surface velocity obtained from an "ideal fluid" solution.

Blasius (8) solved the system of Equations [1, 2, 3] for the case of a flat plate where $(\partial p)/(\partial x) = 0$ and u_0 is constant, being equal to the free-stream velocity. He introduced the new variables

$$z' = \frac{y}{\sqrt{2}}\sqrt{\frac{u_0}{\nu x}}, \quad f = \frac{\psi}{\sqrt{2}\sqrt{\nu x u_0}} \ldots\ldots [4]$$

where

$$u = \frac{\partial \psi}{\partial y}$$

$$v = \frac{\partial \psi}{\partial x}$$

This reduces the partial differential Equations [1], [2] to the ordinary differential equation

$$\frac{d^3 f}{dz'^3} + f\frac{d^2 f}{dz'^2} = 0 \ldots\ldots [5]$$

with boundary conditions

$$\left.\begin{array}{ll} \text{at} & z' = 0, \quad \dfrac{df}{dz'} = 0, \quad f = 0 \\ \text{and at} & z' = \infty, \quad \dfrac{df}{dz'} = 1 \end{array}\right\} \ldots\ldots [6]$$

Temperature Boundary Layer[4]

The energy equation, considering only heat conduction and convection, is

$$k\frac{\partial^2 T}{\partial y^2} = \rho c_p\left(u\frac{\partial T}{\partial x} + v\frac{\partial T}{\partial y}\right) \ldots\ldots [7]$$

Pohlhausen (14), using Blasius' velocity distribution, solved the problem of the temperature field in the vicinity of a heated flat plate placed parallel to the flow field. Introducing the transformation variable [4] and the function

$$\theta(z') = \frac{T - T_s}{T_0 - T_s} \ldots\ldots [8]$$

in Equation [7], the ordinary differential equation

[2] Good discussions can be found in references (1, 2, 3, 4, 5). Numbers in parentheses refer to the Bibliography at the end of the paper.

[3] Recent data indicate that the transition might occur at much higher Reynolds numbers under favorable conditions (see reference 7).

[4] Good discussion of the topic can be found in references (9, 10, 11, 12, 13).

$$\frac{d^2\theta}{dz'^2} + N_{Pr} f \frac{d\theta}{dz'} = 0 \quad \ldots\ldots [9]$$

where

$$N_{Pr} \equiv \frac{\nu\rho c_p}{k}$$

is obtained.

This equation, together with Equation [5] and boundary conditions

$$\left.\begin{array}{l} \text{at} \quad z' = 0 \quad f = 0 \quad \dfrac{df}{dz'} = 0 \quad \theta = 0 \\ \text{and at} \\ \qquad z' = \infty \quad \dfrac{df}{dz'} = 1 \quad \theta = 1 \end{array}\right\} \quad \ldots\ldots [10]$$

determines the thermal boundary layer along a flat plate. The actual solution obtained by Pohlhausen is

$$N_{Nu(x)} = 0.332 N_{Re}^{1/2} N_{Pr}^{1/3} \quad \ldots\ldots [11]$$

It is interesting to notice, in comparing Equations [9] and [5], that if $N_{Pr} = 1$, the dynamic and thermal boundary layers are of equal thickness. If, for instance, N_{Pr} is larger than 1, the thermal boundary layer is thinner than the dynamic layer. In the next section, where diffusion theory is discussed, another equation, similar to Equations [9] and [5], will be derived for the diffusion boundary layer, and again it will be seen that only if a dimensionless number, namely, the Schmidt number, equals 1, are the boundary layers of equal thickness.

Theory of Gaseous Diffusion and Diffusion Boundary Layer[5]

In 1866 Maxwell derived the diffusion coefficient for a binary mixture by treating gas molecules as points which repel one another with a force which falls off as the inverse fifth power of the distance between them. The fifth power was chosen since it presented the least mathematical difficulties. It was not until 1916 that Chapman (15) and Enskog (16) succeeded in treating the more general case of point molecules which repel each other according to the law λr^{-s}, where λ is the "reduced" mass, r is the distance between molecules, and s is an arbitrary integer, and were able to predict the phenomenon of thermal diffusion, i.e., the condition that a temperature gradient in a mixture of two gases causes a gradient of the concentration of the two constituents.

The phenomenon is of limited interest in ordinary engineering problems and will not be considered any further except to mention that its effect can be included by adding to the left-hand side of the following equation a term D_T grad ln T where D_T is a thermal-diffusion coefficient (17). A phenomenon of "pressure diffusion" also has been predicted theoretically but it has never been observed experimentally.

The basic equation of ordinary diffusion, i.e., neglecting thermal and pressure diffusion, of a binary gas mixture, as derived from kinetic theory, is[6]

$$-\frac{\mathfrak{D}_{12} p_t}{(RT)^2} \text{ grad } p_1 = \frac{\rho_1\rho_2}{M_1 M_2} (\vec{q_1} - \vec{q_2}) \quad \ldots\ldots [12]$$

Subscripts 1 and 2 designate respective gases; $\rightarrow$ designates a vector quantity.

An intuitive approach is presented by Maxwell (18) who says in his classic paper on diffusion:

"If we apply the ordinary language about fluids to a single gas of the mixture, we may distinguish the forces which act on an element of volume as follows:

"(1) Any external forces, such as gravity or electricity (X).

"(2) The difference of the pressure of the particular gas on opposite sides of the element of volume. (The pressure due to other gases is to be considered of no account.)

"(3) The resistance arising from the percolation of the gas through the other gases which are moving with different velocities. The resistance, due to encounters with the molecules of any other gas, is proportional to the velocity of the first gas relative to the second, to the product of their densities, and to the coefficient C_{ij} which depends on the nature of the gases and on the temperature. The equation of motion of one gas of a mixture is, therefore, of the form

$$\rho_1 \frac{du_1}{dt} + \frac{dp_1}{dx} - X_1\rho_1 + C_{12}\rho_1\rho_2(u_1 - u_2) + C_{13}\rho_1\rho_3(u_1 - u_3) + \ldots\ldots = 0" \quad \ldots [12a]$$

It is apparent that Equation [12] is a special case of Equation [12a] since the acceleration of the molecules 1 and any external forces have been neglected.

It is evident from an inspection of the two equations that

$$C_{12} = \frac{(RT)^2}{M_1 M_2 \mathfrak{D}_{12} p_t}$$

In order to simplify the appearance of this and succeeding expressions, the quantity

$$\frac{M_1 M_2 \mathfrak{D}_{12} p_t}{(RT)^2}$$

will be designated by the symbol α_{12} and will be called "the pressure diffusivity." Thus

$$\alpha_{12} = \frac{M_1 M_2 \mathfrak{D}_{12} p_t}{(RT)^2} = \frac{1}{C_{12}} \quad \ldots\ldots [12b]$$

The x-component of Equation [12] is

$$-\frac{\mathfrak{D}_{12} p_t}{(RT)^2} \frac{\partial p_1}{\partial x} = \frac{\rho_1\rho_2}{M_1 M_2} (u_1 - u_2) \quad \ldots\ldots [13]$$

Rearranging terms in Equation [13] and letting $(\dot{m}_1)_x$ and $(\dot{m}_2)_x$ represent, respectively, the rate of diffusion per unit area in the x-direction of gases 1 and 2, i.e.

$$(\dot{m}_1)_x = u_1\rho_1, \quad (\dot{m}_2)_x = u_2\rho_2 \quad \ldots\ldots [14]$$

one obtains

$$\left.\begin{array}{l} (\dot{m}_1)_x = -\dfrac{\mathfrak{D}_{12} p_t}{(RT)^2} \dfrac{M_2 M_1}{\rho_2} \dfrac{\partial p_1}{\partial x} + \dfrac{\rho_1}{\rho_2} (\dot{m}_2)_x \\ \qquad = -\dfrac{\alpha_{12}}{\rho_2} \dfrac{\partial p_1}{\partial x} + \dfrac{\rho_1}{\rho_2} (\dot{m}_2)_x \end{array}\right\} \quad \ldots [15]$$

[5] A good discussion of diffusion theory, according to the kinetic theory, is found in chapter 8 of "Introduction to the Kinetic Theory of Gases," by J. H. Jeans, Cambridge University Press, 1940. For applied diffusion theory, see "Absorption and Extraction," by T. K. Sherwood and R. L. Pigford, McGraw-Hill Book Co., Inc., New York, N. Y., 1937, and "Heat Transfer Notes," by L. M. K. Boelter, et al., University of California Press, chapter 16, 1946. For a rate-process consideration of diffusion, "The Theory of Rate Processes," by S. Glasstone, K. J. Laidler, and Henry Eyring, chapter 10, McGraw-Hill Book Company, Inc., New York, N. Y., 1941. An interesting article is "On the Elementary Explanation of Diffusion Phenomena in Gases," by W. H. Furry, *American Journal of Physics*, vol. 16, 1948, pp. 63–78.

[6] See reference (15), equation [7], p. 144. The notation has been altered to conform to the present author's nomenclature.

Similar equations can, of course, be written for the y and z-direction.

In the special case of equal molal diffusion of gases 1 and 2 in opposite directions, i.e. $\left(\frac{u_1\rho_1}{M_1}\right) = -\left(\frac{u_2\rho_2}{M_2}\right)$, Equation [13] reduces to

$$(\dot{m}_1)_x = -\frac{\mathfrak{D}_{12}}{\frac{R}{M_1}T}\frac{\partial p_1}{\partial x} \quad \ldots\ldots [16]$$

(Incidentally, the ideal-gas law will be assumed throughout this discussion.) It is indeed unfortunate that frequently Equation [16] is exhibited in the literature as the basic diffusion equation, which unequivocally it is not.

The $\mathfrak{D}_{12}$ in the various expressions is the so-called "normal diffusion coefficient" calculated in textbooks of kinetic theory of gases; the reason for the preference of $\mathfrak{D}_{12}$ over α_{12} is, of course, that equal molal diffusion usually is the only case considered.

Occasionally it is convenient to choose a weight diffusivity α'_{12} which is defined by the equation

$$(\dot{m}_1)_x = -\alpha'_{12}\frac{\partial \rho_1}{\partial x} + \frac{\rho_1}{\rho_2}(\dot{m}_2)_x \quad \ldots\ldots [17]$$

The relation between the three different diffusivities is

$$\alpha_{12} = \frac{M_2M_1p_t}{(RT)^2}\mathfrak{D}_{12} = \frac{\rho_2M_1}{RT}\alpha'_{12} \quad \ldots\ldots [18]$$

and their dimensions are

$$\left.\begin{aligned} |\alpha'_{12}| &= \left|\frac{\text{length}^2}{\text{time}}\right| \\ |\alpha_{12}| &= \left|\frac{\text{mass}}{\text{area time}}\right| \\ |\mathfrak{D}_{12}| &= \left|\frac{\text{length}^2}{\text{time}}\right| \end{aligned}\right\} \quad \ldots\ldots [18a]$$

Corresponding to Equation [15], an equation for the mass $(\dot{m}_2)_x$ diffusing through gas 1 can be written

$$(\dot{m}_2)_x = -\frac{\alpha_{21}}{\rho_1}\frac{\partial p_2}{\partial x} + \frac{\rho_2}{\rho_1}(\dot{m}_1)_x \quad \ldots\ldots [19]$$

If the total pressure is constant and equal to the sum of the partial pressures, so that

$$dp_1 = -dp_2 \quad \ldots\ldots [20]$$

it is easily seen, by simply rearranging the terms in Equation [19] and comparing them with Equation [15], that

$$\alpha_{12} = \alpha_{21}, \quad \mathfrak{D}_{12} = \mathfrak{D}_{21} \quad \ldots\ldots [21]$$

Notice, however, that α'_{12} is not equal to α'_{21} under these conditions.

Consider a cubical volume ($dx\,dy\,dz$) located in the gas mixture and write a conservation-of-mass relation for the gas species 1 crossing its surface area. The net gain of gas 1 across the faces equals the mass increase inside the cube, or mathematically

$$\frac{\partial}{\partial x}(\dot{m}_1)_x + \frac{\partial}{\partial y}(\dot{m}_1)_y + \frac{\partial}{\partial z}(\dot{m}_1)_z = -\frac{\partial \rho_1}{\partial t} \quad \ldots\ldots [22]$$

where the subscripts indicate the axis perpendicular to the faces across which the mass passes. Substituting Equation [15] and corresponding relations for the y and z-directions in Equation [22] and remembering that

$$(\dot{m}_2)_x = \rho_2 u_2$$
$$(\dot{m}_2)_y = \rho_2 v_2$$
$$(\dot{m}_2)_z = \rho_2 w_2$$

it becomes evident that

$$\frac{\partial}{\partial x}\left(-\frac{\alpha_{12}}{\rho_2}\frac{\partial p_1}{\partial x} + \frac{\rho_2 p_1 u_2}{\rho_2}\right) + \frac{\partial}{\partial y}\left(-\frac{\alpha_{12}}{\rho_2}\frac{\partial p_1}{\partial y} + \frac{\rho_2\rho_1}{\rho_2}v_2\right) + \frac{\partial}{\partial z}\left(-\frac{\alpha_{12}}{\rho_2}\frac{\partial p_1}{\partial z} + \frac{\rho_2\rho_1}{\rho_2}w_2\right) = -\frac{\partial \rho_1}{\partial t} \quad \ldots\ldots [23]$$

Rearranging terms, Equation [23] becomes

$$-\left[\frac{\partial}{\partial x}\left(\frac{\alpha_{12}}{\rho_2}\frac{\partial p_1}{\partial x}\right) + \frac{\partial}{\partial y}\left(\frac{\alpha_{12}}{\rho_2}\frac{\partial p_1}{\partial y}\right) + \frac{\partial}{\partial z}\left(\frac{\alpha_{12}}{\rho_2}\frac{\partial p_1}{\partial z}\right)\right] + \left[\frac{\rho_1}{\rho_2}\frac{\partial}{\partial x}(\rho_2 u_2) + \frac{\rho_1}{\rho_2}\frac{\partial}{\partial y}(\rho_2 v_2) + \frac{\rho_1}{\rho_2}\frac{\partial}{\partial z}(\rho_2 w_2)\right] + \left[\rho_2 u_2\frac{\partial}{\partial x}\frac{\rho_1}{\rho_2} + \rho_2 v_2\frac{\partial}{\partial y}\frac{\rho_1}{\rho_2} + \rho_2 w_2\frac{\partial}{\partial z}\frac{\rho_1}{\rho_2}\right] = -\frac{\partial \rho_1}{\partial t} \quad \ldots\ldots [24]$$

Looking at the second square bracket on the left, it can be seen that it equals ρ_1/ρ_2 times the left side of Equation [22] if subscript 1 is replaced by 2. Hence the bracket equals

$$-\frac{\rho_1}{\rho_2}\frac{\partial \rho_2}{\partial t}$$

Making use of the identity

$$\rho_2\frac{\partial \frac{\rho_1}{\rho_2}}{\partial t} = \frac{\partial \rho_1}{\partial t} - \frac{\rho_1}{\rho_2}\frac{\partial \rho_2}{\partial t} \quad \ldots\ldots [25]$$

and introducing it in Equation [24], the following result is obtained

$$-\left[\frac{\partial}{\partial x}\left(\frac{\alpha_{12}}{\rho_2}\frac{\partial p_1}{\partial x}\right) + \frac{\partial}{\partial y}\left(\frac{\alpha_{12}}{\rho_2}\frac{\partial p_1}{\partial y}\right) + \frac{\partial}{\partial z}\left(\frac{\alpha_{12}}{\rho_2}\frac{\partial p_1}{\partial z}\right)\right] + \rho_2\left[\frac{\partial\,\rho_1/\rho_2}{\partial t} + u_2\frac{\partial}{\partial x}\frac{\rho_1}{\rho_2} + v_2\frac{\partial}{\partial y}\frac{\rho_1}{\rho_2} + w_2\frac{\partial}{\partial z}\frac{\rho_1}{\rho_2}\right] = 0 \quad \ldots\ldots [26]$$

The quantity inside the second square bracket can be written as

$$\frac{d}{d_2t}\left(\frac{\rho_1}{\rho_2}\right)$$

where the subscript 2 indicates that the velocities in this expansion are those of carrier gas 2, i.e., the gas through which 1 is diffusing. The final expression is, therefore

$$-\operatorname{div}\frac{\alpha_{12}}{\rho_2}\operatorname{grad} p_1 + \rho_2\frac{d}{d_2t}\frac{\rho_1}{\rho_2} = 0 \quad \ldots\ldots [26a]$$

or in symbolic notation

$$-\nabla\frac{\alpha_{12}}{\rho_2}\nabla\cdot p_1 + \rho_2\frac{d}{d_2t}\frac{\rho_1}{\rho_2} = 0$$

In the special case of equal molal diffusion, it can be seen, by substituting Equation [16] in [22] that

$$\frac{\partial}{\partial x}\frac{\mathfrak{D}_{12}}{\frac{R}{M_1}T}\frac{\partial p_1}{\partial x} + \frac{\partial}{\partial y}\frac{\mathfrak{D}_{12}}{\frac{R}{M_1}T}\frac{\partial p_1}{\partial y} + \frac{\partial}{\partial z}\frac{\mathfrak{D}_{12}}{\frac{R}{M_1}T}\frac{\partial p_1}{\partial z} = \frac{\partial \rho_1}{\partial t} \quad \ldots\ldots [27]$$

which becomes for isothermal conditions

$$\nabla \mathfrak{D}_{12} \nabla \cdot \rho_1 = \frac{\partial \rho_1}{\partial t}$$

Equation [26] can be simplified for the special case when $\rho_2 \gg \rho_1$, making it a good approximation to consider ρ_2 constant. In addition, α_{12} will be assumed independent of position.

Incidentally, it might be well to point out in this connection that, according to kinetic theory (19), $\mathfrak{D}_{12}$ varies as (T^{1+s}/p_t), where $s = 1/2$ for elastic spheres and $s = 1$ for Maxwellian molecules. According to Equation [18] it would seem, therefore, that α_{12} is practically invariant with respect to temperature and total pressure.

Inserting the approximations, mentioned previously, for isothermal conditions

$$\frac{d\rho_1}{d_2 t} = \frac{\alpha_{12} RT}{M_1 \rho_2} \nabla^2 \rho_1 \quad \ldots\ldots [28]$$

where ∇^2 is the Laplacian operator

or

$$\frac{d\rho_1}{d_2 t} = \mathfrak{D}_{12} \frac{p_t}{p_2} \nabla^2 \rho_1$$

In order to be consistent with the assumption $\rho_1 \ll \rho_2$, p_t/p_2 is usually set equal to 1. The resulting equation

$$\frac{d\rho_1}{d_2 t} = \mathfrak{D}_{12} \nabla^2 \rho_1 \quad \text{or} \quad \frac{dp_1}{d_2 t} = \mathfrak{D}_{12} \nabla^2 p_1 \quad \ldots\ldots [29]$$

is another example of a specialized expression which has assumed in many articles the status of a fundamental diffusion relation.

The similarity between Equations [29] and [7] forms the basis of the similarity approach which has found such widespread use in the field of diffusion. If

$$\pi(z') = \frac{\rho - \rho_s}{\rho_0 - \rho_s}$$

where ρ_s is the concentration at a surface and ρ_0 is the concentration of gas 1 in the free stream, then analogous to Equation [9], one obtains the diffusion boundary-layer equation

$$\frac{d^2\pi}{dz'^2} + N_{Sc} f \frac{d\pi}{dz'} = 0 \quad \ldots\ldots [30]$$

where

$$N_{Sc} = \frac{\nu}{\mathfrak{D}_{12}} \text{ (Schmidt number)}$$

It can be seen that only if $N_{Sc} = N_{Pr} = 1$ will the three boundary layers be of equal thickness.

It is well known from both experimental forced-convection heat-transfer results and theoretical analyses, as evidenced by Equation [11], that low-velocity, forced-convection heat-transfer data can be correlated by an equation of the form

$$N_{Nu} = \phi_1(N_{Re}, N_{Pr}) \quad \ldots\ldots [31]$$

where ϕ_1 indicates a function.

The heat transfer from a medium to a surface can be represented by the equation

$$q_y = -k \left(\frac{\partial T}{\partial y} \right)_s \quad \ldots\ldots [32a]$$

(Subscript s refers to conditions at the surface) or

$$q_y = h(T_0 - T_s). \quad \ldots\ldots [32b]$$

where subscript 0 indicates conditions of the free stream, q_y represents the rate of heat transfer per unit area, and y is the coordinate perpendicular to the body surface.

Similar to Equation [32b], it is possible to write an expression

$$(\dot{m}_1)_s = \beta(\rho_0 - \rho_s) \quad \ldots\ldots [33a]$$

or

$$(\dot{m}_1)_s = \frac{\beta}{\frac{R}{M_1} T} (p_0 - p_s) \quad \ldots\ldots [33b]$$

where β is defined, analogous to h, as the mass-transfer coefficient with dimensions (length/time). In general, β is not independent of the partial pressure difference. Two special cases will now be considered:

1 For steady-state equal-molal diffusion, it can be seen, by integrating Equation [16] between the limits $x = 0$ and $x = \delta$ and respective partial pressures p_s and p_0 of gas 1, that

$$(\dot{m}_1)_s = -\frac{\mathfrak{D}_{12}}{\delta \frac{R}{M_1} T} (p_0 - p_s) \quad \ldots\ldots [34a]$$

or

$$(\dot{m}_1)_s = \frac{\beta}{\frac{R}{M_1} T} (p_0 - p_s) \quad \ldots\ldots [34b]$$

For this particular case, β is not a function of the partial pressure difference.

2 As another illustration, consider the diffusion of gas 1 through a stagnant layer of gas 2. Then one can write from Equations [15] and [19]

$$\left.\begin{aligned} (\dot{m}_1)_x &= -\frac{\alpha_{12}}{\rho_2} \frac{\partial p_1}{\partial x} + 0 \\ (\dot{m}_2)_x &= 0 = -\frac{\alpha_{21}}{\rho_1} \frac{\partial p_2}{\partial x} + u_1 \rho_1 \end{aligned}\right\} \quad \ldots\ldots [35]$$

Assuming $dp_1 = -dp_2$, it is possible to separate variables and integrate

$$\int_0^\delta \frac{\dot{m}_1}{\frac{R}{M_2} T} dx = -\int_{p_s}^{p_0} \frac{\alpha_{12}}{p_t - p_1} dp_1 \quad \ldots\ldots [35a]$$

where

p_t = total pressure = $p_1 + p_2$ = const
δ = effective film thickness
p_0 = partial pressure of gas 1 at the plane $x = \delta$
p_s = partial pressure of gas 1 at the plane $x = 0$, which is permeable to gas 1 only

For steady-state conditions, $\dot{m}$ is independent of x. If α_{12} is assumed constant, Equation [35a] becomes

$$\left.\begin{aligned} (\dot{m}_1)_s &= \frac{RT\alpha_{12}}{M_2 \delta} \ln \frac{p_t - p_0}{p_t - p_s} \\ \text{or} \\ (\dot{m}_1)_s &= \frac{p_t \mathfrak{D}_{12}}{\frac{R}{M_1} T\delta} \ln \frac{p_t - p_0}{p_t - p_s} \end{aligned}\right\} \quad \ldots\ldots [36]$$

This can be written in the alternate form

$$\left.\begin{aligned} \dot{m}_1 &= -\frac{\mathfrak{D}_{12}}{\frac{R}{M_1}T\delta}\frac{p_i}{p_0-p_s}\ln\frac{p_i-p_s}{p_i-p_0}(p_0-p_s) \\ &= \frac{\beta}{\frac{R}{M_1}T}(p_0-p_s) \end{aligned}\right\} \quad \ldots\ldots[37]$$

Here the partial pressure dependence of the mass-transfer coefficient is clearly exhibited. In the case of small partial pressures of the diffusing gas, so that p_0/p_i and $p_s/p_i \ll 1$, the logarithm in Expression [37] can be expanded in an algebraic series

$$\ln\frac{1-\frac{p_s}{p_i}}{1-\frac{p_0}{p_i}} = \frac{p_0-p_s}{p_i}+\frac{1}{2}\left[\left(\frac{p_0}{p_i}\right)^2-\left(\frac{p_s}{p_i}\right)^2\right]+\ldots\ldots[38]$$

Retaining only the first term of the power series, it can be seen that under this condition the mass transfer of gas 1 through a stagnant gas layer equals approximately

$$\dot{m}_1 = -\frac{\mathfrak{D}_{12}}{\frac{R}{M_1}T\delta}(p_0-p_s) = \frac{\beta}{\frac{R}{M_1}T}(p_0-p_s)\ldots\ldots[39]$$

where the mass-transfer coefficient is substantially independent of the partial pressure difference.

Under this condition, it is possible to write, analogous to Equation [31], a functional relationship

$$\frac{\beta x}{\mathfrak{D}_{12}} = \phi_2(N_{Re}, N_{Sc})\ldots\ldots[40]$$

If β is not independent of the pressure, a dimensionless pressure relationship would have to appear in ϕ_2. The quantity $\frac{\beta x}{\mathfrak{D}_{12}}$ will be called the Taylor number and will be designated by N_{Ta}.

Nusselt (20) assumed a function ϕ_1 in Equation [31] of the form

$$\phi_1 = b_1(N_{Re})^{m_1}(N_{Pr})^{n_1}\ldots\ldots[41a]$$

and, similarly for ϕ_2, he wrote

$$\phi_2 = b_2(N_{Re})^{m_2}(N_{Sc})^{n_2}\ldots\ldots[41b]$$

Equations [30] and [9] are identical in form. If, therefore, the heat and mass transfer occur across the same geometrical boundary surfaces and have the same boundary conditions, then it is necessary that

$$b_1 = b_2 = b, \quad m_1 = m_2 = m, \quad n_1 = n_2 = n\ldots.[41c]$$

where b, m, and n can be determined from either heat-transfer or diffusion experiments.

At first glance it might appear that the boundary conditions can never be identical since in a diffusion field, if the surface acts like a permeable membrane toward the diffusing gas, the normal component of the velocity must be finite at the surface. However, as has been pointed out in the derivation of Equation [39], only the velocities of the carrier gas appear in the equation, and they are zero at the surface. Schuh (21) calculated the velocity and concentration fields, assuming a nonvanishing boundary-surface velocity. Since he used Equation [29] for the evaluation of the concentration field, these results must be viewed with some measure of doubt.

The exactness of the analogy, as expressed by Equation [41c], can be strictly valid only if the flow fields associated with the temperature and diffusion fields are identical. This condition, however, can never be exactly true since in the case of the latter field, the flow profile is perturbed by the mass transfer. In spite of this nonconformity of similarity conditions, if the concentration ρ_1 of the diffusing gas is small, as has been assumed in the derivation of Equation [29], the analogy condition yields very satisfactory results.

Returning now to the "dimensionless number" relations, it is found that if Equation [31] is divided by Equation [40], and the conditions expressed in Equations [41a], [41b], and [41c] are introduced, then

$$\frac{h\mathfrak{D}_{12}}{\beta k} = \left(\frac{N_{Pr}}{N_{Sc}}\right)^n \quad \text{or} \quad \frac{\mathfrak{D}_{12}h}{\beta k} = \left(\frac{\mathfrak{D}_{12}\rho_1 c_p}{k}\right)^n \ldots\ldots[42]$$

Since Equation [29] has been derived under the assumption of isothermal conditions and small partial pressures of the diffusing gas, it is apparent that the theory developed so far is only valid within such restricted boundaries. In the general case of simultaneous convective heat transfer and diffusion at low velocities, dimensionless relationships of the form

$$N_{Nu} = N_{Nu}\{N_{Re}, N_{Sc}, N_{Pr}\}\ldots\ldots[43a]$$

$$N_{Ta} = N_{Ta}\{N_{Re}, N_{Sc}, N_{Pr}, \psi[p_s, p_0, p_i]\}\ldots\ldots[43b]$$

(ψ indicates a function) will probably have to be used.

Based on the analogy existing between heat, mass, and momentum transfer processes for a given system, Colburn and Chilton (22) have presented a useful correlation. For heat and momentum transfer systems

$$j_h = \frac{N_{Nu}}{N_{Re}N_{Pr}}N_{Pr}^{2/3} = \frac{h}{\rho_0 u_0 c_{p0}}(N_{Pr})_f^{2/3}\ldots\ldots[44a]$$

where j_h is the Colburn function, which can be correlated as a unique function of the Reynolds number in a form analogous to that of the correlation of the friction factor of the Fanning equation for pressure drop in fluid flow. Similarly to Equation [44a], it was suggested to correlate mass-transfer phenomena by an analogous equation

$$j_d = \frac{N_{Ta}}{N_{Re}N_{Sc}}N_{Sc}^{2/3} = \frac{\beta p_M}{\rho_0 u_0 \frac{R}{M_0}T}(N_{Sc})_f^{2/3}\ldots\ldots[44b]$$

where p_M = mean partial pressure of the nondiffusing gas.

Over wide ranges of Reynolds numbers, it has been determined that $j_h = j_d$. This reduces to the relation given by Equation [42].

Summary

Based on the foregoing discussion, the relationships relevant to the diffusion boundary layer can be summarized as follows:

For the diffusion of a gaseous, binary mixture, the mass transport per unit area in the x-direction of constituents 1 and 2, respectively, can be computed by means of the equations

$$(\dot{m}_1)_x = -\frac{\alpha_{12}}{\rho_2}\frac{\partial p_1}{\partial x}+\frac{\rho_1}{\rho_2}(\dot{m}_2)_x$$

$$(\dot{m}_2)_x = -\frac{\alpha_{21}}{\rho_1}\frac{\partial p_2}{\partial x}+\frac{\rho_2}{\rho_1}(\dot{m}_1)_x$$

where

$$\alpha_{12} = \frac{M_2M_1p_i\mathfrak{D}_{12}}{(RT)^2}$$

Only in the special case of equal molal diffusion, i.e. $(u_1\rho_1/M_1) = -(u_2\rho_2/M_2)$ do these equations reduce to the simple expressions

$$(\dot{m}_1)_x = -\frac{\mathfrak{D}_{12}}{\frac{R}{M_1}T}\frac{\partial p_1}{\partial x}$$

$$(\dot{m}_2)_x = -\frac{\mathfrak{D}_{12}}{\frac{R}{M_2}T}\frac{\partial p_2}{\partial x}$$

These equations can be considered analogous to the heat-transfer equation

$$q_y = -k\left(\frac{\partial T}{\partial y}\right)$$

The differential equations and boundary conditions describing the dynamic and temperature boundary layers can be reduced to a similar form. If the Prandtl number is 1, the two boundary layers for a given system have equal thickness. The general equations and boundary conditions for the diffusion boundary layer, however, cannot be reduced to such an analogous form. Only if the equations are specialized, i.e., it is assumed that (*a*) isothermal, equal molal diffusion exists, (*b*) the density ρ_1 of the diffusing gas is much smaller than the density ρ_2 of the transport gas, so that the partial pressure of gas 2 is almost equal to the pressure of the mixture, can the diffusion equations and boundary conditions be put in a form similar to those for the dynamic and thermal boundary layer. Then, and only then, can these analogous relations between the thermal and diffusion boundary layer be written as follows:

Thermal	Diffusion
Differential equation	
$\frac{dT}{dt} = \frac{k}{\rho c_p}\nabla^2 T$	$\frac{dp_1}{d_2 t} = \mathfrak{D}_{12}\nabla^2 p_1$
$q = h(T_0 - T_s)$	$\dot{m}_1 = \frac{\beta}{\frac{R}{M_1}T}(p_0 - p_s)$
Dimensionless correlation	
$N_{Nu} = \phi_1(N_{Re}, N_{Pr})$	$N_{Ta} = \phi_2(N_{Re}, N_{Sc})$
$\frac{h\mathfrak{D}_{12}}{\beta k} = \left(\frac{N_{Pr}}{N_{Sc}}\right)^n$	$n \sim \frac{1}{3}$

BIBLIOGRAPHY

1 "Boundary Layer in Compressible Fluid," Monograph V, Wright Field, Dayton, Ohio, No. F-TR-1179, ND.

2 "Aerodynamic Theory," by W. F. Durand, J. Springer, Berlin, Germany, vol. 3, 1935, p. 34 ff.

3 "Modern Developments in Fluid Mechanics," by S. Goldstein, Oxford University Press, New York, N. Y., vol. 1, 1938.

4 "Handbuch der Experimentalphysik," edited by W. Wien and F. Harms, vol. 4, part 1, under "Boundary Layer Theory."

5 "Boundary Layer Theory," by H. Schlichting, NACA Technical Memo No. 1217, part 1, "Laminar Flows," and No. 1218, part 2, "Turbulent Flows," Washington, D. C., April, 1949.

6 "A Design Manual for Determining the Thermal Characteristics of High Speed Aircraft," AAF Technical Report 5632, Wright Field, pp. 1–5.

7 "A Free-Flight Investigation of the Possibility of High Reynolds Number Supersonic Laminar Boundary Layers," by J. Sternberg, *Journal of the Aeronautical Sciences*, vol. 19, 1952, pp. 721–733.

8 "Boundary Layers in Fluids of Small Viscosity," by H. Blasius, *Zeitschrift für Mathematik und Physik*, vol. 56, 1908, pp. 1–37.

9 "Modern Developments in Fluid Dynamics," by S. Goldstein, Oxford University Press, New York, N. Y., vol. 2, 1938.

10 "Aerodynamic Theory," by W. F. Durand, J. Springer, Berlin, Germany, vol. 6, section T, 1936.

11 "La convection forcée de la chaleur en regime d'ecoulement turbulent," by Ribaud and Brun, Memorial des Sciences Physiques, Fascicule XIVI, Gauthier-Villars, Paris, France, 1942.

12 "Heat Transfer," by M. Jakob, John Wiley & Sons, Inc., New York, N. Y., 1949.

13 "Einige Probleme der Strömung, des Wärmeüberganges und der Diffusion bei Laminarströmung langs einer ebenen Platte," by H. Schuh, Österreichisches Ingenieur-Archiv 2 (5), 1948, p. 346.

14 "Der Wärmeaustausch zwischen festern Körpern und Flüssigkeiten mit kleiner Reibung und kleiner Wärmeleitung," by E. Pohlhausen, *Zeitschrift für angewandte Mathematik und Mechanik*, vol. 1, 1921, pp. 115–121.

15 "On the Law of Distribution of Molecular Velocities, and on the Theory of Viscosity and Thermal Conduction, in a Non-Uniform Simple Monatomic Gas," by S. Chapman, Philosophical Transactions of the Royal Society of London, series A, vol. 216, 1916, pp. 279–348. See a very thorough discussion in Chapman and Cowling, "The Mathematical Theory of Non-Uniform Gases," Cambridge University Press, New York, N. Y., 1939.

16 "Kinetische Theorie der Vorgänge in mässig verdünnten Gasen," by D. Enskog, Doctoral Dissertation, Uppsala, New York, N. Y., 1917.

17 "The Separation of Isotopes by Thermal Diffusion," by R. C. Jones and W. H. Furry, *Reviews of Modern Physics*, vol. 18, 1946, pp. 151–224. "On the Theory of the Thermal Diffusion Coefficient for Isotopes," by R. C. Jones; I *Physical Review*, vol. 58, 1940, pp. 111–122; II *Physical Review*, vol. 59, 1941, pp. 1019–1033.

18 "The Scientific Papers of James Clark Maxwell," vol. II, Cambridge University Press, New York, N. Y., 1890, paper LXXXIX "Diffusions."

19 "The Mathematical Theory of Non-Uniform Gases," by S. Chapman and T. G. Cowling, The Macmillan Company, New York N. Y., 1939, p. 248, equation 1.

20 "Wärmeübergang, Diffusion und Verdunstung," by W. Nusselt, *Zeitschrift für angewandte Mathematik und Mechanik*, Band 10, Heft 2, April, 1930, pp. 105–121.

21 "Einige Probleme der Strömung, des Wärmeüberganges und der Diffusion bei Laminarströmung langs einer ebenen Platte," by H. Schuh, *Österreichisches Ingenieur-Archiv*, vol. 2, 1948, p. 346.

22 "Mass Transfer (absorption) Coefficients," by T. H. Chilton and A. P. Colburn, *Industrial and Engineering Chemistry*, vol. 26, 1934, pp. 1183–1187.

Application of Saint Venant's Principle in Dynamical Problems

By B. A. BOLEY,[1] NEW YORK, N. Y.

The propagation of stresses in bars under time-dependent self-equilibrating end loads is discussed by means of a simple model. It is found that high stresses are restricted to a short region near the end of the bar if the loads are applied comparatively slowly, but extend to longer portions if the loads are rapidly applied.

THE principle of Saint Venant (1, 2)[2] is useful in the solution of steady-state problems of elasticity, since it permits, for example, the replacement of a complicated system of surface tractions by a mathematically simpler statically equivalent system of loads. The error thus introduced is therefore that resulting from a self-equilibrating loading, and, according to Saint Venant's principle, will be small at large distances from the applied loads. Such a principle, of course, could be similarly employed in the solution of dynamical problems. The extension of the principle to cases of transient disturbances therefore would be valuable, and it is the purpose of this paper to examine briefly whether this extension is possible, and, if so, to what extent.

The meaning and proper formulation of the principle have been greatly clarified, for static loadings, in some recent investigations (3, 4); these have shown that the customary (1, 2) statements of the principle, though they may hold for bodies of certain special shapes (such as thin plates or long cylinders) cannot be applied with complete generality. It is not the intention of this note to extend that type of analysis but rather to examine the validity of the principle in simple cases of time-dependent loadings. To this end a simple idealized structure is first studied; generalizations to some other types of bodies are briefly indicated later.

Study of Idealized Structure

Consider then the structure of Fig. 1, which is made up of three semi-infinite bars connected by "shear springs" of stiffness k_S per unit of length. With the symmetry of the structure and the sign convention as indicated in that figure, the governing equations are

$$EA_1 \frac{\partial^2 u}{\partial x^2} + k_S(v - u) = \rho A_1 \frac{\partial^2 u}{\partial t^2} \quad \ldots\ldots [1]$$

$$EA_2 \frac{\partial^2 v}{\partial x^2} + 2k_S(u - v) = \rho A_2 \frac{\partial^2 v}{\partial t^2} \quad \ldots\ldots [2]$$

where A_1 and A_2 are the areas of the bars indicated in the sub-

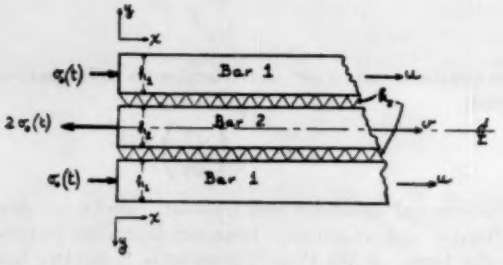

FIG. 1 STRUCTURE, NOMENCLATURE, AND SIGN CONVENTION FOR NUMERICAL EXAMPLES

script, ρ is the density, and E is Young's modulus for the bar material.

If only self-equilibrating loads are considered, the relation

$$v = -2u(A_1/A_2) \quad \ldots\ldots [3]$$

must hold; then Equations [1] and [2] reduce to

$$a^2 \frac{\partial^2 u}{\partial x^2} - \frac{\partial^2 u}{\partial t^2} - \frac{k_S}{\rho}\left(\frac{A_2 + 2A_1}{A_1 A_2}\right) u = 0 \quad \ldots\ldots [4]$$

where $a = (E/\rho)^{1/2}$. Consider the special case

$$h_1 = h_2 = h;\ A_1 = A_2 = bh \quad \ldots\ldots [5a]$$

and let

$$k_S = Gb/h;\ x_1 = x/(3h);\ t_1 = at/(3h) \quad \ldots\ldots [5b]$$

where G is the shear modulus, and let dots and primes indicate derivatives with respect to t_1 and x_1, respectively. Then Equation [4] becomes

$$u'' - \ddot{u} - (27G/E)u = 0 \quad \ldots\ldots [6]$$

Under steady-state conditions, the solution of this equation gives the stresses σ_1 and σ_2 in bars 1 and 2, respectively, as

$$\sigma_1 = -(\sigma_2/2) = [E/(3h)]u' = \sigma_0 e^{-x_1\sqrt{27G/E}} \quad \ldots\ldots [7]$$

These stresses are plotted as the short-dash line of Fig. 2 for a value $(27G/E) = 10.4$; it is clear that high stresses (of the order of magnitude of the applied stress σ_0) occur only within short distance (of order of magnitude $3h$) in the immediate vicinity of the applied load, and that therefore Saint Venant's principle holds in the conventional sense.

Consider now the case in which $\sigma_0 = \sigma_0(t_1)$; then it follows from the hyperbolic nature of Equation [6] that the stresses will propagate along the structure (with a constant velocity a) and that their magnitude at the wave front $(x_1 = t_1)$ is given by

$$\sigma_1 = -(\sigma_2/2) = \sigma_0(0) \quad \ldots\ldots [8]$$

Thus every point in the bar will in its turn be subjected to a stress of the order of magnitude of the initial applied stress $\sigma_0(0)$. Specifically, the displacements and the stresses corresponding to a

---

[1] Associate Professor of Civil Engineering, Columbia University.

[2] Numbers in parentheses refer to the Bibliography at the end of the paper.

Contributed by the Applied Mechanics Division and presented at the Annual Meeting, New York, N. Y., November 28–December 3, 1954, of THE AMERICAN SOCIETY OF MECHANICAL ENGINEERS.

Discussion of this paper should be addressed to the Secretary, ASME, 29 West 39th Street, New York, N. Y., and will be accepted until July 11, 1955, for publication at a later date. Discussion received after the closing date will be returned.

NOTE: Statements and opinions advanced in papers are to be understood as individual expressions of their authors and not those of the Society. Manuscript received by ASME Applied Mechanics Division, March 10, 1954. Paper No. 54—A-30.

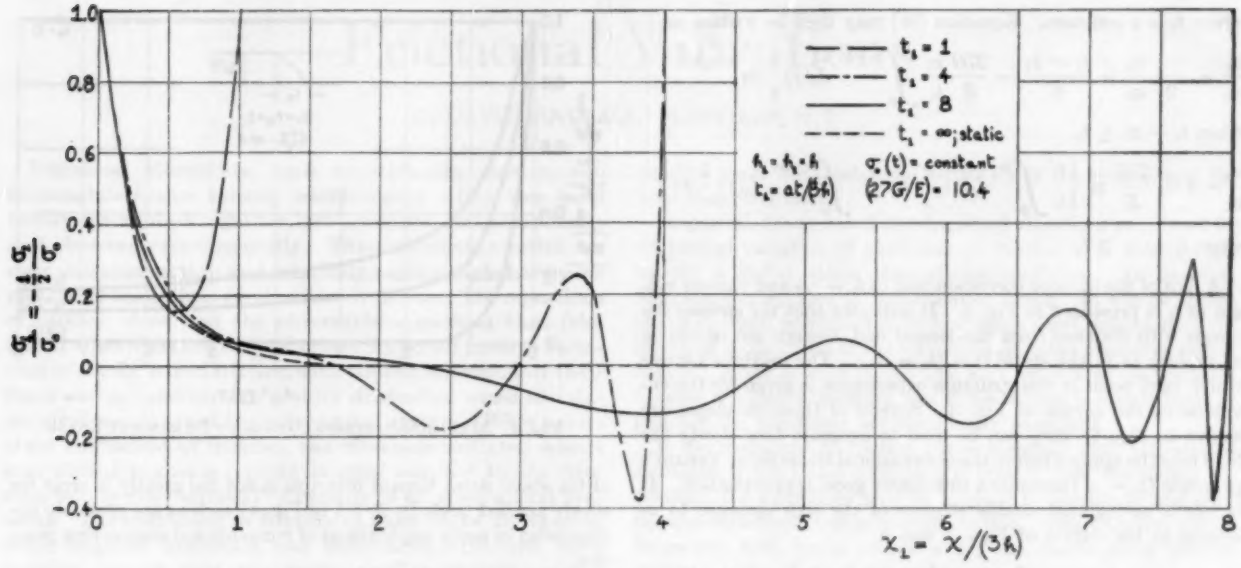

FIG. 2 VARIATION OF STRESSES IN STRUCTURE OF FIG. 1 FOR A SUDDENLY APPLIED LOAD

prescribed variation of applied stress are, respectively, given by (5)

$$u = -(3h/E)\int_0^{t_1-x_1} J_0(z)\sigma_0(\tau)d\tau \quad \ldots\ldots\ldots [9a]$$

$$\sigma_1 = -(\sigma_2/2) = [E/(3h)]u' = \sigma_0(t_1 - x_1) - (27G/E)x_1\int_0^{t_1-x_1} J_1(z)\sigma_0(\tau)(1/z)d\tau \quad \ldots [9b]$$

when $t_1 \geq x_1$, where

$$z = \sqrt{(27G/E)[(t_1-\tau)^2 - x_1^2]} \quad \ldots\ldots\ldots [9c]$$

and where J_n indicates the Bessel function of the first kind, of order n. Both the stresses and the displacements vanish when $t_1 < x_1$.

The stresses caused by a suddenly applied stress σ_0 are plotted in Fig. 2 for the cases in which the wave has traveled down the bar distances equal to 1, 4, 8 times the height $(3h)$ of the structure (as well as for the case $t_1 = \infty$). These three curves show that high stresses are again restricted to a short portion of the bar; but whereas in the static case this portion occurred solely in the immediate neighborhood of the applied load, it is now split in two parts. The second of these travels with the wave front (becoming shorter with increasing time) and thus eventually subjects all points of the bar to a stress equal to σ_0. Thus the conventional principle of Saint Venant certainly does not hold in this case.

The situation is somewhat different if the load is gradually applied, so that $\sigma_0(0) = 0$. Let, for example

$$\left.\begin{aligned} \sigma_0(t_1) &= \sigma_0 t_1/t_0 \quad \text{when } 0 \leq t_1 \leq t_0 \\ &= \sigma_0 \quad \text{when } t_1 \geq t_0 \end{aligned}\right\} \quad \ldots\ldots\ldots [10]$$

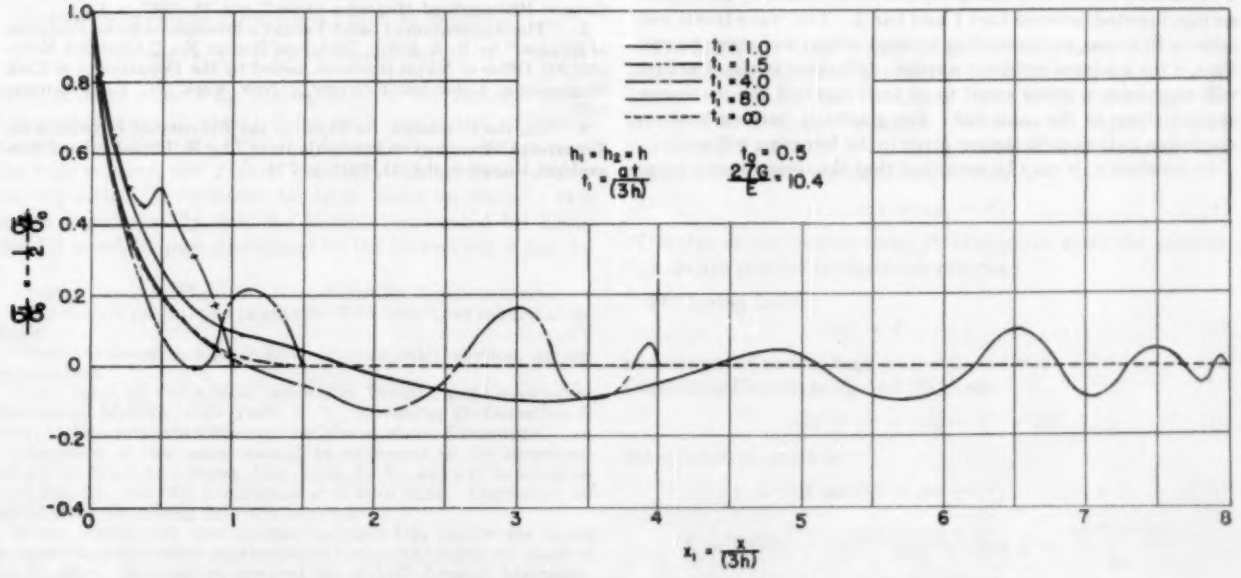

FIG. 3 VARIATION OF STRESSES IN STRUCTURE OF FIG. 1 FOR A GRADUALLY APPLIED LOAD

where t_0 is a constant. Equation [9b] may then be written as

$$\frac{\sigma_1}{\sigma_0} = \frac{-1}{2}\frac{\sigma_2}{\sigma_0} = \frac{t_1 - x_1}{t_0} - \frac{27G}{E}\frac{x_1}{t_0}\int_0^{t_1-x_1} J_1(z)\frac{\tau}{z}\,d\tau$$

when $t_1 - x_1 \leq t_0$

$$\frac{\sigma_1}{\sigma_0} = 1 - \frac{27G}{E}x_1\left\{\frac{1}{t_0}\int_0^{t_0} J_1(z)\,\frac{\tau}{z}\,d\tau - \int_{t_0}^{t_1-x_1} J_1(z)\,\frac{1}{z}\,d\tau\right\}$$

when $t_1 - x_1 \geq t_0$

A plot of the stresses corresponding to $t_0 = 1/2$ and various values of t_1 is presented in Fig. 3. It indicates that the stresses decrease with distance from the loaded end, though not of course as rapidly as in the static case ($t_0 = \infty$). The maximum stress which each point in the structure experiences is given by the envelope of the curves of Fig. 3. Several of these envelopes are shown in Fig. 4; they can be used to estimate how slowly the load must be applied before the conventional static Saint Venant's principle ($t_0 = \infty$) becomes a sufficiently good approximation. It is worth noting that sizable stresses of the sign opposite to σ_0 appear in the curves of Figs. 2 and 3.

General Remarks

These results need some modification in order to hold for time-dependent loads applied to a more general type of structure. Take, for example, the case of a semi-infinite bar under a self-equilibrating system of loads applied at its end; it can be shown (6) that here three wave fronts will arise, traveling with velocities a, $a\sqrt{G/E}$, $0.9194a\sqrt{G/E}$ (for $\nu = 0.25$), corresponding, respectively, to longitudinal, shear, and surface waves. Thus, if the loads are applied suddenly, each point in the bar will experience a stress equal to at least one third the maximum applied stress. If the loads are applied gradually, a set of curves similar to those of Fig. 4 can be constructed for each of the three wave fronts. The curves of that figure can be used for purposes of rough estimates of stress magnitudes.

Some of the results presented here were first described in reference (7) which also included a discussion of the behavior of the model of Fig. 1 when the outer bars are allowed to move in the y-direction. The motion of these bars is then governed by the Timoshenko theory of bending (8) and is restrained by additional springs inserted between bars 1 and bar 2. Two wave fronts will arise in this case, corresponding to longitudinal and shear waves; thus, if the loads are suddenly applied, each point in the structure will experience a stress equal to at least one half the maximum applied stress in the same bar. For gradually varying loads, a discussion analogous to the one given in the foregoing will apply.

In conclusion, it may be remarked that the conventional usage

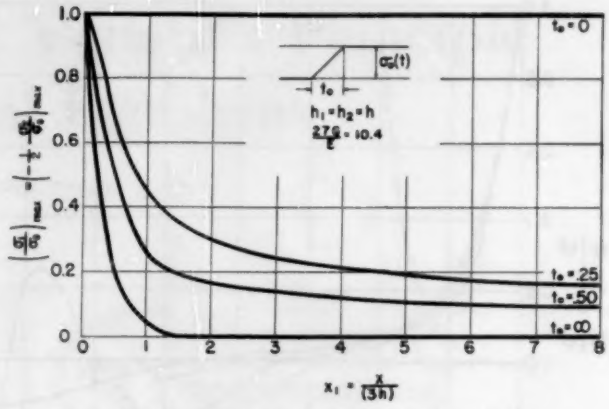

Fig. 4 Maximum Stresses Caused by Dynamical Loads

of the static Saint Venant principle is not too greatly in error for slowly applied loads ($t_0 \gg 0.5$ in Fig. 4) such as are probably encountered in many applications of conventional engineering practice.

Acknowledgment

The author wishes to thank Mr. Paul Bierley and Dr. T. F. H. T. Liu for their help in obtaining the numerical results, and the Office of Naval Research, U. S. Navy, for its support of the research project of which the present investigation is part.

BIBLIOGRAPHY

1 "A Treatise on the Mathematical Theory of Elasticity," by A. E. H. Love, Dover Publications, New York, N. Y., fourth edition, 1944.

2 "Theory of Elasticity," by S. Timoshenko and J. N. Goodier, McGraw-Hill Book Company, Inc., New York, N. Y., second edition, 1951.

3 "On Saint Venant's Principle," by R. von Mises, Bulletin of the American Mathematical Society, vol. 51, 1945, p. 555.

4 "On Saint Venant's Principle," by E. Sternberg, *Quarterly of Applied Mathematics*, vol. 11, no. 4, January, 1954, p. 393.

5 "Differential Equations," by H. Bateman, Longmans, Green and Company, London, England, 1918.

6 "The Propagation of Elastic Waves in a Rod," by J. L. B. Cooper, *Philosophical Magazine*, series 7, vol. 38, 1947, p. 1.

7 "The Application of Saint Venant's Principle in Some Problems of Impact," by B. A. Boley, Technical Report No. 2, Contract Nonr-266(20), Office of Naval Research, issued by the Department of Civil Engineering, Columbia University, New York, N. Y., February, 1953.

8 "On the Correction for Shear of the Differential Equations for Transverse Vibrations of Prismatic Bars," by S. Timoshenko, *Philosophical Magazine*, vol. 41, 1921, p. 744.

Frictional Vibrations

By DAVID SINCLAIR,[1] MANVILLE, N. J.

Frictional vibrations, such as stick-slip motion and automobile-brake squeal, which occur when two solid bodies are rubbed together, are analyzed mathematically and observed experimentally. The conditions studied are slow uniform motion and relatively rapid simple harmonic motion of brake lining over a cast-iron base. The equations of motion show and the observations confirm that frictional vibrations are caused primarily by an inverse variation of coefficient of friction with sliding velocity, but their form and occurrence are greatly dependent upon the dynamical constants of the mechanical system. With a constant coefficient of friction, the vibration initiated whenever sliding begins is rapidly damped out, not by the friction but by the "natural" damping of all mechanical systems. The coefficient of friction of most brake linings and other organic materials was essentially invariant with velocity, except that the static coefficient was usually greater than the sliding coefficient. Most such materials usually showed a small decrease in coefficient with increasing temperature. The persistent vibrations resulting from the excess static friction were reduced or eliminated by treating the rubbing surfaces with polar organic compounds which produced a rising friction characteristic.

Introduction

WHEN two solid bodies are rubbed together, intermittent motion of some type frequently occurs which may, in general, be called "frictional vibrations." The playing of a violin (1),[2] the squeal of an automobile brake, or the creaking of a door hinge are familiar examples of frictional vibrations. Frictional vibrations frequently have been investigated in connection with the study of metallic friction (2, 3, 4). This paper is concerned chiefly with automobile-brake squeal, the frictional vibrations that occur when a brake lining is rubbed against metal, usually cast iron.

The general equation of motion of a rubbing solid is

$$m\ddot{x} + R\dot{x} + kx = F(\dot{x}) + P(t) \quad \ldots\ldots [1]$$

Here, m is the mass of the moving body, R the natural[3] damping constant (usually small), k the force constant or stiffness of the support of the body, $F(\dot{x})$ the friction force, constant or varying with velocity, and $P(t)$ an externally applied force, usually varying with time. $\dot{x}$ stands for dx/dt, and $\ddot{x}$ for d^2x/dt^2. It is shown experimentally that the motion represented by Equation [1] is only in part determined by the friction but is also dependent upon the mechanical constants of the system and the type of applied force.

In general, it was found that frictional vibrations are caused by an inverse variation of coefficient of friction with velocity (1), usually a higher static than sliding coefficient. In practice, significant exceptions to this situation occur. It will be shown that a constant coefficient of friction (known as Coulomb friction) produces no damping of the vibrations initiated whenever sliding begins. If the motion is uniform, such vibrations are transient because of natural damping, but if the motion is intermittent or periodic the vibrations are continually re-excited.

If the coefficient of friction varies inversely with velocity, or especially if the static coefficient is greater than the sliding coefficient, the vibrations tend to increase in amplitude and may become persistent even in uniform motion. This situation occurs frequently with brake linings where the excess static friction overcomes the effect of natural damping, causing brake squeal.

On the other hand, when the friction is artificially altered to have a rising characteristic the frictional vibrations may be damped completely in either uniform or periodic motion. This effect was studied in detail with the idea that it might provide a method for the elimination of automobile-brake squeal.

Equations of Motion

These statements may be illustrated by the following examples which represent the experimental conditions used.

A block of brake lining of mass m, loaded with a weight W (which does not participate in the motion, see below) is pulled along a fixed cast-iron base I, by a spring of stiffness k, whose free end moves with a constant velocity v, in the positive direction of x, as illustrated in Fig. 1.

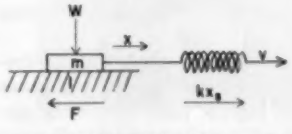

Fig. 1 Schematic Diagram for Intermittent Sliding

The block will begin to slide when the spring force, kx_s, just exceeds the oppositely directed static friction force, $F_0 = f(W + mg)$, where f is the coefficient of friction, and x_s is the extension of the spring from its neutral position. After motion begins, suppose the sliding friction $F < F_0$. Neglecting natural damping, the equation of motion during sliding is then

$$m\ddot{x} = kx_s - F \quad \ldots\ldots [2]$$

(The sign of the friction force, F, is negative since the velocity was always positive in these experiments.)

The spring force

$$kx_s = F_0 - kx + kvt \quad \ldots\ldots [3]$$

assuming that motion begins ($x = 0$) at $t = 0$.
Combining Equations [2] and [3] gives

$$m\ddot{x} + kx = (F_0 - F) + kvt \quad \ldots\ldots [4]$$

the solution of which is

$$x = -A \sin(wt + \phi) + (F_0 - F)/k + vt \quad \ldots\ldots [5]$$

$$A = \sqrt{(F_0 - F)^2/k^2 + v^2/w^2}, \quad \tan \phi = \frac{w(F_0 - F)}{kv}$$

where $w = \sqrt{k/m}$, the natural angular frequency.

---

[1] Senior Research Physicist, Johns-Manville Research Center.

[2] Numbers in parentheses refer to the Bibliography at the end of the paper.

[3] Positive damping arising from internal solid friction, air resistance, etc.

Contributed by the Applied Mechanics Division and presented at the Annual Meeting, New York, N. Y., November 28–December 3, 1954, of The American Society of Mechanical Engineers.

Discussion of this paper should be addressed to the Secretary, ASME, 29 West 39th Street, New York, N. Y., and will be accepted until July 11, 1955, for publication at a later date. Discussion received after the closing date will be returned.

Note: Statements and opinions advanced in papers are to be understood as individual expressions of their authors and not those of the Society. Manuscript received by ASME Applied Mechanics Division, July 31, 1953. Paper No. 54—A-46.

From Equation [5] it is seen that the amplitude of vibration increases with increasing difference between the static and sliding friction and with increasing applied velocity. In general, the velocity of the block increases from zero to a maximum, $v + wA$, when $wt = \pi - \phi$, and back to zero when $wt = 2(\pi - \phi)$. After this, Equation [5] no longer applies and the block remains at rest until the spring force increases to F_0, when the motion is repeated.

If the static and sliding friction are equal (Coulomb friction), the velocity increases from zero to $2v$ and back during one complete period, $2\pi/w$, so that the block comes to rest only instantaneously. In this case, the sinusoidal component of the motion is the same as a free vibration without friction, except that it takes place about the extended position of the spring which just balances the constant friction force. The energy dissipated in friction is supplied by the driver, but the vibration is unaffected.

If v is very small compared to w, the phase angle $\phi \approx \pi/2$ so that the block comes to rest when $wt \approx \pi$, after which Equation [5] no longer applies. In this case the motion consists of a series of sudden slips through a distance, $x \approx 2(F_0 - F)/k$ between periods of stick, resulting in the familiar stick-slip motion. When the block comes to rest, the spring force is approximately $2F - F_0$, which is negative if $F < {}^1/_2F_0$. The motion will be repeated when the spring force again equals F_0, or after a stick of duration, $2(F_0 - F)/kv$.

It is important to note that the velocity will not reverse even when $F \ll F_0$, provided the static-friction value is recovered instantly when the block comes to rest. Sampson (4) and associates observed that appreciable time was required for the recovery of the static friction of metals. In their case $F \approx {}^1/_3F_0$ and the motion did reverse. Rabinowicz (5) also found that appreciable displacement occurs after motion begins before the static friction falls to the sliding value.

This type of motion is observed only approximately since natural damping is always present. If a natural damping term, $R\dot{x}$, be included in Equation [4] the general solution is somewhat involved and space does not permit its presentation. Some properties of the motion can be found by considering the limiting cases which follow:

If the static and sliding friction are nearly equal, which is frequently true for brake linings, the block theoretically will never come to rest but will oscillate with exponentially decreasing amplitude. In practice, the oscillation will usually be quickly damped and the block will thereafter move with constant velocity, v. This condition is frequently observed with brake linings when v is not too small.

When v is very small, the block will come to rest when $wt \approx \pi$, resulting in stick-slip motion. This condition is illustrated in Figs. 12 and 13.

At high velocities, approximately sinusoidal vibrations can occur as in automobile-brake squeal. A sinusoidal vibration of this type was observed in the laboratory when the spring was driven in simple harmonic motion.

The experiments with brake linings showed that as the applied velocity was increased the motion changed from stick-slip to uniform sliding depending on the friction characteristic and the mass and stiffness of the system. In most cases, stick-slip motion was not observed until the applied velocity was reduced to a few thousandths of an inch per second, when the slip was a few thousandths of an inch.

To observe the friction characteristics in detail and to produce persistent frictional vibrations, a mechanical vibrator was used to drive the spring and attached brake block in simple harmonic motion. In Fig. 2 the motion of the block is assumed to begin at angle θ_1, measured from the beginning of the stroke at the left, at time $t = 0$. The friction force F is assumed constant throughout the motion and natural damping is neglected. If θ_0 is the angle at which the spring is in its neutral position

$$F = kr(\cos\theta_0 - \cos\theta_1) \quad [6]$$

The spring force at any time during motion of the block is

$$kx_s = kr\cos\theta_0 - kr\cos(w_0t + \theta_1) - kx \quad [7]$$

where x_s is the extension of the spring from its neutral position, r the eccentric (short compared to the connecting rod), and w_0 the angular frequency of the vibrator.

Combining Equations [2], [6], and [7] gives

$$m\ddot{x} + kx = kr\cos\theta_1 - kr\cos(w_0t + \theta_1) \quad [8]$$

The complete solution of Equation [8] is

$$x = A\cos(wt + \phi) - B\cos(w_0t + \theta_1) + r\cos\theta_1 \quad [9]$$

$$A = [w_0^2r/(w^2 - w_0^2)]\sqrt{1 + (w^2/w_0^2 - 1)\sin^2\theta_1}$$

$$B = w^2r/(w^2 - w_0^2),\ \tan\phi = (w/w_0)\tan\theta_1,\ w = \sqrt{k/m}$$

In the experiments to be described, the quantity actually observed was the spring extension

$$x_s = -A\cos(wt + \phi) + C\cos(w_0t + \theta_1) + F/k \quad [10]$$

$$C = w_0^2r/(w^2 - w_0^2)$$

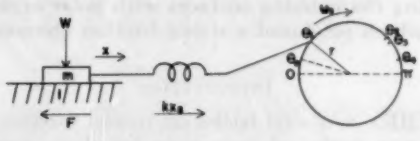

FIG. 2 SCHEMATIC DIAGRAM OF MECHANICAL VIBRATOR

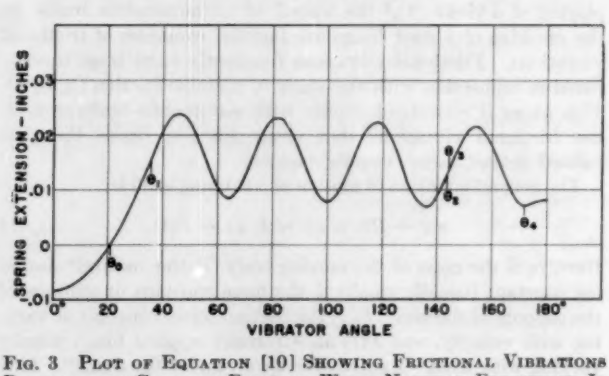

FIG. 3 PLOT OF EQUATION [10] SHOWING FRICTIONAL VIBRATIONS PRODUCED BY COULOMB FRICTION WHEN NATURAL FREQUENCY IS TEN TIMES APPLIED FREQUENCY

(Sliding begins at θ_1 and stops at θ_2, begins again at θ_3 and stops at θ_4.)

Fig. 3 shows a plot of Equation [10] for one half cycle of the vibrator. Convenient values for the constants were chosen to coincide approximately with the experimental conditions. The curve shows the neutral point θ_0, the two starting points θ_1 and θ_3, and the two stopping points θ_2 and θ_4, which occurred under these conditions. During the periods of rest from θ_2 to θ_3 and from θ_4 to θ_1, Equation [10] no longer applies and the curve is given by the motion of the vibrator, $r[1 - \cos(w_0t + \theta_1)]$. [The general form of Fig. 3 is similar to each half of Fig. 6(a), an oscillogram of one cycle of the vibrator.]

As will be shown, the experimental curves were used to calculate the coefficient of friction. In many cases the form of the experimental curves differed appreciably from that of Fig. 3 and the

calculations gave the coefficient of friction as a function of velocity.

Experimental Method

Fig. 4 is a photograph of the mechanical vibrator. The connecting rod C, 6 in. long, eccentrically mounted on the flywheel shaft at a radius of 1/8 in. (1/4 in. in later experiments), drives the piston P, in simple harmonic motion. The piston drives a leaf spring S, which slides a loaded block of brake lining B, along a stationary base I, made of cast iron of the type used in brake drums. The brake block is loaded by means of a weight (not

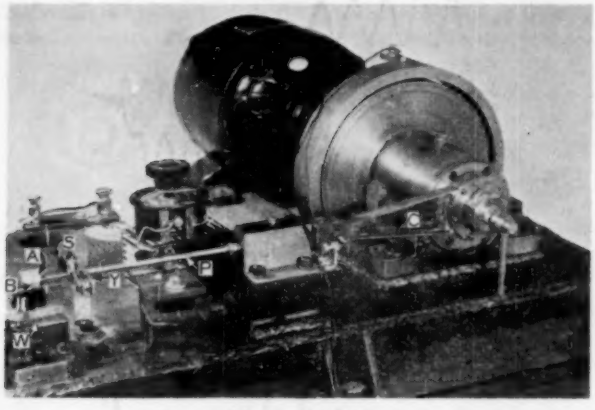

Fig. 4 Mechanical Vibrator
(C, connecting rod; P, piston; S, leaf spring; W, piano wire supporting weight; B, brake block; I, cast-iron base; Y, yoke; A, loading plate.)

shown) suspended from the ends of a piano wire W, which passes over the brake block and down through two holes in the base. A small plate of aluminum A, placed between the wire and brake block, distributes the load and prevents cutting of the brake block. The wire is long enough that motion of the load, usually 30 lb, is so small that it does not affect the vibration appreciably. The leaf spring is mounted on a very stiff yoke Y, attached to the piston, so that the system has only one degree of freedom. The vibrating system then consists of the mass m of brake block and fastenings, including 1/3 the weight of the spring (6), and the spring of stiffness $k = 1000$ lb/in. With this system the vibrator was run at 30 cycles per sec (cps).

The brake block, 1/4 in. thick, 1/2 in. long (in the direction of motion), and 3/4 in. wide, is screwed to a bolt extending from the center of the spring through a 1/16-in. hole in the block. The center of this hole is located 3/32 in. from the rubbing surface to minimize rocking. After suitably locating the aluminum plate the brake block moved back and forth without rocking or twisting. Before running in, noticeable twisting about a vertical axis sometimes occurred because of a variation in coefficient of friction across the width of the block.

The vibration was observed by means of resistance-wire strain gages cemented to the spring at points of maximum flexure. Four SR-4 strain gages (Type C-7, res. 495 ohms, gage factor 3.25), two on each side of the spring, were connected in the form of a Wheatstone-bridge circuit. A d-c potential of 15 to 20 volts was connected across one diagonal of the bridge and a cathode-ray oscilloscope across the other. The sensitivity of this extensometer was 15.8 lb per in. vertical deflection on the oscilloscope.

The photographs of the oscilloscope trace show a horizontal row of points, located approximately on the line of zero spring deflection, which were obtained from a commutator (not shown in Fig. 4) that short-circuited the oscilloscope every 30 deg. The points marked 0 deg and 180 deg, Fig. 6(a), correspond to the end points of the stroke. These points, used to determine the phase of the vibration, were particularly necessary since the sweep velocity was not constant but decreased noticeably from left to right.

The friction force F, at a given point, was calculated from a number of oscillograms with the aid of Equation [2]. The spring force, kx_s, is proportional to the oscilloscope deflection and was measured on photographic enlargements. The block acceleration $\ddot{x} = w_0^2 r \cos\theta - \ddot{x}_s$. The first term is the acceleration of the vibrator. The second term $\ddot{x}_s = KV^2 d^2Y/dX^2$, where dY/dX is the slope of the curve at a given point, $V = dX/dt$, the sweep velocity on the enlargement, and K is the ratio of unit extension of the spring to unit deflection Y, measured on the enlargement.

The corresponding block velocity $\dot{x} = w_0 r \sin\theta - \dot{x}_s$. The first term is the velocity of the vibrator, and $\dot{x}_s = KVdY/dX$.

The leaf-spring extensometer clearly shows the form of the vibrations which are persistent in the presence of Coulomb friction but transient in forced vibration without friction. To simplify the calculations and provide higher sliding velocities, a more rigid extensometer was constructed from a thin-walled aluminum tube. The stiffness of this device was about 60,000 lb/in. in the longitudinal direction, and the vibrations were longitudinal at a natural frequency of about 4500 cps. Fig. 5 shows the extensometer E, attached at one end to the piston P, and at the other end to the brake block B, through the rod R; L is the loading plate, of aluminum, steel, or lead, used to vary the vibrating mass as well as to distribute the load hung from the piano wire W.

Four SR-4, Type C-7 strain gages G were cemented around the tube and connected as before in the form of a Wheatstone-bridge

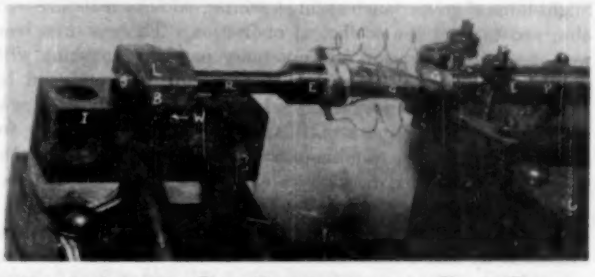

Fig. 5 Aluminum-Tube Extensometer and Brake Block
(P, piston; E, extensometer; G, strain gages; R, fastening rod; B, brake block; L, loading plate; W, piano wire; I, cast-iron base, water-cooled.)

circuit. Maximum sensitivity was obtained by cementing two of the gages longitudinally, i.e., parallel to the axis of the tube, and two transversely around the circumference of the tube. With 30 volts across the bridge the sensitivity was 25.5 lb per in. vertical deflection on the oscilloscope. With this extensometer the vibrator eccentric could be increased to 1/4 in. and the vibrator could be run at frequencies up to 57.5 cps, providing rubbing velocities up to 7 1/2 fps.

In the oscillograms obtained with this extensometer the frictional vibrations are small enough that the average value of the vertical deflection $\bar{x}_s$ can be obtained with reasonable accuracy. These values lie near a point of inflection where $\ddot{x}_s \approx 0$, so that $F = k\bar{x}_s - mw_0^2 r \cos\theta$. In some of these oscillograms commutator points were obtained at 0 deg and 180 deg by unbalancing the bridge a known constant amount, which served to calibrate the sensitivity in addition to locating the angle θ.

The effect of temperature on the coefficient of friction and the frictional vibrations was observed by using a hollow base which could be cooled by tap water or allowed to heat by friction, which often was sufficient to heat the base to 500 F. Tempera-

tures were measured with a thermocouple inserted in a small hole in the side of the base just below the rubbing surface. The observed temperature was somewhat less than that of the rubbing surfaces but provided a lower limit. By this means the effect of temperature and velocity could be observed independently.

Observations of stick-slip motion were made by gearing down the vibrator to provide low sliding velocities. Over a short distance at any part of the stroke the velocity is practically constant. Stick-slip motion of large amplitude usually occurred near the ends of the stroke but disappeared toward the center of the stroke. Stick-slip motion was observed either with a strain recorder or by high-speed strip-film photography of the transient oscilloscope trace produced during slip.

Results

Before reproducible measurements could be made it was necessary to run in the brake block for several minutes to remove surface films. In the study of the friction of metals (7) extreme cleanliness is required for reproducible results. It is particularly important to prevent the formation of films of grease or organic materials. When friction is measured in the atmosphere, films of oxide (7) and moisture (8) are always present to some extent. In fact, the existence of the phenomenon of friction depends on the presence of some such films. When really clean (outgassed) metals (9, 10) are tested in a vacuum the microscopic areas of real contact adhere so firmly that the original surfaces are virtually destroyed and sliding becomes difficult if not impossible.

Cleanliness is equally important in the study of composite friction materials, even though they consist of a somewhat heterogeneous mixture of rubber and/or resin binders, carbon, sulphur, asbestos fiber, catalysts, metal particles, mineral fillers, and so on. Slight films of grease (such as fingerprints), oxide, or moisture were observed to alter the coefficient of friction. The cast-iron base was cleaned by abrasion on fine emery paper or polishing with rouge and water. The brake-block surface was prepared by grinding with a low-speed emery wheel. When the vibrator was first started the friction was usually less than after running for several minutes. The running-in process was aided by wetting the rubbing surfaces with distilled water which served to wash away the wear particles and expose the freshly cleaned surface.

Fig. 6(a) shows the oscillogram observed with the leaf-spring extensometer and a resin-and-rubber-bonded block after running in until dry. The natural frequency of this system was 348 cps. The exposure for this photograph was $^1/_{10}$ sec so that three traces are shown superposed. The temperature near the rubbing surfaces, not measured in this test, was probably about 200 F.

Fig. 7(a) shows the coefficient of friction as ordinates and the block velocities at the corresponding points as abscissas calculated from Fig. 6(a) by the method just described. The coefficient of friction is independent of block velocity within the limits of experimental error. A possible increase in friction at zero velocity is not shown but measurement at low vibrator speeds (see below) showed that it usually was small.

Fig. 6(b) shows the motion occurring when the same block was damp but not wet with water. The vibration amplitude is about the same as before but the average deflection from the zero line is somewhat greater. Fig. 7(b) shows that the coefficient of friction has increased from 0.45 to 0.55 in average.

Fig. 6(c) shows the motion immediately after wetting the same block with water. The vibration amplitude increases rapidly during the stroke. Fig. 7(c) shows the coefficient of friction versus block velocity. The water, probably a water film between the brake block and base, has lowered the friction greatly and produced a falling friction characteristic. A similar result was obtained with lubricating oil; the coefficient of friction dropped to about 0.1, but the frictional vibrations increased.

It is worth noting that even with the violent vibration shown in Fig. 6(c) the velocity of the block is nowhere reversed. At the point of maximum slope (point p, at about 118 deg) the two terms in the velocity equation are equal and give the point at zero velocity in Fig. 7(c).

These results, with minor variations, are typical of all friction materials tested. The 20 per cent or so increase in friction of a damp over a dry block illustrates the phenomenon known as "water sensitivity." The 60 per cent average decrease in friction when the block is wet [which causes at least 80 per cent (11) loss of effectiveness in a self-actuating brake] illustrates the almost com-

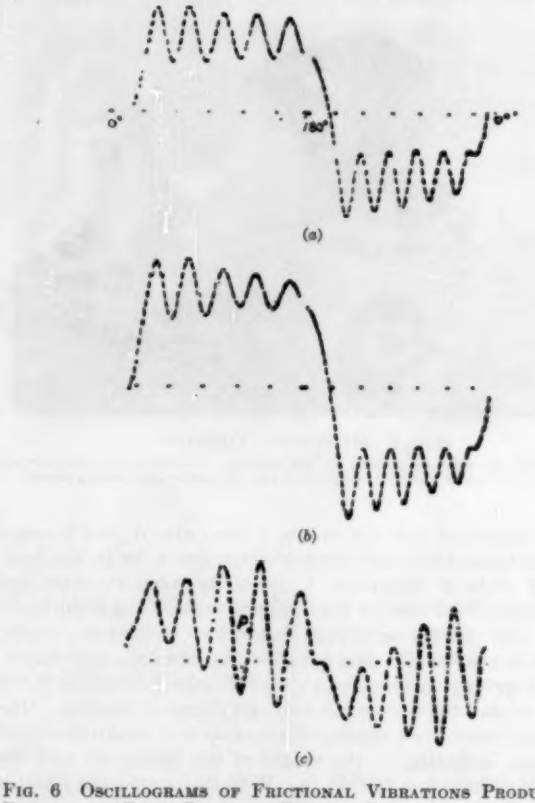

Fig. 6 Oscillograms of Frictional Vibrations Produced by Rubber-and-Resin-Bonded Brake Block for Different Moisture Conditions

(Natural frequency, 348 cps. Vibrator or sweep frequency, 30 cps. a, Dry, observed frequency, 348 cps; b, damp, observed frequency, 348 cps; c, wet, observed frequency, 311 cps.)

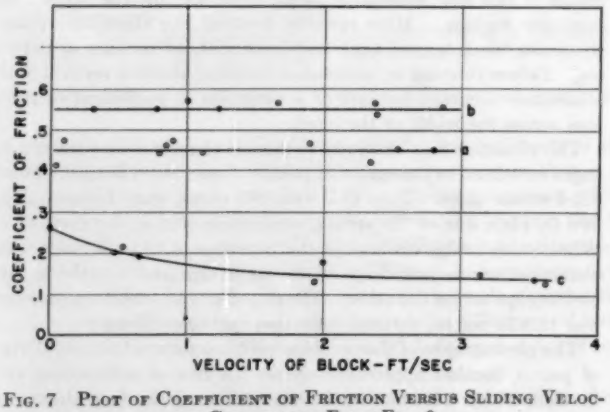

Fig. 7 Plot of Coefficient of Friction Versus Sliding Velocity Calculated From Fig. 6

(a, Dry block; b, damp block; c, wet block.)

plete loss of brakes when soaked with rain. Furthermore, the increased frictional vibration shows why wet brakes may be more noisy than dry brakes even though much less effective.

The wet block illustrates the general effect of a negative damping constant (1) in producing self-excited vibrations in which the amplitude increases with time. The vibration frequency in Fig. 6(*c*) is 311 cps, considerably less than the natural frequency of 348 cps observed in Figs. 6(*a*) and 6(*b*). This is another well-known effect of negative damping (1).

The opposite effect of positive damping was observed by "lubricating" the brake block with a small amount of soap or fatty acid. In many cases the frictional vibrations were almost completely damped, even though the average coefficient of friction was not reduced. Fig. 8(*a*) shows the vibrations of a dry, rubber-bonded block at a natural frequency of about 560 cps; Fig. 8(*b*), the result of lubrication with Ivory soap plus a little glycerine. Fig. 9 shows the coefficient of friction versus block velocity calculated from Fig. 8. It is evident that the vibration has been damped by a coefficient of friction which increased with velocity.

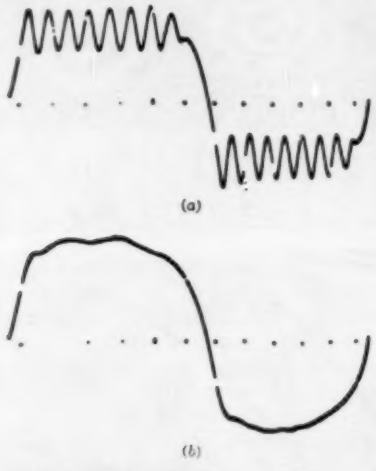

FIG. 8 OSCILLOGRAMS OF LOW-FREQUENCY FRICTIONAL VIBRATIONS SHOWING DAMPING BY SURFACE TREATMENT
(Natural frequency, 560 cps. Sweep frequency, 30 cps. *a*, Dry block; *b*, same block lubricated with soap and glycerine.)

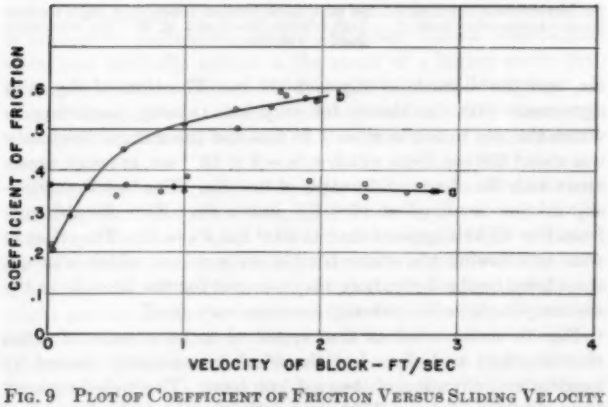

FIG. 9 PLOT OF COEFFICIENT OF FRICTION VERSUS SLIDING VELOCITY FROM FIG. 8
(*a*, Dry block; *b*, block lubricated with soap and glycerine.)

The aluminum-tube extensometer gave essentially similar results although it did not show the form of the frictional vibrations. A large number of friction materials was measured, as well as a few types of wood and some plastics such as nylon and bakelite. The results showed that for clean, dry materials the coefficient of friction was nearly constant for velocities up to $7^1/_2$ fps, except that the static friction was often somewhat greater. An increase in temperature to about 500 F usually lowered the coefficient of friction slightly and decreased the frictional vibrations by decreasing the static friction relative to the sliding friction.

Fig. 10(*a*) shows the vibration observed with the aluminum-tube extensometer using a third type of dry brake block at a temperature of 140 F and a vibrator frequency of $57^1/_2$ cps. The frictional vibrations have a much lower amplitude than those observed with the leaf spring and they are damped out during each stroke. The calculated coefficient of friction was constant at 0.45.

Fig. 10(*b*) shows the effect of allowing the block to heat to 450 F. The frictional vibrations are slightly reduced and the coefficient of friction decreased to 0.40. This illustrates the phenomenon known as "fade," a loss in friction caused by high temperature occurring when brakes are applied at high velocity.

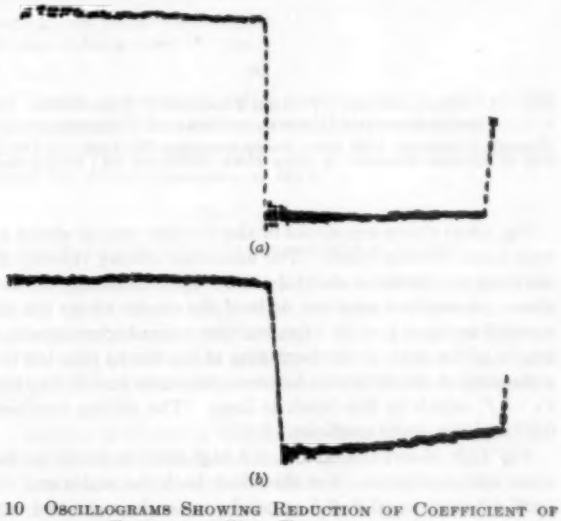

FIG. 10 OSCILLOGRAMS SHOWING REDUCTION OF COEFFICIENT OF FRICTION AT HIGH TEMPERATURE
(Natural frequency, 4500 cps. Sweep frequency, $57^1/_2$ cps. *a*, Dry block at 140 F; *b*, dry block at 450 F.)

Fig. 11(*a*) shows the violent frictional vibrations sometimes observed with a dry brake block when the coefficient of friction varies inversely with velocity. The vibrator frequency was $57^1/_2$ cps, and the eccentric $^1/_4$ in. The coefficient of friction decreased gradually from 0.5 at rest to 0.43 at 4 fps and remained at 0.43 up to $7^1/_2$ fps.

Fig. 11(*b*) shows the effect of lubricating the same block with lithium stearate. Here the vibrator eccentric was $^1/_8$ in. to avoid excessive local heating and abrasion of the rubbing surfaces. The measured temperature was 340 F, about the maximum allowable for vibration elimination. Further heating or abrasion greatly reduced the damping effect of soap and fatty acid. Furthermore, when too hot, these substances behaved more like true lubricants and greatly reduced the coefficient of friction. Such materials proved to be of no practical value for the elimination of brake squeal in automotive brakes where high temperatures, severe abrasion, and surface contamination are unavoidable.

More detailed observation of the friction at low velocity was made by running the vibrator at very low speeds, using the leaf-spring extensometer. Fig. 12 shows the stick-slip motion of brake blocks as reproduced on the circular chart of a Baldwin-Southwark strain recorder.

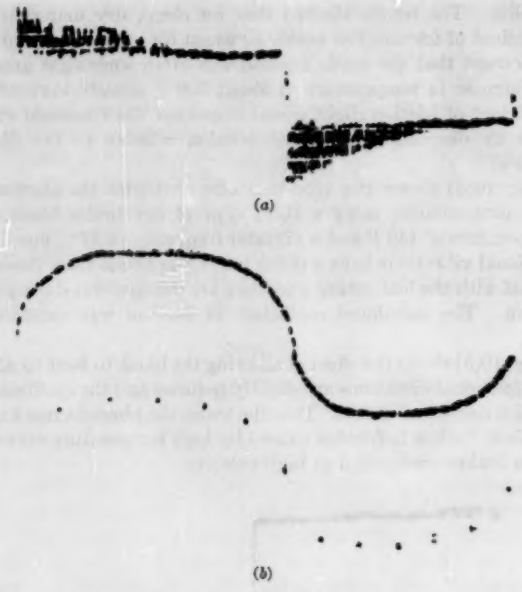

FIG. 11 OSCILLOGRAMS OF HIGH-FREQUENCY FRICTIONAL VIBRATIONS SHOWING DAMPING BY SURFACE TREATMENT
(Natural frequency, 4500 cps. Sweep frequency 57½ cps. *a*, Dry block, 0.25 in. vibrator eccentric; *b*, same block lubricated with lithium stearate, 0.125 in. eccentric.)

Fig. 12(*a*) shows one stroke of the vibrator run at about 1 rpm with a low friction block. The maximum sliding velocity at the center of the stroke is about 2×10^{-3} fps. Stick-slip motion becomes pronounced near the ends of the stroke where the sliding velocity is about 4×10^{-3} fps, but dies out at higher speeds. The height of the peak at the beginning of the stroke (the left end) is a measure of the difference between the static and sliding friction $F_0 - F$, which in this block is large. The sliding coefficient is 0.25 and the static coefficient 0.37.

Fig. 12(*b*) shows the motion of a high-friction block under the same test conditions. For this block both the static and sliding coefficient are equal to 0.5 as nearly as can be measured, and no true stick-slip motion occurs until near the end of the stroke. This result is in general agreement with the predictions of the theory for equal static and sliding coefficients and low velocity. The oscillations are quickly damped out by natural damping and the block then moves with the velocity of the driver. Throughout most of the stroke the motion is irregular, due probably to variations in the real contact area over the rough surface of the block. It has been shown (12, 13) that the real area of contact is less than one per cent of the apparent area. Even the smoothest surfaces are rough compared to molecular dimensions; hence contact occurs only at microscopic high spots and continually shifts from one set of high spots to another as sliding proceeds. Such variations would be pronounced over the inhomogeneous surface of a brake block.

Fig. 12(*c*) shows the stick-slip motion obtained by running the same block, as in Fig. 12(*b*), at about $^1/_{12}$ rpm, giving a maximum sliding speed of about 2×10^{-4} fps. The portion of the chart shown is near the beginning of the stroke where the velocity is about 3×10^{-5} fps. The time between slips is about 2 sec. The duration of the slip itself cannot be determined because the chart shows the much longer response time of the recorder.

The duration of the slip was measured with an Edgerton strip-film camera at about 15 fps film speed. Fig. 13 shows the slip observed with the same high friction block under the same test conditions as in Fig. 12(*c*). The duration of the slip is 6×10^{-4} sec, and the distance of slip is 0.001 in. The time of slip is in agreement with the theory for very low velocity, according to which the slip time $t \approx \pi/w$. In this test the natural frequency was about 600 cps, from which $\pi/w = 8 \times 10^{-4}$ sec, in rough agreement with the observed duration of the slip. The fact that stick-slip motion occurred at 10^{-4} fps shows that $F_0 > F$, although from Fig. 12(*b*) it appears that at 10^{-3} fps, $F_0 = F$. The effect of time in allowing the static friction to increase, which was not considered in the derivation, may account for the increase in the slip amplitude as the velocity becomes very small.

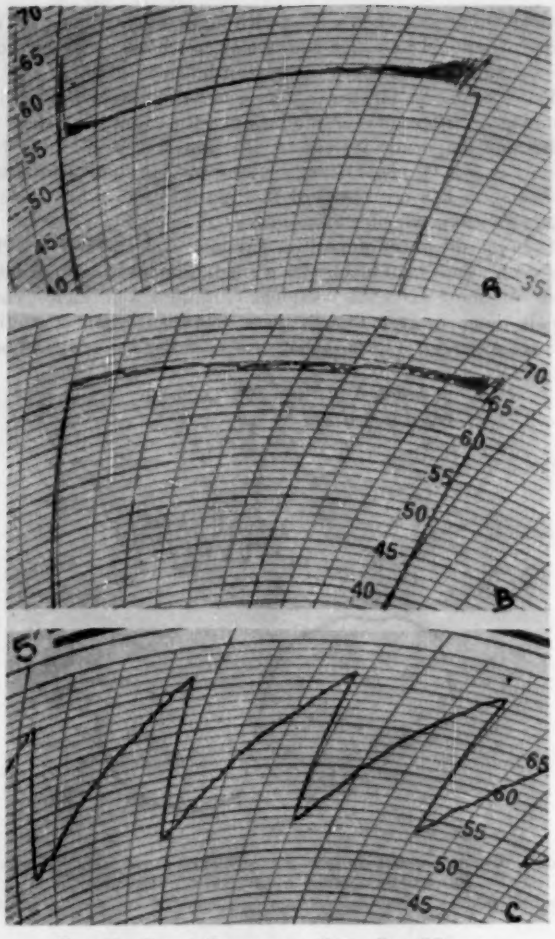

FIG. 12 CHART RECORDS OF STICK-SLIP MOTION
(*a*, Low-friction block at 0.1 fps maximum applied velocity; *b*, high-friction block—same velocity as *a*; *c*, high-friction block at 2×10^{-4} fps maximum applied velocity.)

Fig. 13 shows what at first appeared to be a series of much shorter sticks and slips, but the effect was actually caused by longitudinal vibration of the cast-iron base. The high-frequency base vibration (about 7000 cps) is initiated at the instant of breakaway and carries the block backward at the beginning of the slip. The base vibration continues during the slip and persists far into the stick period.

Base vibration frequently occurred while running the vibrator at the higher speeds. The frequency of the base vibration, measured by amplifying the sweep length, was sometimes as high as 16,000 cps. This type of vibration commonly occurred with high friction blocks, particularly when the static coefficient was appreciably higher than the sliding coefficient. It frequently could be eliminated or minimized by careful adjustment of the position of the load on the brake block.

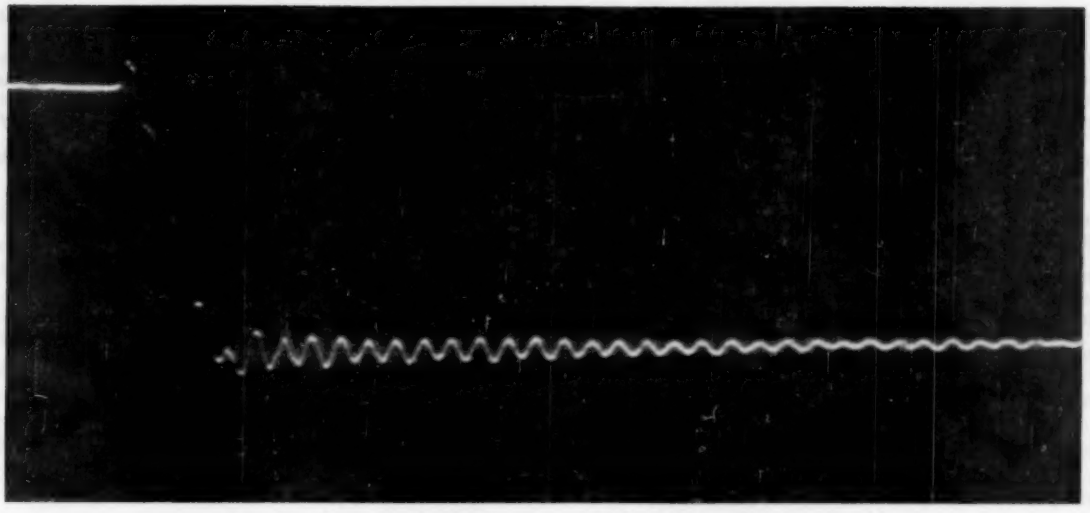

FIG. 13 OSCILLOGRAM OF STICK-SLIP MOTION AND BASE VIBRATION
(Strip-film photograph at 15 fps film speed. Applied velocity about 10^{-4} fps.)

DISCUSSION

The observations show the great variety of frictional vibrations possible from the interaction of the frictional and mechanical properties of rubbing solids. These results were obtained without reference to the cause of the phenomenon of friction itself. It is apparent that whether friction is caused by adhesion (2) at the real areas of contact or by lifting over the microscopic surface irregularities (14, 15), the macroscopic effects are greatly dependent upon the relative velocity, natural frequency, and damping of the rubbing bodies.

It has been suggested (16) and disputed (17) that stick-slip motion in metals is the cause of higher static than sliding friction because the high-velocity slip melts the microscopic areas of contact forming welds at each stick. However, this mechanism cannot explain the observed stick-slip in brake linings where welding is impossible, particularly at low velocities. These observations show that stick-slip motion is the result of a higher static than sliding friction sufficient to overcome natural damping. If natural damping were absent, stick-slip motion would occur even with constant friction because of the dynamics of an elastic system.

The present work provides no explanation of why the static friction is greater than the sliding friction or why the sliding friction sometimes decreases with velocity and sometimes is constant. As indicated in the foregoing (4), there is evidence that time is required for the static friction to develop. A similar explanation might account for the inverse variation with velocity; the surface adhesions decrease and/or the surfaces tend to ride higher on their irregularities because of the short contact time at high velocity. In the case of brake lining at high velocity, the rubbing surfaces are greatly altered by abrasion and high temperature which could readily account for any observed decrease in friction with velocity.

Whatever the cause of the excess static friction coefficient, it is sufficient to account for frictional vibrations, particularly squeal in automobile brakes where the loads are great. When the load is large, even a small decrease in the friction coefficient produces a large decrease in the friction force. For example, at a total normal load on the lining of 1000 lb (50 psi on a lining 10 in. long $\times$ 2 in. wide) a 10 per cent decrease in friction coefficient from 0.5 to 0.45 would cause a decrease in friction force of 50 lb. This is an unbalanced force which accelerates the relative motion whenever sliding begins, in particular, after every period of stick during vibration. Once a vibration is initiated, this intermittent force is applied once each vibration cycle and in the right direction to maintain the vibration.

CONCLUSIONS

The results obtained may be summarized as follows:

1 Frictional vibrations, such as automobile-brake squeal, are caused by an inverse variation of coefficient of friction with sliding velocity, usually a higher static than sliding coefficient.

2 The type of vibration and its occurrence are greatly influenced by the dynamical properties of the mechanical system involved.

3 Constant or Coulomb friction produces no damping of the vibrations initiated whenever sliding begins.

4 Frictional vibrations may be eliminated or reduced by treating the rubbing surfaces to produce a coefficient of friction that varies directly with velocity. Although this method was effective in the laboratory, it was ineffective in eliminating brake squeal because of abrasion and high temperature which destroyed the surface treatment of brake linings.

5 The coefficient of friction of most brake linings and other organic materials in the clean, dry condition is essentially constant over all sliding velocities up to $7\frac{1}{2}$ fps. At zero velocity the static coefficient is usually somewhat greater than the sliding coefficient.

6 The phenomenon known as fade, a decrease in friction observed at high velocity, is caused by the high temperatures developed at high velocity rather than by the high velocity itself.

ACKNOWLEDGMENT

It is a pleasure to acknowledge the assistance of Dr. Paul Greebler in the mathematical analysis and of Mr. E. G. Apgar (no longer in this laboratory) and Mr. Walter Gulick in performing the experiments.

BIBLIOGRAPHY

1 "Mechanical Vibrations," by J. P. den Hartog, McGraw-Hill Book Company, Inc., New York, N. Y., third edition, 1947.

2 "The Friction and Lubrication of Solids," by F. P. Bowden and D. Tabor, Oxford University Press, New York, N. Y., 1950, chapter 5.

3 "X. Studies in Lubrication. Friction Phenomena and the

Stick-Slip Process," by F. Morgan, M. Muskat, and D. W. Reed, *Journal of Applied Physics*, vol. 12, 1941, pp. 743–752.

4 "XII. Studies in Lubrication. Friction Behavior During the Slip Portion of the Stick-Slip Process," by J. B. Sampson, F. Morgan, D. W. Reed, and M. Muskat, *Journal of Applied Physics*, vol. 14, 1943, pp. 689–700.

5 "The Nature of the Static and Kinetic Coefficients of Friction," by Ernest Rabinowicz, *Journal of Applied Physics*, vol. 22, 1951, pp. 1373–1379.

6 "Mechanical Springs," by A. M. Wahl, Penton Publishing Company, Cleveland, Ohio, 1944, p. 233.

7 Reference (2), chapter 4.

8 "Surface Deformation and Friction of Metals at Light Loads," by J. R. Whitehead, Proceedings of the Royal Society, London, England, series A, vol. 201, 1950, pp. 109–124.

9 Reference (2), chapter 7.

10 "Electric Contacts," by R. Holm, Hugo-Gebers vörlag, Stockholm, Sweden, 1946.

11 "Self-Actuating Brakes," by David Sinclair, unpublished report.

12 "The Area of Contact Between Stationary and Between Moving Surfaces," by F. P. Bowden and D. Tabor, Proceedings of the Royal Society, vol. 169, pp. 391–413; also, Reference 2, chapter 1.

13 "Graphite Lubrication," by R. H. Savage, *Journal of Applied Physics*, vol. 19, 1948, pp. 1–10.

14 "Surface Roughness and Sliding Friction," by J. J. Bikerman, *Reviews of Modern Physics*, vol. 16, 1944, pp. 53–68.

15 "On the Magnitude of the Mechanical Component of Solid Friction," by C. D. Strang and C. R. Lewis, *Journal of Applied Physics*, vol. 20, 1949, pp. 1164–1167.

16 "The Nature of Sliding and the Analysis of Friction," by F. P. Bowden and L. Leben, Proceedings of the Royal Society, vol. 169, 1939, pp. 371–390.

17 "Static Coefficient of Friction and Area of Contact," by R. C. Parker and D. Hatch, Proceedings of the Physical Society of London, England, series B, vol. 63, 1950, pp. 185–197.

A Kinematic Notation for Lower-Pair Mechanisms Based on Matrices[1]

By J. DENAVIT[2] and R. S. HARTENBERG,[3] EVANSTON, ILL.

A symbolic notation devised by Reuleaux to describe mechanisms did not recognize the necessary number of variables needed for complete description. A reconsideration of the problem leads to a symbolic notation which permits the complete description of the kinematic properties of all lower-pair mechanisms by means of equations. The symbolic notation also yields a method for studying lower-pair mechanisms by means of matrix algebra; two examples of application to space mechanisms are given.

Introduction

An approach to the problem of rationalizing kinematics into a science by means of a symbolic language was proposed by Reuleaux (2, 3)[4] in 1875. It was his hope that a symbolic language would permit a complete description of the kinematic properties of a mechanism, and that this would be additionally useful not only for the analysis of existing mechanisms but also for the synthesis of new mechanisms. Unfortunately, the symbolism that he devised did not include all variables needed for a complete description of a mechanism, and this limited its usefulness. However, Reuleaux did give several concepts that appear to be fundamental. When exploited, these concepts lead to a manipulative symbolic notation. This notation gives the data necessary for deriving the relative displacements in any lower-pair mechanism. This description is in the form of a symbolic equation, the terms of which are shown to be equivalent to matrices. It is from these matrices that the manipulative properties derive.

The mechanisms to be discussed here are formed from a succession of rigid parts coupled end to end to form a single closed chain. When the motion of each part is constrained or guided in unique fashion the purpose of the mechanism is to transform one motion into another, as the transformation of the linear motion of a piston engine into a continuous circular motion. The connections permitting relative motion are made by means of contact between adjacent boundary surfaces of the parts. The designing of mechanisms consists of finding the proper combination of parts so proportioned that the given input motion yields a desired output motion.

Since the connections are made by the contact of adjacent boundary surfaces, two surfaces will be involved in any connection. One surface lies on one part, and one surface lies on the adjacent part. Taken together, these two surfaces are called a pair, i.e., pairs of contact surfaces, each surface being called one element of the pair. If the mutual contact is made by two mating surfaces, sliding with respect to each other, they then constitute a lower pair. If the mutual contact is confined to a line (as in rollers, cams, or gear teeth) or to a point (as in ball bearings), this then constitutes a higher pair.

Because of their apparent relative simplicity, lower pairs have been studied first. The only possible lower pairs are the following:

1 The spheric pair, as a ball-and-socket joint. It allows a rotation about each of three rectangular axes.

2 The plane pair. It allows two translations along the axes defining the plane and a rotation about an axis perpendicular to the plane.

3 The right circular cylinder pair, or cylindric pair. It allows a rotation about the cylinder axis and a translation along the axis.

4 The screw pair. It gives rise to a helical movement in terms of the fixed axial advance per revolution, or lead.

5 The revolute pair. Both contact surfaces are defined as surfaces of revolution, generated by any profile. It allows a rotation about its axis.

6 The prismatic pair or prism pair. Both contact surfaces are cylinders other than the right circular. It allows a translation parallel to a generatrix.

Reuleaux noted that the revolute pair and the prismatic pair represent limiting cases of the screw pair: When the lead of the screw pair becomes zero, a revolute pair results; when the lead becomes infinite, a prismatic pair results. It also may be remarked that each of the three pairs is completely defined with respect to a system of co-ordinates by its axis; in the case of a prismatic pair the axis is an arbitrary line parallel to a generatrix. It will be convenient to use and exploit the symbol S_L to represent a screw pair of lead L. In addition, it will be convenient to indicate the variable u needed to define the unique possible motion, thus $S_L(u)$ where u is either the angle of rotation or the equivalent advance. The symbol for a revolute (pair) may be written $S_0(u)$, but it will simplify the notation to designate the revolute by $R(u)$. Similarly, the symbol for a prism (prismatic pair) may be written $S_\infty(u)$, but to write $P(u)$ will be simpler. No symbols are needed for the spheric pair, the right circular cylinder pair, or the plane pair, for each of these is formed from and described by the appropriate revolute and/or prism pairs needed to give the motion.

Unfortunately, there is no accepted standard nomenclature for kinematics. The names may seem stilted but there is an association between the name and the symbol of the pair by considering the nature of the contact. This is more or less true for English, French, and German, as Grodzinski (4) points out.

The two elements of a pair are distinguished by two additional symbols: $S_L{}^+$ means the element given by the surface of the screw, or the full body; and $S_L{}^-$ means the element that is the

---

[1] The results presented in this paper were obtained in the course of research sponsored by the Office of Naval Research (1).[4]

[2] Graduate Student, The Technological Institute, Northwestern University.

[3] Associate Professor of Engineering Mechanics, The Technological Institute, Northwestern University. Mem. ASME.

[4] Numbers in parentheses refer to the Bibliography at the end of the paper.

Contributed by the Applied Mechanics Division and presented at the Annual Meeting, New York, N. Y., November 28–December 3, 1954, of The American Society of Mechanical Engineers.

Discussion of this paper should be addressed to the Secretary, ASME, 29 West 39th Street, New York, N. Y., and will be accepted until July 11, 1955, for publication at a later date. Discussion received after the closing date will be returned.

Note: Statements and opinions advanced in papers are to be understood as individual expressions of their authors and not those of the Society. Manuscript received by ASME Applied Mechanics Division, December 14, 1953. Paper No. 54—A-34.

nut, or hollow body. The positive and negative signs are used for the element designations of other pairs as well.

Development of the Symbolic Notation

The position of a screw-pair element in a machine part is determined by the position of its axis. The position of the axis may be described in a number of ways, and the apparent number of parameters needed depends on the manner of the description. Thus the line L of Fig. 1 passing through the point $P(x, y, z)$ needs the angles β and γ to complete the description, and it would seem that five parameters constitute the necessary and sufficient number. However, the line also could be defined by the equations $x = Az + B$ and $y = Cz + D$, and here four coefficients suffice.

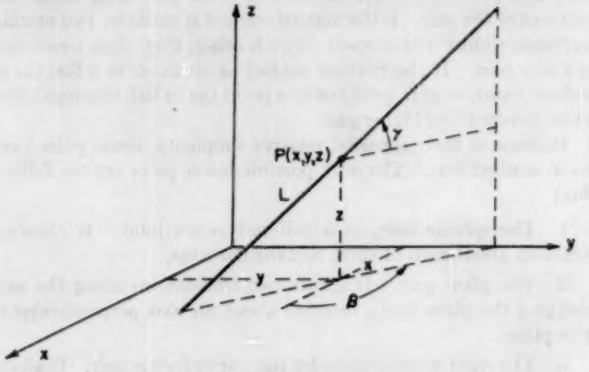

Fig. 1 Parameters x, y, z, β, and γ Defining Line L

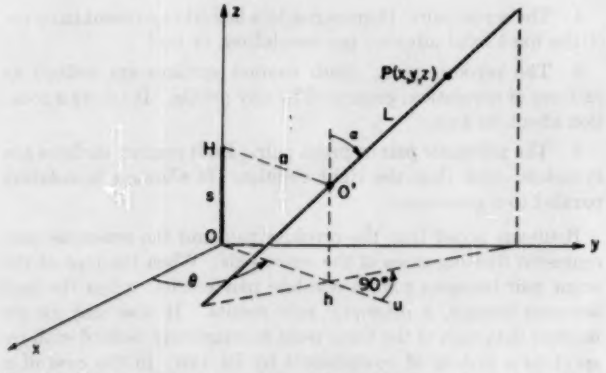

Fig. 2 Parameters a, α, θ, and s Defining Line L, or Axis of a Screw or Revolute Pair

Turning to Fig. 2, the description is based on the use of the unique common perpendicular HO' of length a between Oz and the line L. The angle θ lies between Ox and the common perpendicular, s is the distance from O to H, and α the angle between Oz and L.

Again there are four parameters, and that they are sufficient to define a unique line in the x, y, z-co-ordinate system may be demonstrated by supposing the angle θ given, Fig. 2. The line Ou is then drawn in the xy-plane, and the distance a laid off from O defines the point h. A perpendicular at h of length s defines O'. The plane perpendicular to Oh and containing O' is unique, and in this plane only one straight line L will have an angle α with hO'. The line L or the axis of a screw pair is therefore completely determined by a, α, θ, and s. The axis of a revolute pair also is determined completely by the same four parameters.

Since the axis of a prism pair is an arbitrary line parallel to a generatrix, it may be chosen as going through the origin ($a = 0$, $s = 0$) as shown in Fig. 3. The direction of the axis is then determined completely by θ and α.

A description of a mechanism will involve a description of the relative positions of the successive-pair axes, and this may be done by use of the unique common perpendicular between successive pair axes. The manner of describing the relative positions of successive-pair axes is given by Fig. 4 which depicts two machine parts from a space mechanism. The two parts are connected by the complete revolute pair R_1 with the revolute elements R_0^+ and R_2^- showing where connections are made to the rest of the mechanism. The axes z_0, z_1, and z_2 define the space positions of the revolutes chosen for the illustration but they equally well would define the locations of screw or prism pairs. The axis x_1 is chosen as an extension of the common perpendicular of length a_0 between z_0 and z_1. The axis y_1 is chosen to give a right-handed rectangular system. Similarly, x_2 is the extension of the common perpendicular of length a_1 between z_1 and z_2 with y_2 completing a right-handed system. The position of the pair element R_2^- is thus defined completely with respect to the pair R_1 by the four parameters a_1, α_1, θ_1, and s_1.

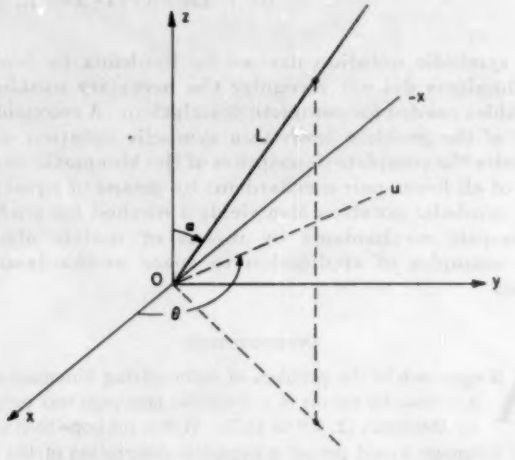

Fig. 3 Parameters α and θ Define Line L or Axis of a Prism Pair ($a = 0$, $s = 0$)

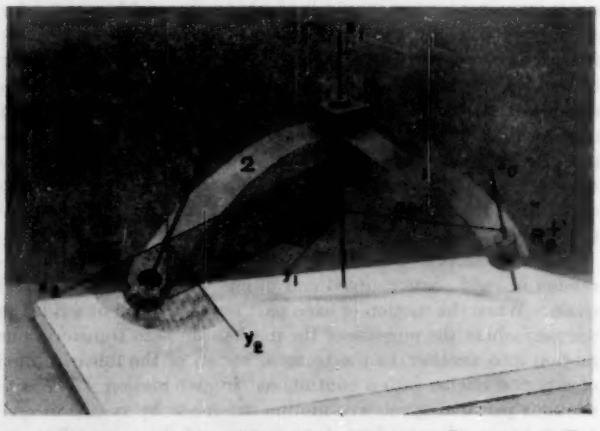

Fig. 4 Parts of a Space Mechanism, Showing Parameters Relating Axes of Three Pairs

A compact way of writing the defining relations between the pair elements of a machine part is to assemble all the data in a block, as shown in Fig. 5. This represents part 2 of Fig. 4. Part 1

cannot be described since the parameters θ_0 and s_0 are dependent on part 0 which precedes part 1.

As an example of how a complete plane mechanism composed of only revolute and prism pairs may be described, consider the slider crank of Fig. 6. The four machine parts are identified for convenience as 1, 2, 3, and 4; they are connected as shown by the pairs P_1, R_2, R_3, and R_4. Each of the parts will be completely described if the geometry of its ends, i.e., its pair elements, is given. The description of the parts leads to a description of the complete mechanism.

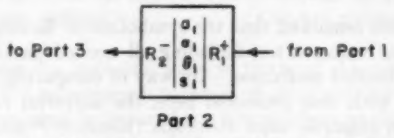

FIG. 5 BLOCK DIAGRAM FOR PART 2 OF FIG. 4

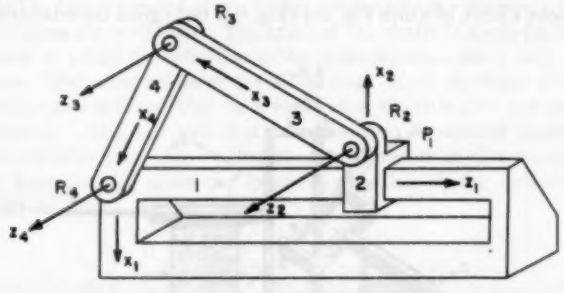

FIG. 6 SLIDER-CRANK MECHANISM, SHOWING PAIRS AND AXES

The location of the prism P_1 is described by the direction of its axis z_1; the revolutes R_2, R_3, and R_4 are described by the location of their axes z_2, z_3, and z_4. In the symbolic description of the mechanism, the angles between successive z-axes is given by α. For the present mechanism the angle between z_1 and z_2 is 90 deg or $\alpha_1 = 90$ deg; the angle between z_2 and z_3 is zero, or $\alpha_2 = 0$; the angle between z_3 and z_4 is also zero, or $\alpha_3 = 0$; and the angle between z_4 and z_1 is 90 deg or $\alpha_4 = 90$ deg.

These angles α are not sufficient for a complete description; obviously certain lengths and other angles are necessary. To find the missing parameters it will be necessary to show the x-axes. The axis x_1 is defined in the machine part 1 along the common perpendicular between z_4 and z_1; x_2 is defined in the part 2 along the common perpendicular between z_1 and z_2; x_3 in part 3 is along the common perpendicular between z_2 and z_3; and x_4 in part 4 is along the common perpendicular between z_3 and z_4. The y-axes are not shown, since no angles are measured from them, but they are considered present to form right-handed systems.

In a symbolic description of the mechanism the perpendicular distances between z-axes will be designated by the latter a. For the present mechanism, the distance between z_4 and z_1 is zero, or $a_4 = 0$; between z_1 and z_2 the distance is a_1; between z_2 and z_3 the distance is a_2; and between z_3 and z_4 the distance is a_3. These distances are illustrated in Fig. 7.

The angles between x-axes are designated by θ. For the present mechanism the angle between x_1 and x_2 is $\theta_1 = 180$ deg, the angles between x_2 and x_3, x_3 and x_4, and x_4 and x_1 are θ_2, θ_3 and θ_4, respectively. These last three angles are the pair variables of the revolutes; their values change with the motion of the mechanism.

The perpendicular distances between x-axes are designated by s, Fig. 7. The perpendicular distance between x_1 and x_2 is s_1, which is also the pair variable of the prism; the distances between x_2 and x_3, x_3 and x_4, x_4 and x_1 are all zero, i.e., $s_2 = 0$, $s_3 = 0$, $s_4 = 0$.

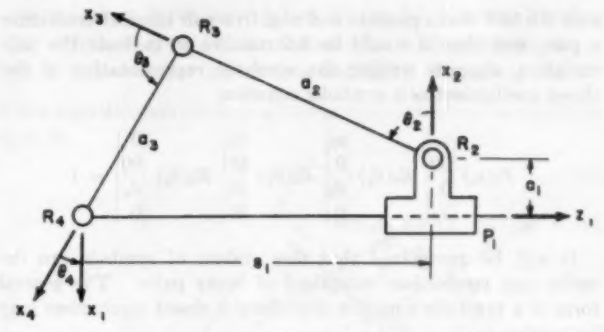

FIG. 7 SCHEMATIC OF SLIDER-CRANK MECHANISM SHOWING PAIR VARIABLES θ AND s

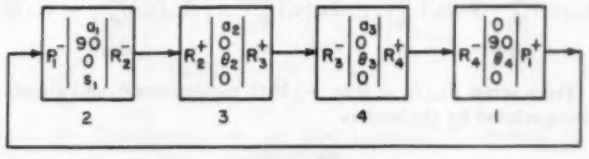

FIG. 8 BLOCK DIAGRAM REPRESENTING SLIDER-CRANK MECHANISMS OF FIGS. 6 AND 7

A representation of this mechanism is given by assembling all these data in blocks, one block to each part, as shown in Fig. 8. Each box represents a machine part; in each block are indicated its pair elements, the parameters defining the machine part itself, and the relations of the part to the preceding machine part. Since the chain of blocks so obtained forms a closed loop, it is seen that the description of the chain may be started at any pair element and may proceed in either direction.

This way of representing a mechanism is cumbersome. A more concise but equally definitive description in the form of an equation would have a manipulative property, particularly if a mathematical interpretation could be shown. Such an equation can be developed from the considerations outlined later. A rigorous justification for the arguments is given under Matrix Interpretation of the Symbolic Equation.

With the aid of Fig. 4 the relations between successive co-ordinate systems were seen to be dependent on the values of the intervening a, α, θ, and s. Such a relation is a linear transformation between the two systems involved, and each linear transformation may be represented by a matrix M; the elements of the matrix are functions of a, α, θ, and s, and each matrix represents the machine part between co-ordinate systems.

On the mechanism of Fig. 6 there are four co-ordinate systems, and hence four linear transformations (taken in succession) would give a return to the original co-ordinate system. The successive linear transformations from one co-ordinate system to another may be effected by multiplying the corresponding matrices. The product of all matrices is the unit matrix when there is a return to the original system. This is the case for a closed chain or mechanism, and for the example of the slider crank the matrix equation would be

$$M_3 \times M_2 \times M_4 \times M_1 = 1 \quad \ldots\ldots\ldots\ldots [1]^5$$

This equation contains the solution to the displacement relations of the mechanism.

The analogy between this equation and Fig. 8 lies in the fact that the matrices of Equation [1] depend on the parameters a, α, θ, and s, appearing between "verticals" in Fig. 8. This, together

[5] In this equation, and all matrix equations to follow, the symbol 1 stands for the unit matrix.

with the fact that a positive and negative-pair element constitute a pair, and that it would be informative to indicate the pair variables, suggests writing the symbolic representation of the closed mechanism as a symbolic equation

$$P_1(s_1)\begin{vmatrix}a_1\\90\\0\\s_1\end{vmatrix}\ R_2(\theta_2)\begin{vmatrix}a_2\\0\\\theta_2\\0\end{vmatrix}\ R_3(\theta_3)\begin{vmatrix}a_3\\0\\\theta_3\\0\end{vmatrix}\ R_4(\theta_4)\begin{vmatrix}0\\90\\\theta_4\\0\end{vmatrix} = 1$$

It will be recognized that this system of symbols can describe any mechanism comprised of lower pairs. The general form of a symbolic equation describing a closed mechanism may be written as

$$S_{L1}(u_1)\begin{vmatrix}a_1\\\alpha_1\\\theta_1\\s_1\end{vmatrix}\ S_{L2}(u_2)\begin{vmatrix}a_2\\\alpha_2\\\theta_2\\s_2\end{vmatrix}\ \ldots\ S_{Li}(u_i)\begin{vmatrix}a_i\\\alpha_i\\\theta_i\\s_i\end{vmatrix}\ \ldots\ S_{Ln}(u_n)\begin{vmatrix}a_n\\\alpha_n\\\theta_n\\s_n\end{vmatrix} = 1 \quad [2]$$

For a screw $S_{Li}(L_i \neq 0 \text{ or } \infty)$ both parameters θ_i and s_i vary, being related by the lead as

$$\frac{\Delta\theta_i}{2\pi} = \frac{\Delta s_i}{L_i}$$

Here $\Delta\theta_i$ and ΔS_i are the variations, and consequently either θ_i or s_i may be taken as the pair variable u_i.

For a revolute ($L_i = 0$) the parameter θ_i is the pair variable u_i; the other parameters, a_i, α_i, and s_i do not change with movement.

For a prism ($L_i = \infty$) the parameter s_i is the pair variable u_i; the other parameters a_i, α_i, and θ_i do not change with movement.

The right circular cylinder pair is equivalent to a coaxial revolute and prism and is written

$$R_1(\theta_1)\begin{vmatrix}0\\0\\\theta_1\\0\end{vmatrix}\ P_2(s_2)\begin{vmatrix}a_2\\\alpha_2\\0\\s_2\end{vmatrix}$$

The plane pair is equivalent to a combination of a revolute and two prisms at right angles to each other and the revolute axis and is written

$$R_1(\theta_1)\begin{vmatrix}0\\90\\\theta_1\\0\end{vmatrix}\ P_2(s_2)\begin{vmatrix}0\\90\\90\\s_2\end{vmatrix}\ P_3(s_3)\begin{vmatrix}a_3\\\alpha_3\\\theta_3\\s_3\end{vmatrix}$$

The spheric pair is equivalent to a combination of three revolutes whose axes are mutually perpendicular at a common point of intersection and is written

$$R_1(\theta_1)\begin{vmatrix}0\\90\\\theta_1\\0\end{vmatrix}\ R_2(\theta_2)\begin{vmatrix}0\\90\\\theta_2\\0\end{vmatrix}\ R_3(\theta_3)\begin{vmatrix}a_3\\\alpha_3\\\theta_3\\s_3\end{vmatrix}$$

The symbolic notation presented in the foregoing has been developed from the kinematic chain-and-pair-element concepts of Reuleaux by establishing the complete and sufficient mathematical description of the relations between pairs. The matrix interpretation of the data between "verticals" endows the new symbolism with an analytical power that only a mathematical procedure possesses.

The literature of kinematics seems to show no similar approach. Dimentberg (6, 7), who has worked in the same general area of lower-pair space mechanisms, has developed a method for studying displacements based on Clifford's dual numbers (taken from the realm of pure algebra). The abstracts do not mention the development of a systematic, manipulative notation generalized to all lower-pair mechanisms.

Comparison of the New Symbolism With That of Reuleaux

It has been remarked that the symbolism of Reuleaux was incomplete by reason of not including all needed parameters and hence had limited usefulness. By way of comparing Reuleaux's symbolism with that presented here, the universal joint will be taken as an example, since Reuleaux (Kennedy)[8] discusses it at some length as follows:

"We may take for a second illustration a universal joint, or Hooke's joint, of which Fig. 181 (Fig. 9 of text) gives the schematic

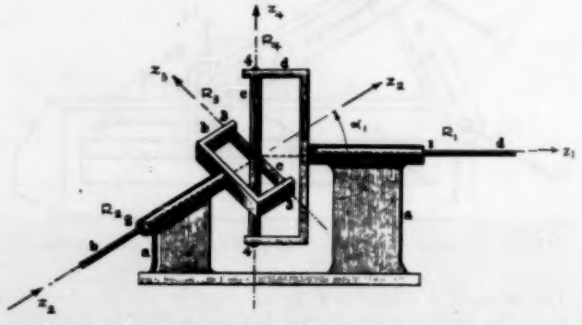

Fig. 9 Reuleaux's Fig. 181, the Universal Joint
(Pairs and axes have been identified in terms of the symbolic notation.)

representation. The chain which constitutes this joint has four links, which are marked on the figure with the letters *a*, *b*, *c*, and *d*. The link *a* is paired with *b* by the turning-pair 2. Normal to this turning-pair is another, 3, which has its open cylinder in the fork of *d* and its full cylinder in the sloping arm of the piece *c*; the link *b* must therefore be written $C^+ \ldots \perp \ldots C^-$. It must be noted that the lower and upper arms of the fork form together one piece only and must be reckoned as such; the same is true of the two ends of the arm *c*, which kinematically forms a single element only. The piece *c* consists of two solid cylinders 3 and 4, having their axes crossing at right angles, and it must therefore be written $C^+ \ldots \perp \ldots C^+$. The third link, the fork and the spindle *d*, is similar to *b* and will be written in the same way. The fourth link *a*, lastly, consists of two open cylinders, 1 and 2, oblique to each other, and so must be written $C^- \ldots \angle \ldots C^-$; it is a fixed link, as its form in the figure shows. The complete formula, therefore (to which we have added the letters and numbers that were used in the foregoing to distinguish the links and pairs), runs thus

$$\underbrace{\underset{2}{C^+}\ldots\perp\ldots\underset{3}{C^-}}_{b} = \underbrace{\underset{3}{C^+}\ldots\perp\ldots\underset{4}{C^+}}_{c} = \underbrace{\underset{4}{C^-}\ldots\perp\ldots\underset{1}{C^+}}_{d} = \underbrace{\underset{1}{C^-}\ldots\angle\ldots\underset{2}{C^-}}_{a} =$$

"There is one geometrical property of the chain which is not shown by our formula, namely, that the axes of the pairs 1, 2, 3, and 4 have a common point of intersection. But unless the chain possessed this property it would not be possible, on our supposi-

[8] Reference (2), pp. 260-261.

tion that all its pairs are closed.[7] No special indication of this property is therefore commonly necessary. Our formula shows, however, that the three links b, c, and d are again identical. This circumstance is very notable, and we shall later on have to deal with it in another form; the common construction of the joint so entirely conceals it as to make it almost unrecognizable."

Reuleaux (Kennedy)[8] remarks that "the formula or symbolic description may in many cases be greatly shortened." The shortened form he calls the contracted formula[9] says:

"The chain forming the universal joint, Fig. 181, —to take another example—allows itself to be written ($C_3^1\ C\angle$) in words, C normal three C oblique"; . . . . . (End of comment on universal joint.)

To describe the universal joint in terms of the new symbolic notation it will be necessary to establish the identities of the four pairs (all revolutes) in terms of the new symbols, as shown in Fig. 9. The z-axes are the axes of the revolutes, and it will be convenient to start numbering at one end of the frame and then proceed to the other end of the frame. Since all axes intersect, the distances a are all zero. The angle of the shafts is given by the angle α_1 which by definition is the angle between the z_1 and z_2-axes. The other angles α are all 90 deg. Each shaft (or revolute) rotation is specified by a value of θ, which is also the pair variable. The four values of s become zero because of mutual axis intersection. Assembling these parameters in the manner of Equation [2] gives the symbolic equation of the universal joint as

$$R_1(\theta_1)\begin{vmatrix}0\\ \alpha_1\\ \theta_1\\ 0\end{vmatrix} R_2(\theta_2)\begin{vmatrix}0\\ 90\\ \theta_2\\ 0\end{vmatrix} R_3(\theta_3)\begin{vmatrix}0\\ 90\\ \theta_3\\ 0\end{vmatrix} R_4(\theta_4)\begin{vmatrix}0\\ 90\\ \theta_4\\ 0\end{vmatrix} = 1 \ldots\ldots [3]$$

This symbolic equation shows all parameters needed to describe completely the universal joint in a geometric manner.

It is to be noted, Reuleaux commented, that the geometrical property of mutual axis intersection was not given in his formula, and that he could write no formula for a mechanism unless he knew beforehand that it moved. Consequently, Reuleaux's symbolism cannot be used to establish the relative displacements of the parts of a mechanism. The new symbolism obviates these shortcomings by indicating all parameters from whose relations the possibility of motion may be deduced.

Matrix Interpretation of the Symbolic Equation

The application of matrix algebra to the description of a mechanism has been outlined in the example of the slider crank. To justify that use of matrices, and to analyze the displacements occurring in a closed mechanism, each matrix must be related to its values of a, α, θ, and s. In the following, the elements of the matrix corresponding to each machine part will be established.

Consider two co-ordinate systems $x_1y_1z_1$ and $x_2y_2z_2$, Fig. 10. A point M is given by its co-ordinates x_2, y_2, z_2 with respect to $x_2y_2z_2$; the problem is to determine the co-ordinates x_1, y_1, z_1 of M with respect to $x_1y_1z_1$. The vector relation

$$\vec{O_1M} = \vec{O_1O_2} + \vec{O_2M}$$

gives by projection on the axes the following system of equations

$$\begin{aligned}
x_1 &= (x_0)_1 + x_2\cos(x_2, x_1) + y_2\cos(y_2, x_1) + z_2\cos(z_2, x_1)\\
y_1 &= (y_0)_1 + x_2\cos(x_2, y_1) + y_2\cos(y_2, y_1) + z_2\cos(z_2, y_1)\\
z_1 &= (z_0)_1 + x_2\cos(x_2, z_1) + y_2\cos(y_2, z_1) + z_2\cos(z_2, z_1)
\end{aligned}$$

These equations are nonhomogeneous with respect to the variables x_2, y_2, z_2.

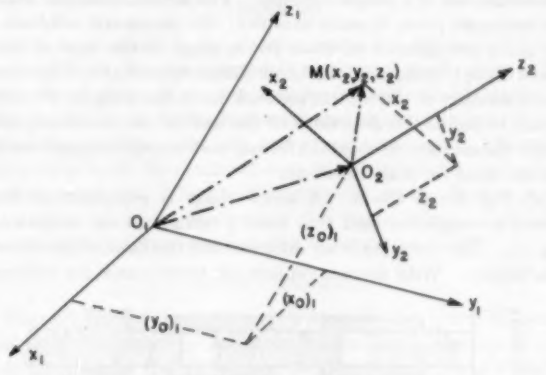

Fig. 10 Transformation of Rectangular Cartesian Co-Ordinates

If, however, the equations are put into homogeneous form, they then may be represented by a square matrix. The introduction of a new set of variables defined by

$$X_1 = x_1H_1,\ Y_1 = y_1H_1,\ Z_1 = z_1H_1$$

and

$$X_2 = x_2H_2,\ Y_2 = y_2H_2,\ Z_2 = z_2H_2$$

with

$$H_1 = H_2$$

will produce the homogeneous system

$$\left.\begin{aligned}
H_1 &= H_2\\
X_1 &= (x_0)_1H_2 + \cos(x_2, x_1)X_2 + \cos(y_2, x_1)Y_2 + \cos(z_2, x_1)Z_2\\
Y_1 &= (y_0)_1H_2 + \cos(x_2, y_1)X_2 + \cos(y_2, y_1)Y_2 + \cos(z_2, y_1)Z_2\\
Z_1 &= (z_0)_1H_2 + \cos(x_2, z_1)X_2 + \cos(y_2, z_1)Y_2 + \cos(z_2, z_1)Z_2
\end{aligned}\right\} \ldots [4]$$

which can be represented by the square matrix of its coefficients

$$M_2 = \begin{vmatrix}1 & 0 & 0 & 0\\ (x_0)_1 & \cos(x_2, x_1) & \cos(y_2, x_1) & \cos(z_2, x_1)\\ (y_0)_1 & \cos(x_2, y_1) & \cos(y_2, y_1) & \cos(z_2, y_1)\\ (z_0)_1 & \cos(x_2, z_1) & \cos(y_2, z_1) & \cos(z_2, z_1)\end{vmatrix} \ldots [5]$$

Equation [5] was developed for the general case of rectangular Cartesian co-ordinates shown in Fig. 10. When applied to the rectangular systems related by the parameters a, α, θ, and s shown in Fig. 4, the matrix representing part 2 takes the following form

$$M_2 = \begin{vmatrix}1 & 0 & 0 & 0\\ a_1\cos\theta_1 & \cos\theta_1 & -\sin\theta_1\cos\alpha_1 & -\sin\theta_1\sin\alpha_1\\ a_1\sin\theta_1 & \sin\theta_1 & \cos\theta_1\cos\alpha_1 & \cos\theta_1\sin\alpha_1\\ s_1 & 0 & -\sin\alpha_1 & \cos\alpha_1\end{vmatrix} \ldots [6]$$

The inverse of this matrix, also useful for computation, is

$$M_2^{-1} = \begin{vmatrix}1 & 0 & 0 & 0\\ -a_1 & \cos\theta_1 & \sin\theta_1 & 0\\ s_1\sin\alpha_1 & -\sin\theta_1\cos\alpha_1 & \cos\theta_1\cos\alpha_1 & -\sin\alpha_1\\ -s_1\cos\alpha_1 & -\sin\theta_1\sin\alpha_1 & \cos\theta_1\sin\alpha_1 & \cos\alpha_1\end{vmatrix} . [7]$$

[7] To avoid confusion, it must be noted that the word "closed" meant two things to Reuleaux, (*a*) that the last machine part is in contact with the first, i.e., the chain of machine parts constitutes a completed loop, and (*b*) that the mechanism actually possesses movability. See Reuleaux (Kennedy) (2) pp. 46–49. The authors use closed in only the first sense.

[8] Reference (2), p. 263

[9] Ibid., p. 264.

Examples

To demonstrate the nature of the matrix manipulations involved in establishing the functional relations of the displacement of different parts, two examples of space mechanisms will be presented. The first example, that of the screw chain, is included for demonstration of a simple example. The second example, that of the universal joint, is more complex; the geometric relations of the parts are difficult to draw (as is usual in the case of space mechanisms) because of the three dimensions that are involved. The reasoning of the matrix method needs the support of only a sketch to define the directions of the axes of the revolutes, after which the solution proceeds in formal mathematical manner without the need for scale drawings.

(*a*) *The Screw Chain.* A screw chain is composed of three screws so connected that they have a common axis, as shown in Fig. 11. The three leads are different and the hand of the threads is arbitrary. With a common axis all three z-axes are collinear,

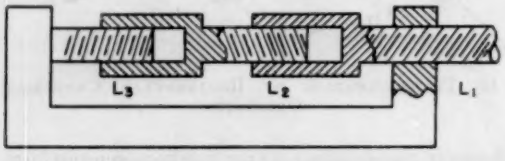

Fig. 11 Screw Chain, General Case

which means that $a_1 = 0$, $a_2 = 0$, and $a_3 = 0$ as well as $\alpha_1 = 0$, $\alpha_2 = 0$, and $\alpha_3 = 0$. Each screw has its own θ and s. Assembling these data in the fashion of Equation [2], the symbolic equation describing the screw chain[10] becomes

$$S_{L_1}(u_1)\begin{vmatrix}0\\0\\\theta_1\\s_1\end{vmatrix} S_{L_2}(u_2)\begin{vmatrix}0\\0\\\theta_2\\s_2\end{vmatrix} S_{L_3}(u_3)\begin{vmatrix}0\\0\\\theta_3\\s_3\end{vmatrix} = 1$$

There are three parts, each of which may be represented by a matrix. The matrix equation of the screw chain is then (cf. Equation [1])

$$M_2 \times M_3 \times M_1 = 1$$

Since each matrix is of the form of Equation [6], the expanded matrix equation of the screw chain is given by

$$\begin{vmatrix}1 & 0 & 0 & 0\\ 0 & \cos\theta_2 & -\sin\theta_2 & 0\\ 0 & \sin\theta_2 & \cos\theta_2 & 0\\ s_2 & 0 & 0 & 1\end{vmatrix} \times \begin{vmatrix}1 & 0 & 0 & 0\\ 0 & \cos\theta_1 & -\sin\theta_1 & 0\\ 0 & \sin\theta_1 & \cos\theta_1 & 0\\ s_1 & 0 & 0 & 1\end{vmatrix}$$

$$\times \begin{vmatrix}1 & 0 & 0 & 0\\ 0 & \cos\theta_3 & -\sin\theta_3 & 0\\ 0 & \sin\theta_3 & \cos\theta_3 & 0\\ s_3 & 0 & 0 & 1\end{vmatrix} = 1$$

The result of this multiplication is given in the following and the unit matrix is expressed in terms of its elements

$$\begin{vmatrix}1 & 0 & 0 & 0\\ 0 & \cos(\theta_1+\theta_2+\theta_3) & -\sin(\theta_1+\theta_2+\theta_3) & 0\\ 0 & \sin(\theta_1+\theta_2+\theta_3) & \cos(\theta_1+\theta_2+\theta_3) & 0\\ s_1+s_2+s_3 & 0 & 0 & 1\end{vmatrix} = \begin{vmatrix}1&0&0&0\\0&1&0&0\\0&0&1&0\\0&0&0&1\end{vmatrix}$$

[10] In Reuleaux's notation this screw chain is given as S'_3 (reference 2, p. 546). The prime sign denotes a common axis.

Identifying the elements of the two matrices leads to the displacement relations

$$\theta_1 + \theta_2 + \theta_3 = 0 \text{ and } s_1 + s_2 + s_3 = 0$$

When L_1, L_2, and L_3 are different from zero and infinity, then either θ or s could be the pair variable u. Choosing θ to represent the pair variable

$$s_1 = L_1\frac{\theta_1}{2\pi},\ s_2 = L_2\frac{\theta_2}{2\pi},\ \text{and}\ \ s_3 = L_3\frac{\theta_3}{2\pi}$$

whence

$$L_1\theta_1 + L_2\theta_2 + L_3\theta_3 = 0$$

Taking θ_1 as the independent variable (input), the functional relations become

$$\theta_2 = -\frac{L_1 - L_3}{L_2 - L_3}\theta_1 \quad \text{and} \quad \theta_3 = -\frac{L_1 - L_2}{L_3 - L_2}\theta_1$$

If s_1 were taken as the independent variable, then the functional relations are given by

$$s_2 = -\frac{\frac{1}{L_1} - \frac{1}{L_3}}{\frac{1}{L_2} - \frac{1}{L_3}}s_1 \quad \text{and} \quad s_3 = -\frac{\frac{1}{L_2} - \frac{1}{L_1}}{\frac{1}{L_2} - \frac{1}{L_3}}s_1$$

Similar relations are shown by Beyer.[11]

The foregoing relations apply when the three leads are different from zero and infinity; either θ or s may then be taken as the pair variable. However, if the lead of one screw becomes zero, giving a revolute, then θ is the pair variable; and if the lead of one screw becomes infinitely great to form a prism, then s is the pair variable.

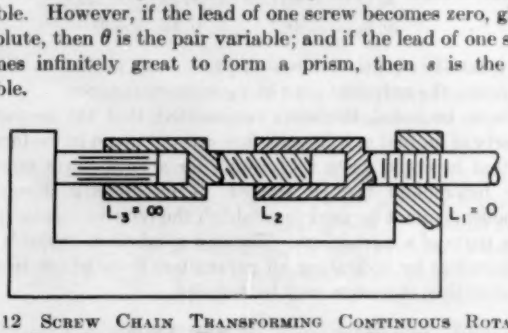

Fig. 12 Screw Chain Transforming Continuous Rotation Into Continuous Translation—or Vice Versa

A special case of practical interest is shown in Fig. 12: it represents the essence of the cross-feed of a lathe, or the feeds of a milling machine table, and so on. Here $L_1 = 0$, $L_2 \neq 0$ or ∞, and $L_3 = \infty$. The functional relations are then

$$\theta_2 = -\frac{\frac{L_1}{L_3} - 1}{\frac{L_2}{L_3} - 1}\theta_1 = -\theta_1$$

and

$$s_3 = -\frac{\frac{1}{L_2} - \frac{1}{L_1}}{\frac{1}{L_2} - \frac{1}{L_3}}\frac{L_1}{2\pi}\theta_1 = -\frac{L_2}{2\pi}\theta_1$$

(*b*) *The Universal Joint.* The symbolic equation has been given already as

[11] Reference (5), p. 46.

$$R_1(\theta_1)\begin{vmatrix}0\\ \alpha_1\\ \theta_1\\ 0\end{vmatrix} R_2(\theta_2)\begin{vmatrix}0\\ 90\\ \theta_2\\ 0\end{vmatrix} R_3(\theta_3)\begin{vmatrix}0\\ 90\\ \theta_3\\ 0\end{vmatrix} R_4(\theta_4)\begin{vmatrix}0\\ 90\\ \theta_4\\ 0\end{vmatrix} = 1 \quad \ldots\ldots [3]$$

In matrix form it is

$$M_2 \times M_3 \times M_4 \times M_1 = 1$$

or with the elements formed from the parameters

$$\begin{vmatrix} 1 & 0 & 0 & 0 \\ 0 & \cos\theta_1 & -\sin\theta_1\cos\alpha & -\sin\theta_1\sin\alpha_1 \\ 0 & \sin\theta_1 & \cos\theta_1\sin\alpha_1 & \cos\theta_1\sin\alpha_1 \\ 0 & 0 & -\sin_1\alpha_1 & \cos\alpha_1 \end{vmatrix}$$

$$\times \begin{vmatrix} 1 & 0 & 0 & 0 \\ 0 & \cos\theta_2 & 0 & -\sin\theta_2 \\ 0 & \sin\theta_2 & 0 & \cos\theta_2 \\ 0 & 0 & -1 & 0 \end{vmatrix} \times \begin{vmatrix} 1 & 0 & 0 & 0 \\ 0 & \cos\theta_3 & 0 & -\sin\theta_3 \\ 0 & \sin\theta_3 & 0 & \cos\theta_3 \\ 0 & 0 & -1 & 0 \end{vmatrix}$$

$$\times \begin{vmatrix} 1 & 0 & 0 & 0 \\ 0 & \cos\theta_4 & 0 & -\sin\theta_4 \\ 0 & \sin\theta_4 & 0 & \cos\theta_4 \\ 0 & 0 & -1 & 0 \end{vmatrix} = \begin{vmatrix} 1 & 0 & 0 & 0 \\ 0 & 1 & 0 & 0 \\ 0 & 0 & 1 & 0 \\ 0 & 0 & 0 & 1 \end{vmatrix}$$

The appearance of this last equation, in particular M_2, suggests that the conventional matrix multiplication would be quite tedious, and that this labor would be reduced by the use of the inverse matrix, viz.

$$M_2^{-1} \times M_2 \times M_3 \times M_4 \times M_1 = M_2^{-1} \times 1$$

Since $M_2^{-1} \times M_2 = 1$ the equation becomes

$$M_3 \times M_4 \times M_1 = M_2^{-1}$$

The general form of the inverse matrix M_2^{-1} expressed in terms of a_1, α_1, θ_1, and s_1 has been given as Equation [7]. The matrix multiplication. now reduced to three operations, i.e., $M_3 \times M_4 \times M_1$, is set equal to the inverse matrix M_2^{-1}. This is shown as follows

$$\begin{vmatrix} 1 & 0 & 0 & 0 \\ 0 & \cos\theta_2\cos\theta_3\cos\theta_4 + \sin\theta_2\sin\theta_4 & \cos\theta_2\sin\theta_3 & -\cos\theta_2\cos\theta_3\sin\theta_4 + \sin\theta_2\cos\theta_4 \\ 0 & \sin\theta_2\cos\theta_3\cos\theta_4 - \cos\theta_2\sin\theta_4 & \sin\theta_2\sin\theta_3 & -\sin\theta_2\cos\theta_3\sin\theta_4 - \cos\theta_2\cos\theta_4 \\ 0 & -\sin\theta_3\cos\theta_4 & \cos\theta_3 & \sin\theta_3\sin\theta_4 \end{vmatrix}$$

$$= \begin{vmatrix} 1 & 0 & 0 & 0 \\ 0 & \cos\theta_1 & \sin\theta_1 & 0 \\ 0 & -\sin\theta_1\cos\alpha_1 & \cos\theta_1\cos\alpha_1 & -\sin\alpha_1 \\ 0 & -\sin\theta_1\sin\alpha_1 & \cos\theta_1\sin\alpha_1 & \cos\alpha_1 \end{vmatrix}$$

Identification of the elements of the two matrices leads to the set of nine equations

$$\begin{aligned} \sin\theta_2\sin\theta_4 &= \cos\alpha_1 \\ \cos\theta_3 &= \cos\theta_1\sin\alpha_1 \\ \sin\theta_3\cos\theta_4 &= \sin\theta_1\sin\alpha_1 \\ \sin\theta_2\sin\theta_3 &= \cos\theta_1\cos\alpha_1 \\ \cos\theta_2\sin\theta_3 &= \sin\theta_1 \\ \cos\theta_2\cos\theta_3\cos\theta_4 + \sin\theta_2\sin\theta_4 &= \cos\theta_1 \\ -\cos\theta_2\cos\theta_3\sin\theta_4 + \sin\theta_2\cos\theta_4 &= 0 \\ \sin\theta_2\cos\theta_3\cos\theta_4 - \cos\theta_2\sin\theta_4 &= -\sin\theta_1\cos\alpha_1 \\ -\sin\theta_2\cos\theta_3\sin\theta_4 - \cos\theta_2\cos\theta_4 &= -\sin\alpha_1 \end{aligned}$$

Taking θ_1 as the independent variable of the input shaft, the relations for the other three pair variables are found to be

$$\tan\theta_2 = \frac{\cos\alpha_1}{\tan\theta_1},\ \cos\theta_3 = \sin\alpha_1\cos\theta_1,\ \tan\theta_4 = \frac{1}{\tan\alpha_1\sin\theta_1}$$

These relations satisfy all nine equations.

The relation for $\tan\theta_2$ is identical with that given by Beyer.[12]

Summary

This paper presents the development of a symbolic notation that is able to describe completely lower-pair mechanisms. This symbolic notation furnishes a powerful and reliable analytical procedure since the operations are based on matrix algebra. The use of the notation also puts lower-pair problems of kinematics into a form ready for electrical computation methods, as has been demonstrated (8). The matrix manipulation involved in establishing the functional relations of the displacements of different parts of space mechanisms is shown by examples.

Acknowledgment

The authors wish to express their appreciation to the following: Prof. J. F. Calvert, who called their attention to the useful symbolic language of the one-degree-of-freedom systems of electrical circuits and urged the investigation of kinematics; Prof. M. B. Gamet, who made available funds that enabled an extension of the work; and Prof. B. H. Jennings, whose constant encouragement was invaluable.

BIBLIOGRAPHY

1 "Developing Problem-Solving Skills in Engineering," by J. F. Calvert, R. S. Hartenberg, R. A. Kliphardt, H. P. Shelley, and J. Denavit, Final Technical Report of Project NR 151-144, completed under Contract N7-onr-45012, Northwestern University, Evanston, Ill., August, 1953; Part D, "The Development of a Manipulative Symbolic Notation for the Description and Synthesis of Kinematic Mechanisms," by J. Denavit and R. S. Hartenberg.

2 "Kinematics of Machinery," by F. Reuleaux, translation by A. B. W. Kennedy, Macmillan and Company, Ltd., London, England, 1876.

3 "Theoretische Kinematik," by F. Reuleaux, F. Vieweg und Sohn, Braunschweig, Germany, vol. 2, 1900.

4 "A Practical Theory of Mechanisms," by P. Grodzinski, Emmot and Company, Manchester-London, England, 1947.

5 "Technische Kinematik," by R. Beyer, Johann Ambrosius Barth, Leipzig, Germany, first edition, 1931 (Edwards Brothers, Ann Arbor, Mich., lithoprint).

6 "A General Method for Finite Displacements of Spatial Mechanisms and on Certain Passive Constraints," by F. M. Dimentberg, Akad. Nauk SSSR, Trudy Sem. Teorii Mashin i Mekhanizmov, vol. 5, no. 17, 1948. Identical abstracts are in *Mathematical Reviews*, vol. 12, 1951, and *Applied Mechanics Reviews*, vol. 4, no. 9, Sept., 1951.

7 "The Determination of the Positions of Spatial Mechanisms," by F. M. Dimentberg, Izdat. Akad. Nauk SSSR, Moscow, USSR 1950. This text of 142 pages is given identical reviews in *Mathematical Reviews*, vol. 12, 1951, and *Applied Mechanics Reviews*, vol. 5, Jan., 1952.

8 "A Symbolic Approach to Mechanisms Leading to Electrical Computation Methods," by J. Denavit, MS thesis, Northwestern University, Evanston, Illinois, June, 1953.

[12] Reference (5), p. 90.

Acceleration in Mechanisms

By R. T. HINKLE,[1] C. IP,[2] and J. S. FRAME,[3] E. LANSING, MICH.

An equation is derived for finding the instantaneous radii of curvature for the paths of relative motion described by the coincidental points of contact of direct-contact mechanisms, and a graphical method for solving the equation for these radii is developed. A proof of the validity of the equivalent linkage for direct-contact mechanisms is presented.

Radii of Curvature of the Path of Relative Motion

IN Fig. 2 link 2 drives link 4 by direct contact with P_2 and P_4 as points of contact at this instant. Both links have arbitrary curves. C and D are centers of curvature of link 2 and link 4, respectively, at the point of contact. It is required to find

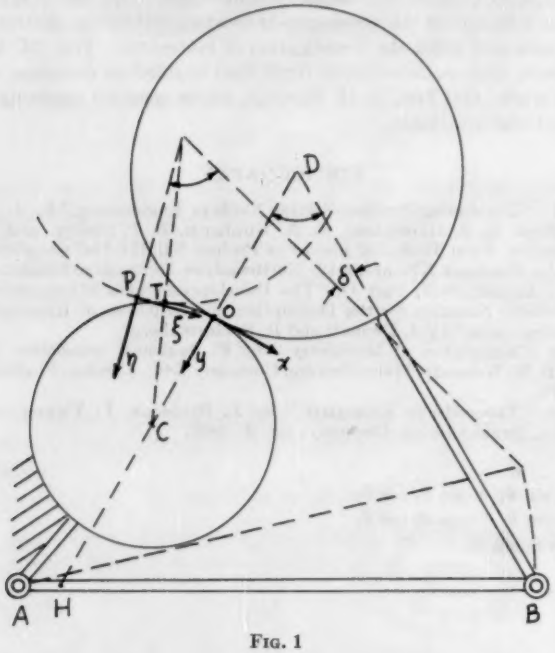

Fig. 1

R_{24} and R_{42}, the radii of curvature of the paths of relative motion. In finding R_{24} link 4 is the reference frame and hence considered stationary. In finding R_{42} link 2 is considered stationary. Essentially, these two cases give two mechanisms obtainable from the mechanism in Fig. 2 by inversion. Since the two cases are

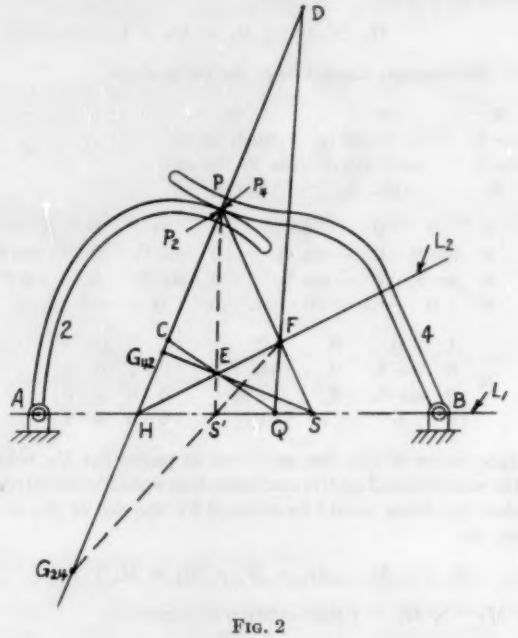

Fig. 2

similar we will work with the inverted mechanism in Fig. 1. The curves in contact are now shown as circles. This will be explained later.

At time $t = 0$, let the instantaneous contact point O be the origin of co-ordinates (x, y) in the fixed link and of co-ordinates (ξ, η) in the moving member chosen so that x and ξ-axes are tangent to the respective curves. The center of curvature C, of the fixed link at the contact point (O, O) is (O, r). The curvature is k. Let the curvature at the point P, which is at (O, O) when $t = 0$, on the moving curve be κ so that its center of curvature D is (O, ρ) measured positive toward the fixed member. Here $k = 1/r$, $\kappa = 1/\rho$. Let the contact point T at time t have co-ordinates $[x(s), y(s)]$ and $[\xi(\sigma), \eta(\sigma)]$ in the two co-ordinate systems, referred to arc lengths $(OT) = s$ and $(PT) = \sigma$. Then since

$$\left(\frac{dx}{ds}\right)^2 + \left(\frac{dy}{ds}\right)^2 = 1 \text{ and } x = 0, \frac{dx}{ds} = 1 \text{ when } t = 0,$$

we have[4]

$$\left.\begin{aligned} x &= s - k^2\frac{s^3}{3!} - 3kl\frac{S^4}{4!} + \cdots\cdots \\ y &= k\frac{s^2}{2!} + l\frac{s^3}{3!} + \cdots\cdots \end{aligned}\right\} \cdots\cdots [1]$$

and for similar reasoning as shown in the Appendix

$$\left.\begin{aligned} \xi &= \sigma - \kappa^2\frac{\sigma^3}{3!} - 3\kappa\lambda\frac{\sigma^4}{4!} + \cdots\cdots \\ \eta &= \kappa\frac{\sigma^2}{2!} + \lambda\frac{\sigma^3}{3!} + \cdots\cdots \end{aligned}\right\} \cdots\cdots [2]$$

Let P have co-ordinates (X, Y) in the fixed system. The curvature $K = 1/R$ of the curve, traced by P and determined by Y as

[4] See Appendix to this paper.

[1] Professor, Mechanical Engineering, Michigan State College. Mem. ASME.

[2] Assistant Professor, Mechanical Engineering, Michigan State College. Assoc. Mem. ASME.

[3] Professor and Head of Mathematics, Michigan State College.

Contributed by the Applied Mechanics Division and presented at the Annual Meeting, New York, N. Y., November 28–December 3, 1954, of The American Society of Mechanical Engineers.

Discussion of this paper should be addressed to the Secretary, ASME, 29 West 39th Street, New York, N. Y., and will be accepted until July 11, 1955, for publication at a later date. Discussion received after the closing date will be returned.

Note: Statements and opinions advanced in papers are to be understood as individual expressions of their authors and not those of the Society. Manuscript received by ASME Applied Mechanics Division, September 16, 1953. Paper No. 54—A-33.

a function of X, is sought. The position vectors in exponential form are

$$Z = X + iY, \quad z = x + iy, \quad \text{and } \zeta = \xi + i\eta$$

Then

$$Z = z - \zeta e^{i\delta} \ldots\ldots\ldots\ldots\ldots\ldots [3]$$

where $\delta(t)$ is the angular rotation of the moving link. Differentiation of Equation [3] with respect to time yields

$$\dot{Z} = \dot{z} - \dot{\zeta}e^{i\delta} - i\zeta\dot{\delta}e^{i\delta} \equiv Ve^{i\tau} \ldots\ldots\ldots\ldots [4]$$

where $V = (ds)/(dt)$ is the speed of P relative to O, and τ is the phase angle of the velocity vector. Further differentiation yields

$$\ddot{Z} = \ddot{z} - \ddot{\zeta}e^{i\delta} - 2i\dot{\zeta}\dot{\delta}e^{i\delta} + \zeta\dot{\delta}^2e^{i\delta} - i\zeta\ddot{\delta}e^{i\delta} = e^{i\tau}(\dot{V} + iV\dot{\tau}) = e^{i\tau}\left(\dot{V} + iV^2\frac{d\tau}{ds}\right) \ldots [5]$$

where

$$\dot{\tau} = \frac{d\tau}{ds}\frac{ds}{dt} = V\frac{d\tau}{ds}$$

But

$$\frac{d\tau}{ds} = K = \frac{1}{R}$$

Dividing Equation [5] by [4] we have

$$\frac{\ddot{Z}}{\dot{Z}} = \frac{\dot{V}}{V} + i\frac{V}{R} = \frac{\ddot{z} - \ddot{\zeta}e^{i\delta} - 2i\dot{\zeta}\dot{\delta}e^{i\delta} + \zeta\dot{\delta}^2e^{i\delta} - i\zeta\ddot{\delta}e^{i\delta}}{\dot{z} - \dot{\zeta}e^{i\delta} - i\zeta\dot{\delta}e^{i\delta}} \ldots\ldots [6]$$

Evaluating for $t = 0$ at which time $\delta = 0$ and $\zeta = 0$ we have

$$\frac{V_0}{R} = \text{Imag}\left[\frac{\ddot{z} - \ddot{\zeta} - 2i\dot{\zeta}\dot{\delta}}{\dot{z} - \dot{\zeta}}\right] = \frac{\ddot{y} - \ddot{\eta} - 2\dot{\sigma}\dot{\delta}_0}{\dot{s}_0 - \dot{\sigma}_0} = \frac{\ddot{y} - \ddot{\eta} - 2\dot{\sigma}_0\dot{\delta}}{V_0} \ldots\ldots [7]$$

$\dot{z} = \dot{s}$ and $\dot{\zeta} = \dot{\sigma}$ at $t = 0$ since all of the velocities are then tangent to the curves.

From Equation [7] and the second derivations of y and η in Equations [1] and [2] with $s \to 0$, $\sigma \to 0$, when $t \to 0$, we have the curvature

$$K = \frac{1}{R} = \frac{k\dot{s}_0^2 - \kappa\dot{\sigma}_0^2 - 2\dot{\sigma}_0\dot{\delta}_0}{(\dot{s}_0 - \dot{\sigma})^2} \ldots\ldots [8]$$

The condition of tangency at T gives

$$\left(\frac{dz}{ds}\right) = \left(\frac{d\zeta}{d\sigma}\right)e^{i\delta} \ldots\ldots [9]$$

Differentiating Equation [9] with respect to time by taking the derivatives, first with respect to the arc length and then with respect to time, of Equations [1] and [2], we have at $t = 0$, $s = 0$, $\sigma = 0$

$$ik\dot{s}_0 = i\kappa\dot{\sigma}_0 + i\dot{\delta}_0 \ldots\ldots [10]$$

whence

$$\dot{\delta}_0 = k\dot{s}_0 - \kappa\dot{\sigma}_0$$

Clearly then the curvature of the path of P relative to the fixed curve depends only on the two curvatures k and κ and some first derivatives of arc length.

Theorem I. For the purpose of finding the acceleration of a moving contact point, the two arbitrary curves in contact can be replaced by two circles having centers, respectively, at the centers of curvature of the arbitrary curves at the point of contact. From Equation [8] we have

$$k - K = \frac{k\dot{s}_0^2 - 2k\dot{s}_0\dot{\sigma}_0 + k\dot{\sigma}_0^2 - k\dot{s}_0^2 + \kappa\dot{\sigma}_0^2 + 2k\dot{s}_0\dot{\sigma}_0 - 2\kappa\dot{\sigma}_0^2}{(\dot{s}_0 - \dot{\sigma}_0)^2} = \frac{\dot{\sigma}_0^2(k - \kappa)}{(\dot{s}_0 - \dot{\sigma}_0)^2} = \frac{1}{(k - \kappa)}\left(\frac{k\dot{\sigma}_0 - \kappa\dot{\sigma}_0}{\dot{s}_0 - \dot{\sigma}_0}\right)^2 = \frac{1}{(k - \kappa)}\left[k - \frac{k\dot{s}_0 - \kappa\dot{\sigma}_0}{\dot{s}_0 - \dot{\sigma}_0}\right]^2$$

Hence

$$(k - K)(k - \kappa) = (k - u)^2 \ldots\ldots [11]$$

where

$$u = \frac{k\dot{s}_0 - \kappa\dot{\sigma}_0}{\dot{s}_0 - \dot{\sigma}_0} = \frac{\dot{\delta}_0}{V_0} = \frac{\text{angular velocity of moving link}}{\text{velocity of } P}$$

Let $h = (PH)$ where H is O_{42} the instantaneous center of relative velocity of links 2 and 4. It is the intersection of the common normal with the line of pivoted centers. From the definition of the instantaneous center and the fact that one link (say, link 2) is stationary

$$V_P = \omega_{42}(PO_{42}) = \omega_4 h$$

or

$$h = \frac{V_P}{\omega_4} = \frac{1}{u} \ldots\ldots [12]$$

Expressing Equation [11] in terms of the radii, we have

Theorem II. The radius of curvature of the path of relative motion can be found by the relationship

$$\left(\frac{1}{r} - \frac{1}{R}\right)\left(\frac{1}{r} - \frac{1}{\rho}\right) = \left(\frac{1}{r} - \frac{1}{h}\right)^2 \ldots\ldots [13]$$

Solving Equation [11] for K we have

$$K = k - \frac{(k - u)^2}{k - \kappa} = \frac{k\kappa + 2ku - u^2}{k - \kappa}$$

Now if $K = 1/R_{42}$ and if R_{24} $(= 1/K')$ the radius of curvature of the other relative path is sought, K' can be obtained from the foregoing expression by interchanging the fixed and the moving links, i.e., by interchanging k and κ. Thus

$$K' = \frac{k\kappa + 2\kappa u - u^2}{\kappa - k}$$

Adding the two equations we have

$$K + K' = \frac{2(k - \kappa)u}{(k - \kappa)} = 2u \ldots\ldots [14]$$

or

$$\frac{1}{R} + \frac{1}{R'} = \frac{2}{h} \ldots\ldots [15]$$

Specifically in this case

$$\frac{1}{R_{42}} + \frac{1}{R_{24}} = \frac{2}{h}$$

Theorem III. The distance h between the contact point and the instantaneous center has a value equal to the harmonic mean of the two radii of curvature of the relative paths, R and R'.

Graphical Solution of Equation [13]

The radii R_{42} and R_{24} are to be found. First determine R_{42}. Let P be the contact position of the points P_2 and P_4. Let C be the

center of curvature of the reference (fixed) link 2, and D the center of curvature of the moving link 4. Let H be the point where the common normal DPC cuts the line of centers AB. Then

$$(PH) = h, (PC) = r, \text{ and } (PD) = \rho$$

Note that ρ is a negative quantity here by our sign convention.

The Construction. Draw any two lines L_1 and L_2 through H (we use the line of centers AB as L_1 for convenience). Join an arbitrary point Q on L_1 to C and D, respectively. Let QC meet L_2 in E, and let QD meet L_2 in F. Let PF meet L_1 in S and let ES meet CD in G_{42}. Then G_{42} is the required center of curvature. Or $(PG_{42}) = R_{42}$.

The Theory. The essential feature is the construction of a quadrangle $QEFS$ having H as one diagonal point and having three of its remaining four sides (or diagonals) passing through C, D, and P. The fourth then goes through G_{42}. Rewriting Equation [13] in the form

$$\left(\frac{\rho - r}{\rho - o}\right)\left(\frac{h - o}{h - r}\right) = \left(\frac{h - r}{h - o}\right)\left(\frac{R - o}{R - r}\right) \quad \ldots . \quad [13a]$$

We see that the cross ratio of the four points (CP, DH), with co-ordinates r, o, ρ, h, is equal to the cross ratio of the four four points (CP, HG_{42}) with co-ordinates r, o, h, R. G_{42} is located by projecting C, P, D, H from Q onto PF, followed by a projection from E onto CD. D moves via F to H, and H moves via S to G_{42}, whereas P is fixed and C returns to C on QE.

The Converse Problem. If link 4 is the reference (fixed) link and R_{24} is sought it is easily seen that the construction will be the same except for the dotted lines. Let PE meet L_1 in S' and let FS' meet CD in G_{24}. Then $(PG_{24}) = R_{24}$.

Examples

Example 1. An interesting example is the shaper mechanism shown in Fig. 3. The center of curvature $R_{24} = \infty$ is obvious since the path of relative motion in this case is a straight line. Both R_{24} and R_{42} can be obtained by the graphical construction, or even more simply found from Equation [11], thus:

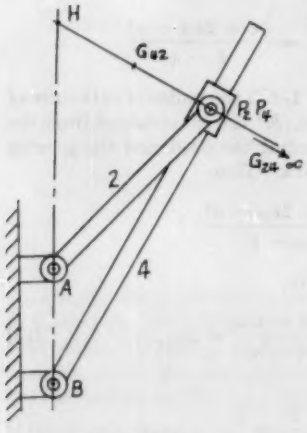

Fig. 3

(*a*) Link 4 as the reference link. Here $r = \infty$, and $\rho = 0$; i.e., $k = 0$ and $\kappa = \infty$; $u = 1/h = 1/(PH)$ is finite.

From Equation [11], first let $K \to o$, and then let $\kappa \to \infty$, we have

$$K = \frac{u^2}{\kappa} = 0 \quad \text{or} \quad R_{24} = \infty$$

(*b*) Link 2 as the reference link. Here $r = 0$, and $\rho = \infty$; i.e., $k = \infty$, and $\kappa = 0$. Expanding Equation [11] we have

$$k^2 = (K + \kappa)k + K\kappa = k^2 - 2ku + u^2$$

Simplifying and dividing both sides by $-k$ we have

$$R_{42} = \frac{1}{K} = \frac{h}{2} \text{ when } (k = \infty, \kappa = o)$$

The fact that $R_{24} = \infty$ results in $R_{42} = h/2$, agrees with Equation [15].

Here, $(PG_{42}) = (PH)/2$ locates the other center readily.

Example 2—Disk Cam With Flat Rocking Follower (Fig. 4). This problem does not lend itself easily to other methods of analysis. It will be worked here as a numerical example. The following given angular velocity and angular acceleration apply to the problem

$$\omega_2 = 1 \text{ rad/sec}, \alpha_2 = 1.5 \text{ rad/sec}^2, \text{ and } AB = 4.48 \text{ in.}$$

The angular acceleration α_4 of the rocking follower is sought.

The velocity polygon is shown in Fig. 4(*b*). By measurement $V_{P_4} = 0.81$ ips, $V_{P_4P_2} = 1.64$ ips.

The acceleration polygon is shown in Fig. 4(*c*). The primary solution using the radius of curvature of the path that P_4 traces on

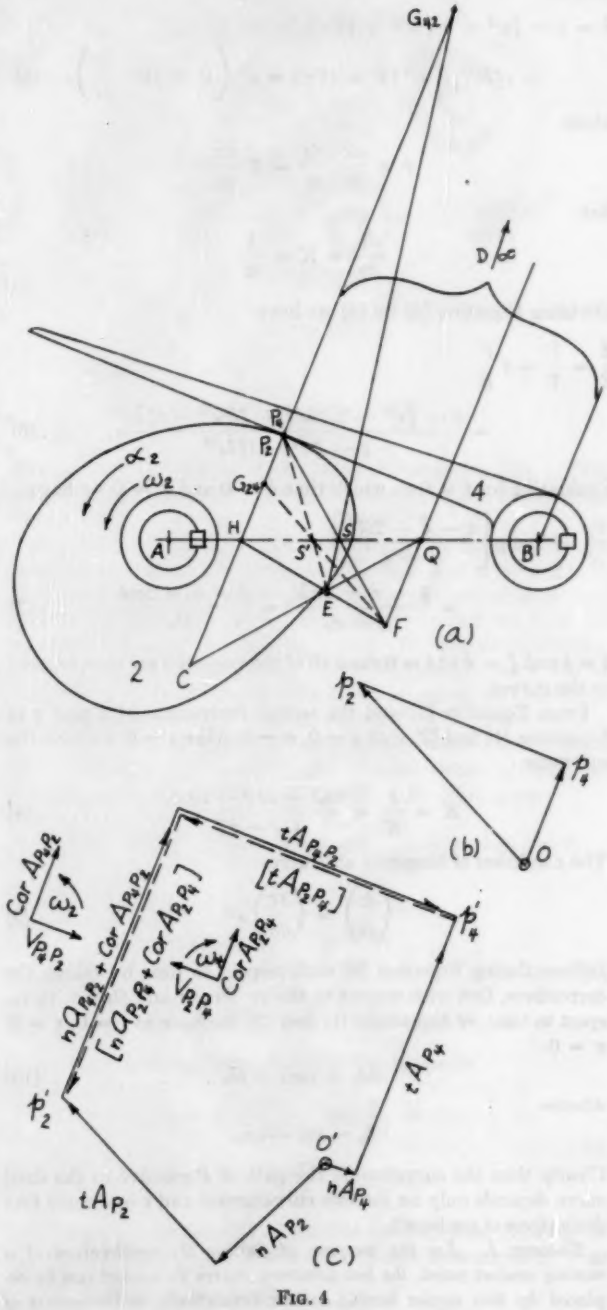

Fig. 4

2 will be considered first. The vectors are calculated and laid off in the following order

$${}_nA_{P_2} = \omega_2^2(AP) = 1.83 \text{ in/sec}^2$$

$${}_tA_{P_2} = \alpha_2(AP) = 1.5 \times 1.83 = 2.74 \text{ in/sec}^2$$

$${}_nA_{P_4} = \frac{V^2_{P_4}}{AP} = \frac{(0.81)^2}{1.83} = 0.358 \text{ in/sec}^2$$

$$A_{P_4P_2} = {}_na_{P_4P_2} +\!\!\rightarrow \text{cor } A_{P_4P_2} +\!\!\rightarrow {}_tA_{P_4P_2}$$

$${}_na_{P_4P_2} = \frac{V^2_{P_4P_2}}{R_{42}} = \frac{(1.64)^2}{5.55} = 0.485 \text{ in/sec}^2$$

$$\text{cor } A_{P_4P_2} = 2V_{P_4P_2}\,\omega_2 = 2 \times 1.64 \times 1 = 3.28 \text{ in/sec}^2$$

$${}_na_{P_4P_2} +\!\!\rightarrow \text{cor } A_{P_4P_2} = 3.77 \text{ in/sec}^2$$

The directions of ${}_tA_{P_4}$ and ${}_tA_{P_4P_2}$ are known. These are laid off and the intersection p'_4 is obtained. By measurement

$${}_tA_{P_4} = 3.35 \text{ in/sec}^2$$

$$\alpha_4 = \frac{{}_tA_{P_4}}{(BP)} = \frac{3.34}{3.34} = 1 \text{ rad/sec}^2$$

The vectors for the secondary or inverse solution are shown with dotted lines.

$$A_{P_2P_4} = {}_na_{P_2P_4} +\!\!\rightarrow \text{cor } A_{P_2P_4} +\!\!\rightarrow {}_tA_{P_2P_4}$$

$${}_na_{P_2P_4} = \frac{V^2_{P_2P_4}}{R_{24}} = \frac{(1.64)^2}{0.59} = 4.56 \text{ in/sec}^2$$

$$\text{cor } A_{P_2P_4} = 2V_{P_2P_4}\left(\frac{V_{P_4}}{BP}\right) = 2 \times 1.64 \times \frac{0.81}{3.34} = 0.79 \text{ in/sec}^2$$

These two vectors are in opposite directions, hence

$${}_na_{P_2P_4} +\!\!\rightarrow \text{cor } A_{P_2P_4} = 4.56 - 0.79 = 3.77 \text{ in/sec}^2$$

which agrees with the primary solution.

Equivalent Linkages

Acceleration analysis of most direct contact mechanisms can be made using equivalent linkages. A simple example having two circular contact members of radii R_1 and r_1 is shown in Fig. 5. The equivalent four-bar linkage, *A-B-C-D*, can be used in making the acceleration analysis of the original mechanism. *C* and *D* are the centers of curvature of members 2 and 4. The angular-velocity-ratio theorem is included in most textbooks on kinematics; it states, "the angular velocities of driver and follower are inversely as the segments cut on the line of centers by the line of transmission." In direct-contact mechanisms the line of transmission and the common normal at the point of contact coincide. The common normal at the point of contact always passes through the centers of curvature of the two contacting members. For the phase shown solid in Fig. 5, the common normal cuts the line of centers, *AB*, at *M*. The angular-velocity ratio of driver and follower is

$$\frac{\omega_2}{\omega_4} = \frac{BM}{AM}$$

In the linkage *A-B-C-D* the line of transmission lies along link *CD*. The lines of transmission for the two mechanisms coincide. The angular-velocity ratio of links *AC* and *BD* is the same as for 2 and 4.

The direct-contact mechanism is shown with broken lines in another phase. The angular-velocity ratio of 2 and 4 is

$$\frac{\omega_2}{\omega_4} = \frac{BM'}{AM'}$$

The lengths *DC* and *D'C'* are equal. The link *D'C'* coincides with the line of transmission for the direct-contact mechanism. The angular-velocity ratio of *AC'* and *BD'* is again the same as for 2 and 4. For any series of displacements the velocity ratios of *AC* and *BD* will equal the ratios of 2 and 4 for corresponding phases.

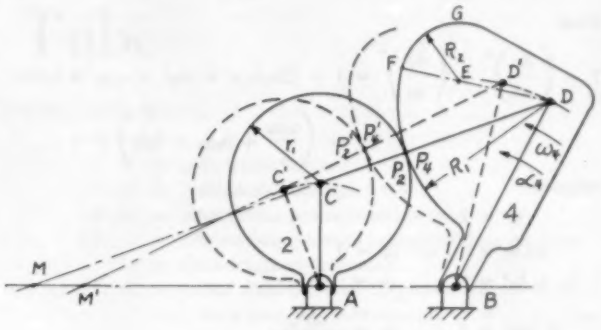

Fig. 5

Therefore the equivalent linkage can be used in making acceleration analyses. When the angular velocity and acceleration of *BD* are made equal to that of 4, then the angular velocity and acceleration of *AC* will be equal to that of 2.

A portion of the profile *FG* of link 4 is of radius R_2. When a point on the profile between *F* and *G* is in contact with link 2 a new equivalent linkage results. The length of the links are *AC*, *BE*, and $R_2 + r_1$. For the phase in which point *F* of member 4 contacts member 2, both linkages result. Both are correct and both should be analyzed. This represents a discontinuity in the acceleration ratio of links 2 and 4 because of the finite change in radius from R_1 to R_2.

If the radius of curvature of the profile of one or of both members changes continuously then the equivalent linkage changes continuously and must be determined for each phase. In the proof for the construction of the radius of curvature of the path that a coincident point traces on the other member it was shown that the acceleration depends only on the instantaneous radii of curvature of the profiles of the contact point. Hence *C* and *D* on the equivalent linkage are the centers of curvature of the two members at the point of contact.

Theorem IV. The angular acceleration ratio of the two links in a direct-contact mechanism is the same as that of the two crank arms of the four-bar mechanism, whose crank arms are formed by joining the centers of rotation to the respective centers of curvature, at the point of contact, of the two direct-contact mechanism links.

Appendix

Co-ordinates x and y expressed as power series of the arc length s. Let *x* and *y* be expressed by the Maclaurins' series

$$x = a_1 s + a_2 \frac{s^2}{2!} + a_3 \frac{s^3}{3!} + a_4 \frac{s^4}{4!} + \ldots .$$

$$y = b_1 s + b_2 \frac{s^2}{2!} + b_3 \frac{s^3}{3!} + b_4 \frac{s^4}{4!} + \ldots .$$

with the coefficients $a_1, a_2, \ldots .$ and $b_1, b_2, \ldots .$ yet to be determined.

Differentiating the series we have

$$\frac{dx}{ds} = a_1 + a_2 s + a_3 \frac{s^2}{2!} + a_4 \frac{s^3}{3!} + \ldots .$$

$$\frac{dy}{ds} = b_1 + b_2 s + b_3 \frac{s^2}{2!} + b_4 \frac{s^3}{3!} + \ldots\ldots$$

Since the axis is chosen tangential to the curve at the origin

$$\left.\frac{dx}{ds}\right|_0 = a_1 = 1 \quad \text{and} \quad \left.\frac{dy}{ds}\right|_0 = b_1 = 0$$

Now

$$1 = \left(\frac{dx}{ds}\right)^2 + \left(\frac{dy}{ds}\right)^2 = 1 + (2a_1a_2)s + (a_2^2 + a_1a_3 + b_2^2)s^2 + \left(\frac{a_1a_4}{3} + a_2a_3 + b_2b_3\right)s^3 + \ldots\ldots$$

whence

$$a_1 = 1$$
$$2a_1a_2 = 0 \quad \text{so} \quad a_2 = 0$$
$$a_3 + b_2^2 = 0 \qquad a_3 = -b_2^2$$
$$\frac{a_4}{3} + b_2b_3 = 0 \qquad a_4 = -3b_2b_3$$

Differentiating the series once again we have

$$\frac{d^2x}{ds^2} = a_3 s + a_4 \frac{s^2}{2!} + \ldots.$$

$$\frac{d^2y}{ds^2} = b_2 + b_3 s + b_4 \frac{s^2}{2!} + \ldots.$$

But the curvature of the curve at the origin is

$$k = \left[\frac{dx}{ds}\frac{d^2y}{ds^2} - \frac{dy}{ds}\frac{d^2x}{ds^2}\right]_0 = [1.b_2 - 0.0] = b_2$$

Tabulating the coefficients we have

$a_1 = 1$	$b_1 = 0$
$a_2 = 0$	$b_2 = k$
$a_3 = -k^2$	$b_3 = l$
$a_4 = -3kl$	....
.....	....

where l is a quantity of higher order than the curvature k. Its physical meaning is not important here.

Hence the power series are

$$x = s - k^2 \frac{s^3}{3!} - 3kl \frac{s^4}{4!} + \ldots.$$

$$y = k \frac{s^2}{2!} + l \frac{s^3}{3!} + \ldots\ldots$$

The Effect of a Surrounding Fluid on Pressure Waves in a Fluid-Filled Elastic Tube[1]

By M. C. JUNGER,[2] CAMBRIDGE, MASS.

The analysis of the transmission of pressure waves in a fluid-filled elastic tube has been extended to the case where the tube is surrounded by a fluid medium. The sound pressure inside the tube is the resultant of a number of modes, some of which are nonpropagating, while others propagate at their own characteristic phase velocities. Neglecting end effects, and for continuously generated waves, it is found that only the modes whose velocity is larger than the sound velocity of the surrounding medium radiate sound energy radially outward. These modes will be damped out by radiation losses, while modes having a phase velocity smaller than this sound velocity are propagated without attenuation (if viscous and heat-transfer losses are neglected). Consequently, if the fluid is the same in the surrounding medium and in the tube only the lowest mode, which resembles a plane wave, propagates unattenuated. In any case, the mass-loading of the surrounding fluid lowers the phase velocities of the propagating modes, particularly at intermediate frequencies. It is shown that in this application the membrane theory of shells will lead to incorrect results, even in thin-walled tubes. This is illustrated by comparison with experimental data.

Nomenclature

The following nomenclature is used in the paper:

a = radius of tube
c_i, c_s = sound velocity of fluid inside tube and in fluid surrounding tube, respectively (velocities corresponding to an unbounded medium)
c_t = compressional wave velocity in tube wall, $\sqrt{\frac{E}{(1-\nu^2)\rho_t}}$
c_{ph} = phase velocity of mode n in fluid column
E = Young's modulus of tube material
h = half-thickness of tube wall
$H_n^{(2)}(x)$ = Hankel function of second kind
$J_n(x)$ = Bessel function
j = $-\sqrt{-1}$
k = ω/c, wave number
$N_n(x)$ = Neumann function
$p(r, z)$ = alternating pressure inside tube
$P(r, z)$ = alternating pressure in surrounding medium
r, z = cylindrical co-ordinates
$u_i(r, z), u_s(r, z)$ = radial fluid-particle displacement in fluid in tube and fluid surrounding tube
u_t, v_t = radial and axial displacement components of tube wall, respectively
$\delta(x - \xi)$ = Dirac delta function, defined by identity $\int_{-\infty}^{\infty} f(\xi)\delta(x-\xi)\,d\xi = f(x)$
ν = Poisson's ratio
ρ_i, ρ_s, ρ_t = density of fluid in tube, of fluid surrounding tube, and of tube material, respectively
ω = circular frequency

Introduction

The transmission of pressure waves in a fluid column bounded by a cylindrical tube having a finite impedance has attracted the attention of a number of investigators. Among more recent analyses are those by Morse (1),[3] who applies the concept of impedance ratios, and by Thomson (2), who considers this impedance to be purely reactive and caused by the inertial and elastic forces in the cylindrical tube. Kuhl (3) gives experimental results related to this problem. For a more extended biography one may refer to Kuhl's paper.

In the present analysis it is assumed that the elastic tube itself is surrounded by a fluid medium whose impedance is not negligible. A system of this nature, for example, would be a metal tube filled with water and submerged in water.[4] End effects are neglected; i.e., the solution is based on the assumption that the tube is of infinite length. The wave source is assumed to generate a continuous train of waves. If the excitation is in the form of pulses of finite length generated at regular intervals, the present analysis can be applied to each component of the Fourier series representing such an excitation. The medium being dispersive, the group velocities of these pulses will differ from the phase velocities obtained from this analysis but can be calculated from the results presented here by means of commonly known relations.

The sound pressure in the fluid column is governed by a solution of the wave equation which is well known from the classical problem of propagation of pressure waves in elastic tubes surrounded by a vacuum (1); the sound pressure is the resultant of a summation of partial pressures, each of which is associated with a mode having its own phase velocity. In practice, it is the dynamic configuration of the wave source which determines which modes are excited. The dynamic configuration expressed as a function of the radius can be expanded in the form of a series, and its coefficients b_n, appearing later in Equation [5], evaluated. The

[1] This research has been aided by funds made available under a contract with the ONR.

[2] Research Fellow in Acoustics, Acoustics Research Laboratory, Harvard University; currently, Partner, Cambridge Acoustics. Mem. ASME.

Contributed by the Applied Mechanics Division and presented at the Annual Meeting, New York, N. Y., November 28–December 3, 1954, of The American Society of Mechanical Engineers.

Discussion of this paper should be addressed to the Secretary, ASME, 29 West 39th Street, New York, N. Y., and will be accepted until July 11, 1955, for publication at a later date. Discussion received after the closing date will be returned.

Note: Statements and opinions advanced in papers are to be understood as individual expressions of their authors and not those of the Society. Manuscript received by ASME Applied Mechanics Division, October 24, 1953. Paper No. 54—A-93.

[3] Numbers in parentheses refer to Bibliography at end of paper.

[4] This problem was studied in connection with the design of an underwater sound source of this form.

analysis presented here is general and permits, in theory, the investigation of this problem, whatever the cross-sectional distribution of the excitation, provided it is axially symmetrical.

The dynamic behavior of the tube is analyzed by means of equations given by Kennard (4). These equations, which are based on Epstein's theory of elastic shells, have been derived by consistent and systematic elimination of higher-order terms; they differ significantly from Love's equations. The solution of the classical problem which is obtained from the present analysis (by neglecting the term representing the impedance of the surrounding fluid medium) therefore will differ somewhat from results obtained by previous investigators (2).

The phenomena in the surrounding fluid medium are described by a solution of the wave equation representing outgoing waves; the proper z-dependence is introduced by means of Fourier transforms. When the solutions thus derived for the dynamic behavior of the fluid column, of the elastic shell, and of the surrounding medium are combined, one obtains a transcendental characteristic equation whose roots are the "eigenvalues" of the composite system.

Phenomena in Fluid Column

The solution of this part of the problem is well known and will be summarized briefly. The alternating pressure connected with a continuous train of waves in a fluid column satisfies the steady-state, cylindrical wave equation (1, 2)

$$\frac{1}{r}\frac{\partial}{\partial r}\left(r\frac{\partial p}{\partial r}\right)+\frac{\partial^2 p}{\partial z^2}+k_i^2 p=0 \qquad [1]$$

Imposing the condition that the pressure be finite at $r = 0$, one obtains solutions in the form

$$p_n(r, z)=a_n J_0(k_{rn}r)e^{j(\omega t-k_{zn}z)} \qquad [2]$$

The wave numbers satisfy the relation

$$k_{rn}^2+k_{zn}^2=k_i^2 \qquad [3]$$

These numbers are the roots of the transcendental equation which characterize the boundary conditions of the system and are therefore as yet unknown. A mode n whose wave number k_{zn} has a real component propagates down the tube. All modes whose index is larger than a certain number, determined essentially by the frequency, have purely imaginary wave numbers and are therefore nonpropagating; their effect is negligible except in the vicinity of the wave source. The $n = 0$ mode comes closest to being a plane wave; it propagates at all frequencies with a real velocity c_{z0} which is smaller than the characteristic sound velocity c_i. In most cases this mode is the only one that need be considered in practice.

The boundary condition $u_i(a, z) = u_i(z)$ relates the foregoing solution to the radial displacement of the tube. For any mode n, the fluid particle displacement $u_{in}(a, z)$ at the inner surface of the tube is given by the relation

$$u_{in}(a, z)=\frac{1}{\rho_i\omega^2}\left.\frac{\partial p_n(r, z)}{\partial r}\right|_{r=a}=-\frac{k_{rn}a_n}{\rho_i\omega^2}J_1(k_{rn}a)e^{j(\omega t-k_{zn}z)} \qquad [4]$$

When this expression is substituted in the boundary condition stated above, it is seen that the radial deflection $u_i(z)$ of the tube is expressed by a summation of terms of the form

$$u_{in}(z)=b_n e^{j(\omega t-k_{zn}z)} \qquad [5]$$

where

$$b_n=-\frac{k_{rn}a_n}{\rho_i\omega^2}J_1(k_{rn}a)$$

Using this expression one can solve for a_n in terms of u_{in}; when this is substituted in Equation [2], the pressure p_n becomes, in terms of u_{in}

$$p_n(r, z)=\frac{j\rho_i\omega u_{in}J_0(k_{rn}r)}{k_{rn}J_1(k_{rn}a)} \qquad [6]$$

Phenomena in Surrounding Fluid Medium

The pressure in the surrounding medium also satisfies the wave Equation [1]. A general expression for a z-dependent solution representing outgoing waves may be written in the form of a Fourier integral as follows (5)

$$P(r, z)=e^{j\omega t}\int_{-\infty}^{\infty}F(k_Z)H_0^{(2)}\left(\sqrt{k_e^2-k_Z^2}\,r\right)e^{-jk_Z z}\,dk_Z \qquad [7]$$

The function $F(k_Z)$ may be derived from the boundary condition at $r = a$. For this purpose, the radial component of the tube-wall deflection, which was obtained in the preceding section, also will be expressed in terms of a Fourier transform

$$\left.\begin{aligned}u_i(k_Z)&=\frac{e^{j\omega t}}{2\pi}\sum_{n=0}^{\infty}b_n\int_{-\infty}^{\infty}e^{-jk_{zn}z}e^{jk_Z z}\,dz\\&=e^{j\omega t}\sum_{n=0}^{\infty}b_n\delta(k_Z-k_{zn})\end{aligned}\right\} \qquad [8]$$

The boundary condition $u_e(a, z) = u_i(z)$ requires that

$$\left.\begin{aligned}&u_i(k_Z)=\frac{1}{\rho_e\omega^2}\left.\frac{\partial P(r, k_Z)}{\partial r}\right|_{r=a}\\&\text{i.e.}\\&F(k_Z)=-\frac{\rho_e\omega^2}{\sqrt{k_e^2-k_Z^2}\,H_1^{(2)}\left(\sqrt{k_e^2-k_Z^2}\,a\right)}\sum_{n=0}^{\infty}b_n\delta(k_Z-k_{zn})\end{aligned}\right\} \qquad [9]$$

When this expression is substituted in Equation [7] and the integration performed, the sound pressure becomes

$$P(r, z)=-e^{j\omega t}\rho_e c_e\omega\sum_{n=0}^{\infty}\frac{b_n e^{-jk_{zn}z}}{\sqrt{1-(k_{zn}/k_e)^2}}\frac{H_0^{(2)}\left(\sqrt{k_e^2-k_{rn}^2}\,r\right)}{H_1^{(2)}\left(\sqrt{k_e^2-k_{zn}^2}\,a\right)} \qquad [10]$$

This can be rewritten in terms of Equation [5] as

$$P(r, z)=\rho_e c_e\sum_{n=0}^{\infty}u_{in}\zeta_e(k_{Rn}r) \qquad [11]$$

where the acoustic impedance ratio ζ_e is found to be, by comparison with Equation [10], and after some manipulation

$$\zeta_e(k_{Rn}r)=j\frac{H_0^{(2)}(k_{Rn}r)}{\sqrt{1-(c_e/c_{zn})^2}\,H_1^{(2)}(k_{Rn}a)} \qquad [12]$$

The wave number k_{Rn} is related to k_{zn} by the equation

$$\left.\begin{aligned}&k_{Rn}^2+k_{zn}^2=k_e^2\\&\text{i.e.}\\&k_{Rn}=k_e\sqrt{1-(c_e/c_{zn})^2}\end{aligned}\right\} \qquad [13]$$

It is noted that k_{Rn} is imaginary when $c_{zn} < c_s$. k_{Rn} can be related to k_{rn} by eliminating k_{zn} between Equations [13] and [3].

$$k_{Rn}^2 = k_s^2 - k_t^2 + k_{rn}^2 \quad \ldots\ldots [14]$$

The impedance ratio ζ_s is the complex sum $(\theta_s + j\chi_s)$ of a resistance ratio θ_s, indicating sound radiation, and of a reactance ratio χ_s connected with the acceleration of the surrounding fluid by the vibrating tube wall. Focusing the attention on the value of the pressure at the tube surface, these ratios may be calculated by taking the real and imaginary parts of ζ_s (as given by Equation [12]) for $r = a$. After some manipulation one obtains

$$\left.\begin{aligned} \theta_s(k_{Rn}a) &= \\ &\frac{2}{\pi k_{Rn}a\,\sqrt{1-(c_s/c_{zn})^2}\,\left|H_1^{(2)}(k_{Rn}a)\right|^2} \\ \chi_s(k_{Rn}a) &= \\ &\frac{J_0(k_{Rn}a)J_1(k_{Rn}a) + N_0(k_{Rn}a)N_1(k_{Rn}a)}{\sqrt{1-(c_s/c_{zn})^2}\,\left|H_1^{(2)}(k_{Rn}a)\right|^2} \end{aligned}\right\} \text{for } c_{zn} > c_s$$

$$\left.\begin{aligned} \theta_s(k_{Rn}a) &= 0 \\ \chi_s(k_{Rn}a) &= \frac{K_0(|k_{Rn}|a)}{\sqrt{(c_s/c_{zn})^2 - 1}\,K_1(|k_{Rn}|a)} \end{aligned}\right\} \text{for } c_{zn} < c_s \quad \ldots [15]$$

(The function K_n is defined later in Equation [25].) In the latter case, (i.e., $c_{zn} < c_s$) no power is radiated radially outward; the sound field forms a circular bundle of plane waves around and parallel to the tube (6).

If the fluids in the tube and in the surrounding medium have the same characteristic sound velocity ($c_i = c_s$), Equation [14] reduces to $k_{Rn} = k_{rn}$; since for the 0-mode $c_{z0} < c_i$, this condition also implies $c_{z0} < c_s$. This most important mode therefore will be propagated without being attenuated by radiation, since the corresponding resistive impedance is zero, as seen from Equation [15].

Dynamics of Tube

When dynamic deflections in the form of Equation [5] are substituted in the equations of motion of a cylindrical shell (4), one obtains

$$\left.\begin{aligned} -\rho_t\omega^2 u_{tn} &= \frac{-E}{1-\nu^2}\left(-j\,\frac{\nu}{a}\,k_{zn}v_{tn} + \frac{u_{tn}}{a^2}\right) \\ &\quad - \frac{Eh^2}{6(1-\nu^2)}\left(2k_{zn}^4 u_{tn} + \frac{2+\nu}{1-\nu}\,\frac{u_{tn}}{a^4}\right) \\ &\quad + \frac{p(a,z)}{2}\left(\frac{1}{h} - \frac{1-2\nu}{(1-\nu)a}\right) \\ &\quad - \frac{P(a,z)}{2}\left(\frac{1}{h} + \frac{1-2\nu}{(1-\nu)a}\right) \\ -\rho_t\omega^2 v_{tn} &= \frac{-E}{1-\nu^2}\left(k_{zn}^2 v_{tn} + j\,\frac{\nu}{a}\,k_{zn}u_{tn}\right) \end{aligned}\right\} \quad \ldots [16]$$

The latter of Equations [16] can be solved for v_{tn}; noting that $E/(1-\nu^2) = \rho_t c_t^2$, the relation between the axial and radial displacement components becomes

$$v_{tn} = \frac{j\nu k_{zn}u_{tn}}{a(k_t^2 - k_{zn}^2)} \quad \ldots\ldots [17]$$

When this expression is substituted in the former of Equations [16] one eventually obtains

$$\left[-k_t^2a^2 + \frac{\nu^2}{(c_{zn}/c_t)^2 - 1} + 1 + \frac{1}{6}\left(\frac{h}{a}\right)^2 \left(2k_{zn}^4a^4 + \frac{2+\nu}{1-\nu}\right)\right] u_{tn} = \frac{p_n a}{2\rho_t c_t^2}\left(\frac{a}{h} - \frac{1-2\nu}{1-\nu}\right) - \frac{P_n a}{2\rho_t c_t^2}\left(\frac{a}{h} + \frac{1-2\nu}{1-\nu}\right) \quad \ldots\ldots [18]$$

The specific impedance $z_t = p/\dot{u}_t$ of the shell to a force acting on its inner wall can be derived from this equation. The expression for this impedance will be found useful later in the analysis. The impedance is purely reactive. Hence if, in general, $z_t = r_t + jx_t$, then, in this particular case, $r_t = 0$ and

$$x_t = -\frac{2\rho_t c_t}{k_t a}\,\frac{1}{\dfrac{a}{h} - \dfrac{1-2\nu}{1-\nu}}\left[-k_t^2a^2 + 1 + \frac{\nu^2}{(c_{zn}/c_t)^2 - 1} + \frac{1}{6}\left(\frac{h}{a}\right)^2\left(2k_{zn}^4a^4 + \frac{2+\nu}{1-\nu}\right)\right] \quad \ldots\ldots [19]$$

This quantity is seen to be a function of the unknown parameters c_{zn} and k_{zn}, i.e., of k_{rn}. However, the functional dependence is weak for most values of $k_{rn}a$. It is convenient to define the reactance in terms of a reactance ratio $\chi_t(k_{rn}a) = x_t/\rho_t c_t$.

Characteristic Equation

The characteristic equation which determines the velocities of propagation of the different modes can now be constructed. When the partial modal pressures $P_n(a, z)$ and $p_n(a, z)$, given in Equations [11] and [6], respectively, are substituted in the equations of motion of the shell, Equations [18], and dividing all terms by u_{tn}, one obtains the characteristic equation of the problem under investigation

$$-k_t^2a^2 + \frac{\nu^2}{(c_{zn}/c_t)^2 - 1} + 1 + \frac{1}{6}\left(\frac{h}{a}\right)^2\left(2k_{zn}^4a^4 + \frac{2+\nu}{1-\nu}\right) = -\frac{\omega^2\rho_i a}{2k_{rn}\rho_t c_t^2}\,\frac{J_0(k_{rn}a)}{J_1(k_{rn}a)}\left(\frac{a}{h} - \frac{1-2\nu}{1-\nu}\right) - \frac{j\omega a\rho_s c_s \zeta_s(k_{rn}a)}{2\rho_t c_t^2}\left(\frac{a}{h} + \frac{1-2\nu}{1-\nu}\right) \quad \ldots\ldots [20]$$

The wave numbers k_{Rn} and k_{zn} can be expressed in terms of the wave number k_{rn}, by means of Equations [13] and [14]. The fluid-impedance ratio $\zeta_s(k_{Rn}a)$ defined in Equation [15] therefore has been written as a function of $(k_{rn}a)$. The characteristic equation now contains as the only unknown the wave number k_{rn}; values of k_{rn} which satisfy this equation are the wave numbers connected with the different modes; these, in turn, determine the corresponding phase velocities.

Equation [20] can be stated in more concise form when its left side is written in terms of the function $\chi_t(k_{rn}a)$ defined in the preceding section. After some manipulation, the characteristic equation is finally expressed as follows

$$\frac{\chi_t(k_{rn}a)}{k_t a} - j\,\frac{\rho_s}{\rho_i}\,\frac{\zeta_s(k_{rn}a)}{k_s a}\,\frac{1 + \dfrac{h}{a}\dfrac{1-2\nu}{1-\nu}}{1 - \dfrac{h}{a}\dfrac{1-2\nu}{1-\nu}} = \frac{J_0(k_{rn}a)}{k_{rn}aJ_1(k_{rn}a)} \quad \ldots [21]$$

The roots $x_n = k_{rn}a$ which satisfy this transcendental equation determine the velocities of propagation of the different modes. It can be verified from Equation [3] that these velocities are given by the expression

$$c_{zn} = \frac{c_i}{\sqrt{1 - (x_n/k_i a)^2}} \quad \ldots\ldots\ldots\ldots\ldots [22]$$

The roots x_n are complex when $\theta_s \neq 0$, i.e., when $c_{zn} > c_s$, and real (or imaginary, in the case of the $n = 0$ mode) when $\theta_s = 0$, i.e., when $c_{zn} < c_s$.

If $c_i = c_s$, then $\theta_s \neq 0$ for all modes except the quasi-plane ($n = 0$) mode. Consequently, all propagating modes will be attenuated by radiation into the surrounding medium, except the quasi-plane mode which does not radiate. Of course, if c_s is sufficiently large, all modes will radiate and therefore be attenuated.

The Quasi-Plane Wave

The transcendental Equation [21] will be studied for the case where the fluid in the tube is the same as in the surrounding medium. Only the $n = 0$ mode need be studied as the other propagating modes, if any, will be damped out by radiation, as explained previously. Under these conditions $c_i = c_s$, $\rho_i = \rho_s$, $k_i = k_s$, and k_{r0} and the root x_0 are imaginary; hence

$$\left.\begin{aligned} x_0 &= -j|x_0| \\ &= -jk_i a \sqrt{(c_i/c_{z0})^2 - 1} \end{aligned}\right\} \quad \text{or} \quad \left.\begin{aligned} c_{z0} &= \frac{c_i}{\sqrt{1 + (|x_0|/k_i a)^2}} \end{aligned}\right\} \quad \ldots\ldots\ldots [23]$$

The tube reactance given in Equation [19] may be written explicitly in terms of $|x_0|$ by making use of Equation [23] to eliminate c_{z0} and k_{z0}

$$\chi_t(|x_0|) = -\frac{2}{k_i^2 a^2}\frac{\rho_t}{\rho_i}\frac{\frac{k_i a}{\frac{a}{h}} - \frac{1-2\nu}{1-\nu}}{\left\{-k_i^2 a^2 + 1 + \frac{\nu^2}{\frac{(c_i/c_t)^2}{1 + (|x_0|/k_i a)^2} - 1}\right.}$$

$$\left. + \frac{1}{6}\left(\frac{h}{a}\right)^2\left[2(k_i^2 a^2 + |x_0|^2) + \frac{2+\nu}{1-\nu}\right]\right\} \quad \ldots\ldots [24]$$

The reactance ratio χ_s and the resistance ratio $\theta_s (= 0)$ are obtained from the latter two Equations [15]. When the Bessel and Hankel functions of imaginary argument are replaced by the modified functions

$$\left.\begin{aligned} I_n(|x_0|) &= (-j)^{-n} J_n(-j|x_0|) \\ \text{and} \\ K_n(|x_0|) &= \frac{\pi}{2}(-j)^{n+1} H_n^{(2)}(-j|x_0|) \end{aligned}\right\} \quad \ldots\ldots\ldots [25]$$

the transcendental Equation [21] takes the form

$$\frac{I_0(|x_0|)}{|x_0| I_1(|x_0|)} + \frac{K_0(|x_0|)}{|x_0| K_1(|x_0|)} \frac{1 + \frac{h}{a}\frac{1-2\nu}{1-\nu}}{1 - \frac{h}{a}\frac{1-2\nu}{1-\nu}} + \frac{\chi_t(|x_0|)}{k_i a} = 0 \quad \ldots [26]$$

The transcendental Equation [26] has been solved for the case of a brass tube (in CGS units: $E = 9.93 \times 10^{11}$, $\rho_t = 8.50$, $\nu = 0.3$) filled with water and surrounded by water ($c_i = c_s = 14.3 \times 10^4$, $\rho_i = \rho_s = 1.0$) for ratios of h/a equal to $1/16$ and $1/100$; (see Fig. 1). The mass-loading effect of the surrounding fluid is seen to be largest for intermediate values of frequency, where it causes a reduction of c_{z0} of the order of 35 per cent for $h/a = 100$ and of 13 per cent for $h/a = 1/16$. At very low frequencies this effect is of little importance because inertia forces are small in comparison to elastic forces; at high frequencies the effect also is small, the surrounding fluid being compressed rather than accelerated. It may be noted that the curve for $h/a = 1/16$, for a tube in vacuum, differs by a few per cent from the results obtained by Thomson (2) for the same numerical values of the parameters; this is due to the discrepancy between Kennard's and the usual equations of motion for cylindrical shells.

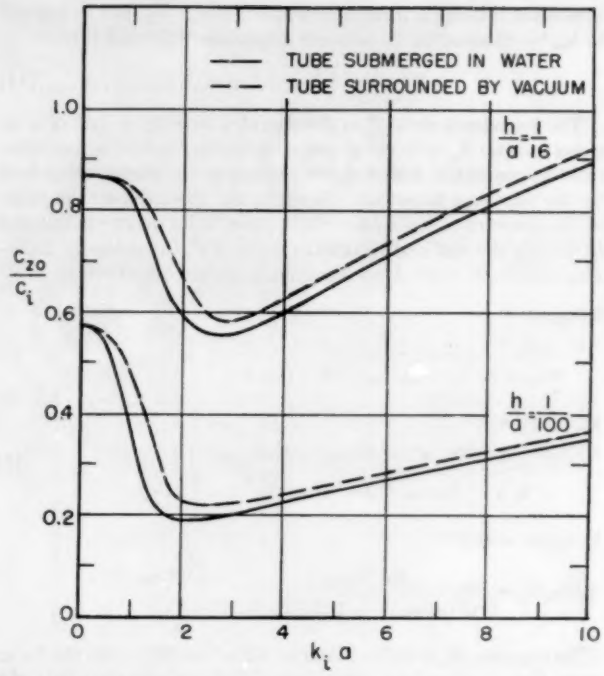

FIG. 1 RATIO OF PHASE VELOCITY c_{z0} TO CHARACTERISTIC SOUND VELOCITY c_i FOR QUASI-PLANE WAVE. ALL OTHER MODES ARE EITHER ATTENUATED BY RADIATION, OR NONPROPAGATING
(Brass tube filled with water and submerged in water; a is the tube radius and $2h$ its wall thickness.)

Inadequacy of Membrane Theory

Since the first two terms in Equation [26] are positive for $|x_0|$ real, this equation admits real roots (i.e., real values of c_{z0}) only if $\chi_t(|x_0|) < 0$, i.e., if the shell is "stiffness controlled." Should the motion of the shell be "mass controlled," even the quasi-plane wave would not propagate. It is seen that such a situation would arise for sufficiently large values of $k_i a$, except for the flexural term in $(h/a)^2$ which is related to changes in curvature. Without this term, which is neglected in the membrane theory of shells, the curves in Fig. 1 would steadily tend toward zero, instead of going through a minimum value.

The reason the flexural term prevents the tube from becoming mass-controlled above the frequency which coincides with the natural frequency of the 0-mode of the tube, as given by the membrane theory of shells, is as follows: When the first-order terms in the expression for χ_t tend to cancel, i.e., when $k_i a \leq 1$, the higher-order terms involving h^2 become significant, however small the ratio h/a, because as χ_t tends to zero, so must the I_n and K_n terms, in order to satisfy the transcendental Equation [26]; this, in turn, means that $|x_0|$ must grow beyond bounds; the factor $|x_0|^4$, which appears in the h^2-term, will thus always cause this term to become sizable. Physically, this can be interpreted as follows:

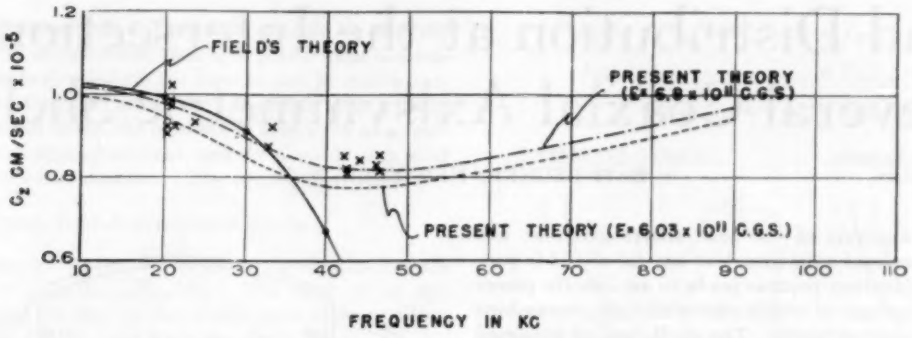

FIG. 2 DISPERSION CURVE FOR ZERO-ORDER MODE OF PROPAGATION OF ULTRASONIC WAVES IN COLUMN OF NAPHTHA CONTAINED IN A GLASS TUBE: x x FIELD AND BOYLE'S EXPERIMENTAL POINTS (7)

(———Field's theory (7), equivalent to membrane theory; – – – present theory using Field's values of parameters of system; —·—·— present theory using a Young's modulus for glass of $E = 6.80 \times 10^{11}$ CGS instead of Field's value of $E = 6.03 \times 10^{11}$. Discrepancy between two theories is not important for higher modes.)

The flexural stresses, represented by the h^2-term, become comparable to the membrane stresses in the region $k_r a \leqq 1$ because, as the phase velocity, and therefore the wave length, decreases without a similar reduction in the radial deflection, the changes in curvature become very large. Also, the shell wall is no longer "thin" when measured in terms of wave lengths, thus invalidating the fundamental assumption of the membrane theory. A very unusual situation thus obtains, in that the membrane theory will lead to incorrect results, however small the value of h/a.

These considerations are illustrated by the experimental study by Field and Boyle (7) on the propagation of ultrasonic waves in a glass tube ($E = 6.03 \times 10^{11}$, $\rho = 2.6$, $\nu = 0.215$, $h = 0.07$, $a = 1.62$, CGS units), filled with naphtha ($\rho = 0.74$, $c = 1.21 \times 10^5$, CGS); see Fig. 2. This figure shows experimental points obtained by Field and Boyle (7) together with their theoretical curve based on an analysis which is appproximately equivalent to the membrane theory. In addition, a dispersion curve obtained by analyzing the tube dynamics by means of the present theory has been plotted. It is quite obvious that the latter curve shows a better agreement with the experimental points in that it does not display a cutoff phenomenon. By assuming a somewhat larger value of Young's modulus ($E = 6.80 \times 10^{11}$) than the one given by Field and Boyle, the agreement can be made completely satisfactory. This assumed value of Young's modulus is entirely reasonable as E for most types of glass lies between 6 and 8×10^{11} CGS.

It is interesting to note that a "dead zone" can be brought into existence in the following manner: If closely spaced circular grooves are machined into the outer surface of a cylindrical shell, the alternating weak and thick sections thus obtained act, respectively, as discrete spring and inertia elements; the elastic energy connected with flexural stresses is then negligible, and the zero-order does display a "low-pass" cutoff behavior. This has been verified experimentally by Kuhl (3), who notes the discrepancy between the results of Field's analysis and of the observed data pertaining to the zero-mode. Kuhl suggests neglecting the inertia force in the tube wall to avoid the cutoff phenomenon predicted by the membrane theory. (In the present analysis, of course, it is the presence of flexural stresses which keeps the tube wall always stiffness-controlled.) Kuhl's heuristic procedure is less satisfactory than the present approach, particularly since he finds that the inertia force must be brought back into the picture if the theoretical curve is to agree with the experimental points pertaining to the higher modes. The reason why the membrane theory is satisfactory for these modes is that, in contradistinction to the zero-order mode, the wave length is always relatively long, so that strains connected with changes of curvature are never large.

It is interesting to note that the membrane theory also leads to erroneous conclusions when applied to the analysis of the propagation of stress waves in thin cylindrical shells (8).

A remark is in order about the case where a pressure pulse consisting of a finite number of cycles is sent down the tube. If the corresponding boundary condition is substituted in Equation [8], and the foregoing procedure carried through, it will be found that the resistance ratio θ_r never vanishes, i.e., that some power is always radiated, so that all modes are attenuated to some extent. The same applies to the case where a continuous train of pressure waves is sent along a tube of finite length. However, a length of the order of 20 wave lengths is sufficient to make the end effects insignificant.

ACKNOWLEDGMENT

The help of Mrs. E. B. Bockelman of the Acoustics Research Laboratory, Harvard University, in performing the calculations is gratefully acknowledged.

BIBLIOGRAPHY

1 "Vibration and Sound," by P. M. Morse, McGraw-Hill Book Company, Inc., New York, N. Y., second edition, 1948, pp. 305–311.

2 "Transmission of Pressure Waves in Liquid Filled Tubes," by W. J. Thomson, Proceedings of the First National Congress of Applied Mechanics, ASME, New York, N. Y., 1953, pp. 927–933.

3 "Die Eigenschaften Wassergefüllter Rohre für Widerstands- und Schall-geschwindigkeitsmessungen," *Acustica*, vol. 3, 1953, pp. 111–123.

4 "The New Approach to Shell Theory: Circular Cylinders," by E. H. Kennard, JOURNAL OF APPLIED MECHANICS, Trans. ASME, vol. 75, 1953, pp. 33–40.

5 "Methods of Theoretical Physics," by P. M. Morse and H. Feshbach, McGraw-Hill Book Company, Inc., New York, N. Y., 1953, section 11.2.

6 "The Physical Interpretation of the Expression for an Outgoing Wave in Cylindrical Coordinates," by M. C. Junger, *Journal of the Acoustical Society of America*, vol. 25, 1952, pp. 40–47.

7 "Dispersion and Selective Absorption in the Propagation of Ultrasound in Liquids Contained in Tubes," by G. S. Field and R. W. Boyle, *Canadian Journal of Research*, vol. 6, 1932, pp. 192–202.

8 "The Propagation of Elastic Waves in Thin-Walled Cylindrical Shells," by M. C. Junger and F. J. Rosato, *Journal of the Acoustical Society of America*, vol. 26, 1954, pp. 709–713.

Load Distribution at the Intersection of Several Coaxial Axisymmetric Shells

By H. BECKER,[1] NEW YORK, N. Y.

A relaxation analysis of the load distribution at the intersection of several axisymmetric coaxial shells is presented. The relaxation process leads to an infinite power series, the summation of which yields explicit expressions for the individual shell loads. The shells are all assumed to be unconstrained axially, thus eliminating axial interaction effects among them. The analysis, consequently, is restricted to radial shear forces and distributed moments at the intersection line, which is taken in a plane perpendicular to the common axis of the shells. Methods of treating temperature and pressure effects are described, and an illustrative example of the analysis of a three-shell intersection is included.

Introduction

A problem of frequent occurrence in pressure-vessel design involves determination of load distribution at the common intersection of several coaxial axisymmetric shells axisymmetrically loaded. Usually only two shells have a common intersection, such as the joint between the cylindrical and head portions of a drum. However, cases exist in which three or more shells intersect at a common latitude. The analysis to be presented yields expressions for the loads in each shell at the intersection circle in terms of the external applied forces and the shell proportions.

The general theory is developed for linearly deforming shells of any shape for which the rigidities are known. The general analysis considers only radial shears and distributed moments at the joint circle. Methods of treating temperature and pressure distributions are described in a subsequent section. An application of the method is included for shells analyzable on the basis of simplified theory.

Theory

The relaxation process to be described follows the same general lines as the well-known process of moment distribution with side sway.[2] It is evident, from an elementary consideration of one point on the line of intersection of the shells, Fig. 1, that a load will be distributed to each shell in proportion to the stiffness of that shell relative to the total stiffness of all the shells. Consider, then, the problem of determining the manner in which an external radial shear is distributed among the various shells at a joint. The shear load V is applied to the joint, which is constrained against rotation but not against radial deflection. The shear load is distributed to each joint in proportion to its shear distribution factor $D_{V(n)}$, and consequently the shear in shell n (see Fig. 1) is then $D_{V(n)}V$. This shear load, because of rotational restraint, induces a moment in shell n at the joint. It is possible to determine the induced moment in terms of the applied shear. The constant which relates induced moment to applied shear is called the shear-moment induction factor and is designated as $I_{VM(n)}$ for shell n. Consequently, the induced moment in shell n is $I_{VM(n)}D_{V(n)}V$. The sum of these moments represents the total moment applied to the joint from the shells, and is the negative of the moment which must be applied externally to the joint in order to prevent it from rotating. These three steps of shear distribution, moment induction, and moment summation, comprise the shear-to-moment, or VM-phase of the distribution process. Use of the terms "positive" and "negative," applied to shells above and below the latitude of the joint, is merely a sign convention to control the signs of the induction factors.

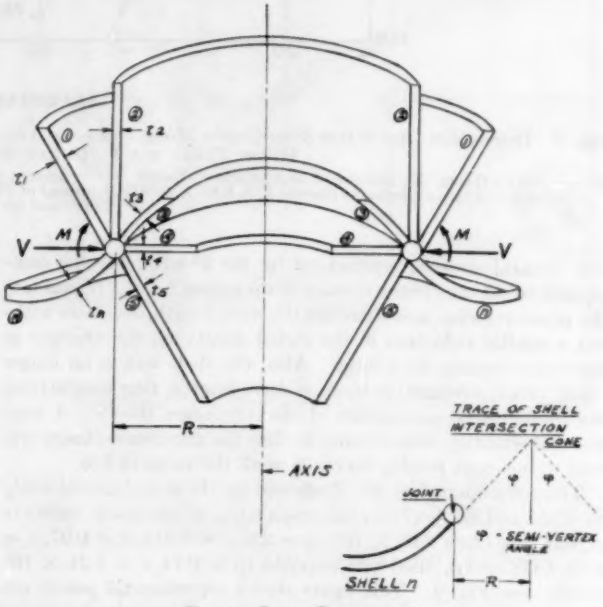

Fig. 1 Joint Geometry

The procedure by which the external joint moment from the VM-phase is distributed among the shells with the joint constrained radially, but not against rotation, is the moment-shear, or MV-phase. The external moment is distributed to each shell in proportion to its moment (with radial restraint) distribution factor, $D_{M(n)}$. The shear induced by the radial restraint is then $I_{MV(n)}D_{M(n)}M$. The summation of these shears is the resultant shear force applied to the radial restraint by the shells, and the negative of this quantity is the new external shear load on the joint.

The shear and moment cycles are developed symbolically later, during which it may be seen that the value of joint load at the beginning of any cycle bears a constant ratio to its value at the be-

[1] Research Division, College of Engineering, New York University.

[2] See, for example, "Theory of Modern Steel Structures," by L. E. Grinter, The Macmillan Company, New York, N. Y., vol. 2, 1937, p. 155.

Contributed by the Applied Mechanics Division and presented at the Annual Meeting, New York, N. Y., November 28–December 3, 1954, of The American Society of Mechanical Engineers.

Discussion of this paper should be addressed to the Secretary, ASME, 29 West 39th Street, New York, N. Y., and will be accepted until July 11, 1955, for publication at a later date. Discussion received after the closing date will be returned.

Note: Statements and opinions advanced in papers are to be understood as individual expressions of their authors and not those of the Society. Manuscript received by ASME Applied Mechanics Division, November 16, 1953. Paper No. 54—A-43.

ginning of the previous cycle. Thus it is possible to add the successive loads on an individual shell by a power-series summation and so obtain in simple form the shear in each joint as a fraction of the external applied shear, the moment in each joint in terms of the external shear, the moment in each joint as a fraction of the external applied moment, and the shear in each joint in terms of the external moment. The development follows.

Shear Load-Distribution Cycle

The net shear in shell n after the first shear distribution cycle is $V_n = V(D_{V(n)} - I_{MV(n)}D_{M(n)}\Sigma I_{VM}D_V)$. The shear to be applied to the joint at the start of the second cycle is the negative of the total shear on the joint from the shells, or

$$+ V \Sigma I_{MV}D_M \Sigma I_{VM}D_V.$$

Let this be designated $QV(Q = \Sigma I_{MV}D_M \Sigma I_{VM}D_V)$. Then the second cycle external shear is QV, the third cycle external shear will be Q^2V, and the ith cycle external shear will be Q^iV. Thus the total shear in shell n after an infinite number of cycles would be

$$V_n = V(D_{V(n)} - I_{MV(n)}D_{M(n)} \Sigma I_{VM}D_V)(1 + Q + \ldots\ldots + Q^i)$$
$$= V(D_{V(n)} - I_{MV(n)}D_{M(n)} \Sigma I_{VM}D_V)/(1 - Q) \text{ (see footnote[3])}$$

or

$$(V_n/VD_{V(n)}) = [1 - (I_{MV(n)}D_{M(n)}/D_{V(n)}) \Sigma I_{VM}D_V]/(1 - Q) \ldots\ldots [1]$$

Similarly, the total moment in shell n would be found from the expression

$$(M_n/VI_{VM(n)}D_{V(n)}) = [1 - (D_{M(n)}/I_{VM(n)}D_{V(n)}) \Sigma I_{VM}D_V]/(1 - Q) \ldots\ldots [2]$$

Moment-Distribution Cycle

The net moment in shell n after the first distribution cycle is $M_n = M(D_{M(n)} - I_{VM(n)}D_{V(n)} \Sigma I_{MV}D_M)$, and the moment to be applied to the joint at the start of the second cycle is QM. Consequently, the final joint moment is expressible as

$$(M_n/MD_{M(n)}) = [1 - (I_{VM(n)}D_{V(n)}/D_{M(n)}) \Sigma I_{MV}D_M]/(1 - Q) \ldots\ldots [3]$$

and the final shear in shell n is expressible as

$$(V_n/MI_{MV(n)}D_{M(n)}) = [1 - (D_{V(n)}/I_{MV(n)}D_{M(n)}) \Sigma I_{MV}D_M]/(1 - Q) \ldots\ldots [4]$$

Special Cases

It is shown in Fig. 2 that induction factors for positive shells (shells above the joint) are positive, whereas for negative shells all induction factors are negative. This follows from the shear-and-moment sign conventions shown in Fig. 2. (In general, irrespective of shear-and-moment sign convention, I for a shell below the joint will be equal to $-I$ for a similar shell above the joint.) On this basis it is possible to examine some special cases of shell arrangements.

(a) A group of j positive equal shells: For this case

$$I_{MV(1)} = I_{MV(2)} = \ldots\ldots = I_{MV(j)} = I_{MV}$$
$$I_{VM(1)} = I_{VM(2)} = \ldots\ldots = I_{VM(j)} = I_{VM}$$
$$D_V = D_M = 1/j \text{ for all shells}$$

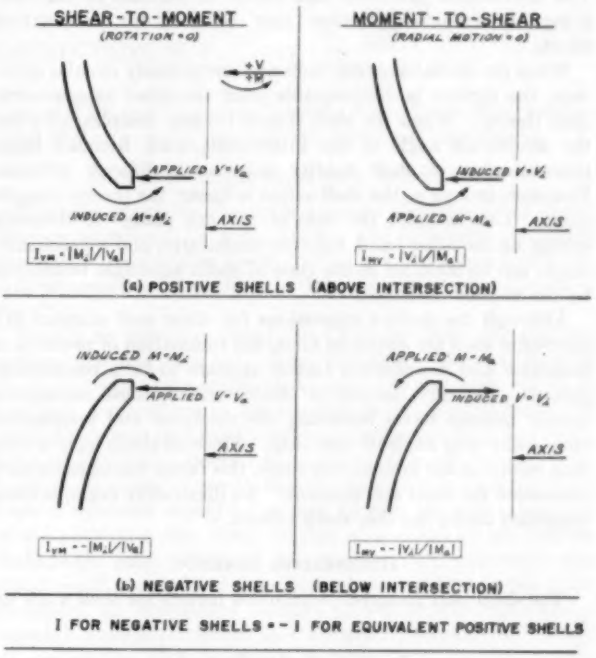

Fig. 2 Induction Factors

Under a radial shear loading V, the joint moment in each shell is

$$(M_n/VI_{VM(n)}D_{V(n)}) = (1 - I_{VM}/I_{VM})/(1 - I_{VM}I_{MV}) = 0$$

and the shear per shell is V/j.

For the case of applied moment, $M_n = M/j$, and $V_n = 0$.

(b) A group of $j/2$ positive shells and $j/2$ negative shells, all with equal rigidities: In this case, because of the difference in sign of I for + and — shells, $\Sigma I_{VM}D_V = \Sigma I_{MV}D_M = 0$, and therefore

$$V_n = V/j, M_n = VI_{VM}/j$$

for shear loading

$$M_n = M/j, V_n = MI_{MV}/j$$

for moment loading.

Additional special cases may be found from examination of Equations 1 to 4. For example, for a flat plate all $I = 0$ and therefore

$$V_n/VD_{V(n)} = M_n/MD_{M(n)} = 1, M_n/V = V_n/M = 0$$

Applications of Method

The results developed in the preceding section may be utilized for any shell intersection at which the loading conditions are known. These loads may be externally applied radial shears or distributed moments, for which conditions the analysis was developed, or they may be forces arising from the application of loads to one or more shells that reach the intersection. For example, the effects on each shell generated by external pressure loads on any one shell may be found by assuming the loaded shell

[3] This summation is permissible if $Q < 1$. It may be demonstrated, using elementary shell theory, that $Q < 1/2$. Since the demonstration is lengthy, and contributes nothing to an understanding of the distribution method, it is not presented.

to be fuliy fixed at the joint (no rotation, no radial deflection). The fixed end moment on the loaded shell at the joint, and the restraint shear, may then be found, after which these forces are reversed in sign and then applied to the joint as external loads. The distribution processes then follow as outlined in the foregoing. A similar application may be used for temperature effects.

When the shells have thin walls and are virtually circular cylinders, the rigidity is determinable from simplified axisymmetric shell theory. When the shell shapes become complex, or when the semivertex angle of the intersection cone becomes large, determination of shell rigidity may be a difficult problem. However, as long as the shell action is linear, the theory is applicable. This includes the case of the flat plate. A Belleville spring, on the other hand, behaves nonlinearly, and consequently might not be included in the class of shells amenable to analysis by the method described.

Although the derived expressions for shear and moment in a particular shell are simple in form, the summation of products of induction and distribution factors appears to be a complicated process. Actually, as will be demonstrated, these expressions merely become terms involving the thickness and intersection cone semivertex angle of each shell. Since all shells have a common radius at the intersection circle, this factor vanishes for each expression for shear and moment. An illustrative example using simplified theory for thin shells follows.

Illustrative Example

The shear and moment distribution factors for shell n are defined as

$$D_{V(n)} = (V/\Delta)_n/\Sigma\,(V/\Delta)$$

and

$$D_{M(n)} = (M/\theta)_n/\Sigma\,(M/\theta)$$

where (V/Δ) and (M/θ) are the shear and moment rigidities determined on the bases described above.

It can be shown (using the thin-wall theory of conical shell behavior to find the deflections of any shell with an intersection cone semivertex angle φ, and wall thickness, t) that[4]

$$D_{V(n)} = t_n^{5/2}\cos^{-1/2}\varphi_n/\Sigma t^{5/2}\cos^{-1/2}\varphi$$

$$D_{M(n)} = t_n^{5/2}\cos^{1/2}\varphi_n/\Sigma t^{5/2}\cos^{1/2}\varphi$$

Then, using the values of I found in accordance with Fig. 2, it may be shown, using elementary shell theory, that

$$I_{VM(n)} = (1/2)/I_{MV} = s_n a t_n^{1/2}\cos^{1/2}\varphi_n$$

$$(a = 0.778\,R^{1/2} \text{ when Poisson's ratio} = 0.3)$$

Consequently

$$(I_{MV(n)}D_{M(n)}/D_{V(n)})\,\Sigma\,I_{VM}D_V = U_n = (1/2)(C/B)s_n t_n^{1/2}\cos^{1/2}\varphi_n$$

$$(D_{M(n)}/I_{VM(n)}D_{V(n)})\,\Sigma\,I_{VM}D_V = 2U_n$$

$$(I_{VM(n)}D_{V(n)}/D_{M(n)})\,\Sigma\,I_{MV}D_M = W_n = (1/2)(C/A)s_n t_n^{-1/2}\cos^{-1/2}\varphi_n$$

$$(D_{V(n)}/I_{MV(n)}D_{M(n)})\,\Sigma\,I_{MV}D_M = 2W_n$$

$$\Sigma\,I_{MV}D_M\,\Sigma\,I_{VM}D_V = Q$$

$$A = \Sigma\,t^{3/2}\cos^{-1/2}\varphi,\ B = \Sigma\,t^{5/2}\cos^{1/2}\varphi,\ C = \Sigma\,st^2,\ Q = C^2/2\,AB$$

Therefore

$$V_n/VD_{V(n)} = (1 - U_n)/(1 - Q)$$

$$M_n/VI_{VM(n)}D_{V(n)} = (1 - 2U_n)/(1 - Q)$$

$$M_n/MD_{M(n)} = (1 - W_n)/(1 - Q)$$

$$V_n/MI_{MV(n)}D_{V(n)} = (1 - 2W_n)/(1 - Q)$$

The symbol s refers to the sign of the shell, and is + or − accordingly.

[4] For shell deflections and rotations, see "Stresses and Deformations of Flanged Shells," by G. Horvay and I. M. Clausen, Journal of Applied Mechanics, Trans. ASME, vol. 76, 1954, pp. 109–116.

Solving Highly Complex Elastic Structures in Easy Stages

By GABRIEL KRON,[1] SCHENECTADY, N. Y.

A systematic procedure is presented to solve quickly very large elastic structures, containing hundreds of component elements. The method is not competitive with existing techniques of solving sets of linear equations and is to be used only when other methods prove inadequate to cope with the capacity of the available computer (slide rule or electronic). Extension of the method—shown here for beams with one dominant dimension only—to structural components having more general and arbitrary shapes should be obvious to those versed in the art of structural analysis.

INTRODUCTION

Interconnecting Equations of State

THE performance of most physical systems is usually represented by a set of simultaneous relations between the known and unknown variables, to be called here "equations of state." The solution of the same physical system is similarly represented by another set of simultaneous equations, to be called here "equations of solutions."

The author has spent several decades developing rules to establish in a routine manner the equations of state of complex physical systems—both linear and nonlinear—by tearing the given system apart into several smaller systems and setting up the equations of state of each small system. In highly complex engineering systems it was expedient to continue the tearing apart of the physical system into successively smaller systems, until the ultimate components were reached, whose equations of state could be more easily established by the basic equations of Lagrange, or by Hooke's law, and so on. With the equations of state of the ultimate "primitive" system established, a set of routine transformations (linear or nonlinear) interconnected the equations of state of the smaller systems into those of the original large system. (Of course each stage of physical tearing is usually accompanied by auxiliary sets of co-ordinate transformations into more appropriate physical or hypothetical reference frames.)

The process of tearing apart physical systems always has demanded the introduction of "tensors" and "geometric objects" in order to tie together the various types of physical objects scattered among the component subdivisions. The establishment of all tensors and geometric objects inherent in a physical system may be looked upon as tearing the system apart into "functional subdivisions," as opposed to physical subdivisions. Each tensor performs a different physical function, so that the totality of all functions correctly represents the actual physical system. The success of the tearing method is chiefly due to the parallel development of the theory of physical and functional subdivisions.

Interconnecting Equations of Solutions

Since the equations of solutions consist also of a set of simultaneous equations between known and unknown variables, eventually the question arose: "Why not tear apart and interconnect equations of solutions in the same way as are equations of state?"

Having an extensive background in interconnecting physical systems first and then only their equations of state, a little reflection showed to the author that a new type of duality, which he has been emphasizing in his previous works, fits perfectly the parallel relations that exist between equations of state and equations of solutions. Instead of a convenience, it became now, however, an actual necessity, that the interconnection of the equations of solutions should follow step by step the interconnection of the physical system itself, or that of a model of the system. Perhaps the most significant difference between interconnecting equations of state and equations of solutions is that in the latter procedure all connection tensors **C** are usually nonsingular (square), while in the former all **C** are usually rectangular. (That is, part of the always existing nonsingular **C** became usually irrelevant to the problem under consideration.)

Purpose of the "Method of Tearing"

The method of tearing always leads to a set of equations of solutions first and then only to some particular numerical solution or solutions. Hence this new analytical tool is primarily an "inversion procedure," not a solution technique. Its merits and demerits must be viewed accordingly from that angle.

The method of tearing is not intended to compete with any existing inversion or solution method. It should be used only when other methods have proved unsatisfactory to cope with the limitations of the available computer, be it a slide rule, a desk calculator, or an electronic digital computer, such as a CPC or the "Whirlwind." The method is ideal especially for problems whose equations are so large in number, or so complicated, that one does not even attempt to write the equations down. The new method requires only the existence of a physical system (or a model of it) and the equations of any convenient subdivisions thereof. In case of a large elastic-beam structure, for instance, it is sufficient to have available the equations of each isolated beam only (or of any small or large combination of them). The tearing method supplies an almost automatic procedure to establish the equation of solution of the entire system.

The equations of solutions come out in an entirely new form containing a large number of zero elements. If the number of subdivision is n, the new type of inverse ("factorized" inverse or "orthogonal" inverse) contains only about $1/\sqrt{n}$ nonzero elements, compared with that of a conventional inverse matrix. In this new form it is comparatively easy to augment the physical system and its equations of solution in a parallel manner, as well as diminish them or alter them in unison. In structures where a finished design is often modified to suit new conditions, the advantage of an easily alterable solution is obvious. Spatial motions

---

[1] Consulting Engineer, General Electric Company, Schenectady, N. Y.

Contributed by the Applied Mechanics Division and presented at the Annual Meeting, New York, N. Y., November 28–December 3, 1954, of The American Society of Mechanical Engineers.

Discussion of this paper should be addressed to the Secretary, ASME, 29 West 39th Street, New York, N. Y., and will be accepted until July 11, 1955, for publication at a later date. Discussion received after the closing date will be returned.

Note: Statements and opinions advanced in papers are to be understood as individual expressions of their authors and not those of the Society. Manuscript received by ASME Applied Mechanics Division, October 19, 1953. Paper No. 54—A-25.

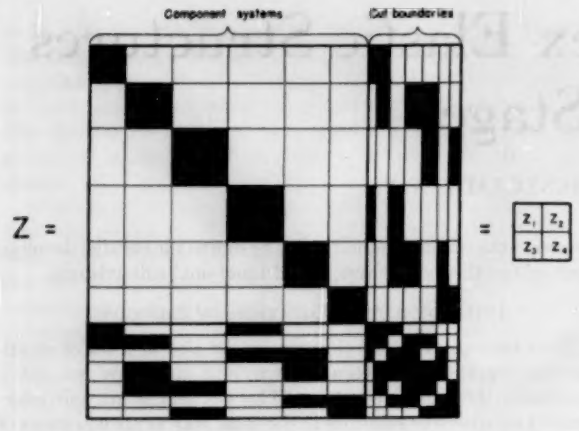

FIG. 1 INVERSE MATRIX INVOLVING CUT BOUNDARIES

or rotations of parts into a large number of new positions may be taken care of easily without starting the solutions of the stationary and rotating parts all over again for each new position. When each portion of a system could be built up from several different types of material (as in a nuclear reactor), the few types of subdivisions may be interconnected into quite a large variety of resultant systems with little extra work.

The author visualizes the equations of solution of standardized pieces of structures being stored away in file cabinets in the same manner as standardized manufactured products are stored in warehouses. When the equations of solutions of a new structure are needed, the partial solutions stored away years ago are recombined with the solutions of any new component parts to form quickly the equations of solution of the new structure. The latter in turn are to be stored away for the eventual solution of still bigger structures. It is the hope of the author to be able to re-employ, for instance, two-dimensional solutions of partial differential equations for use in the solution of three-dimensional problems and the latter in turn to solve four-dimensional ones, without starting the analysis from the very beginning each time a new and larger problem arises.

All efforts of the author, all his formulations and methods of reasoning, are inspired with such distant goals in mind.

EXAMPLE OF "PARTITIONING" A MATRIX

Since the "tearing apart" of a physical system at first sight appears to be analogous to the step of partitioning a matrix,[2] it is instructive to point out one of the significant differences that already excludes any competition between the two methods for the purposes outlined in the foregoing.

Let a physical system with equations $\mathbf{I} = \mathbf{YE}$ be torn apart into three component parts. In terms of a partitioned matrix the equations of state might assume the form

$$\begin{bmatrix} \mathbf{I}_1 \\ \mathbf{I}_2 \\ \mathbf{I}_3 \end{bmatrix} = \begin{bmatrix} \mathbf{Y}_1 & & \mathbf{Y}_3 \\ & \mathbf{Y}_2 & \mathbf{Y}_4 \\ \mathbf{Y}_5 & \mathbf{Y}_6 & \mathbf{Y}_7 \end{bmatrix} \begin{bmatrix} \mathbf{E}_1 & \mathbf{E}_2 & \mathbf{E}_3 \end{bmatrix} \quad \ldots\ldots\ldots\ldots\ldots [1]$$

(This equation should not be construed as a statement that a set of equations may be partitioned in the same manner as a physical system can be torn apart. The foregoing form of the equations is assumed only for the sake of the argument to follow.)

The equations might be inverted by the following steps:

[2] See for instance reference (3). Numbers in parentheses refer to the Bibliography at the end of the paper.

1 Find the inverse of $\mathbf{Y}_1$ and $\mathbf{Y}_2$ as $\mathbf{Z}_1$ and $\mathbf{Z}_2$. (That is, solve the first two equations for $\mathbf{E}_1$ and $\mathbf{E}_2$, respectively.)

2 Substitute $\mathbf{E}_1$ and $\mathbf{E}_2$ into the third equation. (This step requires a large number of matrix multiplications.)

3 Find the inverse of the new submatrix occupying the place of $\mathbf{Y}_7$ and call it $\mathbf{Z}_7$. The resulting $\mathbf{E} = \mathbf{ZI}$ equations are

$$\begin{bmatrix} \mathbf{E}_1' \\ \mathbf{E}_2' \\ \mathbf{E}_3' \end{bmatrix} = \begin{bmatrix} \mathbf{E}_1 + \mathbf{Z}_1\mathbf{Y}_3\mathbf{E}_3 \\ \mathbf{E}_2 + \mathbf{Z}_2\mathbf{Y}_4\mathbf{E}_3 \\ \mathbf{E}_3 \end{bmatrix} = \begin{bmatrix} \mathbf{I}_1 & & \mathbf{I}_2 & \mathbf{I}_3 \\ \mathbf{Z}_1 & & & \\ & & \mathbf{Z}_2 & \\ -\mathbf{Z}_7\mathbf{Y}_5\mathbf{Z}_1 & & -\mathbf{Z}_7\mathbf{Y}_6\mathbf{Z}_2 & \mathbf{Z}_7 \end{bmatrix} \quad \ldots\ldots [2]$$

The reader unacquainted with "invariant" transformations, physical or hypothetical reference frames, and similar concepts of tensor analysis, would exclaim: "Here is a set of equations of solution $\mathbf{E} = \mathbf{ZI}$ of a physical system. Let us go and interconnect this set with the similar equations of one or several other physical systems in the same manner as the method of tearing does."

The answer is that such an interconnection cannot be performed. In the foregoing equations the $\mathbf{E}'$ are in a reference frame different from that of the I. Before the matrix can be interconnected with a similar matrix, it is necessary to eliminate $\mathbf{E}_3$ from the first two equations and completely fill the inverse matrix, in order to assume the tensor or physically existing equations of solution.

$$\begin{bmatrix} \mathbf{E}_1 \\ \mathbf{E}_2 \\ \mathbf{E}_3 \end{bmatrix} = \begin{bmatrix} \mathbf{Z}_1 & \mathbf{Z}_2 & \mathbf{Z}_3 \\ \mathbf{Z}_4 & \mathbf{Z}_5 & \mathbf{Z}_6 \\ \mathbf{Z}_7 & \mathbf{Z}_8 & \mathbf{Z}_9 \end{bmatrix} \begin{bmatrix} \mathbf{I}_1 & \mathbf{I}_2 & \mathbf{I}_3 \end{bmatrix} \quad \ldots\ldots\ldots\ldots\ldots [3]$$

Now both $\mathbf{E}$ and $\mathbf{I}$ are in the same physical reference frame (the same frame as that of Equation [1]) and the $\mathbf{Z}$ can now be interconnected with similar $\mathbf{Z}$, as directed by the method of tearing.

EXAMPLE OF THE METHOD OF "TEARING"

Compare with the foregoing steps next how the method of tearing establishes a set of new types of equations of solutions, that can also be interconnected.

1 Given the equations of state of three isolated structures (the primitive system) as

$$\begin{bmatrix} \mathbf{I}_1 \\ \mathbf{I}_2 \\ \mathbf{I}_3 \end{bmatrix} = \begin{bmatrix} \mathbf{Y}_1 & & \\ & \mathbf{Y}_2 & \\ & & \mathbf{Y}_3 \end{bmatrix} \begin{bmatrix} \mathbf{E}_1 & \mathbf{E}_2 & \mathbf{E}_3 \end{bmatrix} \quad \ldots\ldots\ldots\ldots\ldots [4]$$

2 Find the inverse of the three Y as $\mathbf{Z}_1$, $\mathbf{Z}_2$, $\mathbf{Z}_3$

$$\begin{bmatrix} \mathbf{E}_1 \\ \mathbf{E}_2 \\ \mathbf{E}_3 \end{bmatrix} = \begin{bmatrix} \mathbf{Z}_1 & & \\ & \mathbf{Z}_2 & \\ & & \mathbf{Z}_3 \end{bmatrix} \begin{bmatrix} \mathbf{I}_1 & \mathbf{I}_2 & \mathbf{I}_3 \end{bmatrix} \quad \ldots\ldots\ldots\ldots\ldots [5]$$

3 Interconnect the three isolated structures by a routine procedure, that involves only a rearrangement of the rows and columns of the three Z without any multiplications.[3] The resultant form is

$$\begin{bmatrix} \mathbf{E}_1 \\ \mathbf{E}_2 \\ \mathbf{E}_3 \\ 0 \end{bmatrix} = \begin{bmatrix} \mathbf{Z}_1 & & & \mathbf{Z}_4 \\ & \mathbf{Z}_2 & & \mathbf{Z}_5 \\ & & \mathbf{Z}_3 & \mathbf{Z}_6 \\ \mathbf{Z}_7 & \mathbf{Z}_8 & \mathbf{Z}_9 & \mathbf{Z}_{10} \end{bmatrix} \begin{bmatrix} \mathbf{I}_1 & \mathbf{I}_2 & \mathbf{I}_3 & \mathbf{i} \end{bmatrix} \quad \ldots\ldots\ldots\ldots\ldots [6]$$

[3] The connection matrix $\mathbf{C}$ contains usually only plus or minus unity and zero. The interconnection itself is performed by the law of transformation $\mathbf{C}_i\mathbf{ZC}$, that involves only additions and permutations of rows and columns. If a digital computer is not equipped to perform such interchange, it may be done by clerical work with sciissors and Scotch tape.

In these equations of solutions all **E** and **I** are in identical physical reference frame (the same as in Equation [1]). Hence the **Z**-matrix is now ready to be interconnected with several other similar **Z** to form the **Z** of a still larger physical system. The **Z** of Equation [6] also may be altered in the same manner as the physical system is modified.

In the foregoing equations the extra variables **i** are the unknown currents (or forces) appearing at the cuts. (No such new concept appears in partitioning a matrix.) Since the three **I** are assumed to be known, the unknown **i** may be found by simply solving (not even inverting) the corner matrix $\mathbf{Z}_{10}$. There is no necessity to eliminate the **Z** in the last column as was the case with the **Y** of a partitioned matrix of Equation [1] in step 2.

The "Factorized" Inverse

Although this new type of inverse **Z** of Equation [6] has more variables than the conventional inverse Equation [3], nevertheless it contains far less nonzero elements. If the number of subdivision is n, the ratio of nonzero elements is about $1/\sqrt{n}$ matrix. That is, each time a new set of known **I** are assumed, the unknown **E** may be found by about a fraction of $1/\sqrt{n}$ fewer number of multiplications than by the use of the conventional inverse. This quasidiagonal nature of the factorized inverse offers hopes that very large problems with many thousands of variables eventually will be inverted without carrying along unduly large number of nonzero elements.

It should be noted that—since the reference frames of both types of inverses are identical—the factorized inverse of Equation [6] becomes identical with the conventional inverse of Equation [3], if the last row and column of the boundary constraints **i** are eliminated. As the conventional inverse of Equation [3] may be factorized into the elements of Equation [6], the latter is called a factorized inverse. However, the reverse step, the introduction of the auxiliary variables **i**, and the consequent decrease in the number of nonzero elements, cannot be performed without going through the reasonings of the method of tearing.

Since the k-dimensional abstract space of the k constraint variables **i** is orthogonal to the n-dimensional abstract space of the n-force variables **I** (and **i** is a dual of **I**), the factorized inverse of Equation [6] also may be called "orthogonal" inverse, to differentiate it from the conventional inverse of Equation [6]. Another designation may be "augmented" inverse.

Comparison With "Elimination" Methods

The factorized inverse of a physical system can be used not only for the construction of the factorized inverse of still bigger physical systems, but also can be used to get numerical solutions for the system in question for a large variety of boundary conditions. Since a conventional inverse matrix also can be used for both purposes, it is of interest to compare the computation time of the two types of inverse matrices. (The computation time does not involve input and output time, or the clerical work, only actual machine computation time of multiplications and divisions.) As a standard norm for calculating inverses the Gauss or Crout elimination method will be assumed, in which the number of multiplications is approximately N^3, where N is the number of equations (or variables).

If a system is torn into n-parts, the inverse calculation of each part involves approximately $1/n^3$ of that of the original inverse. The inverse of the n-parts (Equation [5]) involves $1/n^2$ calculation. The interconnection of the subdivision involves no multiplications, only additions (mostly an interchanging of rows and columns). Ignoring the computer time for addition and for the interchange of rows and columns, the establishment of the factorized inverse of Equation [6]—valid already for the construction of still bigger structures—involves thus $1/n^2$ of that of the conventional inverse of Equation [3].

If the factorized inverse is to be used also to solve for the unknown variables **E** numerically, (eventually all inverses are to be used for such purposes) then it is still necessary to solve (or calculate the inverse of) the lower corner matrix $\mathbf{Z}_{10}$ of Equation [6] for the unknown constraints **i** appearing at the cuts. In this additional calculation it is possible to use all devices of the theory of matrices such as partitioning, and so on, since it is possible to transform the auxiliary reference frame of the boundary currents **i** in an arbitrary manner, without destroying the reference frame of the original variables **I** and **E**.

These additional calculations roughly may be expected to take as much machine time as the inversion of all the n-component parts, namely, $1/n^2$. (In two-dimensional partial differential equations this assumption was found to be reasonable. However, in three-dimensional problems and in problems with more complex cuts, this rough estimate may prove to be too optimistic.) Hence the total machine time of the factorized inverse should take a fraction of about $2/n^2$ of that of the conventional inverse. (The rule, of course, breaks down when n is too small or too large compared with N, the number of equations. The clerical work involved in changing tapes, and the like, is not considered in the given reasoning.)

In connection with the foregoing rule of thumb two considerations must be emphasized:

1 If not the elimination method but some specialized technique, such as the partitioning of matrices, is used for inversion, then the foregoing rule of thumb cannot be used and should not be used for time estimate. The rule should be changed in accordance with the specialized inversion method used.

2 If the purpose of the computation is merely to solve a given set of equations already available, and if iterative, triangulation, Lanczos, conjugate gradient, or other types of solutions are practicable on the available computer, in such cases the establishment of an inverse is never even contemplated. Hence the rule of thumb $2/n^2$ similarly should not enter into consideration in comparing solution time. Any comparison is irrelevant, since the method of tearing should not be used if other solution methods are available and are practicable. (It should be noted that the method of tearing may employ any of the techniques mentioned for the solution of the constraint variables **i** of Equation [6].)

Construction of the orthogonal inverse should be undertaken only in view of the advantages expressed in the foregoing and in references (11 to 14). As emphasized before, the method of tearing is not a competitive procedure. Rather, it charts its own course through a hitherto untrodden territory. Any numerical example worked out for educational purposes (such as that in reference 13) should not be viewed as a proposed alternative procedure for existing inverse or solution techniques.

Field of Application of the Method of Tearing

While the most obvious application of the method of tearing is for the solution of simple types of linear systems, requiring merely the inversion of a matrix, that step of course only begins to touch its wide field of use. Even the very first practical application of the method of tearing to the calculation of losses in the transmission networks of several interconnected electric-utility companies (14) has led to a highly elaborate set of equations, transformations, and new concepts. The extension of the loss problem of steam systems to include their economic operations with hydroelectric systems and their reservoirs has involved the method of tearing in the calculus of variations, in the solution of the Hamilton-Jacobi partial-differential equation, and in contact transformations. Even an extension of the present paper to solve

more general elastic structures where the subdivisions have no supports, leads already to more elaborate equations of solution than $\mathbf{E} = \mathbf{ZI}$.

The author sees no limitations for the possible application of the method of tearing to linear and to certain special types of nonlinear problems with very large number of variables, except the imagination of the engineer and his intellectual courage to experiment with new techniques against great odds.

Necessity of a Physical Model

It should be noted that the method of interconnecting piecewise solutions assumes the existence of a physical model, in addition to the existence of a set of equations. The rules developed are applicable only to the tearing apart of a physical (or geometrical) system itself or its model, and not to the tearing apart of its conventional equations. Of course the model consists of only a drawing on a piece of paper, without implying any physical realizability.

The reason for the necessity of a physical model may come as a surprise to many an engineer. A physical model, such as an electrical circuit, contains far more information about the physical system to be solved than the conventional set of equations does that describes the system. The equation of a system (such as the dynamical equations of Lagrange, or the partial differential equation of the elastic field) do contain sufficient information to solve for the unknown variables. However, the processes of tearing apart and interconnection of systems demand additional informations that are not contained explicitly in the conventional equations.

Now, the electric-circuit (or any other correct) model does contain all such additional information needed, provided the model was formed by following the rules of tensor analysis, that is, provided the equations modeled were tensor or tensor-density equations. These additional informations are discussed in detail in reference (11). As the understanding of these new concepts involves some acquaintance with a few basic rules of tensor analysis, constant reference will have to be made in the paper also to the book "Tensor Analysis of Networks" (9) as TAN.

SCHEMATIC MODEL OF AN ELASTIC STRUCTURE

Electrical Model of a Beam

The electric-circuit model of a long thin beam, having six degrees of freedom at each of its ends (three translations and three rotations), has been established in a paper entitled "Tensorial Analysis and Equivalent Circuits of Elastic Structures" (10) to which constant reference will be made as TES. The model of each beam is equivalent to a six-phase transmission network, containing positive and negative resistances. Since the two ends of the transmission lines are mutually coupled, the stiffness coefficients $\mathbf{Y}$ of each beam are arranged into a matrix with twelve rows and columns. Each beam is assumed to lie in a general direction in space and its ends may be subjected to arbitrary constraints. Many of the representative scalar equations are given in Tables I–XI of TES. (These researches were based upon the concepts of Southwell (8).) Other types of electric-circuit models for beams, valid also for natural-frequency studies, are given in reference (7).

In the previous article the purpose of the electric-circuit model was to solve the elastic structural equations on the a-c analyzer. For that purpose the model had to be physically realizable. In consequence, it had to assume a rather detailed form, containing a large number of units, as shown in Fig. 2(a) for a two-dimensional beam lying in a grid frame and having both ends rigid (reproduced from Fig. 13(a) of TES). For the present purpose the model need not be physically realizable and it will be sufficient to

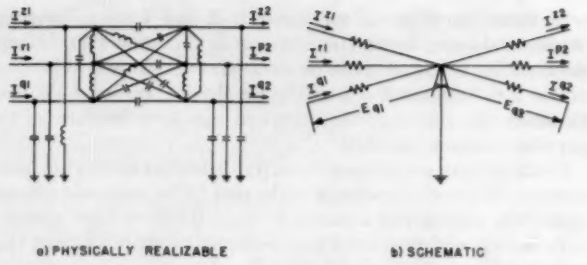

Fig. 2 Representations of a Two-Dimensional Beam

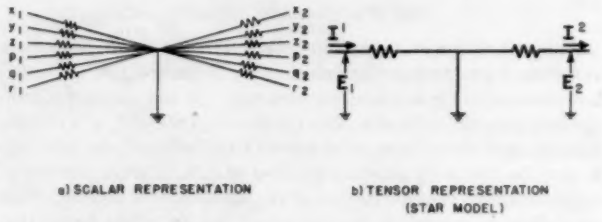

Fig. 3 Schematic Representations of a General Three-Dimensional Beam

represent the same beam by the schematic circuit of Fig. 2(b). For the most general three-dimensional beam the new model is shown in Fig. 3(a). It consists of twelve resistances, all mutually coupled (the coupling arrows are left out) and all of them grounded at a common central point. Depending on the type of constraints existing at the joints, some of the beams may contain five or less resistances at each end or at both ends in all combination (TES, p. 418).

As a matter of fact, for the present purpose it will be sufficient to represent each beam by two coils only, mutually coupled and grounded at a common point. Since each coil now actually stands for six scalar coils, it is drawn with heavy lines and called a tensor coil, Fig. 3(b). Similarly, the stiffness coefficients of each beam will be represented analytically by a matrix with two rows and columns, in which each bold-face element actually represents a six-by-six matrix

$$\mathbf{Y} = \begin{array}{c} \\ 1 \\ 2 \end{array} \begin{array}{c} \begin{array}{cc} 1 & 2 \end{array} \\ \begin{bmatrix} \mathbf{Y}^{11} & \mathbf{Y}^{12} \\ \mathbf{Y}^{21} & \mathbf{Y}^{22} \end{bmatrix} \end{array} \quad \ldots\ldots\ldots\ldots\ldots\ldots [7]$$

where $\mathbf{Y}^{21}$ is the transpose of $\mathbf{Y}^{12}$.

If so desired, the schematic star-connected two coils may be replaced by three coils connected in a tee, or a delta, or in a pi as shown in Fig. 4. In the analytical study of TES the pi form was used. All these forms, however, require the same method of analysis without any change.

The mass and moment of inertia tensor $\omega^2\mathbf{M}$ (with six degrees of freedom) may be represented by a tensor coil, Fig. 5, attached between a junction of two beams and the ground (see also Fig. 9 of TES).

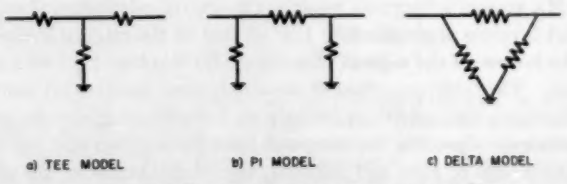

Fig. 4 Other Tensor Representations of a Beam

Since the new model is only schematic, the following treatment is valid not only for long, thin beams, but, in general, for beams—short and thick—having one dominant dimension. The components of **Y**, given in TES, must be generalized for such more general beams.

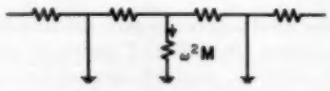

FIG. 5 TENSORIAL REPRESENTATION OF MASS AND MOMENT OF INERTIA ω^2M

It should be emphasized that these new types of schematic (physically nonrealizable) models basically are not electrical, but geometrical (topological) models of the physical system. However, it is much more convenient to use electrical terminology as "impress a current at a junction" than to use topological parlance, such as "draw the boundaries of a 1-chain on an *O*-cell." It is not the intention of the author to inflict upon the harassed mechanical engineer concepts from electrical engineering. Nevertheless, he is convinced that to translate basic scientific (geometrical) concepts into engineering parlance, the choice of electrical terminology is the least of three possible evils (not because of his electrical background but because of the basic inadequacy of mechanical analogs).

NOMENCLATURE

To clarify the statements to follow for engineers who are not acquainted with electrical models, a parallel mechanical and electrical terminology is given:

Mechanical		Electrical	
Stiffness matrix	= **Y**	Admittance matrix	= **Y**
Flexibility matrix	= **Z**	Impedance matrix	= **Z**
External force	= **F**	Current impressed	= **I**
Internal force	= **f**	Circulating current	= **i**
Displacement	= **D**	Absolute potential	= **E**

The six displacements **D** at each end of a beam represent three linear displacements along x, y, and z and three angular displacements around the same axes (p, q, r). Similarly, three of six forces are linear (stress and shear) and three are angular (torque and bending moment).

EQUATIONS OF AN ELASTIC STRUCTURE

The equations of state of an interconnected elastic structure are written as

$$\mathbf{I} = \mathbf{YE} \mid \mathbf{F} = \mathbf{YD} \quad \ldots\ldots [8]$$

The joints may be rigid or subjected to arbitrary constraints. The applied forces **F** at the joints are represented as currents **I**, the displacements **D** of joints by differences of potential **E** appearing between the end points and the ground. The stiffness coefficients are represented by an admittance matrix **Y**. Expressed in another way, the given mechanical beam network is looked upon as a "junction" network, in which all voltages and currents are defined between two joints (TAN, p. 359).

To simplify the presentation of the central theme of tearing and interconnecting, it will be assumed that all applied forces **I** are known and all displacements **E** are unknown. (In the general case, of course, part of **I** and part of **E** may be known; the rest of the **I** and **E** are unknown.) The problem thus is to establish the equations of solution

$$\mathbf{E} = \mathbf{ZI} \mid \mathbf{D} = \mathbf{ZF} \quad \ldots\ldots [9]$$

where **Z** is the inverse of the given matrix **Y** and contains the flexibility (or influence) coefficients. An example to establish the equations of state of a structure with five beams and two masses is worked out in detail in Equations [33] to [36] of TES. Also, reference (2) contains several other general examples and reference (1), some simpler ones.

THE GENERAL PROBLEM

THREE SYSTEMS WITH ANALOGOUS EQUATIONS

It so happens that the three previous publications, in which the author has explained the idea of solving large physical systems by interconnecting solutions of their subdivisions, all involved also the solution of junction networks, having equations of state in the form **I** = **YE**. However, the method of solution of the present physical system differs from that of the other three systems, just as the solution of the latter three differed from each other. Hence a separate treatment of the present physical system is needed.

The first series of publications (14) covered the I^2R loss calculation of an extended electrical power-transmission network, jointly operated by several power companies forming a "power pool." The second publication (11) involved the solution of the partial differential equation of Poisson

$$\text{Div y grad } E = I \quad \ldots\ldots [10]$$

The third publication (12) treated the steady-state solution of the two-dimensional field equations of Maxwell

$$\left.\begin{array}{l|l} \text{Curl } \mathbf{E} + \dfrac{\partial \mathbf{B}}{\partial t} = \mathbf{O} & \text{Div } \mathbf{B} = 0 \\ \text{Curl } \mathbf{H} = \dfrac{\partial \mathbf{D}}{\partial t} + \mathbf{I} & \text{Div } \mathbf{D} = 0 \end{array}\right\} \quad \ldots\ldots [11]$$

or of the diffusion equation

$$\text{Div y grad } E + yE = I \quad \ldots\ldots [12]$$

(The electrical network configurations are the same for both types of equations, but the physical interpretations of the network quantities are different.) The difference equations of all three types of partial differential equations assume the form **I** = **YE**, just as the equations of state of an elastic structure do.

However, the electric-circuit models in the three publications assume two radically different basic forms. In the Maxwell network and in the diffusion network every junction is grounded through an impedance, while in the entire Poisson network and in the electrical power network only one ground point exists or none at all. Because of this difference in network structure, the process of interconnection involves more steps in the Poisson and the power networks. When no ground exists, it is necessary to determine the differences of potentials existing between the various torn-up structures. When each of the subdivisions is grounded, no differences of potential arise between them.

SPECIAL NATURE OF ELECTRIC-POWER NETWORKS

Attention is called to a special feature in the study of electrical power networks of reference (14) that can be adapted for the treatment of elastic structures also. Since a comparatively small number of electrical power plants supplies a very large number of loads, it is customary to replace all loads existing within a territory by one "equivalent" load. Thereby the actual electrical network is replaced by a hypothetical network by means of a series of three transformations and it is the hypothetical network that actually is being studied.

In an analogous manner it is also customary to replace large actual elastic structures by smaller and simpler "equivalent" structures. In consequence, the concept of "beam" occurring in these pages, having six degrees of freedom, can just as well be

assumed to represent an equivalent beam having any large number of degrees of freedom. All diagrams, formulas, and reasoning of this paper remain, nevertheless, unchanged, since each tensor and each beam may represent unspecified degrees of freedom.

Another special feature also exists in the treatment of electric-power networks, that makes their study unpalatable to all but specialists. In the hour-by-hour operation of a power system the numerical values of **E** and **I** occurring in the basic solutions **E** = **ZI** are unknown. Instead of knowing the voltages **E** and currents **I**, the operating engineers only know the numerical values of the "real powers" **P**. Hence it is necessary to transform **E** = **ZI** to a new form **L** = **MP** by a series of three additional transformations and thus to perform all tearing apart and interconnections in terms of the unfamiliar concepts of **P** and **L** (directional losses).

In problems involving combined dynamical and elastic properties and especially when thermal and perhaps chemical, or the like, properties also are included, the tearing apart and interconnections are to be performed not in the actual physical reference frame, but in some artificial, hypothetical frame. In the solution of such torn-apart complex problems the more advanced concepts of tensor analysis become indispensable.

Special Nature of Elastic Structures

The electrical model of the elastic structure is analogous to the Maxwell and diffusion networks of reference (12) inasmuch as the circuit of every beam is grounded. Hence the method of interconnection of their subdivisions is also analogous. Any difference arising between their interconnection is more in the nature of convenient procedure rather than a matter of circuit configuration. In particular:

1 Elastic structures will always be cut at the end of a beam and not in its middle. (Of course, a beam always can be assumed as composed of two or more beams in series.)

2 An applied force often will be assumed to exist right at the cut.

3 For the elastic structure, all drawings and concepts will be given and all tearings and interconnections performed in terms of six-dimensional tensors **I** and **E** only, instead of ordinary scalars. Nevertheless, the tensor procedure is analogous to the scalar steps, with the appropriate precautions (TAN, p. 216).

In the entire structural analysis there will be no necessity to differentiate between tensile forces, shear, and bending moments, and their accompanying linear displacements and angular rotations. The tensorial thinking and concepts automatically will take care of all such complicated interrelations. The engineer will have to manipulate only a simple single-line electrical circuit with many grounded points.

However, in setting up the equations of solutions of elastic structures an important basic consideration arises which sharply differentiates the analysis of mechanical structures from those of electric circuits. The stiffness matrix **Y** of a single beam, or of any group of beams, has zero determinant and the inverse of **Y** cannot be found. To find the inverse of any **Y**-matrix, it is necessary to assume that one point in the structure is rigidly fixed in space and no rigid-body translation or rotation can take place. (This fixed support in the mechanical structure and the ground point in the electrical model of a beam should not be confused. The two concepts are unrelated. The electrical ground represents the reference point from which the displacements are measured.

The Method of Attack

The author proposes the following method of attack of elastic tructures to take care of these extra complications:

1 Tear the system apart into any convenient number of independent smaller systems.

2 Set up the equations of state of each subdivision (the primitive system) as given in TES

$$\mathbf{I} = \mathbf{YE} \mid \mathbf{F} = \mathbf{YD} \qquad [13]$$

3 Assume one fixed support in each subdivision.

4 Find the inverse (flexibility) **Z** matrix of each constrained subdivision. In addition, establish also an asymmetrical transfer matrix $\boldsymbol{\lambda}$ from **Y** and **Z** by a method to be shown later.

5 Establish the inverse equation of solution of each subdivision as

$$\boldsymbol{\lambda}\mathbf{E} = \mathbf{ZI} \mid \lambda_\alpha{}^\beta \mathbf{E}_\beta = \mathbf{Z}_{\alpha\beta}\mathbf{I}^\beta \qquad [14]$$

6 Represent each solution by an equivalent electrical star network such as shown in Fig. 8. (No special knowledge of electrical circuits is needed for this step.)

7 Interconnect the star networks into the resultant network (such as Fig. 10).

8 Perform the identical interconnections analytically in terms of the component **Z** and $\boldsymbol{\lambda}$ matrices by means of nonsingular (square) matrix of transformation **C**.

9 Form the new $\mathbf{Z}'$ and $\boldsymbol{\lambda}'$ matrices by a routine transformation, establishing thereby the equation of solution of the interconnected system as

$$\boldsymbol{\lambda}'\mathbf{E}' = \mathbf{Z}'\mathbf{I}' \qquad [15]$$

This step requires again only additions and no multiplications. (It should be noted from the indexes of Equation [14] that $\boldsymbol{\lambda}$ has a different law of transformation from that of **Z** or **Y**.)

The resulting equations of solution are ready to be altered along the same lines as the physical system is modified and also are ready to be interconnected with those of other structures to form the equations of solutions of superstructures.

If it is necessary to solve for the displacements in this structure (or in the superstructure), three more steps are needed:

10 The unknown constraint forces appearing at the cuts (**i** of Equation [6]) are eliminated or solved for.

11 All supports except one (or more if the problem requires it) are removed by finding an inverse or by elimination.

12 The equation of the fixed support is simply dropped from view. The remaining equations assume the form

$$\mathbf{E}'' = \mathbf{Z}''\mathbf{I}'' \mid \mathbf{D}'' = \mathbf{Z}''\mathbf{F}'' \qquad [16]$$

It should be mentioned that the equations of solutions (Equation [15]) may be altered, or interconnected to construct superstructures, not only after step 9 but also after steps 10 or 11, or at any intermediate point. However, if a fixed support is dropped as in step 12, the resulting equation, such as Equation [16], no longer can be interconnected and therefore cannot rightly be called equations of solutions.

THE SIMPLIFIED PROBLEM

Retaining the Supports

In order not to make the present paper too lengthy, in the example to follow the single rigid support assumed in each subdivision will not be removed. Thereby no $\boldsymbol{\lambda}$ matrix will have to be calculated and the reactions in the supports will not appear as variables. A detailed study of the more general case is intended to be undertaken in another publication.

The simplified problem to be analyzed now may be stated as follows:

1 Given a set of isolated structures (the primitive system)

each with one support and each having an equation of solution of the form

$$\mathbf{E} = \mathbf{ZI} \mid \mathbf{D} = \mathbf{ZF} \quad \ldots\ldots\ldots\ldots\ldots\ldots [17]$$

These equations may be set up by any method.

2 Establish a schematic electric-circuit model for the equations.

3 Set up a nonsingular (square) connection tensor **C** relating the internal forces appearing at the cut boundaries and elsewhere.

4 Establish the equations of the interconnected system as

$$\mathbf{E}' = \mathbf{Z}'\mathbf{F}' \mid \mathbf{D}' = \mathbf{Z}'\mathbf{F}' \quad \ldots\ldots\ldots\ldots\ldots\ldots [18]$$

5 Eliminate (or solve for) the unknown constraints **i** appearing at the cut.

The resultant equations (as they stand) cannot be used for the construction of superstructures, only to calculate the displacements **D** for an assumed **F**.

On the Use of Influence Coefficients

Structural engineers in the past have been analyzing elastic structures with equations expressed in terms of influence coefficients **Z** (references 1, 4, 5, 6). Attention is called especially to the papers by Wehle and Lansing (5) and by Langefors (1). They employ influence coefficients **Z** to analyze highly simplified structures carrying normal forces only, or shear forces only. However, Wehle and Lansing do not put to use the concept of connection tensor **C**, the law of transformation of various tensors, and other invariant concepts that form the nerves and sinews of the present treatment. Langefors does use tensorial methods. Since his structures are pin-jointed and are first made statically determinate by hypothetical cuts, his method of attack differs from that of the author.

One of the contributions of the present paper is to show how to set up the connection tensor (or matrix of transformation) **C** of a general beam structure when its influence coefficients **Z** are known instead of its stiffness matrix **Y**. (Each member of the structure may carry stresses and shear, as well as bending moments and torques and each joint may be subjected to arbitrary constraints.) In the previous paper TES the interconnection of isolated beams has been performed in terms of the known **Y** by the aid of a connection tensor **A**, which is the transposed inverse of the present **C**

$$\mathbf{A} = \mathbf{C}_t^{-1} \mid \mathbf{C} = \mathbf{A}_t^{-1} \quad \ldots\ldots\ldots\ldots\ldots\ldots [19]$$

In the present paper, where equations of solutions are interconnected, **C** is always square (nonsingular). However, in TES, where equations of states were interconnected, the **A** was usually rectangular and not square. (Though **A** is always square, just as **C** is, the problem at hand did not require the use of the missing reference axes.)

Statement of the Problem

Let the three-dimensional elastic structure of Fig. 6 with 225 beams be given, all beams lying in a general direction. Let arbitrary forces and moments be applied at all the 82 joints. Some of the joints may be pinned, some rigid, and others may be subjected to arbitrary constraints, so that many of the beam ends may have less degrees of freedom than others. Four of the joints are rigid supports. Each beam may be the equivalent of a whole collection of other beams, so that in general each end of a beam may have more than six degrees of freedom.

For purposes of analysis the structure of Fig. 6 is subdivided into four smaller structures shown by dotted lines, where each subdivision contains one support. The isolated four component structures are shown in Fig. 7. At the points of separation each joint has general forces applied to it, as yet unknown.

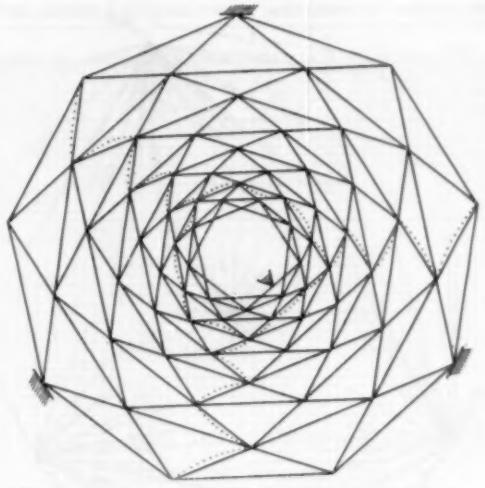

Fig. 6 Three-Dimensional Elastic Structure

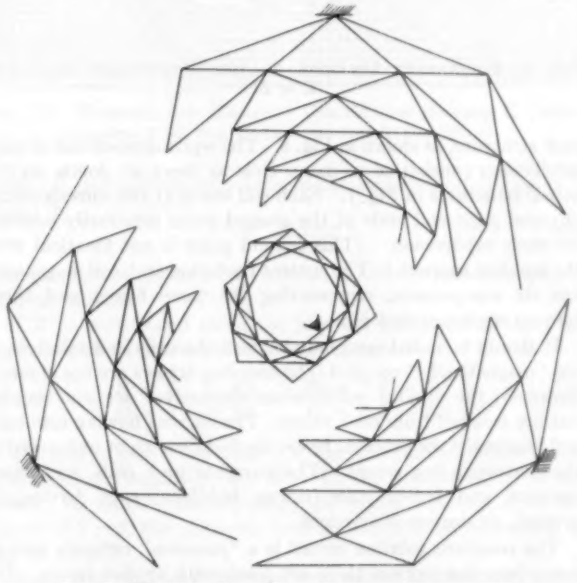

Fig. 7 Tearing Into Four Smaller Structures

It will be assumed that the equations of solutions **E** = **ZI** (or **D** = **ZF**) of each of the four structures have already been determined by any method available. If so desired, it is possible to employ the tensorial method of attack for the solution of each subdivision given in TES (pp. 437–440); that is, subdivide each subdivision into its ultimate elements, the individual beams. Then establish first the **I** = **YE**, and afterward the **E** = **ZI** equations of each subdivision. (For additional examples see reference 2.)

The **Z**-matrices of each of the four structures are arranged along the diagonal of a large matrix, representing the **Z** of the primitive system of Fig. 7, existing before the interconnection. (In analogy to Equation [33] of TES.) The problem ahead is then to establish the connection tensor **C** showing how the four smaller structures are interconnected into the larger structure.

Equivalent Circuits of the Component Solutions

With the equations **E** = **ZI** for each subdivision available, the first step is to set up schematic equivalent circuits on paper for

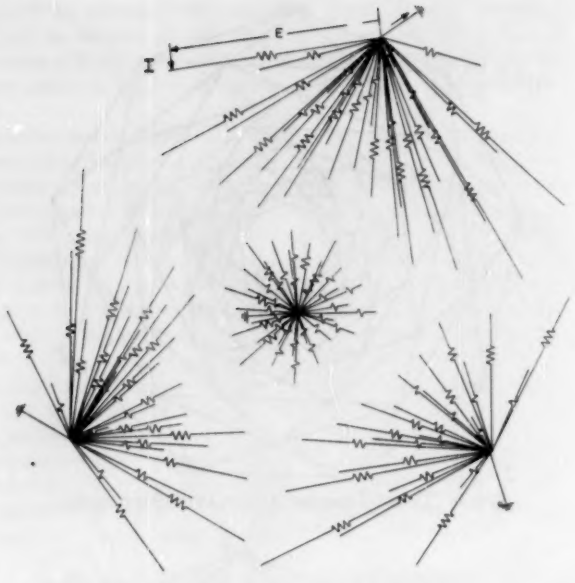

FIG. 8 EQUIVALENT CIRCUITS OF THE COMPONENT SOLUTIONS (E = ZI)

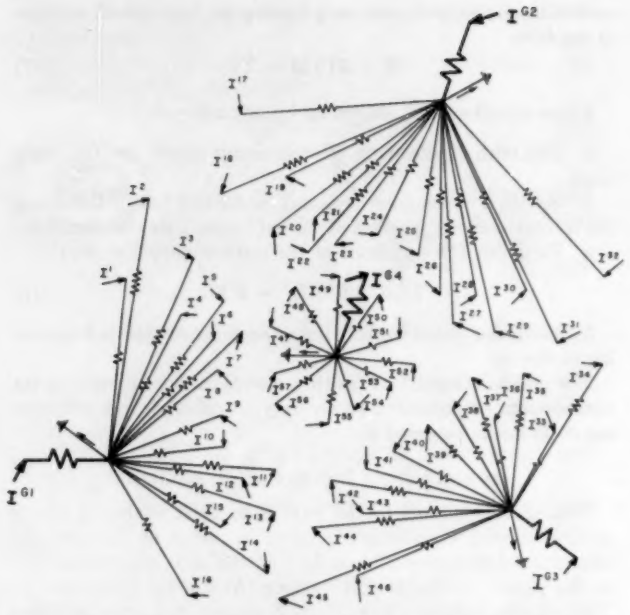

FIG. 9 COMBINING ALL NONBOUNDARY TENSOR COILS INTO ONE "COMPOUND" TENSOR COIL

each structure, as shown in Fig. 8. The equivalent circuit of each subdivision consists of as many coils as there are joints on the actual structures in Fig. 7. Each coil starts at the corresponding physical joint and ends at the ground point arbitrarily selected for each subdivision. (This ground point is not identical with the point of support.) The current **I** entering each coil, in general, has six components, representing the three forces and three torques applied at each joint.

It should be noted especially that all the coils in a subdivision are "magnetically" coupled (the coupling arrows are not shown). However, the various subdivisions themselves are not coupled but are isolated from each other. The current flowing into each coil represents the external forces applied (known or unknown) at the corresponding joints. The currents and coils are tensor currents and tensor coils (drawn boldface) each having, in general, six degrees of freedom.

The resultant solution circuit is a "junction" network with as many junction-pairs as there are joints with applied forces. If a joint has no applied forces, the corresponding row and column is left out from **Z** and so is the corresponding coil from the equivalent circuit. But a joint at the boundary cannot be left out.

It should be noted especially, that although Fig. 8 is a junction network, its defining equations are not the customary $I^{\alpha} = Y^{\alpha\beta}E_{\beta}$ but $E_{\alpha} = Z_{\alpha\beta}I^{\beta}$, a type of equation that customarily is associated with a mesh network. Herein lies the secret of interconnecting successfully equations of solutions, as opposed to interconnecting equations of state. If an attempt is made to set up the customary mesh equivalent circuit for **E** = **ZI**, instead of the junction network of Fig. 8, it will be found that the solutions cannot be interconnected. To avoid just such mistakes in logic is the reason why in TAN the equations of mesh networks are denoted with lower-case letters as **e** = **zi**. The equations with capital letters are reserved for junction networks.

In order to simplify the presentation to follow, all coils and impressed currents that do not form part of the cut boundaries are combined into one "compound" tensor-coil and one "compound" tensor-current (TAN, p. 216) as shown with extra-bold-faced lines in Fig. 9.

THE INTERCONNECTED SYSTEM

All boundary coils are shown interconnected in Fig. 10. Along the boundaries between two neighboring systems only two coils are joined together. At several points where three neighboring systems meet, three of the coils are joined into one junction point. It is assumed that at every boundary-junction point a known force is impressed.

The resulting network contains both meshes and junction pairs. It is absolutely necessary to set up the equations of solutions for all meshes and all junction pairs; that is, the resulting solution network must be viewed as an orthogonal network possessing a nonsingular (square) connection tensor **C** (TAN, p. 407).

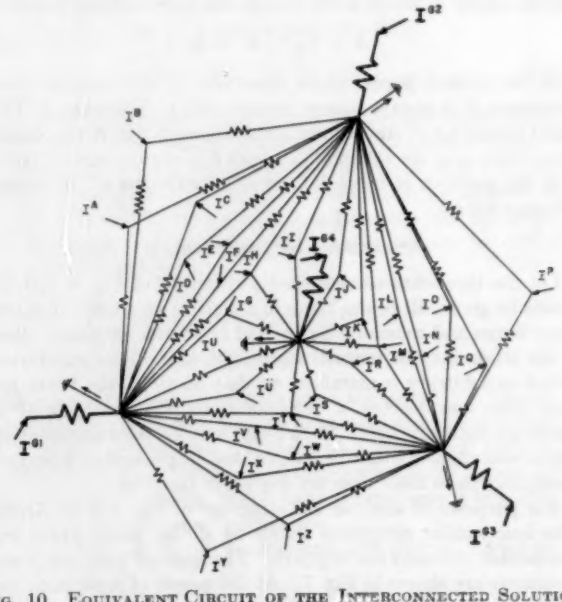

FIG. 10 EQUIVALENT CIRCUIT OF THE INTERCONNECTED SOLUTION (Assumed junction pairs shown.)

The known junction-currents **I** are assumed to flow from a junction to the next ground through one of the coils arbitrarily selected, as shown in Fig. 10. If some of the junctions possess no impressed forces, the corresponding junction current may be left out from Fig. 10 and the connection tensor **C** is no longer square. But the coils on both sides of the junctions are retained so that the number of meshes is not decreased.

The number of meshes is equal to the number of coils (61) minus the number of junction pairs (28). Hence the number of meshes is 61 — 28 = 33 (TAN, p. 75). (The four grounds shown are equivalent to one junction point only.) Although there are numerous possibilities for selecting the meshes, each mesh will be assumed to start and end at two different ground points, as shown in Fig. 11. Expressed in another manner, each mesh current passes through one boundary point where two coils meet. At points where three coils (beams) meet, two mesh currents will flow through, such as i^{a1} and i^{a2}. In general, at a junction of n beams n — 1 mesh currents will flow by.

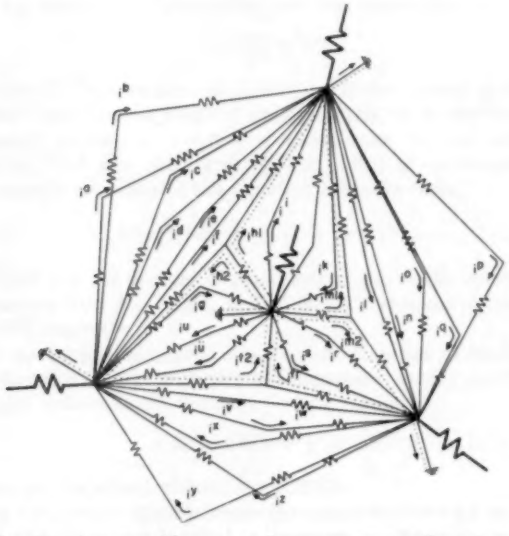

FIG. 11 ASSUMED MESHES OF INTERCONNECTED SOLUTIONS

The unknown mesh currents **i** represent the internal beam forces appearing at the joints.

THE CONNECTION TENSOR C

The matrix of transformation **C** is established by setting up a relation $\mathbf{I} = \mathbf{CI}'$ between the "old" currents flowing in Fig. 9 and the "new" currents shown in Figs. 10 and 11. The resulting **C** is given in Fig. 12. It is square and in the present example it has 61 rows and columns (as many as there are total numbers of coils in the interconnected system of Fig. 10).

As an example, in coil 52 of Fig. 9 flows, before interconnection, I^{52}. After interconnection two types of currents flow in the same coil. In particular:

1 In Fig. 10 the impressed junction current I^M.

2 In Fig. 11 two of the mesh currents i^{m1} and i^{m2} flow in the opposite direction. Hence

$$I^{52} = I^M - i^{m1} - i^{m2} \quad \ldots\ldots [20]$$

Each unity in **C** of Fig. 12 represents a unit matrix with six diagonal elements.

THE EQUATIONS OF SOLUTIONS

With **C** established and **Z** of the primitive system of Fig. 9

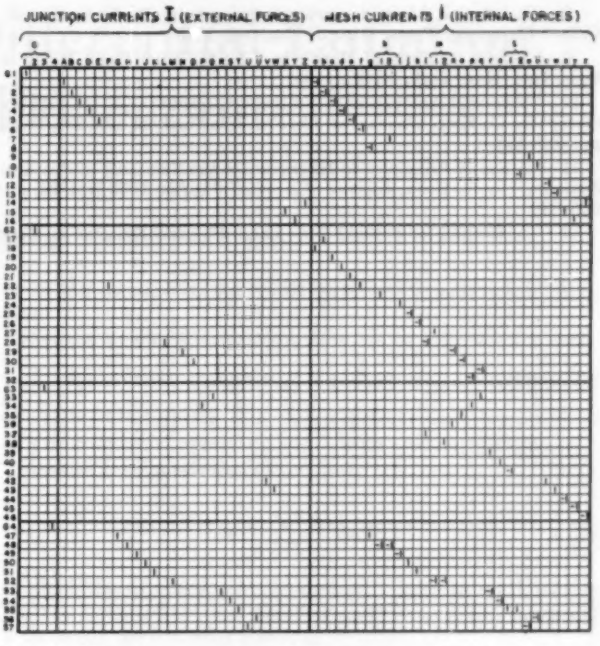

FIG. 12 NONSINGULAR (SQUARE) CONNECTION TENSOR **C** INTERCONNECTING THE FOUR COMPONENT SOLUTIONS

available, the impedance matrix of the interconnected system is found by

$$\mathbf{Z}' = \mathbf{C}_t\mathbf{ZC} \quad \ldots\ldots [21]$$

The calculation requires only additions and the interchanging of rows or columns.

If $\mathbf{Z}'$ is partitioned along the junction pairs and meshes, the equations of the interconnected systems are

$$\left.\begin{aligned} \mathbf{E} &= \mathbf{Z}_1\mathbf{I} + \mathbf{Z}_2\mathbf{i} \\ \mathbf{O} &= \mathbf{Z}_3\mathbf{I} + \mathbf{Z}_4\mathbf{i} \end{aligned}\right| \quad \left.\begin{aligned} \mathbf{D} &= \mathbf{Z}_1\mathbf{F} + \mathbf{Z}_2\mathbf{f} \\ \mathbf{O} &= \mathbf{Z}_3\mathbf{F} + \mathbf{Z}_4\mathbf{f} \end{aligned}\right\} \quad \ldots\ldots [22]$$

The known quantities are $\mathbf{I} = \mathbf{F}$, the external impressed forces. The unknown quantities are $\mathbf{E} = \mathbf{D}$, the displacements at the joints As an intermediary step, the second equation gives the values of $\mathbf{i} = \mathbf{f}$, the unknown internal beam forces appearing at the cut joints.

When **D** at each joint has been determined, the internal forces **i** appearing at each end of all beams may be found from the stiffness equation $\mathbf{I} = \mathbf{YD}$ where **Y** is the stiffness matrix of the primitive system built up of isolated beams.

BIBLIOGRAPHY

1 "Analysis of Elastic Structures by Matrix Transformation With Special Regard to Semimonocoque Structures," by B. Langefors, *Journal of the Aeronautical Sciences*, vol. 19, 1952, pp. 451–458.

2 "Analysis of Rigid Frames by an Electronic Digital Computer," by R. K. Livesley, *Engineering*, vol. 176, Aug. 21, 1953, p. 230, Aug. 28, 1953, p. 277.

3 "The Partitioning of Matrices in Structural Analysis," by S. V. Benscoter, JOURNAL OF APPLIED MECHANICS, Trans. ASME, vol. 70, 1948, pp. 303–307.

4 "Vibrations of Composite Structures," by H. Serbin, *Journal of the Aeronautical Sciences*, vol. 12, 1945, pp. 108–112.

5 "A Method for Reducing Analysis of Complex Redundant Structures to a Routine Procedure," by L. B. Wehle and W. Lansing, *Journal of the Aeronautical Sciences*, vol. 19, 1952, p. 677.

6 "The Combination of Dynamical Systems," by T. G. Sofrin, *Journal of the Aeronautical Sciences*, vol. 13, 1946, pp. 281–288.

7 "Beam-Vibration Analysis With the Electric Analog Computer," by G. D. McCann and R. H. MacNeal, JOURNAL OF APPLIED MECHANICS, Trans. ASME, vol. 72, 1950, p. 13.

8 "Relaxation Methods in Engineering," by R. V. Southwell, Oxford University Press, Oxford, England, 1940.

9 "Tensor Analysis of Networks," by G. Kron, John Wiley & Sons, Inc., New York, N. Y., 1939.

10 "Tensorial Analysis and Equivalent Circuits of Elastic Structures," by G. Kron, *Journal of The Franklin Institute*, vol. 238, 1944, pp. 400–452.

11 "A Set of Principles to Interconnect the Solutions of Physical Systems," by G. Kron, *Journal of Applied Physics*, 1953, vol. 24, pp. 965–980.

12 "A Method for Solving Very Large Physical Systems in Easy Stages," by G. Kron, Proceedings of the Institute of Radio Engineers, vol. 42, 1954, pp. 680–686.

13 "Inverting a 256 × 256 Matrix on the CPC in 16 Hours," by G. Kron, *Engineering*, vol. 179, March 11, 1955, pp. 309–312.

14 "Tensorial Analysis of Integrated Transmission Systems—IV," by G. Kron, Trans. AIEE, 1953, pp. 827–839.

15 "Tensorial Analysis of Control Systems," by G. Kron, JOURNAL OF APPLIED MECHANICS, Trans. ASME, vol. 70, 1948, p. 107.

16 "Equivalent Circuits of the Elastic Field," by G. Kron, JOURNAL OF APPLIED MECHANICS, Trans. ASME, vol. 66, 1944, p. A-149.

On the Nonlinear Differential Equation for Beam Deflection

$$EI\, d^2y/dx^2 = M(x)[1 + (dy/dx)^2]^{3/2}$$

By E. J. SCOTT[1] and D. R. CARVER,[1] MANHATTAN, KAN.

A general solution of the nonlinear beam equation is given for all problems in which the moment can be expressed as a function of the independent variable alone.

Introduction

IN the theory of bending of uniform bars it is shown that the bending moment at any section is proportional to the resulting curvature. In equation form this relation is

$$M/(EI) = 1/\rho$$

in which E is the modulus of elasticity, I is the moment of inertia of the beam section about a principal axis, M is the bending moment acting in a plane perpendicular to the axis of bending, and ρ is the corresponding radius of curvature. In rectangular co-ordinates this equation takes the form

$$M(x)/(EI) = y''/[1 + (y')^2]^{3/2} \quad [1]$$

in which y is the vertical displacement of the elastic curve at a distance x from the origin, and y' and y'' represent dy/dx and d^2y/dx^2, respectively.

In most engineering problems the deflections are so small that the quantity $(y')^2$ is negligible in comparison to unity and Equation [1] reduces to the ordinary linear equation

$$M(x)/(EI) = y''(x) \quad [2]$$

which may be solved without any difficulty.

For exceedingly flexible beams the quantity $(y')^2$ may be quite large and one is not justified in dropping it. Then one is confronted with the nonlinear Equation [1] and the problem becomes much more difficult.

Solutions of the nonlinear beam equation for particular loading conditions have been obtained before.[2] It is the purpose of this paper to show that the reversion method gives a general solution to the nonlinear beam equation for all cases in which the moment expression can be formulated in terms of the independent variable alone, and to illustrate the method with several examples.

The Reversion Method

We shall describe the method for an integral power series. For the more general nonintegral power series, which include our series as a special case, the reader is referred to an article by A. C. Sim.[3]

Suppose that a differential equation can be written in the form

$$\Phi_1 y + \Phi_2 y^2 + \Phi_3 y^3 + \ldots + \Phi_n y^n + \ldots = \lambda\Psi(x) \quad [3]$$

in which y is a function of x, the coefficients are either functions of x or differential operators, and λ is an auxiliary parameter.

Assume a series solution of the form

$$y = \sum_{n=1}^{\infty} \lambda^n y_n(x) \quad [4]$$

in which the $y_n(x)$ are to be determined. Substituting Equation [4] into Equation [3] and equating coefficients of like powers of λ we obtain the following formulas

$$\Phi_1 y_1 = \Psi(x) \quad [5]$$

$$\Phi_1 y_2 = -\Phi_2 y_1^2 \quad [6]$$

$$\Phi_1 y_3 = -\Phi_2 y_1^3 - 2\Phi_2 y_1 y_2 \quad [7]$$

$$\Phi_1 y_4 = -\Phi_4 y_1^4 - 3\Phi_3 y_1^2 y_2 - \Phi_2(y_2^2 + 2y_1 y_3) \quad [8]$$

$$\Phi_1 y_5 = -\Phi_5 y_1^5 - 4\Phi_4 y_1^3 y_2 - 3\Phi_3(y_1 y_2^2 + y_1^2 y_3) - 2\Phi_2(y_1 y_4 + y_2 y_3) \quad [9]$$

$$\Phi_1 y_6 = -\Phi_6 y_1^6 - 5\Phi_5 y_1^4 y_2 - 4\Phi_4(y_1^2 y_2^2 + y_1^3 y_3) - \Phi_3(y_2^3 + 3y_1^2 y_4 + 6y_1 y_2 y_3) - \Phi_2(y_3^2 + 2y_1 y_5 + 2y_2 y_4) \quad [10]$$

and so on.

Other formulas may be derived by using the multinomial theorem. The ones just derived, however, will be sufficient for our purpose.

Thus, if the Φ_i stand for differential operators, the solution of the original nonlinear differential equation has been reduced to the solution of the sequence of ordinary linear differential Equations [5], [6], . . . [10], ...

The auxiliary parameter λ was introduced for the purpose of determining the sequence of linear equations. Having served its purpose, we may replace λ by 1 and obtain for the solution of

$$\Phi_1 y + \Phi_2 y^2 + \Phi_3 y^3 + \ldots + \Phi_n y^n + \ldots = \Psi(x) \quad [11]$$

the series

$$y = y_1 + y_2 + y_3 + \ldots + y_n + \ldots \quad [12]$$

Solution of the Nonlinear Beam Equation

Equation [1] may be written

$$y'' = M(x)[1 + (y')^2]^{3/2}/(EI) \quad [13]$$

Expanding the quantity in the brackets by the binomial theorem and rearranging terms, we obtain

---

[1] Associate Professor of Applied Mechanics, Kansas State College.

[2] "Strength of Materials," by J. E. Boyd, McGraw-Hill Book Company, Inc., New York, N. Y., third edition, 1924, Appendix D.

Contributed by the Applied Mechanics Division and presented at the Annual Meeting, New York, N. Y., November 28–December 3, 1954, of The American Society of Mechanical Engineers.

Discussion of this paper should be addressed to the Secretary, ASME, 29 West 39th Street, New York, N. Y., and will be accepted until July 11, 1955, for publication at a later date. Discussion received after the closing date will be returned.

Note: Statements and opinions advanced in papers are to be understood as individual expressions of their authors and not those of the Society. Manuscript received by ASME Applied Mechanics Division, September 28, 1953. Paper No. 54—A-35.

[3] "A Generalization of Reversion Formulae With Their Application to Nonlinear Differential Equations," by A. C. Sim, *Philosophical Magazine*, series 7, vol. 42, 1951, pp. 228–238.

$$y'' - \frac{M(x)}{EI}\left[\frac{3}{2}(y')^2 + \frac{3}{8}(y')^4 - \frac{1}{16}(y')^6 + \frac{3}{128}(y')^8 - \ldots\right] = \frac{M(x)}{EI} \quad \ldots\ldots [14]$$

Letting $y' = Y$ in Equation [14] we see that

$$\frac{dY}{dx} - \frac{M(x)}{EI}\left[\frac{3}{2}Y^2 + \frac{3}{8}Y^4 - \frac{1}{16}Y^6 + \frac{3}{128}(Y)^8 - \ldots\right] = \frac{M(x)}{EI} \quad \ldots\ldots [15]$$

and this equation is of the form of Equation [11]. Comparing Equation [15] with Equation [11] we observe that

$$\left.\begin{aligned} &(a)\ \Phi_1 = d/dx, \quad (b)\ \Phi_2 = -\frac{3M(x)}{2EI} \\ &(c)\ \Phi_3 = 0, \quad (d)\ \Phi_4 = -\frac{3M(x)}{8EI} \quad (e)\ \Phi_5 = 0, \\ &(f)\ \Phi_6 = \frac{M(x)}{16EI} \quad (g)\ \Phi_7 = 0, \quad (h)\ \Phi_8 = -\frac{3M(x)}{128EI} \cdots \\ &(i)\ \Psi(x) = \frac{M(x)}{(EI)} \end{aligned}\right\} \ldots [16]$$

and for the nonlinear beam equation, Equations [5], [6], [7], and [8] become

$$dY_1/dx = \frac{M(x)}{EI} \quad \ldots\ldots [17]$$

$$dY_2/dx = \frac{3M(x)}{2EI} Y_1^2 \quad \ldots\ldots [18]$$

$$dY_3/dx = \frac{3M(x)}{EI} Y_1 Y_2 \quad \ldots\ldots [19]$$

$$dY_4/dx = \frac{3M(x)}{8EI} Y_1^4 + \frac{3M(x)}{2EI} Y_2^2 + \frac{3M(x)}{EI} Y_1 Y_3 \quad \ldots [20]$$

Other equations could be written but four terms are sufficient.

Equation [17] integrates directly giving

$$Y_1 = \int \frac{M(x)}{EI}\,dx + c \quad \ldots\ldots [21]$$

in which c is a constant of integration. Equations [18], [19], and [20] may now be solved consecutively for any given $M(x)$. Eliminating $M(x)/(EI)$ successively and integrating, we obtain

$$Y_2 = \frac{1}{2} Y_1^2 \quad \ldots\ldots [22]$$

$$Y_3 = \frac{3}{10} Y_1^5 \quad \ldots\ldots [23]$$

$$Y_4 = \frac{3}{40} Y_1^5 + \frac{3}{56} Y_1^7 + \frac{9}{70} Y_1^7 \quad \ldots\ldots [24]$$

Thus

$$dy/dx = Y = Y_1 + \frac{1}{2} Y_1^3 + \frac{3}{8} Y_1^5 + \frac{51}{280} Y_1^7 + \ldots\ldots [25]$$

and the slope of the tangent to the elastic curve may be determined for any beam from Equations [25] and [21].

If one retains only one term on the right-hand side of Equation [25] one obtains the ordinary linear solution for the slope. The slope in the case of larger deflections is thus a power series in the linear solution.

The deflection y may be obtained by integration of Equation [25]. Thus

$$y = \int \left\{Y_1 + \frac{1}{2} Y_1^3 + \frac{3}{8} Y_1^5 + \frac{51}{280} Y_1^7 + \ldots\right\} dx + c_1 \quad \ldots\ldots [26]$$

and the problem is formally solved.

Practically, however, the solution has several limitations. The equation $M/(EI) = 1/\rho$ is valid in the final configuration only, and in problems involving large deflections the geometrical changes during loading can be of considerable magnitude. Also, since $M(x)$ is assumed to be known and to be a function of x alone, only vertical loads and reactions can be treated. A horizontal component of a reaction H would introduce a moment term Hy, and Equation [26] is not valid for a problem of this type.

But solutions of beam problems in which loads and reactions are vertical and in which the moment expression is written from the equilibrium configuration can be of practical importance, and a solution of this kind should prove to be a matter of interest to engineers.

Several examples will be given to illustrate the use of Equation [26].

Centrally Loaded Beam With Vertical Reactions

There is symmetry with respect to the center line, Fig. 1, in this case and only the left portion of the beam will be considered.

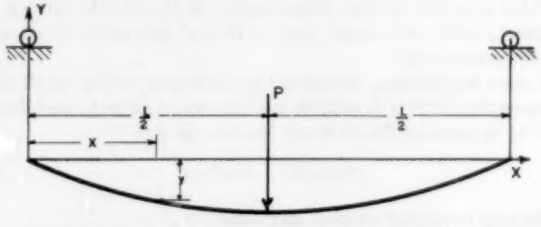

Fig. 1 Centrally Loaded Beam With Vertical Reactions

The moment function here is

$$M(x) = Px/2 \qquad 0 \le x \le L/2$$

From Equation [21]

$$Y_1 = \int \frac{M(x)}{EI}\,dx + c = \int \frac{Px}{2EI}\,dx + c = \frac{Px^2}{4EI} + c$$

Replacing c by $c_1/(4EI)$, we have

$$Y_1 = \frac{1}{4EI}(Px^2 + c_1)$$

The slope must be zero at $x = L/2$. If $c_1 = -PL^2/4$, this condition is satisfied and Equation [25] gives

$$dy/dx = \frac{P}{4EI}\left(x^2 - \frac{L^2}{4}\right) + \frac{1}{2}\left(\frac{P}{4EI}\right)^3\left(x^2 - \frac{L^2}{4}\right)^3 + \frac{3}{8}\left(\frac{P}{4EI}\right)^5\left(x^2 - \frac{L^2}{4}\right)^5 + \frac{51}{280}\left(\frac{P}{4EI}\right)^7\left(x^2 - \frac{L^2}{4}\right)^7 + \ldots$$

It should be noticed that the first term on the right is the usual linear equation expression for dy/dx. Integrating

$$y = \frac{P}{4EI}\left(\frac{x^3}{3} - \frac{L^2x}{4}\right) + \frac{1}{2}\left(\frac{P}{4EI}\right)^3\left(\frac{x^7}{7} - \frac{3L^2x^5}{20} + \frac{L^4x^3}{16} - \frac{L^6x}{64}\right)$$
$$+ \frac{3}{8}\left(\frac{P}{4EI}\right)^5\left(\frac{x^{11}}{11} - \frac{5L^2x^9}{36} + \frac{5L^4x^7}{56} - \frac{L^6x^5}{32} + \frac{5L^8x^3}{768} - \frac{L^{10}x}{1024}\right)$$
$$+ \frac{51}{280}\left(\frac{P}{4EI}\right)^7\left(\frac{x^{15}}{15} - \frac{7L^2x^{13}}{52} + \frac{21L^4x^{11}}{176} - \frac{35L^6x^9}{576}\right.$$
$$\left. + \frac{35L^8x^7}{1792} - \frac{21L^{10}x^5}{5120} + \frac{7L^{12}x^3}{12,288} - \frac{L^{14}x}{16,384}\right)$$

The center deflection is

$$y(L/2) = -\frac{PL^3}{48EI} - \left(\frac{PL^2}{4EI}\right)^3\frac{L}{560} - \left(\frac{PL^3}{4EI}\right)^5\frac{L}{14,784}$$
$$- \left(\frac{PL^2}{4EI}\right)^7\frac{51L}{28,828,000} - \ldots$$

Cantilever Beam With a Concentrated Load P at the Free End

In this case, Fig. 2, the moment at any section x is

$$M(x) = -P(L - x)$$

with the boundary conditions $y(0) = y'(0) = 0$.

From Equation [21]

$$Y_1(x) = -\frac{P}{EI}\int (L - x)dx + c_1 = \frac{P}{2EI}(L - x)^2 + c_1$$

Since $y'(0) = 0$, then $c_1 = -(PL^2/2EI)$ and

$$Y_1(x) = \frac{P}{2EI}[(L - x)^2 - L^2] = \frac{P}{2EI}x(x - 2L)$$

Therefore, from Equation [25]

$$dy/dx = \frac{P}{2EI}x(x - 2L) + \frac{1}{2}\left(\frac{P}{2EI}\right)^3[x(x - 2L)]^3$$
$$+ \frac{3}{8}\left(\frac{P}{2EI}\right)^5[x(x - 2L)]^5 + \frac{51}{280}\left(\frac{P}{2EI}\right)^7[x(x - 2L)]^7 + \ldots$$

Integrating and making use of the condition $y(0) = 0$, which makes the constant of integration turn out to be zero, we obtain

$$y(x) = \frac{P}{2EI}\left(\frac{x^3}{3} - Lx^2\right) + \frac{1}{2}\left(\frac{P}{2EI}\right)^3\left(\frac{x^7}{7} - Lx^6\right.$$
$$\left. + \frac{12}{5}L^2x^5 - 2L^3x^4\right) + \frac{3}{8}\left(\frac{P}{2EI}\right)^5\left(\frac{x^9}{11} - Lx^{10} + \frac{40}{9}L^2x^9\right.$$
$$\left. - 10L^3x^8 + \frac{80}{7}L^4x^7 - \frac{16}{3}L^5x^6\right)$$
$$+ \frac{51}{280}\left(\frac{P}{2EI}\right)^7\left(\frac{x^{15}}{15} - Lx^{14} + \frac{84}{13}L^2x^{13} - \frac{70}{3}L^3x^{12}\right.$$
$$\left. + \frac{560}{11}L^4x^{11} - \frac{336}{5}L^5x^{10} + \frac{448}{9}L^6x^9 - 16L^7x^8\right) + \ldots$$

If the load P acts at the end of a cantilever beam of length s the solution is valid as formulated in the foregoing in terms of the horizontal projection L. The value of L may then be determined by solving the equation

$$s = \int_0^L \sqrt{1 + (y')^2}\,dx$$

for L.

Cantilever Beam With Couple Applied at Free End

The moment function here, Fig. 3, is

$$M(x) = M_0$$

with the boundary conditions $y(0) = y'(0) = 0$.

From Equation [21]

$$Y_1(x) = \frac{M_0}{EI}\int dx + c_1 = \frac{M_0}{EI}x + c_1$$

Using the boundary condition $y'(0) = 0$, we find that $c_1 = 0$.

Thus $Y_1(x) = M_0x/(EI)$.

Consequently, from Equation [25]

$$dy/dx = \frac{M_0}{EI}x + \frac{1}{2}\left(\frac{M_0}{EI}\right)^3x^3$$
$$+ \frac{3}{8}\left(\frac{M_0}{EI}\right)^5x^5 + \frac{51}{280}\left(\frac{M_0}{EI}\right)^7x^7 + \ldots$$

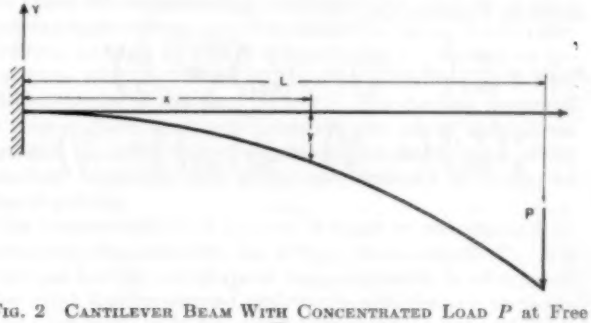

Fig. 2 Cantilever Beam With Concentrated Load P at Free End

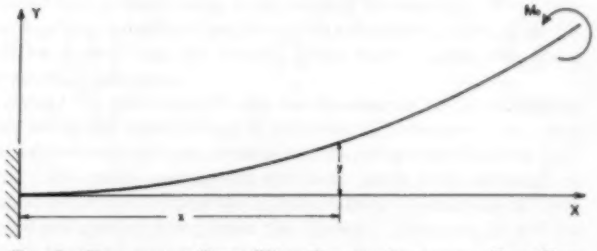

Fig. 3 Cantilever Beam With Couple Applied at Free End

Integrating and making use of the condition $y(0) = 0$, we finally have

$$y(x) = \frac{1}{2}\left(\frac{M_0}{EI}\right)x^2 + \frac{1}{8}\left(\frac{M_0}{EI}\right)^3x^4 + \frac{1}{16}\left(\frac{M_0}{EI}\right)^5x^6$$
$$+ \frac{51}{2240}\left(\frac{M_0}{EI}\right)^7x^8 + \ldots$$

It is known that for $M(x) = M_0$ the deflection curve is an arc of a circle. The foregoing series, since it represents a single-valued function, will give only the lower half of the circle.

Clamped Beam-Concentrated Load at Its Center

For the interval $0 \leq x \leq L/2$, in Fig. 4, the moment function $M(x) = Px/2 - M_0$, in which M_0 is the moment at the left end support. From Equation [21]

$$Y_1 = \int \frac{M(x)}{EI}\,dx + c = \frac{1}{EI}\int (Px/2 - M_0)dx + c$$

$$= \frac{Px^2}{4EI} - \frac{M_0 x}{EI} + \frac{c_1}{EI}$$

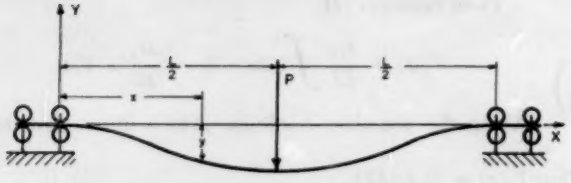

FIG. 4 CLAMPED BEAM-CONCENTRATED LOAD AT ITS CENTER

The conditions $y'(0) = 0$ and $y'(L/2) = 0$ imply that $c_1 = 0$ and $M_0 = PL/8$. Thus

$$Y_1 = \frac{Px^2}{4EI} - \frac{PLx}{8EI} = \frac{P}{4EI}\left(x^2 - \frac{Lx}{2}\right)$$

and from Equation [25]

$$dy/dx = \frac{P}{4EI}\left(x^2 - \frac{Lx}{2}\right) + \frac{1}{2}\left(\frac{P}{4EI}\right)^3\left(x^2 - \frac{Lx}{2}\right)^3$$

$$+ \frac{3}{8}\left(\frac{P}{4EI}\right)^5\left(x^2 - \frac{Lx}{2}\right)^5 + \frac{51}{280}\left(\frac{P}{4EI}\right)^7\left(x^2 - \frac{Lx}{2}\right)^7 + \cdots$$

Integrating, we obtain

$$y(x) = \frac{P}{4EI}\left(\frac{x^3}{3} - \frac{Lx^2}{4}\right) + \frac{1}{2}\left(\frac{P}{4EI}\right)^3\left(\frac{x^7}{7} - \frac{Lx^6}{4}\right.$$

$$\left. + \frac{3L^2x^5}{20} - \frac{L^3x^4}{32}\right) + \frac{3}{8}\left(\frac{P}{4EI}\right)^5\left(\frac{x^{11}}{11} - \frac{Lx^{10}}{4} + \frac{5}{18}L^2x^9\right.$$

$$\left. - \frac{5L^3x^8}{32} + \frac{5L^4x^7}{112} - \frac{L^5x^6}{192}\right) + \frac{51}{280}\left(\frac{P}{4EI}\right)^7\left(\frac{x^{15}}{15} - \frac{Lx^{14}}{4}\right.$$

$$\left. + \frac{21L^2x^{13}}{52} - \frac{35L^3x^{12}}{96} + \frac{35L^4x^{11}}{176}\right.$$

$$\left. - \frac{21L^5x^{10}}{320} + \frac{7L^6x^9}{576} - \frac{L^7x^8}{1024}\right) + \cdots$$

The center deflection is

$$y(L/2) = -\frac{PL^3}{192EI} - \left(\frac{PL^2}{4EI}\right)^3\frac{L}{35{,}840}$$

$$- \left(\frac{PL^2}{4EI}\right)^5\frac{L}{2^{16} \times 231} - \cdots$$

It should be remarked that the results obtained in the paper are formal solutions of the problems. Questions concerning intervals of convergence of series will, in general, arise, and these questions would have to be studied for each problem considered. In many cases the nature of the physical problem at hand suggests the limitations on the solutions.

Problems of Plane Elasticity for Reinforced Boundaries

By J. R. M. RADOK,[1] MELBOURNE, AUSTRALIA

Based on N. I. Muskhelishvili's approach to problems of plane elasticity, a general method has been deduced for the solution of problems of reinforced cutouts in infinitely thin sheets. As an illustration, the circular reinforced hole has been treated in detail and the results have been related to those obtained experimentally and theoretically by other authors. The solution for other shapes of cutouts will be greatly simplified, since full use may be made of the theory of conformal transformations.

Nomenclature

The following nomenclature is used in the paper:

A_k, a_k, a_k' = Fourier coefficients (see Equations [28, 29])
A = area of section of reinforcing material
B_j = see Equations [40]
E = Young's modulus
k = local curvature of boundary (see Equations [13])
N_1, N_2 = principal stresses at infinity
p = stress at infinity
r = local radius of curvature
R = radius of hole (Section 3)
s = arc co-ordinate at boundary
t = thickness of plate
u, v = displacements
$z = x + iy$ = complex variable in original plane
$\bar{z} = x - iy$
R, S = radial and shear forces per unit length at boundary of sheet (Section 2)
F = hoop force in reinforcement
X_x, Y_y, Y_y = stresses in rectilinear co-ordinate system
$\widehat{rr}, \widehat{\theta\theta}, \widehat{r\theta}$ = stresses in curvilinear co-ordinate system in original plane
N', T' = external stresses at boundary
N, T = boundary values of stresses
$\alpha = \frac{A}{t}$
$\alpha' = \frac{A}{tR}$
Γ, Γ', γ = see [31]
ζ = complex variable in image region
θ = polar angle
ϑ = angle between tangent to boundary and some fixed direction
ν = Poisson's ratio
ρ = radius
$\Phi, \Psi, \varphi, \psi$ = stress functions
$\omega(\zeta)$ = conformal transformation
$\frac{\partial}{\partial\theta} = \cdot$
$\frac{d}{d\zeta} = '$

1 Introduction

The use of reinforcements at the boundaries of cutouts and lightning holes is common practice in aircraft construction. For this reason the corresponding boundary-value problems of plane elasticity have received special consideration during recent years. However, as early as 1924 S. Timoshenko (1)[2] deduced an approximate solution. Some of these investigations have been listed at the end of this paper (1 to 6). The theories, developed by these authors, are characterized by the use of the indirect approach, i.e., by the use of solutions which satisfy some of the boundary conditions and which are combined to solve the original problem.

The present method of solution is based on the approach to problems of plane elasticity, due to N. I. Muskhelishvili (7). It is direct and has the advantage of being applicable to all types of holes which may be mapped conformally onto the unit circle exactly or approximately by use of polynomials or rational functions. Only the problem of the reinforced circular hole will be treated here in detail as an illustration of the method. This problem has been considered previously in references (1 to 4, 6) and it will be shown that the results, given there, agree with those obtained in this report.

Except for reference (6) the reinforcements under consideration are in the terminology of reference (5) compact; i.e., they are subject only to hoop stresses and do not possess bending stiffness. The same assumption has been made here, although it should be mentioned that the introduction of the bending stiffness would not greatly complicate the theory. However, it will be shown that the results of the present theory agree as well or even better with the experimental results of reference (6) than those of the theory given there, indicating that the effect of the bending stiffness of the reinforcement is of second order. This fact actually has been suggested already in reference (6).

In Section 2 the general statement of the problem is given for any type of hole in an infinite sheet. The treatment of the circular hole in Section 3 starts from first principles but at the end of the section it is shown how the same formulas could be obtained from the general theory of Section 2. In Section 4 a comparison is made between the results of Section 3 and the theoretical and experimental results of reference (6), while Section 5 makes certain deductions from the results of Section 3 which may be useful to the designer.

Since the conclusion of this work, it has come to the author's notice that in all probability an identical method has been used by G. N. Savin (8) in Russia. The only detail at the author's

---

[1] Senior Scientific Officer, Structures and Materials Division, Aeronautical Research Laboratories, Department of Supply.

Contributed by the Applied Mechanics Division and presented at the Annual Meeting, New York, N. Y., November 28–December 3, 1954, of The American Society of Mechanical Engineers.

Discussion of this paper should be addressed to the Secretary, ASME, 29 West 39th Street, New York, N. Y., and will be accepted until July 11, 1955, for publication at a later date. Discussion received after the closing date will be returned.

Note: Statements and opinions advanced in papers are to be understood as individual expressions of their authors and not those of the Society. Manuscript received by ASME Applied Mechanics Division, February 23, 1954. Paper No. 54—A-92.

[2] Numbers in parentheses refer to the Bibliography at the end of the paper.

disposal at present is given by I. Malkin[3] who mentions that in chapter 5 of Savin's book stress concentrations around reinforced openings have been investigated.

2 General Boundary Condition for Reinforced Holes

The approach of reference (7) to problems of plane elasticity is based on the theory of functions of a complex variable. Representing biharmonic functions in terms of two complex functions Φ and Ψ, it is shown that the stresses and displacements are determined in terms of these functions by the following formulas

$$\left.\begin{aligned} X_x + Y_y &= 2[\Phi(z) + \overline{\Phi(z)}] \\ Y_y - X_x + 2iX_y &= 2[\bar{z}\Phi'(z) + \Psi(z)] \end{aligned}\right\} \quad \ldots\ldots [1]$$

$$2\mu(u + iv) = \kappa\varphi(z) - z\overline{\Phi(z)} - \overline{\psi(z)} \quad \ldots\ldots [2]$$

where

$$\left.\begin{aligned} \kappa &= 3 - 4\nu \\ &\text{for plane strain} \\ \kappa &= 3 - \frac{4\nu}{1+\nu} \end{aligned}\right\} \quad \ldots\ldots [3]$$

for generalized plane stress, and

$$\varphi(z) = \int \Phi(z)dz, \quad \psi(z) = \int \Psi(z)dz \quad \ldots\ldots [4]$$

If L is the boundary of the hole in the homogeneous sheet, the boundary condition for the first fundamental problem—when the stresses on the boundary are given—is

$$\varphi(z) + z\overline{\varphi'(z)} + \overline{\psi(z)} = i\int_0^s (X_n + iY_n)ds \text{ for } z \text{ on } L \quad \ldots [5]$$

where $X_n(s)$, $Y_n(s)$ are the external stress components at the point s of the boundary $\quad \ldots [6]$

Consider now the effect of compact reinforcement, Fig. 1, on the general form of the boundary condition. By Fig. 2 one has for equilibrium

$$\frac{\partial F}{\partial s}ds + Sds = 0, \quad Rds - Fd\vartheta = 0 \quad \ldots\ldots [7a]$$

However, since the forces from inside the boundary are due to stresses in the sheet and the boundary is taken along a co-ordinate line r = const, one has

$$\left.\begin{aligned} R &= \widehat{rr}\, t \\ S &= \widehat{r\theta}\, t \end{aligned}\right\} \quad \ldots\ldots [7b]$$

while, assuming the reinforcement to be made of the same material, F is given by

$$F = A(\widehat{\theta\theta} - \nu\,\widehat{rr}) \quad \ldots\ldots [7c]$$

where A is the area of the reinforcing ring, t the thickness of the sheet, and $\widehat{rr}$, $\widehat{\theta\theta}$, $\widehat{r\theta}$ are the stress components in the sheet in the directions of the relevant curvilinear co-ordinates denoted by (r, θ). It thus follows from Equation [7a] that

$$\frac{\partial}{\partial s}A(\widehat{\theta\theta} - \nu\widehat{rr}) + t\widehat{r\theta} = 0, \quad t\,\widehat{rr} - A(\widehat{\theta\theta} - \nu\widehat{rr})\frac{d\vartheta}{ds} = 0 \quad \ldots\ldots [7d]$$

[3] *Applied Mechanics Reviews*, vol. 5, May, 1952, no. 1318.

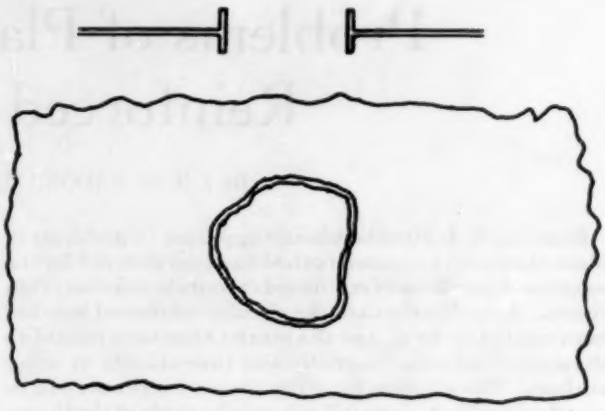

Fig. 1 Compactly Reinforced Hole

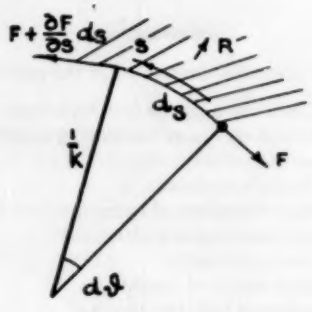

Fig. 2 Forces on Reinforced Boundary

or

$$\widehat{rr} = \frac{\alpha\widehat{\theta\theta}}{\dfrac{ds}{d\vartheta} + \nu\alpha}, \quad \widehat{r\theta} = -\frac{\partial}{\partial s}\left(\frac{\alpha\widehat{\theta\theta}\,\dfrac{ds}{d\vartheta}}{\dfrac{ds}{d\vartheta} + \nu\alpha}\right) \quad \ldots\ldots [7e]$$

where

$$\alpha = \frac{A}{t} \quad \ldots\ldots [8]$$

is a known function of the arc co-ordinate along the boundary, and $(ds)/(d\vartheta)$ is the local radius of curvature of the boundary.

These formulas express the boundary values of $\widehat{rr}$ and $\widehat{r\theta}$ in terms of those of $\widehat{\theta\theta}$ and of its tangential derivative. However, by Equation [1] the stress $\widehat{\theta\theta}$ may be expressed in terms of the functions Φ and Ψ, so that the boundary condition, Equation [5], may be modified by writing, with $r = (ds)/(d\theta)$

$$N = \left(\frac{\widehat{\theta\theta}\,\alpha}{r + \nu\alpha}\right) + N', \quad T = -\frac{\partial}{\partial s}\left(\frac{\alpha r\,\widehat{\theta\theta}}{r + \nu\alpha}\right) + T' \quad \ldots [9]$$

where N', T' are now the external stresses, applied to the reinforced boundary.

In order to solve problems for general shapes of the boundary, use may be made of conformal mapping of the boundaries onto the unit circle. Let

$$z = \omega(\zeta) \quad \ldots\ldots [10]$$

be the function mapping the boundary L in the z-plane onto the unit circle γ in the ζ-plane. When considering the infinite plane

with the hole L, the equation of the hole will be given in terms of the polar angle θ in the ζ plane by

$$z = \omega(e^{i\theta}) \quad \ldots\ldots [11]$$

so that on the boundary

$$z = x + iy = \frac{1}{2}[\omega + \bar{\omega} + (\omega - \bar{\omega})] \quad \ldots\ldots [12]$$

The equation of the original hole is thus given as a function of the parameter θ and one finds for the curvature

$$k = \frac{d\vartheta}{ds} = \frac{\dot{x}\ddot{y} - \dot{y}\ddot{x}}{(\dot{x}^2 + \dot{y}^2)^{3/2}} = -\frac{i}{2}\frac{\bar{\dot{\omega}}\ddot{\omega} - \dot{\omega}\bar{\ddot{\omega}}}{(\dot{\omega}\bar{\dot{\omega}})^{3/2}} \quad \ldots\ldots [13a]$$

where $$\cdot = \frac{\partial}{\partial\theta}$$

However, writing $$\zeta = \rho e^{i\theta} \quad \ldots\ldots [14]$$

one has

$$\left.\begin{aligned} \dot{\omega} &= \frac{\partial}{\partial\theta}\omega = i\zeta\frac{d}{d\zeta}\omega = i\zeta\omega' \\ \ddot{\omega} &= \frac{\partial}{\partial\theta}\dot{\omega} = -\zeta\omega' - \zeta^2\omega'' \end{aligned}\right\} \quad \ldots\ldots [15]$$

and hence from Equation [13]

$$k = \frac{d\vartheta}{ds} = \frac{1}{2}\frac{e^{i\theta}\bar{\omega}'\omega'' + 2\omega'\bar{\omega}' + re^{-i\theta}\omega'\bar{\omega}''}{(\omega'\bar{\omega}')^{3/2}} \quad \ldots\ldots [13b]$$

Next, an expression will be found for $\widehat{\theta\theta}$ in terms of ζ. The formulas, corresponding to Equations [1] and expressing the stress components in the curvilinear directions, are[4]

$$\left.\begin{aligned} \widehat{rr} + \widehat{\theta\theta} &= 2[\Phi(\zeta) + \overline{\Phi(\zeta)}] \\ \widehat{\theta\theta} - \widehat{rr} + 2i\widehat{r\theta} &= \frac{2\zeta^2}{\rho^2\overline{\omega'(\zeta)}}\left[\overline{\omega(\zeta)}\Phi'(\zeta) + \omega'(\zeta)\Psi(\zeta)\right] \end{aligned}\right\} \quad \ldots [16]$$

so that

$$\widehat{\theta\theta} = \Phi(\zeta) + \overline{\Phi(\zeta)} + \frac{\zeta^2}{2\rho^2\overline{\omega'(\zeta)}}\left[\overline{\omega(\zeta)}\Phi'(\zeta) + \omega'(\zeta)\Psi(\zeta)\right] + \frac{\overline{\zeta^2}}{2\rho^2\omega'(\zeta)}\left[\omega(\zeta)\overline{\Phi'(\zeta)} + \overline{\omega'(\zeta)}\overline{\Psi(\zeta)}\right] \quad \ldots\ldots [17]$$

Finally, an expression is required for the derivative with respect to the arc co-ordinates of the original boundary. One has

$$ds = (\dot{x}^2 + \dot{y}^2)^{1/2}d\vartheta = (\dot{\omega}\bar{\dot{\omega}})^{1/2}d\vartheta = (\omega'\bar{\omega}')^{1/2}d\vartheta \quad \ldots [18a]$$

and hence

$$\frac{\partial}{\partial s} = \frac{1}{(\omega'\bar{\omega}')^{1/2}}\frac{\partial}{\partial\vartheta} \quad \ldots\ldots [18b]$$

Thus the condition for the reinforced boundary becomes

$$\Phi(\zeta) + \overline{\Phi(\zeta)} - \frac{\zeta^2}{\overline{\omega'(\zeta)}}\left[\overline{\omega(\zeta)}\Phi'(\zeta) + \omega'(\zeta)\Psi(\zeta)\right] - \frac{\widehat{\theta\theta}\,\alpha}{\dfrac{ds}{d\vartheta} + \nu\alpha} - i\frac{\partial}{\partial s}\frac{\alpha\dfrac{ds}{d\vartheta}\widehat{\theta\theta}}{\dfrac{ds}{d\vartheta} + \nu\alpha} = N' - iT' \quad \ldots\ldots [19]$$

[4] By §50 of reference (7).

for $\zeta = e^{i\vartheta}$, where

$$\widehat{\theta\theta},\ \frac{\partial}{\partial s}\frac{\alpha\dfrac{ds}{d\vartheta}\widehat{\theta\theta}}{\dfrac{ds}{d\vartheta} + \nu\alpha}$$

are given by Equations [17], [13b], and [18b]. The solution of the boundary-value problem, Equation [19], may be effected by a number of different methods, treated in great detail in reference (7). The most elementary of these makes use of complex Fourier series and it is this method which will be applied in the next section. It also should be mentioned that a number of suitable conformal transformations are likewise given in reference (7), and that approximate solutions for other regions, containing, for example, holes with corners, may be obtained by use of polynomials or rational functions.

3 Plane With a Reinforced Circular Hole

In this case the Relations [7e] are easily seen to take the form

$$\widehat{rr} = \frac{\alpha'\widehat{\theta\theta}}{1 + \nu\alpha'}, \quad \widehat{r\theta} = -\frac{d}{d\theta}\left(\frac{\alpha'\widehat{\theta\theta}}{1 + \nu\alpha'}\right) \quad \ldots\ldots [20]$$

where $$\alpha' = \frac{A}{Rt} = \frac{\alpha}{R} \quad \ldots\ldots [21]$$

In polar co-ordinates, the formulas expressing the stresses in terms of the stress functions $\Phi(z)$, $\Psi(z)$ become

$$\left.\begin{aligned} \widehat{rr} + \widehat{\theta\theta} &= 2[\Phi(z) + \overline{\Phi(z)}] \\ \widehat{\theta\theta} - \widehat{rr} + 2i\widehat{r\theta} &= 2[\bar{z}\Phi'(z) + \Psi(z)]e^{2i\theta} \end{aligned}\right\} \quad \ldots\ldots [22]$$

and hence

$$\widehat{\theta\theta} = \Phi(z) + \overline{\Phi(z)} + \frac{1}{2}[z\Phi'(z) + \bar{z}\overline{\Phi'(z)}] + \frac{e^{2i\theta}}{2}\Psi(z) + \frac{e^{-2i\theta}}{2}\overline{\Psi(z)} \quad \ldots\ldots [23]$$

where use has been made of the relations

$$z = Re^{i\theta}, \quad \bar{z} = Re^{-i\theta} \quad \ldots\ldots [24]$$

on the boundary.

Assuming now the area A of the reinforcing ring to be constant, one finds

$$\frac{\partial\widehat{\theta\theta}}{\partial\theta} = i\left\{\frac{3}{2}z\Phi'(z) - \frac{3}{2}\bar{z}\overline{\Phi'(z)} + \frac{z^2}{2}\Phi''(z) - \frac{\bar{z}^2}{2}\overline{\Phi''(z)} + e^{2i\theta}\left[\Psi(z) + \frac{z}{2}\Psi'(z)\right] - e^{-2i\theta}\left[\overline{\Psi(z)} + \frac{\bar{z}}{2}\overline{\Psi'(z)}\right]\right\} \quad \ldots\ldots [25]$$

so that the boundary values of the stresses $N - iT$ are, by Equations [9]

$$N - iT = \frac{\alpha'}{1 + \alpha'\nu}\left\{\Phi(z) + \overline{\Phi(z)} - z\Phi'(z) + 2\bar{z}\overline{\Phi'(z)} - \frac{z^2}{2}\Phi''(z) + \frac{\bar{z}^2}{2}\overline{\Phi''(z)} - \frac{e^{2i\theta}}{2}[\Psi(z) + z\Psi'(z)] + \frac{e^{-2i\theta}}{2}[3\overline{\Psi(z)} + \bar{z}\overline{\Psi'(z)}]\right\} \quad \ldots\ldots [26]$$

The unmodified boundary condition for the present problem is

$$\Phi(z) + \overline{\Phi(z)} - e^{2i\theta}[\bar{z}\Phi'(z)] + \Psi(z) = N - iT \quad \ldots [27]$$

Writing for the functions Φ and Ψ their power series expansions

$$\Phi(z) = \sum_{k=0}^{\infty} a_k z^{-k}, \quad \Psi(z) = \sum_{k=0}^{\infty} a_k' z^{-k} \quad \ldots [28]$$

one finds the following relations between a_k, a_k', and the Fourier coefficients A_k of $N - iT$

$$N - iT = \sum_{-\infty}^{+\infty} A_k e^{ik\vartheta} \quad \ldots [29]$$

where the A_k are now given in terms of a_k and a_k' by Equation [26]

$$\left.\begin{aligned} & a_0 = \Gamma, \quad a_0' = \Gamma' \\ & 2a_0 - \frac{a_2'}{R^2} = A_0, \quad \frac{\bar{a}_1}{R} - \frac{a_1'}{R} = A_1, \quad \frac{\bar{a}_2}{R^2} - a_0' = A_2 \\ & \frac{\bar{a}_n}{R^n} = A_n, \quad a_n' = (n-1)R^2 a_{n-2} - R^n A_{2-n} \end{aligned}\right\} \quad \ldots [30]$$

These formulas, deduced (§56, reference 7) by substitution of the power series in the boundary condition, contain the quantities Γ, Γ' which are defined in terms of the principal stresses at infinity

$$\Gamma = \frac{1}{4}(N_1 + N_2), \quad \Gamma' = -\frac{1}{2}(N_1 - N_2)e^{-2i\gamma} \quad \ldots [31]$$

where γ is the angle between N_1 and the ox-axis.

It is easily seen from Equation [7] that

$$\left.\begin{aligned} A_k &= \frac{1}{R^k}\left[\bar{a}_k\left(1 - \frac{3}{2}k + \frac{k^2}{2}\right) + \bar{a}'_{k+2}\frac{(1-k)}{2R^2}\right]\frac{\alpha'}{1+\nu\alpha'}, \quad k \geqslant 3 \\ A_2 &= -\frac{1}{2}\left[a_0' + \frac{\bar{a}_1'}{R^4}\right]\frac{\alpha'}{1+\nu\alpha'} \\ A_1 &= 0 \\ A_0 &= \left[a_0 + \bar{a}_0 + \frac{a_2' + \bar{a}_2'}{2R^2}\right]\frac{\alpha'}{1+\nu\alpha'} \\ A_{-1} &= \frac{1}{R}\left[a_1 + \bar{a}_1' + \frac{a_3'}{R^2}\right]\frac{\alpha'}{1+\nu\alpha'} \\ A_{-2} &= \left[\frac{3}{2}\bar{a}_0' + \frac{3}{2}\frac{a_4'}{R^4}\right]\frac{\alpha'}{1+\nu\alpha'} \\ A_{-k} &= \frac{1}{R^k}\left[a_k\left(1 + \frac{1}{2}k - \frac{k^2}{2}\right) + a_{k+2}\frac{(k+1)}{2R^2}\right]\frac{\alpha'}{1+\nu\alpha'}, \quad k \geqslant 3 \end{aligned}\right\} \quad \ldots [32]$$

Hence by Equations [30]

$$\left.\begin{aligned} \Phi(z) &= \Gamma + \bar{\Gamma}'\frac{R^2}{z^2}\frac{1+\alpha'\nu+\alpha'}{1+\alpha'\nu+3\alpha'} \\ \Psi(z) &= \Gamma' + 2\Gamma\frac{R^2}{z^2}\frac{(1+\nu\alpha'-\alpha')}{1+\nu\alpha'+\alpha'} + 3\bar{\Gamma}'\frac{R^4}{z^4}\frac{(1+\alpha'\nu-\alpha')}{1+\alpha'\nu+3\alpha'} \end{aligned}\right\} \quad \ldots [33]$$

Consider, for example, the case of uniaxial tension in the x-direction when

$$\Gamma = \frac{p}{4}, \quad \Gamma' = -\frac{p}{2} \quad \ldots [34]$$

Then the stresses are, by Equations [22]

$$\left.\begin{aligned} \widehat{rr} &= \frac{p}{2}\left\{1 - \frac{R^2}{r^2}\frac{(1+\nu\alpha'-\alpha')}{(1+\nu\alpha'+\alpha')} + \cos 2\theta\left[1 - \frac{4R^2}{r^2}\frac{(1+\alpha'\nu+\alpha')}{(1+\alpha'\nu+3\alpha')} + \frac{3R^4}{r^4}\frac{(1+\alpha'\nu-\alpha')}{(1+\alpha'\nu+3\alpha')}\right]\right\} \\ \widehat{\theta\theta} &= \frac{p}{2}\left\{1 + \frac{R^2}{r^2}\frac{(1+\nu\alpha'-\alpha')}{(1+\nu\alpha'+\alpha')} - \cos 2\theta\left[1 + \frac{3R^4}{r^4}\frac{(1+\alpha'\nu-\alpha')}{(1+\alpha'\nu+3\alpha')}\right]\right\} \\ \widehat{r\theta} &= -\frac{p}{2}\left\{1 + \frac{2R^2}{r^2}\frac{(1+\alpha'\nu+\alpha')}{(1+\alpha'\nu+3\alpha')} - \frac{3R^4}{r^4}\frac{(1+\alpha'\nu-\alpha')}{(1+\alpha'\nu+3\alpha')}\right\}\sin 2\theta \end{aligned}\right\} \quad \ldots [35]$$

A useful check is provided by the two extreme cases

$$\alpha' = 0, \quad \alpha' = \infty \quad \ldots [36]$$

The first case gives

$$\left.\begin{aligned} \widehat{rr} &= \frac{p}{2}\left[1 - \frac{R^2}{r^2} + \cos 2\theta\left(1 - \frac{4R^2}{r^2} + 3\frac{R^4}{r^4}\right)\right] \\ \widehat{\theta\theta} &= \frac{p}{2}\left[1 + \frac{R^2}{r^2} - \cos 2\theta\left(1 + \frac{3R^4}{r^4}\right)\right] \\ \widehat{r\theta} &= -\frac{p}{2}\left[1 + \frac{2R^2}{r^2} - \frac{3R^4}{r^4}\right]\sin 2\theta \end{aligned}\right\} \quad \ldots [37]$$

which is the well-known solution deduced by G. Kirsch in 1898. The second case gives for the stresses on the edge of the hole

$$\left.\begin{aligned} \widehat{rr} &= p\left(\frac{1}{\nu+1} - \frac{2\cos 2\theta}{\nu+3}\right) \\ \widehat{\theta\theta} &= p\left(\frac{\nu}{\nu+1} - \frac{2\nu\cos 2\theta}{\nu+3}\right) \\ \widehat{r\theta} &= -\frac{4}{\nu+3}p\sin 2\theta \end{aligned}\right\} \quad \ldots [38]$$

Hence one has for the circumferential strain

$$\widehat{\theta\theta} - \nu\widehat{rr} = 0$$

which is essentially also the first condition of Equations [20], while the shear strain satisfies the second condition of [20].

When applying the general theory of Section 2 to the present problem, one has for the transformation onto the unit circle

$$z = \omega(\zeta) = R\zeta$$

and the formulas, written down directly in this section, are obtained.

Finally, it will be obvious that any desired type of loading at infinity can be attained by varying the expressions for Γ, Γ' in

Equations [33] in conformity with their definitions, Equations [31]. Owing to the existence of a wide range of results for the circular hole, e.g., references (3, 4), it has not been considered necessary here to study any other loading than that treated in this section.

4 Comparison With the Work of Reference (6)

The theory of reference (6) also takes account of bending of the reinforcement, while the present theory neglects this effect, so that the reinforcement is only subject to hoop stresses. Reference (6) gives a comparison between its theoretical and experimental results. In the notation of the present paper one has

$$R = 3.66 \text{ in.}, \quad t = 0.052 \text{ in.}, \quad A = 0.1193 \text{ sq in.}$$

$$E = 10.5 \times 10^6, \quad \nu = \frac{1}{3}, \quad p = 4160 \text{ psi}$$

Hence

$$\alpha' = 0.626$$

and Equation [35] gives

$$\widehat{rr} = 2080\left[1 - 0.318\,\frac{R^2}{r^2} + \cos 2\theta\left(1 - 2.377\,\frac{R^2}{r^2} + 0.566\,\frac{R^4}{r^4}\right)\right]$$

$$\widehat{\theta\theta} = 2080\left[1 + 0.318\,\frac{R^2}{r^2} - \cos 2\theta\left(1 + 0.566\,\frac{R^4}{r^4}\right)\right]$$

$$\widehat{r\theta} = -2080\left(1 + 1.189\,\frac{R^2}{r^2} - 0.566\,\frac{R^4}{r^4}\right)\sin 2\theta$$

From the stresses, tabulated in Table 1 for $\theta = 0, \pi/4, \pi/2$, $r = 5.25$ in., 7.75 in., the corresponding strains may be found using the formulas

$$\epsilon_{rr} = \frac{1}{E}\left(\widehat{rr} - \nu\widehat{\theta\theta}\right), \quad \epsilon_{r\theta} = \frac{2(1+\nu)}{E}\,\widehat{r\theta},$$

$$\epsilon_{\theta\theta} = \frac{1}{E}\left(\widehat{\theta\theta} - \nu\widehat{rr}\right)$$

In Table 2 these strains have been tabulated together with the theoretical and experimental strains of reference (6) and the theoretical strains for the plate with a simple hole.

It is seen that the strains calculated from the present theory are as close or closer to the experimental results, although bending has been neglected, than those based on the theory of reference (6).

TABLE 1 THEORETICAL STRESSES AT $\theta = 0, \pi/4, \pi/2$, $R/r = 0.697, 0.472$

R/r	θ	$\widehat{rr}$	$\widehat{\theta\theta}$	$\widehat{r\theta}$
0.697	0	1712	42	0
0.697	$\pi/4$	1760	2402	−3001
0.697	$\pi/2$	2008	4762	0
0.472	0	2965	89	0
0.472	$\pi/4$	1930	2230	−2573
0.472	$\pi/2$	895	4371	0

This observation seems to bear out the suggestion in reference (6) that the bending stiffness of the reinforcement represents a second-order effect, in spite of the comparatively large value of α'. For smaller values of α' which are most common in practice the foregoing theory will be entirely satisfactory.

5 Numerical Results for Reinforced Circular Hole

The theoretical results of this paper are easily presented in the form of graphs with α' as parameter. Writing the expressions for the stresses in the form

$$\left.\begin{aligned}
\frac{\widehat{rr}}{p} &= 0.5 - \frac{R^2}{r^2}B_1 + \cos 2\theta\left(0.5 - 2\,\frac{R^2}{r^2}B_2 + \frac{R^4}{r^4}B_3\right)\\
\frac{\widehat{\theta\theta}}{p} &= 0.5 + \frac{R^2}{r^2}B_1 - \cos 2\theta\left(0.5 + \frac{R^4}{r^4}B_3\right)\\
\frac{\widehat{r\theta}}{p} &= -\left(0.5 + \frac{R^2}{r^2}B_2 - \frac{R^4}{r^4}B_3\right)\sin 2\theta
\end{aligned}\right\} \quad \ldots [39]$$

where

$$\left.\begin{aligned}
B_1 &= \frac{1}{2}\,\frac{1 + \alpha'\nu - \alpha'}{1 + \gamma\alpha' + \alpha'}\\
B_2 &= \frac{1 + \alpha'\nu + \alpha'}{1 + \alpha'\nu + 3\alpha'}\\
B_3 &= 1.5\,\frac{1 + \alpha'\nu - \alpha'}{1 + \alpha'\nu + 3\alpha'}
\end{aligned}\right\} \quad \ldots [40]$$

The constants B_j have been graphed in Fig. 3, using $\nu = 1/3$.

The maximum stress concentration for $r = R$ is given by

$$\left(\frac{\widehat{\theta\theta}}{p}\right)_{\max} = 1 + B_1 + B_3 \text{ for } \theta = \pi/2 \quad \ldots [41]$$

while the extreme circumferential strain concentration at the edge is given by

$$\lambda = 1 + \frac{4}{3}B_1 - \frac{2}{3}B_2 + \frac{4}{3}B_3, \quad \theta = \pi/2 \quad \ldots [42]$$

These stress and strain concentrations have been graphed in Fig. 4. In particular, it is seen that the curve for λ agrees with that in Fig. 5 of reference (4) for the same quantity.

6 Conclusion

A general method has been deduced for the investigation of the stress distribution around compactly reinforced holes in infinite plates. The solution of such problems has been based on N. I. Muskhelishvili's monograph on plane elasticity. As an application of the method, the case of the circular reinforced hole has been solved completely and comparison with previous theoretical and experimental results shows the correctness of the present approach.

TABLE 2 STRAINS, THEORETICAL AND EXPERIMENTAL

		Equations [35]			Experimental, reference (5)			Theoretical, reference (5)			Theoretical for simple plate		
R/r	θ	$\epsilon_{rr} \times 10^4$	$\epsilon_{\theta\theta} \times 10^4$	$\epsilon_{r\theta} \times 10^4$	$\epsilon_{rr} \times 10^4$	$\epsilon_{\theta\theta} \times 10^4$	$\epsilon_{r\theta} \times 10^4$	$\epsilon_{rr} \times 10^4$	$\epsilon_{\theta\theta} \times 10^4$	$\epsilon_{r\theta} \times 10^4$	$\epsilon_{rr} \times 10^4$	$\epsilon_{\theta\theta} \times 10^4$	$\epsilon_{r\theta} \times 10^4$
0.697	0	1.62	−0.504	0	0.61	−0.504	−0.27	1.62	−0.295	0	0.702	−0.631	0
0.697	$\pi/4$	0.913	1.73	−7.63	0.595	1.94	−7.69	0.935	1.88	−7.62	0.035	2.6	−6.4
0.697	$\pi/2$	0.040	3.90	0	0.94	5.06		0.242	4.07	0	−0.632	5.83	0
0.472	0	2.797	−0.855	0	....	....	....	.....	.....		2.00	0.588	0
0.472	$\pi/4$	1.130	1.55	−6.53	....	.....	.....	.....	.....	....	0.735	1.903	−6.84
0.472	$\pi/2$	−0.585	3.88	0	−0.79	3.91	0.25	−0.488	4.00	0	−0.576	4.35	0

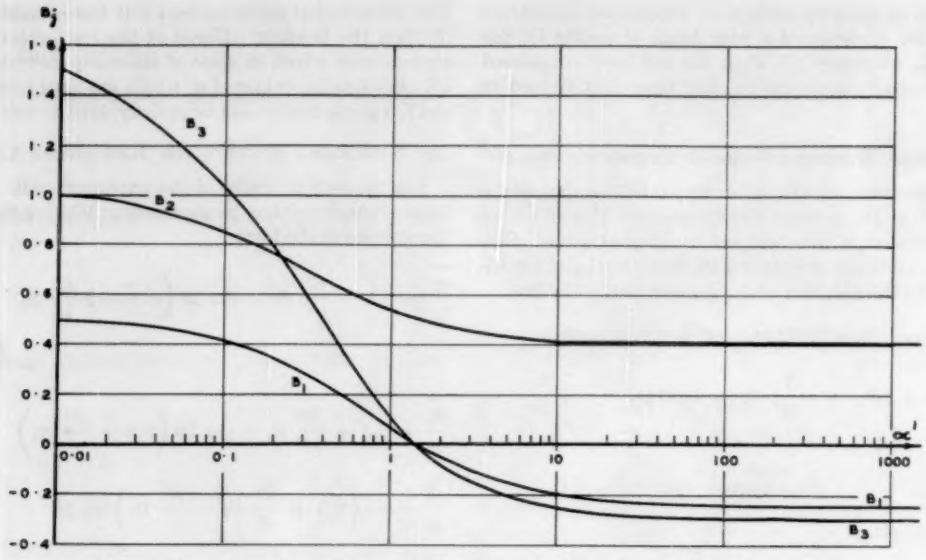

FIG. 3 CONSTANTS B_j, CHARACTERIZING STRESS DISTRIBUTION, EQUATIONS [39]

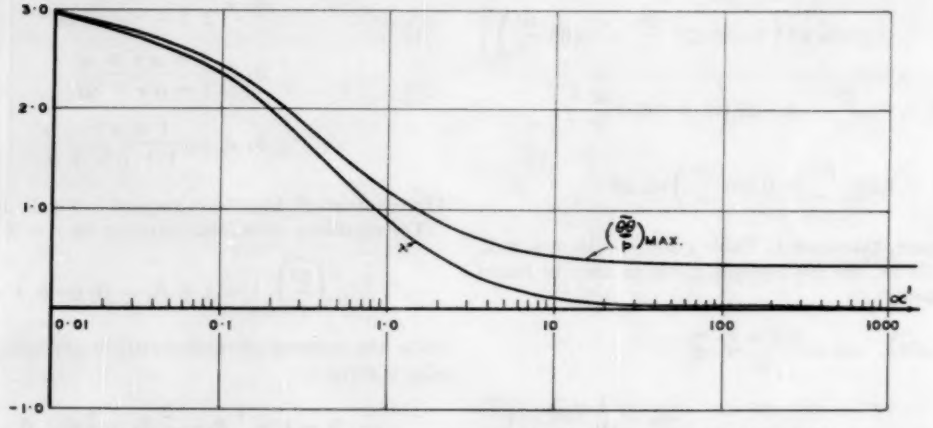

FIG. 4 STRESS AND STRAIN CONCENTRATION FACTORS, EQUATIONS [41] AND [42]

Various possibilities arise with regard to further applications of the theory of this paper. In order to avoid duplication, it would be most desirable to obtain reference (8) before investigating different shapes of holes. However, the present theory also allows the introduction of external loading at the edge of the reinforced hole and, apart from varying the stresses at infinity, certain cases of this type will be of interest. Particular interest will attach to the elliptical hole, since its limiting case is the straight cut. By solving this problem for tangential external stresses, one can obtain the solution of the problem of the infinite plate loaded through an elastic, finite-length rib attached to it. The solution of this problem would be of great interest to aircraft design.

BIBLIOGRAPHY

1 "On Stresses in a Plate With a Circular Hole," by S. Timoshenko, *Journal of The Franklin Institute*, vol. 197, 1924, pp. 505–516.

2 "Strength of Materials," by S. Timoshenko, McGraw-Hill Book Company, Inc., New York, N. Y., vol. 2, 1930.

3 "An Analysis of the Stresses in a Flat Plate With a Reinforced Circular Hole Under Edge Forces," by C. Gurney, R. and M. 1834, February, 1938.

4 "Strengthening of Circular Holes in Plates Under Edge Loads," by L. Beskin, JOURNAL OF APPLIED MECHANICS, Trans. ASME, vol. 66, 1944, p. A-140.

5 "On the Plane Stress Distribution in an Infinite Plate With Rim-Stiffened Elliptical Opening," by A. A. Wells, *Quarterly Journal of Mechanics and Applied Mathematics*, part 1, vol. 2, March, 1950.

6 "Reinforced Circular Cutouts in Plane Sheets," by H. Reissner and M. Morduchow, NACA TN 1852, April, 1949.

7 "Some Basic Problems of the Mathematical Theory of Elasticity," by N. I. Muskhelishvili, N. V. P. Noordhoff, Gronigen, Holland, 1953.

8 "Concentration of Stresses Around Holes," by G. N. Savin, Moscow-Leningrad, Gosud. Izdat. Tekhn.-teor. Lit., 1951 (*Applied Mechanics Reviews*, vol. 5, May, 1952, no. 1318.)

Stress Distribution in a Uniformly Rotating Equilateral Triangular Shaft[1]

By H. T. JOHNSON,[2] CHICAGO, ILL.

An approximate solution for the distribution of stresses in a rotating prismatic shaft, of triangular cross section, is presented in this paper. A general method is employed which may be applied in obtaining approximate solutions for the stress distribution for rotating prismatic shapes, for the cases of either generalized plane stress or plane strain. Polynomials are used which exactly satisfy the biharmonic equation and the symmetry conditions, and which approximately satisfy the boundary conditions.

Introduction

DURING the past half century, many papers have been written dealing with the stresses in both rotating disks and rotating shafts of various shapes. The stresses produced in thin disks and infinitely long shafts of uniform circular cross section rotating about their axes of symmetry are well known (1 to 4).[3] The stresses in rotating disks and shafts of other shapes are also of interest and have been treated extensively in the literature, a complete bibliography of which is beyond the scope of this paper. While the stresses in thin circular disks of uniform thickness rotating eccentrically and the stresses in thin circular disks of nonuniform thickness have received much attention, disks and shafts having other than circular cross sections have not been considered.

In this paper the stresses in a rotating shaft, the cross section of which is a regular polygon, are studied.

Statement of Problem, Residual Problem

A general method is presented in this paper for obtaining approximate solutions for the stress distribution in either thin disks or long shafts, the cross sections of which are regular polygons. The method is applicable only for the cases of either generalized plane stress or plane strain.

Numerical computations are presented for the stress distribution in an equilateral triangular shaft rotating uniformly about its centroidal axis for the case of plane strain. The biharmonic equation is satisfied exactly and the boundary conditions are approximately satisfied by use of a finite number of stress polynomials. By using a combination of twelve stress polynomials, the boundary stresses of the residual problem were approximated with a maximum error of 0.1 per cent, based on the maximum value of the given boundary stress. In addition, a system of equations is presented which facilitates obtaining similar approximations for other problems having the same symmetry properties.

If the body force field is given by

$$\bar{F} = -\text{Grad } \Omega(x, y) \quad [1]$$

then provided the components of stress are related to the Airy stress function, ϕ, according to

$$\sigma_x = \phi_{yy} + \Omega, \quad \sigma_y = \phi_{xx} + \Omega, \quad \tau_{xy} = -\phi_{xy} \quad [2]$$

the compatibility equation for plane strain is

$$\nabla^4\phi = -\frac{(1-2\nu)}{(1-\nu)}\nabla^2\Omega \quad [3]$$

where ν is Poisson's ratio. In the present problem

$$\Omega = -\frac{1}{2}\mu\omega^2 r^2 \quad [4]$$

where μ is the mass density and $r = (x^2 + y^2)^{1/2}$, thus

$$\nabla^4\phi = \frac{2(1-2\nu)\mu\omega^2}{(1-\nu)} \equiv K \quad [5]$$

where K is a constant. The general solution to Equation [5] is

$$\phi(x, y) = \frac{Kr^4}{64} + \Phi(x, y) \quad [6]$$

where

$$\nabla^4\Phi = 0 \quad [7]$$

The normal and shear stresses on the boundaries of the equilateral triangle are identically zero. Referring to Fig. 1, along the boundary AB, the normal and shear stresses are zero, that is

$$\sigma_x(h/3, y) = \tau_{xy}(h/3, y) = 0 \quad [8]$$

or by Equations [2] and [6], along the boundary $x = h/3$

$$\left.\begin{aligned} \Phi_{yy}(h/3, y) &= \alpha[3 - 2\nu + (1 + 2\nu)9y^2/h^2] \\ \Phi_{xy}(h/3, y) &= -6\alpha(1-2\nu)y/h \end{aligned}\right\} \quad [9]$$

where

$$\alpha = \frac{\mu\omega^2 h^2}{72(1-\nu)}$$

The normal and shear stresses are also identically zero on the boundaries BC and CA. These remaining boundary conditions are satisfied automatically if the function ϕ has the symmetry properties

$$\left.\begin{aligned} \phi(x, y) &= \phi(x, -y) \\ \phi(x, y) &= \phi(x', y') \end{aligned}\right\} \quad [10]$$

where

$$\left.\begin{aligned} x' &= \frac{1}{2}\left(-x + \sqrt{3}\,y\right) \\ y' &= \frac{1}{2}\left(-\sqrt{3}\,x - y\right) \end{aligned}\right\} \quad [11]$$

so that the x', y'-system is obtained by rotating counterclockwise through an angle of $2\pi/3$ radians from the x, y-system as shown in

---

[1] This paper was prepared from the author's thesis for the degree of Master of Science in Mechanics at Illinois Institute of Technology.

[2] Research Engineer, Armour Research Foundation of Illinois Institute of Technology. Assoc. Mem. ASME.

[3] Numbers in parentheses refer to the Bibliography at the end of the paper.

Contributed by the Applied Mechanics Division and presented at the Annual Meeting, New York, N. Y., November 28–December 3, 1954, of The American Society of Mechanical Engineers.

Discussion of this paper should be addressed to the Secretary, ASME, 29 West 39th Street, New York, N. Y., and will be accepted until July 11, 1955, for publication at a later date. Discussion received after the closing date will be returned.

Note: Statements and opinions advanced in papers are to be understood as individual expressions of their authors and not those of the Society. Manuscript received by ASME Applied Mechanics Division, December 14, 1953. Paper No. 54—A-91.

Fig. 1. From Equations [6] and [11], Equation [10] is satisfied if

$$\left.\begin{aligned}\Phi(x, y) &= \Phi(x, -y)\\ \Phi(x, y) &= \Phi(x', y')\end{aligned}\right\} \quad \ldots\ldots\ldots\ldots\ldots [12]$$

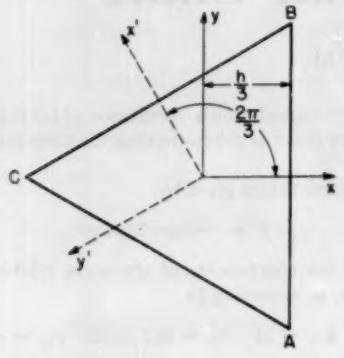

FIG. 1 CORRESPONDING AXES OF SYMMETRY FOR CROSS SECTION OF SHAFT

To obtain the required stresses, it is necessary to solve Equation [7] subject to the boundary conditions expressed in Equation [9] and the symmetry condition given in Equation [12]. This problem will be referred to as the residual problem. Since an exact solution could not be determined, combinations of polynomials were utilized in constructing Φ, which approximated the boundary conditions and which satisfied exactly the biharmonic equation and the symmetry conditions.

POLYNOMIAL APPROXIMATION FOR SOLUTION OF RESIDUAL PROBLEM

The general solution of the biharmonic equation, $\nabla^4\Phi = 0$, can be expressed in the form

$$\Phi = \psi_a + r^2\psi_b \ldots\ldots\ldots\ldots\ldots\ldots [13]$$

where

$$\nabla^2\psi_a = \nabla^2\psi_b = 0 \ldots\ldots\ldots\ldots\ldots\ldots [14]$$

Polynomials of the form

$$\psi = r^{2m}\cos 3m\theta \quad (m = 0, 1, 2, \ldots) \ldots\ldots\ldots [15]$$

where

$$\theta = \arctan (y/x)$$

satisfy Equation [14] and the symmetry conditions, Equation [12]. Since the biharmonic equation is linear, a combination of these polynomials, each multiplied by an undetermined coefficient, also will satisfy the biharmonic equation. Hence we may set

$$\Phi = \sum_{m=0}^{n} \Phi_m^{(A)} + \sum_{m=0}^{n'} \Phi_m^{(B)} \ldots\ldots\ldots\ldots [16]$$

where

$$\left.\begin{aligned}\Phi_m^{(A)} &= A_m' r^{3m}\cos 3m\theta\\ \Phi_m^{(B)} &= B_m' r^{3m+2}\cos 3m\theta\end{aligned}\right\} \quad \ldots\ldots\ldots\ldots [17]$$

These stress polynomials, for convenience, can be expressed in terms of rectangular co-ordinates, x and y, as

$$\left.\begin{aligned}\Phi_m^{(A)} &= A_m(3/h)^{3m-2}\sum_{s=0}^{s=3m/2}\left[\frac{(-1)^s(3m)!}{(2s)!(3m-2s)!}\,x^{3m-2s}y^{2s}\right]\\ \Phi_m^{(B)} &= B_m(3/h)^{3m}\sum_{s=0}^{s=\frac{3m+2}{2}}\left\{\frac{(-1)^s(3m)!}{(2s)!(3m-2s+2)!}\right.\\ &\left.[(3m-2s+2)(3m-2s+1)-2s(2s-1)]x^{3m-2s+2}y^{2s}\right\}\end{aligned}\right\} \quad [18]$$

where

$$A_m' = A_m(3/h)^{3m-2}, \qquad B_m' = B_m(3/h)^{3m}, \qquad s = 0, 1, 2, \ldots$$

The coefficients A_m and B_m are used instead of A_m' and B_m', respectively, so that all the undetermined coefficients will have the same dimensions.

Since the foregoing polynomials satisfy the biharmonic equation and the symmetry conditions, an approximate solution to the residual problem can be determined if a linear combination of these polynomials can be found which approximates the boundary values given in Equation [9] along the line $x = h/3$ with sufficient accuracy. Three different linear combinations were tried, which were obtained by taking n equal to 2, 3, and 6, respectively, and n' equal to $n - 1$, in order to satisfy the boundary conditions as to value, slope, etc., at certain discrete points. This procedure requires the solution of a system of equations of order $2n$ for the coefficients A_m and B_m.

For the case where n equals 6, the properties of Φ along the boundary which were satisfied are

$$\left.\begin{aligned}\Phi_{yy}(h/3, 0) &= Q_1 & \Phi_{xy}(h/3, h/3) &= R_1\\ \Phi_{yy}(h/3, h/3) &= Q_2 & \Phi_{xy}(h/3, h/\sqrt{3}) &= R_2\\ \Phi_{yy}(h/3, h/\sqrt{3}) &= Q_3 & \Phi_{xyy}(h/3, 0) &= R_3\\ \Phi_{yyy}(h/3, h/3) &= Q_4 & \Phi_{xyy}(h/3, h/3) &= R_4\\ \Phi_{yyy}(h/3, h/\sqrt{3}) &= Q_5 & \Phi_{xyy}(h/3, h/\sqrt{3}) &= R_5\\ \Phi_y(h/3, h/\sqrt{3}) - \Phi_y(h/3, 0) &= Q_6\\ \Phi_x(h/3, h/\sqrt{3}) - \Phi_x(h/3, 0) &= R_6\end{aligned}\right\} \ldots [19]$$

Twelve linear equations in the twelve unknown coefficients, A_m and B_m, are obtained by substituting the required derivatives of Φ, from Equations [16] and [18], into Equation [19]. A general solution for this system is given in the Appendix. The values of Q_q and R_q ($q = 1, 2, \ldots n$) are obtained from the boundary values, Equation [9]. For Poisson's ratio ν, equal to 0.3, the values of Q_q and R_q are given in Table 1.

TABLE 1 BOUNDARY-VALUE COEFFICIENTS, Q_q AND R_q

q	Q_q/α	R_q/α
1	2.4	-0.8
2	4.0	$-0.8\sqrt{3}$
3	7.2	$-2.4/h$
4	$9.6/h$	$-2.4/h$
5	$9.6\sqrt{3}/h$	$-2.4/h$
6	$4h/\sqrt{3}$	$-0.4h$

NUMERICAL RESULTS

As already stated, three approximations were tried which were obtained by taking n equal to 2, 3, and 6, respectively, with n' taken equal to $n - 1$. Some of the properties of Φ along the boundary $x = h/3$ are given in Equation [19]. Of this group, those used for the approximation where n equals 2 are Q_1, Q_3, R_2, and R_3; and where n equals 3 are Q_1, Q_3, Q_5, R_2, R_3, and R_5. The values of A_m and B_m for the three approximations are given in Table 2.

TABLE 2 NUMERICAL VALUES OF THE COEFFICIENTS A_m AND B_m

	$n = 2$	$n = 3$	$n = 6$
A_0	0	0	0
A_1	$3.7037 \times 10^{-1}\alpha$	$4.0330 \times 10^{-1}\alpha$	$4.05668 \times 10^{-1}\alpha$
A_2	$-5.9259 \times 10^{-3}\alpha$	$-4.7737 \times 10^{-3}\alpha$	$-4.26923 \times 10^{-3}\alpha$
A_3		$-1.37174 \times 10^{-4}\alpha$	$-1.51334 \times 10^{-4}\alpha$
A_4			$6.33623 \times 10^{-5}\alpha$
A_5			$5.51953 \times 10^{-6}\alpha$
A_6			$-1.285139 \times 10^{-6}\alpha$
B_0	2.1037α	2.1827α	2.18862α
B_1	$-5.9259 \times 10^{-3}\alpha$	$-6.9136 \times 10^{-3}\alpha$	$-7.16625 \times 10^{-3}\alpha$
B_2		$-8.8183 \times 10^{-4}\alpha$	$-1.12697 \times 10^{-3}\alpha$
B_3			$4.83679 \times 10^{-6}\alpha$
B_4			$4.89366 \times 10^{-7}\alpha$
B_5			$-4.15237 \times 10^{-8}\alpha$

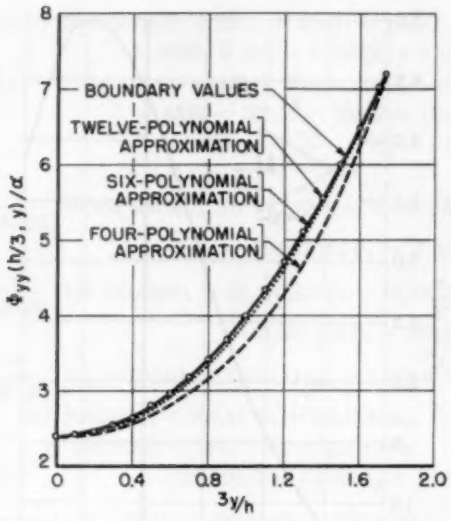

FIG. 2 COMPARISON OF THE BOUNDARY VALUES, $\Phi_{yy}(h/3, y)$, OF RESIDUAL PROBLEMS AND POLYNOMIAL APPROXIMATIONS

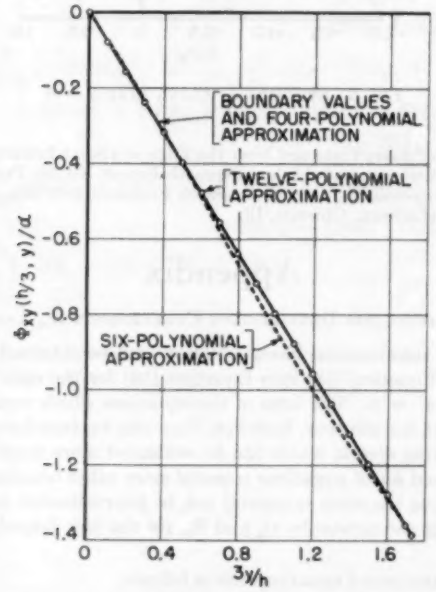

FIG. 3 COMPARISON OF BOUNDARY VALUES, $\Phi_{xy}(h/3, y)$, OF RESIDUAL PROBLEM AND POLYNOMIAL APPROXIMATIONS

Figs. 2 and 3 show how well the boundary values given in Equation [9] are reproduced for each of the three cases. Fig. 4 shows the stresses σ_y along the boundary AB; i.e., the line $x = h/3$. Figs. 5 and 6 show the stresses σ_x and σ_y along the line $y = 0$.

The maximum error in the polynomial approximation of the boundary values $\Phi_{yy}(h/3, y)$ for the cases where n equals 2, 3, and 6 are 0.40α, 0.079α, and 0.0012α, respectively. These values represent errors of 5.6, 1.1, and 0.017 per cent, respectively, based on the maximum value of $\Phi_{yy}(h/3, y)$. The maximum errors in the polynomial approximation of the boundary values $\Phi_{xy}(h/3, y)$ are zero, 0.042α, and 0.00135α, respectively, for each of the three cases. These values represent errors of zero, 3.0, and 0.097 per cent, respectively, based on the maximum value of $\Phi_{xy}(h/3, y)$.

The maximum values of $\sigma_x(x, 0)$ and $\sigma_y(x, 0)$ shown in Figs. 5 and 6, respectively, were computed from the case where $n = 6$ and $n' = 5$. The maximum values of $\sigma_x(x, 0)$ and $\sigma_y(x, 0)$ computed for the case where $n = 2$ and $n' = 1$ were in error by approximately 5.0 per cent and for the case where $n = 3$ and $n' = 2$ they were in error by approximately 0.3 per cent.

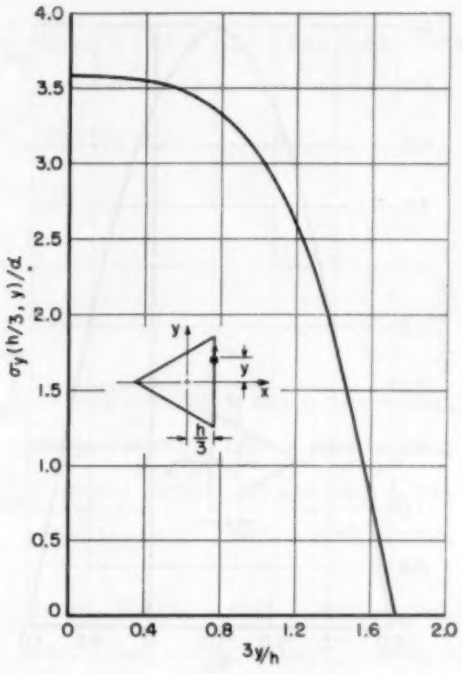

FIG. 4 STRESSES σ_y ALONG BOUNDARY $x = h/3$

The stresses $\sigma_x(x, y)$ can be determined along the boundary $x = h/3$ and along the altitude $y = 0$ from the values of σ_x and σ_y along these lines. If it is assumed that the deflection in the (axial) z-direction, W, is identically zero, the axial stress is

$$\sigma_z = \nu(\sigma_x + \sigma_y) \quad [20]$$

CONCLUSIONS

The maximum principal stresses which occur along the line $y = 0$ in a uniformly rotating equilateral triangular shaft are $\sigma_x = 4.966\alpha$, as shown in Fig. 5, and $\sigma_y = 5.006\alpha$, as shown in Fig. 6. From symmetry, these maximum stresses occur at corresponding points along the other altitudes of the triangular cross section. The maximum principal stress which occurs along the boundary $x = h/3$ is $\sigma_y = 3.577\alpha$, as shown in Fig. 4.

The maximum normal stress along the line $y = 0$ for the triangular shaft is, therefore

$$[\sigma_y(x, 0)]_{max} = 0.0993\mu\omega^2h^2$$

For comparison, the maximum stress in a rotating circular shaft circumscribed about the triangle is at the center and has the value

$$[\sigma_r(r, \theta)]_{max} = 0.1925\mu\omega^2h^2$$

where μ is the mass density and ω is the uniform angular velocity.

The use of stress polynomials of the forms $\Phi = A_m' r^{3m} \cos 3m\theta$ and $\Phi = B_m' r^{3m+2} \cos 3m\theta$ was effective for computing the required stresses. With only four polynomials, the maximum σ_x and σ_y stresses along the line $y = 0$ were only 5 per cent in error relative to the twelve-polynomial solution. With six polynomials the error for the same stresses was only 0.3 per cent.

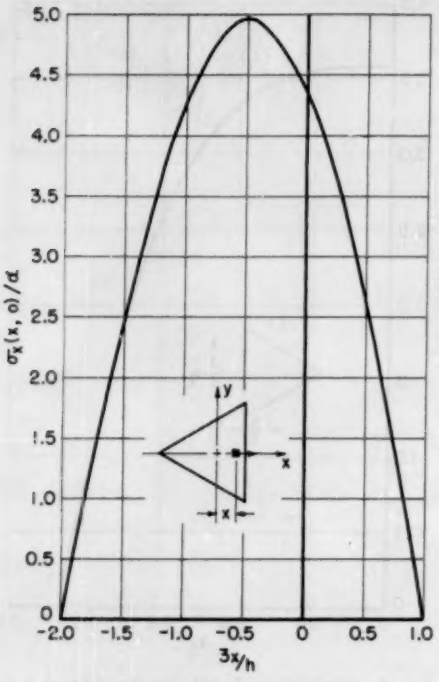

FIG. 5 STRESSES σ_x ALONG LINE $y = 0$

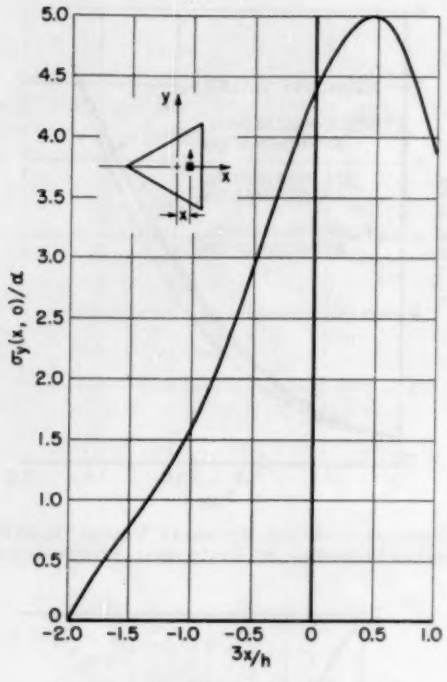

FIG. 6 STRESSES σ_y ALONG LINE $y = 0$

In order to obtain a solution with 12 polynomials, a system of 12 linear equations with 12 unknown coefficients had to be solved. The magnitude of the coefficients varied by factors as large as 10^6. The principal difficulty which this caused was that some of the equations in the triangular system, given in the Appendix, had to be solved with great accuracy in order to obtain all the coefficients with the required accuracy. For example, coefficients B_5 and A_6 had to be computed to 26 significant figures in order to get values for B_0 and A_1 to eight significant figures. However, when all the coefficients A_m and B_m were determined, it was necessary to use each coefficient to only five significant figures in order to satisfy the original system, obtained by substituting Equation [18] into Equation [19], to five significant figures. The difficulty of determining coefficients B_5 and A_6 to the required accuracy would be reduced greatly if digital computing machines were available.

ACKNOWELDGMENT

The author would like to express his appreciation to Dr. K. E. Bisshopp, Senior Research Engineer of the Armour Research Foundation, who suggested the problem and guided the analysis, and to Mr. T. T. Arai, also of the Armour Research Foundation, who assisted by checking some of the algebra.

BIBLIOGRAPHY

1 "The Mathematical Theory of Elasticity," by A. E. H. Love, Dover Publications, New York, N. Y., fourth edition, 1944, pp. 146–148.

2 "Theory of Elasticity," by S. Timoshenko, McGraw-Hill Book Company, Inc., New York, N. Y., first edition, 1934, p. 66

3 "Mathematical Theory of Elasticity," unpublished notes by I. S. Sokolnikoff, Brown University, Providence, R. I., p. 243.

4 "An Introduction to the Theory of Elasticity," by R. V. Southwell, Oxford University Press, London, England, second edition, 1941, p. 395.

5 "Steam and Gas Turbines," by A. Stodola, Lowenstein's translation of the sixth edition, McGraw-Hill Book Company, Inc., New York, N. Y., vol. 1, 1945, pp. 372–406.

6 "Stress Distributions Produced by a Cylindrical Hot Spot at the Center of a Square Plate and Near the Edge of a Semi-Infinite Plate," by K. E. Bisshopp, unpublished Research Report No. 39, Project No. 90-692J, Appendix A, Armour Research Foundation of Illinois Institute of Technology, Chicago, Ill.

Appendix

EQUATIONS FOR DETERMINING COEFFICIENTS A_m AND B_m

Twelve simultaneous linear equations can be obtained by substituting Equation [18] into Equation [19] for the case where $n = 6$ and $n' = 5$. The form of the equations which result is not convenient for solution; however, they can be transformed into the following system which can be evaluated more readily. The transformed set of equations is useful since other boundary tractions having the same symmetry can be approximated simply by evaluating the constants, Q_q and R_q, for the new boundary conditions.

The transformed equations are as follows:

$$-13{,}282{,}894B_5 + 91{,}342{,}629A_6 = P_1$$

$$37{,}200{,}553B_5 + 25{,}909{,}407A_6 = P_2$$

$$5A_5 - 8{,}669{,}510B_5 + 14{,}538{,}657A_6 = P_3$$

$$B_4 - 1{,}076{,}405A_5 + 704{,}527B_5 + 3{,}571{,}701A_6 = P_4$$

$$2A_4 + 2026B_4 - 101{,}945A_5 - 245{,}596B_5 + 1{,}729{,}728A_6 = P_5$$

$$3B_3 - 28{,}784A_4 - 2432B_4 + 216{,}455A_5 - 680{,}226B_5 - 564{,}228A_6 = P_6$$

$$9A_3 - 174B_3 + 1232A_4 + 4290B_4 - 11{,}120A_5 - 37{,}099B_5 + 70{,}074A_6 = P_7$$

$$B_3 + 105A_3 - 621B_3 - 1508A_4 + 20{,}950B_4 - 15{,}020A_5 - 443{,}989B_5 + 602{,}502A_6 = P_8$$

$$A_2 - 2B_2 - 24A_3 + 48B_3 + 384A_4 - 768B_4 - 5120A_5 + 10{,}240B_5 + 61{,}440A_6 = P_9$$

$$B_1 - 28B_2 + 480B_3 - 6656B_4 + 81{,}920B_5 = P_{10}$$

$$A_1 + 2B_1 + 20A_2 + 28B_2 + 84A_3 + 105B_3 + 220A_4 + 260B_4 + 455A_5 + 520B_5 + 816A_6 = P_{11}$$

$$B_0 - 3A_1 - 2B_1 - 15A_2 - 14B_2 - 36A_3 - 35B_3 - 66A_4 - 65B_4 - 105A_5 - 104B_5 - 153A_6 = P_{12}$$

where

$$P_1 = \frac{1}{15{,}552}(20{,}452{,}400D_1 + 11{,}078{,}573D_2 - 8{,}465{,}945D_3 - 10{,}027{,}863D_4 - 17{,}156{,}692D_5)$$

$$P_2 = \frac{1}{15{,}552}(142{,}932{,}208D_1 + 25{,}916{,}857D_2 - 76{,}151{,}797D_3 - 61{,}807{,}131D_4 - 98{,}150{,}468D_5)$$

$$P_3 = \frac{1}{20{,}736}(-1{,}960{,}064Q_1 - 3{,}612{,}114Q_2 - 1{,}289{,}677Q_3 + 109{,}350Q_4 + 201{,}417Q_5 + 6{,}861{,}855Q_6 - 293{,}382R_1 + 275{,}778R_2 - 322{,}816R_3 - 423{,}900R_4 - 53{,}600R_5 + 1{,}635{,}840R_6)$$

$$P_4 = \frac{1}{15{,}552}(-271{,}776Q_1 - 432{,}054Q_2 - 104{,}670Q_3 - 38{,}637Q_4 + 6765Q_5 + 808{,}500Q_6 - 454{,}410R_1 - 292{,}992R_2 - 211{,}680R_3 - 132{,}354R_4 + 11{,}916R_5 + 2{,}159{,}040R_6)$$

$$P_5 = \frac{1}{1152}(-2048Q_1 - 3294Q_2 - 713Q_3 - 336Q_4 + 19Q_5 + 6055Q_6 + 216R_1 + 176R_2 - 832R_3 - 810R_4 - 30R_5 + 2560R_6)$$

$$P_6 = \frac{1}{288}(684Q_2 - 19Q_3 - 45Q_4 + 68Q_5 - 665Q_6 + 498R_1 - 368R_2 - 156R_4 - 6R_5 + 64R_6)$$

$$P_7 = \frac{1}{72}(-3R_1 + 4R_3 + 3R_4 - 8R_6)$$

$$P_8 = \frac{1}{288}(108Q_2 - 18Q_3 + 18Q_5 - 90Q_6 + 3R_1 - 16R_3 - 3R_5 + 32R_6)$$

$$P_9 = \frac{1}{144}(Q_2 - Q_5 - Q_6)$$

$$P_{10} = -\frac{1}{72}Q_3$$

$$P_{11} = \frac{1}{6}R_3$$

$$P_{12} = \frac{1}{2}Q_1$$

and where

$$D_1 = \frac{1}{576}(-160Q_1 - 1674Q_2 + 49Q_3 + 24Q_4 - 163Q_5 + 1785Q_6 - 1080R_1 - 128R_2 + 800R_3 + 378R_4 + 30R_5)$$

$$D_2 = \frac{1}{576}(-864Q_1 - 900Q_2 - 301Q_3 - 183Q_4 + 52Q_5 + 2065Q_6 - 54R_1 - 288R_2 - 672R_3 - 432R_4 + 6R_5 + 2880R_6)$$

$$D_3 = \frac{1}{576}(1120Q_1 + 306Q_2 + 464Q_3 + 261Q_4 - 171Q_5 - 1890Q_6 - 54R_1 + 608R_2 + 1568R_3 + 918R_4 - 6080R_6)$$

$$D_4 = \frac{1}{576}(-1344Q_1 - 5346Q_2 - 415Q_3 + 12Q_4 - 291Q_5 + 7105Q_6 - 3456R_1 - 672R_2 + 832R_3 + 54R_4 + 42R_5 + 6400R_6)$$

$$D_5 = \frac{1}{576}(-544Q_1 + 342Q_2 - 148Q_3 - 219Q_4 + 99Q_5 + 350Q_6 + 594R_1 - 320R_2 - 768R_3 - 324R_4 + 18R_5 + 1600R_6)$$

Further Problems in Orthotropic Plane Stress

By H. D. CONWAY,[1] ITHACA, N. Y.

A solution is given for the infinite orthotropic plate containing an elliptical hole, the plate being subjected to tension at infinity and the axes of the hole and the direction of the tension inclined at arbitrary angles to the principal axes of orthotropy.

Method of Analysis

Problems in orthotropic plane stress require a solution of the equation

$$\left(\frac{\partial^2}{\partial x^2} + \alpha_1^2 \frac{\partial^2}{\partial y^2}\right)\left(\frac{\partial^2}{\partial x^2} + \alpha_2^2 \frac{\partial^2}{\partial y^2}\right)\phi = 0 \quad \ldots\ldots [1]$$

subject to the boundary conditions, the stresses being given by

$$\sigma_x = \frac{\partial^2 \phi}{\partial y^2}, \quad \sigma_y = \frac{\partial^2 \phi}{\partial x^2}, \quad \tau_{xy} = -\frac{\partial^2 \phi}{\partial x \partial y} \quad \ldots\ldots [2]$$

It is assumed that the x, y-axes are the principal axes of orthotropy. The constants α_1^2 and α_2^2 are functions of the elastic moduli expressed, with the usual notations, as

$$\alpha_1^2 \alpha_2^2 = S_{11}/S_{22}, \quad \alpha_1^2 + \alpha_2^2 = (S_{66} + 2S_{12})/S_{22} \quad \ldots [3]$$

Considering a pure rotation β of the x, y-co-ordinate axes by means of

$$x = x_1 \cos\beta - y_1 \sin\beta, \quad y = x_1 \sin\beta + y_1 \cos\beta \quad \ldots [4]$$

Equation [1] becomes

$$\left(\frac{\partial^2}{\partial x_1^2} + \frac{2(\alpha_1^2 - 1)\sin\beta\cos\beta}{\alpha_1^2 \sin^2\beta + \cos^2\beta}\frac{\partial^2}{\partial x_1 \partial y_1} + \frac{\alpha_1^2 \cos^2\beta + \sin^2\beta}{\alpha_1^2 \sin^2\beta + \cos^2\beta}\frac{\partial^2}{\partial y_1^2}\right)$$

$$\left(\frac{\partial^2}{\partial x_1^2} + \frac{2(\alpha_2^2 - 1)\sin\beta\cos\beta}{\alpha_2^2 \sin^2\beta + \cos^2\beta}\frac{\partial^2}{\partial x_1 \partial y_1} + \frac{\alpha_2^2 \cos^2\beta + \sin^2\beta}{\alpha_2^2 \sin^2\beta + \cos^2\beta}\frac{\partial^2}{\partial y_1^2}\right)\phi = 0 \quad \ldots\ldots [5]$$

When discussing plane-stress distributions in aelotropic materials without placing any restriction on the symmetry of the elastic properties, Green[2] has shown that the stresses can be derived from a stress function satisfying an equation of the form

$$\left(\frac{\partial^2}{\partial x_1^2} + m_1 \frac{\partial^2}{\partial x_1 \partial y_1} + n_1^2 \frac{\partial^2}{\partial y_1^2}\right)\left(\frac{\partial^2}{\partial x_1^2} + m_2 \frac{\partial^2}{\partial x_1 \partial y_1} + n_2^2 \frac{\partial^2}{\partial y_1^2}\right)\phi = 0 \quad \ldots\ldots [6]$$

the stresses being given by

$$\sigma_{x1} = \frac{\partial^2 \phi}{\partial y_1^2}, \quad \sigma_{y1} = \frac{\partial^2 \phi}{\partial x_1^2}, \quad \tau_{x1y1} = -\frac{\partial^2 \phi}{\partial x_1 \partial y_1} \quad \ldots\ldots [7]$$

and where m_1, m_2, n_1 and n_2 are functions of the elastic constants given, with the usual notation, by

$$n_1^2 + n_2^2 + m_1 m_2 = (2S_{12} + S_{66})/S_{22}, \; n_1^2 n_2^2 = S_{11}/S_{22}$$
$$m_1 + m_2 = -2S_{26}/S_{22}, \; m_1 n_2^2 + m_2 n_1^2 = -2S_{16}/S_{22} \quad \ldots [8]$$

Equation [5] is seen to be a special case of Equation [6] and this enables Green's solutions to be utilized immediately in solving certain interesting problems in orthotropic plane stress. The latter, of course, could have been solved directly by Green's powerful method.

Examples

As a first example, Green[2] has solved Equation [6] for the case of an infinite plate containing a circular hole, the plate being subjected at infinity to a uniform tensile stress T acting in a direction parallel to the x_1-axis. The stress at the edge of the circular hole is obtained in the closed form

$$\sigma_\theta(1 + \gamma_1^2 + \delta_1^2 - 2\gamma_1 \cos 2\theta - 2\delta_1 \sin 2\theta)$$
$$(1 + \gamma_2^2 + \delta_2^2 - 2\gamma_2 \cos 2\theta - 2\delta_2 \sin 2\theta) = T[(1 + \gamma_1)$$
$$(1 + \gamma_2)(1 + \gamma_1 + \gamma_2 - \gamma_1\gamma_2 - 2\cos 2\theta) + (\delta_1 + \delta_2)^2$$
$$- \delta_1^2\delta_2^2 - \delta_1^2\gamma_2^2 - \delta_2^2\gamma_1^2 + 2\delta_1\delta_2 \cos 2\theta - 2(\delta_1 + \delta_2$$
$$+ \delta_1\gamma_2 + \delta_2\gamma_1)\sin 2\theta] \quad \ldots\ldots [9]$$

where θ is measured from the x_1-axis and

$$\gamma_1 = \frac{n_1^2 - 1}{n_1^2 + 1 + 2\left(n_1^2 - \frac{1}{4}m_1^2\right)^{1/2}},$$

$$\gamma_2 = \frac{n_2^2 - 1}{n_2^2 + 1 + 2\left(n_2^2 - \frac{1}{4}m_2^2\right)^{1/2}}$$

$$\delta_1 = \frac{-m_1}{n_1^2 + 1 + 2\left(n_1^2 - \frac{1}{4}m_1^2\right)^{1/2}},$$

$$\delta_2 = \frac{-m_2}{n_2^2 + 1 + 2\left(n_2^2 - \frac{1}{4}m_2^2\right)^{1/2}} \quad \ldots\ldots [10]$$

In order to make Equations [5] and [6] identically equal, it can easily be shown that

---

[1] Professor of Mechanics, Cornell University. John Simon Guggenheim Fellow, Imperial College of Science, London University. Assoc. Mem. ASME.

[2] "A Note on Stress Systems in Aelotropic Materials-I," by A. E. Green, *Philosophical Magazine*, vol. 34, 1943, pp. 416–420.

Contributed by the Applied Mechanics Division and presented at the Annual Meeting, New York, N. Y., November 28–December 3, 1954, of The American Society of Mechanical Engineers.

Discussion of this paper should be addressed to the Secretary, ASME, 29 West 39th Street, New York, N. Y., and will be accepted until July 11, 1955, for publication at a later date. Discussion received after the closing date will be returned.

Note: Statements and opinions advanced in papers are to be understood as individual expressions of their authors and not those of the Society. Manuscript received by ASME Applied Mechanics Division, March 23, 1954. Paper No. 54—A-48.

$$\gamma_1 = \left(\frac{\alpha_1 - 1}{\alpha_1 + 1}\right)\cos 2\beta,\quad \gamma_2 = \left(\frac{\alpha_2 - 1}{\alpha_2 + 1}\right)\cos 2\beta$$

$$\delta_1 = -\left(\frac{\alpha_1 - 1}{\alpha_1 + 1}\right)\sin 2\beta,\quad \delta_2 = -\left(\frac{\alpha_2 - 1}{\alpha_2 + 1}\right)\sin 2\beta \quad [11]$$

and, by substituting these in Equation [9], the stress is obtained around a circular hole in an orthotropic plate when the tension T at infinity acts at an angle β to the principal axis of orthotropy in the direction of which S_{11} is measured. After some reduction, this stress is obtained as

$$\begin{aligned}8\sigma_\theta[\alpha_1^2\sin^2(\beta-\theta) + \cos^2(\beta-\theta)][\alpha_2^2\sin^2(\beta-\theta) \\ + \cos^2(\beta-\theta)] = T\{8\alpha_1\alpha_2[(\alpha_1+1)(\alpha_2+1)\sin^2 \\ (\beta-\theta)\cos^2\beta - 1] + 8(\alpha_1+1)(\alpha_2+1)\sin^2\beta\cos^2(\beta-\theta) \\ - 2(\alpha_1+1)(\alpha_2+1)(\alpha_1+\alpha_2)\sin 2\beta\sin 2(\beta+\theta) \\ - (\alpha_1-1)^2(\alpha_2-1)^2\sin^2 2\beta\cos^2 2\beta\} \quad [12]\end{aligned}$$

The angle θ is measured from the direction of the tensile stress T. Writing $\beta = 0$ as a special case, it follows that

$$\begin{aligned}\sigma_\theta(\alpha_1^2\sin^2\theta + \cos^2\theta)(\alpha_2^2\sin^2\theta + \cos^2\theta) \\ = T\alpha_1\alpha_2[(\alpha_1 + \alpha_2 + \alpha_1\alpha_2)\sin^2\theta - \cos^2\theta] \quad [13]\end{aligned}$$

which result has been given elsewhere.[3] Writing $\beta = 90$ deg gives Equation [13] with α_1 and α_2 replaced, respectively, by their reciprocals.

In order to get some idea of the numerical values obtainable from Equation [12], calculations have been made for oak, using the elastic constants of Hörig.[4] For oak, α_1^2 and α_2^2 are 5.321 and 1.109, respectively, and, assuming $\beta = 45$ deg, the values of the stresses at $\theta = 0$ and $\theta = 90$ deg are $-0.69T$ and $2.73T$. The corresponding results for $\beta = 0$ are $-2.43T$ and $2.38T$ whereas, for $\beta = 90$ deg, they are $-0.41T$ and $4.36T$.

In order to consider, as a further example, the case of an elliptical hole with the minor axis $2a$ in the x_1-direction and the major axis $2b$ in the y_1-direction, use is made of the transformation $y^* = ky_1$, $k = b/a > 1$, presented in a previous paper.[3] Equation [6] then becomes

$$\left(\frac{\partial^2}{\partial x_1^2} + m_1k\frac{\partial^2}{\partial x_1\partial y^*} + n_1^2k^2\frac{\partial^2}{\partial y^{*2}}\right)\left(\frac{\partial^2}{\partial x_1^2} + m_2k\frac{\partial^2}{\partial x_1\partial y^*} + n_2^2k^2\frac{\partial^2}{\partial y^{*2}}\right)\phi^* = 0 \quad [14]$$

The radius of the circular hole was assumed to be a and the stresses in the elliptical and circular-hole cases are related by the equations

$$k^2\sigma_x^* = \sigma_{x1},\ \sigma_y^* = \sigma_{y1},\ \tau_{xy}^* = \tau_{x1y1} \quad [15]$$

From Equation [14] it is seen that the functions of the elastic constants in the elliptical-hole case are different from those in the circular-hole case, m_1k replacing m_1, $n_1^2k^2$ replacing n_1^2, and so on. Thus, if the values of m_1, n_1^2, m_2, and n_2^2 in the circle case are replaced by m_1/k, n_1^2/k^2, m_2/k, and n_2^2/k^2, respectively, the functions of the elastic constants for the ellipse case will be m_1, n_1^2, m_2, and n_2^2 as defined by Equations [8]. The stresses for the case of an infinite orthotropic plate having an elliptical hole whose minor axis is inclined at β to the principal axis in the direction of which S_{11} is measured and subjected to tension T in the minor axis direction can be obtained from Equation [9] where

$$\left.\begin{aligned}\gamma_1 &= \frac{n_1^2 - k^2}{n_1^2 + k^2 + 2k\left(n_1^2 - \frac{1}{4}m_1^2\right)^{1/2}} \\ \gamma_2 &= \frac{n_2^2 - k^2}{n_2^2 + k^2 + 2k\left(n_2^2 - \frac{1}{4}m_2^2\right)^{1/2}} \\ \delta_1 &= \frac{-m_1k}{n_1^2 + k^2 + 2k\left(n_1^2 - \frac{1}{4}m_1^2\right)^{1/2}} \\ \delta_2 &= \frac{-m_2k}{n_2^2 + k^2 + 2k\left(n_2^2 - \frac{1}{4}m_2^2\right)^{1/2}}\end{aligned}\right\} \quad [16]$$

or, in terms of α_1 and α_2

$$\left.\begin{aligned}\gamma_1 &= \frac{(\alpha_1^2 - k^2)\cos^2\beta - (\alpha_1^2k^2 - 1)\sin^2\beta}{(\alpha_1 + k)^2\cos^2\beta + (\alpha_1k + 1)^2\sin^2\beta} \\ \gamma_2 &= \frac{(\alpha_2^2 - k^2)\cos^2\beta - (\alpha_2^2k^2 - 1)\sin^2\beta}{(\alpha_2 + k)^2\cos^2\beta + (\alpha_2k + 1)^2\sin^2\beta} \\ \delta_1 &= \frac{-2k(\alpha_1^2 - 1)\sin\beta\cos\beta}{(\alpha_1 + k)^2\cos^2\beta + (\alpha_1k + 1)^2\sin^2\beta} \\ \delta_2 &= \frac{-2k(\alpha_2^2 - 1)\sin\beta\cos\beta}{(\alpha_2 + k)^2\cos^2\beta + (\alpha_2k + 1)^2\sin^2\beta}\end{aligned}\right\} \quad [17]$$

From the first of Equations [15] and since the tension is in the x_1-direction, T in Equation [9] must be replaced by Tk^2. The stress σ' at the ends of the minor axis is therefore

$$\begin{aligned}[(1-\gamma_1)^2 + \delta_1^2][(1-\gamma_2)^2 + \delta_2^2]\sigma' = Tk^2[-(1-\gamma_1^2)(1-\gamma_2^2) \\ + (\delta_1 + \delta_2)^2 - \delta_1^2\delta_2^2 - \delta_1^2\gamma_2^2 - \delta_2^2\gamma_1^2 + 2\delta_1\delta_2] \quad [18]\end{aligned}$$

where γ_1, δ_1, γ_2, and δ_2 are given by Equations [17]. Noting that the stress σ'' at the ends of the major axis of the ellipse is in the x_1-direction and, from the first of Equations [15], the stress there is given by

$$\begin{aligned}[(1+\gamma_1)^2 + \delta_1^2][(1+\gamma_2)^2 + \delta_2^2]\sigma'' = T[(1+\gamma_1)(1+\gamma_2) \\ (3 + \gamma_1 + \gamma_2 - \gamma_1\gamma_2) + (\delta_1 + \delta_2)^2 - \delta_1^2\delta_2^2 - \delta_1^2\gamma_2^2 \\ - \delta_2^2\gamma_1^2 - 2\delta_1\delta_2] \quad [19]\end{aligned}$$

where γ_1, δ_1, γ_2, and δ_2 are again given by Equations [17].

For $\beta = 0$

$$\gamma_1 = \frac{\alpha_1 - k}{\alpha_1 + k},\quad \gamma_2 = \frac{\alpha_2 - k}{\alpha_2 + k},\quad \delta_1 = \delta_2 = 0 \quad [20]$$

and it follows from Equation [18] that

$$\sigma' = -\alpha_1\alpha_2T \quad [21]$$

and from Equation [19] that

$$\sigma'' = \left(1 + \frac{\alpha_1 + \alpha_2}{\alpha_1\alpha_2}\frac{b}{a}\right)T \quad [22]$$

For $\beta = 90$ deg

$$\gamma_1 = \frac{-(\alpha_1k - 1)}{\alpha_1k + 1},\quad \gamma_2 = \frac{-(\alpha_2k - 1)}{\alpha_2k + 1},\quad \delta_1 = \delta_2 = 0 \quad [23]$$

[3] "Stress Concentration Due to Elliptical Holes in Orthotropic Plates," by H. D. Conway, JOURNAL OF APPLIED MECHANICS, Trans. ASME, vol. 76, 1954, pp. 42–44.

[4] "Anwendung der Elastizitätstheorie anisotroper Körper auf Messungen an Holz," by H. Hörig, *Ingenieur Archiv*, vol. 6, 1935, pp. 8–14.

and from Equation [18]

$$\sigma' = -\frac{1}{\alpha_1\alpha_2}T \quad \ldots\ldots\ldots\ldots\ldots\ldots [24]$$

and from Equation [19]

$$\sigma'' = \left(1 + [\alpha_1 + \alpha_2]\frac{b}{a}\right)T \quad \ldots\ldots\ldots\ldots [25]$$

These latter results have been obtained previously.

Numerical values of the stresses in Equations [18] and [19] have been obtained for oak for which $\alpha_1^2 = 5.321$, $\alpha_2^2 = 1.109$ and assuming $\beta = 45$ deg and $k = b/a = 2$. The stresses at the ends of the minor and major axes are found to be $-0.69T$ and $4.46T$, respectively. The corresponding values for $\beta = 0$ from Equations [21] and [22] are $-2.43T$ and $3.77T$, whereas for $\beta = 90$ deg and from Equations [24] and [25], they are $-0.41T$ and $7.72T$.

Conclusion

The most general case of an elliptical hole in an orthotropic sheet subjected to uniaxial tension is when the major axis of the ellipse is inclined at an arbitrary angle to a principal axis of orthotropy, and the tension is inclined at an arbitrary but different angle. Assuming that the major axis is inclined at β to the S_{11} axis of orthotropy and the tension T is inclined at ξ to the latter and measured in the same sense, the stress system at infinity can then be resolved into, (a) tension $T\cos^2(\beta - \xi)$ parallel to the major axis of the ellipse, (b) tension $T\sin^2(\beta - \xi)$ parallel to the minor axis of the ellipse, and (c) shear $T\sin(\beta - \xi)\cos(\beta - \xi)$ parallel and perpendicular to the axes of the ellipse. Cases (a) and (b) can be solved in the manner already indicated and the solution for (c) can be developed in the same manner from a circular-hole result also presented by Green.[3] It will be seen that the results will be complex and hence they will not be given here.

Stresses Due to Diametral Forces on a Circular Disk With an Eccentric Hole

By A. M. SEN GUPTA,[1] SIBPORE, HOWRAH, WEST BENGAL, INDIA

In this paper stresses in a circular disk with an eccentric circular hole have been determined when the disk is compressed along the line of centers by two equal and opposite forces acting on its outer edge, the inner edge being unstressed. From the results obtained, the solution of the problem of a semi-infinite plate acted on by a concentrated normal force on its straight boundary and containing an unstressed circular hole has been deduced.

Nomenclature

The following nomenclature is used in the paper:

x, y	=	rectangular co-ordinates
R_1, θ_1; R_2, θ_2	=	polar co-ordinates
α, β	=	orthogonal curvlinear co-ordinates
a	=	a real positive length
$\frac{1}{h}$	=	stretch ratio
$\widehat{\alpha\alpha}, \widehat{\beta\beta}$	=	normal stress components in curvilinear co-ordinates
$\widehat{\alpha\beta}$	=	shearing stress in curvilinear co-ordinates
X	=	stress function
X_0, X_1	=	auxiliary stress functions
$\rho, \sigma, \tau, c, \alpha_1$	=	constants
F	=	applied force
ξ	=	$\alpha - c$
ξ_1	=	$\alpha_1 - c$

Introduction

The first problem discussed in this paper is that of determining stresses in a circular disk having an unstressed eccentric circular hole, the outer edge of the disk being compressed by two equal and opposite forces at the ends of a diameter. The solution which is believed to be new is obtained in bipolar co-ordinates. From the results thus obtained the solution of the problem of a semi-infinite plate containing an unstressed circular hole and subjected to a concentrated external force applied normally to its straight edge is then deduced. A practical application of the latter problem, which also can be solved directly, is that it will provide a first approximation to the general stress distribution in a plate containing a circular hole when acted upon by a cutting tool.

Method of Solution

Let us introduce the curvilinear co-ordinates defined by

$$\alpha + i\beta = \log \frac{x + i(y + a)}{x + i(y - a)} \quad \ldots\ldots [1]$$

Solving for x and y, we have

$$x = \frac{a \sin \beta}{\cosh \alpha - \cos \beta}, \quad y = \frac{a \sinh \alpha}{\cosh \alpha - \cos \beta} \quad \ldots\ldots [2]$$

From the relation

$$\frac{1}{h^2} = \left(\frac{\partial x}{\partial \alpha}\right)^2 + \left(\frac{\partial y}{\partial \alpha}\right)^2$$

we get

$$h = (\cosh \alpha - \cos \beta)/a \quad \ldots\ldots [3]$$

The curves α = const are a set of coaxial circles having $(0, \pm a)$ for limiting points, and β = const another set of circles passing through the limiting points $(0, \pm a)$ and intersecting the other set of circles orthogonally. We have $\alpha = 0$, on the x-axis, while on the y-axis $\beta = 0$, except on the segment joining the limiting points $(0, \pm a)$, where $\beta = \pm\pi$. The co-ordinates of the center of the circle $\alpha = c$ are $(0, a \coth c)$ and its radius is a cosech c.

The stresses in terms of the stress function X are given by Jeffery[2]

$$\widehat{a\alpha\alpha} = \left[(\cosh \alpha - \cos \beta)\frac{\partial^2}{\partial \beta^2} - \sinh \alpha \frac{\partial}{\partial \alpha} - \sin \beta \frac{\partial}{\partial \beta} + \cosh \alpha\right](hX)$$

$$\widehat{a\beta\beta} = \left[(\cosh \alpha - \cos \beta)\frac{\partial^2}{\partial \alpha^2} - \sinh \alpha \frac{\partial}{\partial \alpha} - \sin \beta \frac{\partial}{\partial \beta} + \cos \beta\right](hX)$$

$$\widehat{a\alpha\beta} = -(\cosh \alpha - \cos \beta)\frac{\partial^2(hX)}{\partial \alpha \partial \beta} \quad \ldots\ldots [4]$$

so that we have

$$a(\widehat{\alpha\alpha} - \widehat{\beta\beta}) = (\cosh \alpha - \cos \beta)\left(\frac{\partial^2}{\partial \beta^2} - \frac{\partial^2}{\partial \alpha^2} + 1\right)(hX) \ldots [5]$$

The differential equation satisfied by (hX) is[2]

$$\left(\frac{\partial^4}{\partial \alpha^4} + 2\frac{\partial^4}{\partial \alpha^2 \partial \beta^2} + \frac{\partial^4}{\partial \beta^4} - 2\frac{\partial^2}{\partial \alpha^2} + 2\frac{\partial^2}{\partial \beta^2} + 1\right)(hX) = 0 \quad \ldots\ldots [6]$$

The necessary and sufficient conditions for the boundary α = const to be free from stress are[2] that on the boundary

$$\frac{\partial}{\partial \alpha}(hX) = \rho \quad \ldots\ldots [7]$$

and

$$hX = \rho \tanh \alpha + \sigma(\cosh \alpha \cos \beta - 1) + \tau \sin \beta \ldots [8]$$

---

[1] Lecturer in Mathematics, Bengal Engineering College.

Contributed by the Applied Mechanics Division and presented at the Annual Meeting, New York, N. Y., November 28–December 3, 1954, of The American Society of Mechanical Engineers.

Discussion of this paper should be addressed to the Secretary, ASME, 29 West 39th Street, New York, N. Y., and will be accepted until July 11, 1955, for publication at a later date. Discussion received after the closing date will be returned.

Note: Statements and opinions advanced in papers are to be understood as individual expressions of their authors and not those of the Society. Manuscript received by ASME Applied Mechanics Division, December 14, 1953. Paper No. 54—A-37.

[2] "Plane Stress and Plane Strain in Bipolar Coordinates," by G. B. Jeffery, Philosophical Transactions of the Royal Society of London, England, vol. 221, 1921, pp. 265–293.

where ρ, σ, and τ are Michell's three constants of the boundary.

A Circular Disk Containing an Eccentric Circular Hole and Compressed by Two Equal and Opposite Forces Acting Along a Diameter

Let us consider a circular disk of unit thickness, the (x, y)-plane of Cartesian co-ordinates being the middle plane of the disk. The disk contains an eccentric circular hole. The axis of y is taken to be the line passing through the centers of the disk and the hole and coinciding with the diameter of the disk at the extremities A and B of which two equal and opposite forces each of intensity F per unit thickness are applied.

Let the outer boundary of the disk be defined by $\alpha = c$, $c > 0$, and the hole by $\alpha = \alpha_1$, $\alpha_1 > c$.

We assume that each of the forces (F) produces a simple radial stress distribution, so that the stress function X_0 required to make the boundary of the outer circle free from stress at all points other than A and B is given by[3]

$$X_0 = -\frac{F}{2\pi}\left[2x(\theta_1 + \theta_2) - \frac{R_1^2}{a \operatorname{cosech} c}\right] \quad \ldots\ldots [9]$$

where R_1, θ_1; R_2, θ_2 are the co-ordinates of any point $P(x, y)$ on the disk as shown in Fig. 1.

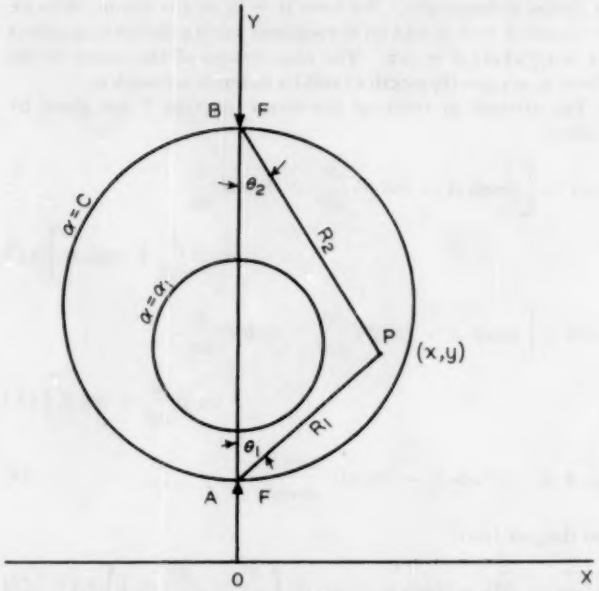

Fig. 1 Problem of the Circular Disk With Eccentric Hole

Noting that for $\alpha > c > 0$

$$\left.\begin{aligned}\theta_1 &= \sum_{n=1}^{\infty}\frac{e^{-n\alpha}}{n}\left[1 + (-1)^{n-1}e^{2nc}\right]\sin n\beta \\ \theta_2 &= \sum_{n=1}^{\infty}\frac{e^{-n\alpha}}{n}\left[e^{2nc} - 1\right]\sin n\beta\end{aligned}\right\} \quad \ldots\ldots [10]$$

[3] "Elementary Distribution of Plane Stress," by J. H. Michell, Proceedings of the London Mathematical Society, London, England, vol. 32, 1900, p. 44.

and $$R_1^2 = a^2\operatorname{sech}^2\frac{c}{2}\,\frac{\cosh(\alpha - c) + \cos\beta}{\cosh\alpha - \cos\beta}$$

we have for $\xi > 0$

$$hX_0 = \frac{F}{\pi}\left\{-e^{-\xi} + \sum_{n=2,4}^{\infty}\left[\frac{e^{-(n-)\xi}}{n-1} - \frac{e^{-(n+1)\xi}}{n+1}\right]\cos n\beta + \tanh\frac{c}{2}(\cosh\xi + \cos\beta)\right\} \quad \ldots\ldots [11]$$

For the auxiliary stress function X_1, we have to assume a function which will produce no stress on the boundary $\alpha = c$ and which is such that the complete stress function $X = X_0 + X_1$ will produce no stress on the boundary $\alpha = \alpha_1$.

We assume

$$hX_1 = \frac{F}{\pi}\left\{B_0[\xi(\cosh\alpha - \cos\beta)\cosh c + \sinh\xi(\cosh\alpha\cos\beta - \cosh^2 c)] + A_1(\cosh 2\xi - 1)\cos\beta + \sum_{n=2}^{\infty}[A_n\{\cosh(n+1)\xi - \cosh(n-1)\xi\} + B_n\{(n-1)\sinh(n+1)\xi - (n+1)\sinh(n-1)\xi\}]\cos n\beta\right\} \quad \ldots\ldots [12]$$

Since on the boundary $\alpha = c$ or $\xi = 0$, $hX_1 = 0$ and $(\partial/\partial\alpha)(hX_1) = 0$, the stresses on the boundary $\alpha = c$ is unaffected by the introduction of X_1, each of the Michell's constants being zero in this case. Further, it can be seen that the displacements produced by hX_1 are single valued.[2]

The complete stress function $X = X_0 + X_1$ given by Equations [11] and [12] must satisfy the Conditions [7] and [8] for the boundary $\alpha = \alpha_1$ or $\xi = \xi_1$.

From the boundary conditions the values of the constants B_0, A_1, A_n, and B_n are determined as

$$\left.\begin{aligned}B_0 &= -\frac{\cosh c\cosh\xi_1\operatorname{cosech}\xi_1}{\sinh\alpha_1\sinh\xi_1 + \sinh c\sinh(\alpha_1 + c)\cosh\xi_1} \\ A_1 &= \frac{1}{2}\,\frac{\cosh c\sinh\alpha_1\operatorname{cosech}\xi_1}{\sinh\alpha_1\sinh\xi_1 + \sinh c\sinh(\alpha_1 + c)\cosh\xi_1}\end{aligned}\right\} \quad \ldots [13]$$

for n even ≥ 2

$$\left.\begin{aligned}A_n[\sinh^2 n\xi_1 - n^2\sinh^2\xi_1] &= -n\sinh^2\xi_1 \\ B_n[\sinh^2 n\xi_1 - n^2\sinh^2\xi_1] &= \frac{1}{n^2-1}\{n^2\sinh^2\xi_1 + n\sinh\xi_1\cosh\xi_1 + e^{-n\xi_1}\sinh n\xi_1\}\end{aligned}\right\} \quad \ldots [14]$$

and for n odd ≥ 3 $\qquad A_n = B_n = 0 \quad \ldots\ldots [15]$

On the hole $\alpha = \alpha_1$, $\widehat{\alpha\alpha} = 0$; so that $\widehat{\beta\beta}$ can be very easily calculated from Equation [5]. We have

$$\widehat{\beta\beta}_{\alpha=\alpha_1} = \frac{F}{\pi a}\,\frac{\cosh^2 c[1 - \coth\xi_1\sinh 2\alpha_1 - 2\operatorname{cosech}\xi_1\sinh c\cos\beta + \cos 2\beta]}{\sinh\alpha_1\sinh\xi_1 + \sinh c\sinh(\alpha_1 + c)\cosh\xi_1} + \frac{4F}{\pi a}(\cosh\alpha_1 - \cos\beta)\sum_{n=2,4,\ldots}^{\infty}R_n\cos n\beta \quad \ldots\ldots [16]$$

where

$$\left[R_n + \frac{n}{n-1}e^{-(n-1)\xi_1}\right](\sinh^2 n\xi_1 - n^2\sinh^2\xi_1) = \frac{n}{n-1}(n^2\sinh^2\xi_1 + n\sinh\xi_1\cosh\xi_1 + e^{-n\xi_1}\sinh n\xi_1)\sinh(n-1)\xi_1 - n^2\sinh^2\xi_1\cosh(n-1)\xi_1$$

The series in Equation [16] converges slowly for small values of ξ_1. To make it rapidly convergent, we put

$$R_n = 2ne^{-n\xi_1}\sinh\xi_1 + Q_n$$

where

$$Q_n[\sinh^2 n\xi_1 - n^2\sinh^2\xi_1] = e^{-n\xi_1}[2n^2\sinh^2\xi_1 + ne^{-n\xi_1}\sinh\xi_1\sinh n\xi_1]$$

Now noting that

$$\sum_{n=2,4,..}^{\infty} ne^{-n\xi_1}\cos n\beta = \frac{\cosh 2\xi_1\cos 2\beta - 1}{(\cosh 2\xi_1 - \cos 2\beta)^2} \quad \ldots [17]$$

we have

$$\widehat{\beta\beta}_{(\alpha=\alpha_1)} = \frac{F}{\pi a}\frac{\cosh^2 c[1 - \coth\xi_1\sinh 2\alpha_1 - 2\,\mathrm{cosech}\,\xi_1\sinh c\cos\beta + \cos 2\beta]}{\sinh\alpha_1\sinh\xi_1 + \sinh c\sinh(\alpha_1 + c)\cosh\xi_1} + \frac{8F}{\pi a}(\cosh\alpha_1 - \cos\beta)\sinh\xi_1 \times \frac{\cosh 2\xi_1\cos 2\beta - 1}{(\cosh 2\xi_1 - \cos 2\beta)^2} + \frac{4F}{\pi a}(\cosh\alpha_1 - \cos\beta)\sum_{n=2,4,..}^{\infty} Q_n\cos n\beta \quad \ldots [18]$$

And for the outer boundary $\alpha = c$

$$\widehat{\beta\beta}_{(\alpha=c)} = \frac{F}{\pi a}(\cosh c - \cos\beta)\left[\frac{(1 + \cosh 2c)\cos\beta - \cosh c\coth\xi_1\sinh 2c}{\sinh\alpha_1\sinh\xi_1 + \sinh c\sinh(\alpha_1 + c)\cosh\xi_1} + \sum_{n=2,4,..}^{\infty} N_n\cos n\beta\right] \quad \ldots [19]$$

where $N_n = 4nA_n$

In Tables 1 and 2 the numerical values of the coefficients N_n and Q_n, respectively, for different values of ξ_1 are given.

The stresses are symmetrical about the y-axis. Hence in Tables 3 and 4 the values of $\widehat{\beta\beta}$ on the boundaries $\alpha = \alpha_1$ and $\alpha = c$, respectively, are given for values of β between 0 and π when $\alpha_1 = .2$ and $c = 0.6$, i.e., when the ratio of the diameter of the disk to the diameter of the hole is

$$\frac{\sinh\alpha_1}{\sinh c} \ (= 5.697)$$

From Table 3 it will be found that the maximum tensions are at the extremities of the diameter of the hole passing through A and B and it is more marked at the point where the distance between the two boundaries is least. The points of zero stresses are found to be approximately at $\beta = \pm 31° 34'$ and at $\beta = \pm 144° 13'$ with the points of maximum compression $10.93F/(\pi a)$ at $\beta = \pm 94°$ approximately. From Table 4 it will be found that the compression is maximum and more marked at the point which is

TABLE 1 NUMERICAL VALUES OF COEFFICIENTS N_n

ξ_1	0.8	1.0	1.2	1.4	1.6	1.8	2
$-N_2$	5.075	2.896	1.756	1.103	0.7081	0.4617	0.3042
$-N_4$	0.3671	0.1223	0.03984	0.01274	0.003995	0.00123	0.0003
$-N_6$	0.03097	0.00489	0.00073	0.000105	0.000015		
$-N_8$	0.00223	0.000159					
$-N_{10}$	0.000142						

TABLE 2 NUMERICAL VALUES OF Q_n

ξ_1	0.8	1.0	1.2	1.4	1.6	1.8	2
Q_2	0.977	0.4810	0.2475	0.1299	0.06936	0.03738	0.0203
Q_4	0.02709	0.005324	0.0009965	0.00018	0.0000316		
Q_6	0.0006855	0.000043					

TABLE 3 VALUES OF $\widehat{\beta\beta}$ ON BOUNDARY $\alpha = \alpha_1$

($\alpha_1 = 2$, $c = 0.6$)

β, deg	$\frac{\pi a}{F}\widehat{\beta\beta}_{(\alpha=\alpha_1)}$	β, deg	$\frac{\pi a}{F}\widehat{\beta\beta}_{(\alpha=\alpha_1)}$	β, deg	$\frac{\pi a}{F}\widehat{\beta\beta}_{(\alpha=\alpha_1)}$	β, deg	$\frac{\pi a}{F}\widehat{\beta\beta}_{(\alpha=\alpha_1)}$
0	4.6608	60	− 6.8547	120	−8.077	180	10.017
15	3.4704	75	− 9.504	135	−3.567		
30	0.4327	90	−10.841	150	2.351		
45	−3.3331	105	−10.463	165	6.869		

TABLE 4 VALUES OF $\widehat{\beta\beta}$ ON BOUNDARY $\alpha = c$

($\alpha_1 = 2$ $c = 0.6$)

β, deg	$\frac{\pi a}{F}\widehat{\beta\beta}_{(\alpha=c)}$	β, deg	$\frac{\pi a}{F}\widehat{\beta\beta}_{(\alpha=c)}$	β, deg	$\frac{\pi a}{F}\widehat{\beta\beta}_{(\alpha=c)}$	β, deg	$\frac{\pi a}{F}\widehat{\beta\beta}_{(\alpha=c)}$
0	−0.1985	60	0.3563	120	0.5809	180	−3.098
15	−0.2019	75	0.8046	135	−0.4485		
30	−0.1662	90	1.144	150	−1.688		
45	0.005058	105	1.123	165	−2.702		

closest to the boundary of the hole. The points of zero stresses are found to be at $\beta = \pm 44° 43'$ and at $\beta = \pm 129° 7'$ approximately with the points of maximum tension $1.192F/(\pi a)$ at $\beta = \pm 97°$ approximately.

A Semi-Infinite Plate With a Circular Hole Subjected to a Concentrated External Force F Applied Normally to Its Straight Edge[4]

In the result of the previous section putting $c = 0$, we have the case of a semi-infinite plate with an unstressed circular hole subjected to a concentrated load F normal to its straight boundary.

Putting $c = 0$ in Equation [18] we have the circumferential stress on the circular hole $\alpha = \alpha_1$ of the semi-infinite plate as

$$\widehat{\beta\beta}_{(\alpha=\alpha_1)} = \frac{4F}{\pi a}\frac{\sinh\alpha_1(\cosh 2\alpha_1\cos 2\beta - 1)}{(\cosh 2\alpha_1 - \cos 2\beta)(\cosh\alpha_1 + \cos\beta)} - \frac{2F}{\pi a}\frac{\cosh 2\alpha_1 - \cos 2\beta}{\cosh 2\alpha_1 - 1} + \frac{4F}{\pi a}(\cosh\alpha_1 - \cos\beta)\sum_{n=2,4,\ldots}^{\infty} M_n\cos n\beta \quad [20]$$

where

$$M_n[\sinh^2 n\alpha_1 - n^2\sinh^2\alpha_1] = e^{-n\alpha_1}[2n^2\sinh^2\alpha_1 + ne^{-n\alpha_1}\sinh\alpha_1\sinh n\alpha_1]$$

And for the straight boundary $\alpha = 0$, we have from Equation [19], putting $c = 0$

$$\widehat{\beta\beta}_{(\alpha=0)} = \frac{F}{\pi a}(1 - \cos\beta)\left(2\operatorname{cosech}^2\alpha_1 + \sum_{n=2,4,\ldots}^{\infty} P_n\cos n\beta\right) \quad \ldots[21]$$

where

$$P_n(\sinh^2 n\alpha_1 - n^2\sinh^2\alpha_1) = -4n^2\sinh^2\alpha_1$$

In Fig. 2 we have the graphs of the stresses in the two boundaries in the case when $\alpha_1 = 1.4$, i.e., when the shortest distance between the two boundaries is nearly equal to the radius of the hole. The general character of the stresses in the two boundaries does not change owing to the proximity of the hole. For the circular boundary the maximum tensions take place at the same places for all distances of the hole from the straight edge, viz., at the extremities of the diameter perpendicular to the straight edge, this being most marked at the extremity nearest the straight edge. But the ratio of the maximum tensions increases as the hole approaches the straight edge and reduces approximately to unity as the hole recedes to a great distance from the straight edge. Thus for $\alpha_1 = 1.4$ this ratio is 6.2 nearly, while for $\alpha_1 = 0.8$ this ratio is 20.5 nearly—the maximum compression in either case occurring between the two.

TABLE 5 COMPRESSION VALUES

α_1	Ratio of distance of center of hole from straight edge to radius of hole	$\frac{\pi a}{F}\widehat{\beta\beta}$ at middle point of straight edge	$\frac{\pi a}{F}\widehat{\beta\beta}$ at nearest point of circular boundary	$\frac{\pi a}{F}\widehat{\beta\beta}$ at most remote point of circular boundary
0.8	1.337	−16.0208	17.92	0.8728
1	1.543	− 8.9428	11.604	0.9056
1.2	1.811	− 5.3486	8.2428	0.9544
1.4	2.151	− 3.3368	6.256	1.016
1.6	2.578	− 2.1328	5.0132	1.0936
1.8	3.108	− 1.388	4.1984	1.1796
2	3.762	− 0.9132	3.6387	1.2704
5	74.21	− 0.00072	2.056	1.946
6	201.7	− 0.000098	2.02	1.996
∞	∞	0	2	2

For the straight boundary the stress at the middle point is minimum for all distances of the hole from the straight edge and follows the same general character as when the hole is at a great distance. But the maximum compression at the middle point increases as the hole approaches the straight edge. Its value for different values of the ratio of the distance of the center of the hole from the straight edge to the radius of the hole as also the stresses at the nearest and most remote points of the circular boundary are given in Table 5.

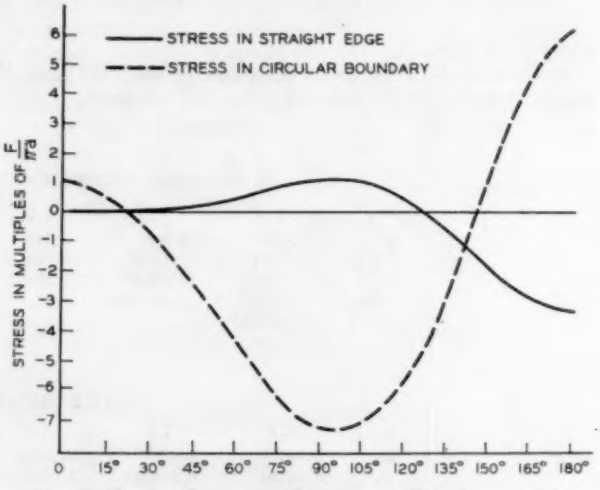

Fig. 2 Stress Curves in Boundaries When $\alpha_1 = 1.4$

Acknowledgment

The author thanks Dr. B. Sen for his kind help in the preparation of this paper.

[4] The author is grateful to the referees for bringing to his notice the paper of A. Barjansky on this problem published in the *Quarterly of Applied Mathematics*, vol. II, 1944, pp. 16–31. It is found that the results obtained here tally with the corresponding results of A. Barjansky. The only justification of the inclusion of this problem in this paper is to show how it can be solved as a particular case of the problem of the compressed circular disk with an eccentric hole.

Bending of Orthogonally Stiffened Plates

By W. H. HOPPMANN, 2ND,[1] BALTIMORE, MD.

In this paper the flexure theory for plates of orthotropic material is applied in the case of orthogonally stiffened plates using an experimental method to determine plate stiffnesses in bending and in twisting. Once these stiffnesses, or elastic moduli, have been determined by test they may be used in calculating bending deflections for plates of identical stiffened construction but any given boundary conditions. As an example, calculated deflections of a stiffened circular plate with clamped edge are compared with those which were determined experimentally. It is also demonstrated that the theory can be applied to the case of vibration of a stiffened plate if in addition to the orthotropic elastic constants the weight per unit area of the plate is determined. The various experimental results show considerable promise for use of the proposed combination of theory and experimental method in the analysis of both statically and dynamically loaded plates with attached stiffeners.

Nomenclature

The following nomenclature is used in the paper:

ϵ_i	=	strain
γ	=	shear strain
σ_i	=	stress
τ	=	shear stress
S_{ij}	=	elastic constants
E_x	=	$1/S_{11}$ = Young's modulus
E_y	=	$1/S_{22}$ = Young's modulus
G_{xy}	=	$1/S_{66}$ = rigidity or shear modulus
ν_{xy}	=	$-E_x . S_{12}$ = Poisson's ratio
ν_{yx}	=	$-E_y . S_{21}$ = Poisson's ratio
W	=	deflection of plate
h	=	thickness of plate (equivalent orthotropic plate)
a	=	width of plate (bending)
b	=	length of plate (bending)
c	=	length of side of plate (twisting)
x, y	=	co-ordinates of point on surface of plate
A, B, C	=	constants of integration
A_x, A_y, A_{xy}	=	constants in differential equation of plate and are expressions in terms of elastic constants
$F(x, y, t)$	=	force applied normally to face of plate
ρ	=	mass density
t	=	time
P_{mn}	=	circular frequency of m, n mode of vibration of rectangular plate
m, n	=	mode numbers corresponding to x-direction and y-direction, respectively
r_0	=	radius of circular plate

[1] Associate Professor, Department of Mechanical Engineering, The Johns Hopkins University. Mem. ASME.

Contributed by the Applied Mechanics Division and presented at the Annual Meeting, New York, N. Y., November 28–December 3, 1954, of The American Society of Mechanical Engineers.

Discussion of this paper should be addressed to the Secretary, ASME, 29 West 39th Street, New York, N. Y., and will be accepted until July 11, 1955, for publication at a later date. Discussion received after the closing date will be returned.

Note: Statements and opinions advanced in papers are to be understood as individual expressions of their authors and not those of the Society. Manuscript received by ASME Applied Mechanics Division, September 19, 1953. Paper No. 54—A-31.

Introduction

Flexure theory for flat plates of homogeneous orthotropic material has been in existence for many years (1).[2] An application of it to the case of plates with attached stiffeners was introduced more recently by several investigators (2, 3, 4, 5). For this latter case, an isotropic plate with stiffeners attached in each of two orthogonal directions is assumed to be approximately an orthotropic plate. The stiffeners are identical, parallel, and fairly closely spaced. A repeating unit is regarded as an infinitesimal element of an equivalent orthotropic plate of corresponding stiffness factors or compliances. The entire composite structure will bend and twist approximately the same as a homogeneous orthotropic plate of equivalent stiffness. This type of analysis is particularly applicable for composite structures such as stiffened bottoms in ships and fuselages of airplanes (6, 7, 8, 9).

Examination of the technical literature shows that investigators invariably attempt to estimate the appropriate unit stiffness factors or compliances for stiffened plates on a theoretical basis, using beam theory as a guide. Cross-contraction effects associated with a Poisson's type ratio are usually neglected.

In the present paper the theory is applied in conjunction with an experimental method for the determination of the effective stiffness moduli of the actual stiffened structure. Rectangular portions or "patches" of the plate containing a sufficient number of the stiffeners to be representative are subjected to pure bending and twisting couples distributed along their edges. From these tests elastic constants for the stiffened material are determined.

The use of the method with dynamical problems is illustrated by the study of flexural vibrations of simply supported plates.

Theory of Equivalent Orthotropic Plate

Consideration of an experimental method for the determination of elastic constants of homogeneous orthotropic plate material of constant thickness (12, 13) suggests that one might utilize the same method to determine effective elastic constants for a plate with attached system of stiffeners.

For the purpose, a stiffened plate is considered as if it were approximately a plate of homogeneous orthotropic material of some definite thickness. It is assumed that the elastic constants of this equivalent orthotropic plate can be chosen in such a manner that it will have approximately the bending and twisting stiffnesses or compliances of the given orthogonally stiffened plate. The validity of this assumption must be investigated by experiment.

Now suppose that conveniently sized but sufficiently representative rectangular and square test plates are fabricated just like sections from the stiffened prototype. These test plates may themselves be considered as small orthotropic plates. The rectangular models will serve for bending tests and square ones for twisting tests. The elastic constants determined from test on the samples will be assumed to be those corresponding to the stiffened material of which the prototype is fabricated.

It will be assumed further that the plates are effectively homogeneous and orthotropic and therefore have three axes of symmetry at each point. The edges of the test plates are parallel to the stiffeners and hence parallel to the principal directions of stiffness.

[2] Numbers in parentheses refer to the Bibliography at the end of the paper.

In the usual notation (10) the stress-strain relation of the equivalent orthotropic material may be written for the strains in terms of the elastic constants and stresses as

$$\epsilon_i = S_{ij}\sigma_j \ (i, j = 1, 2)$$

$$\gamma = S_{66}\tau \ldots\ldots\ldots\ldots\ldots\ldots\ldots\ldots\ldots\ldots [1]$$

Three planes of symmetry are assumed and there are four independent constants of elasticity $S_{ij}(S_{12} = S_{21})$.

The differential equation for the free flexural vibrations was given by Voigt (1). Using the notation used by Timoshenko (10) it may be written for forced vibrations as

$$A_x \frac{\partial^4 w}{\partial x^4} + A_{xy} \frac{\partial^4 w}{\partial x^2 \partial y^2} + A_y \frac{\partial^4 w}{\partial y^4} + \rho h \frac{\partial^2 w}{\partial t^2} = F(x, y, t) \ldots\ldots [2]$$

The constants A_x, A_y, and A_{xy} can readily be put in terms of the elastic constants S_{ij}.

In order to determine the effective S_{ij} for stiffened plates we take the acceleration and applied force F identically zero in Equation [2]. These equations then can be solved for certain simple boundary conditions which can be approximated on tests in the laboratory. These tests enable us to determine S_{ij} and they will now be described briefly.

Experimental Determination of Orthotropic Elastic Constants of Orthogonally Stiffened Plate

In order to determine what tests to make it may be observed that the differential equation for static bending is solved for certain simple boundary loadings (11, 12, 13). Specifically, the deflection equation for rectangular plates with uniformly distributed couples on two opposite edges is known. Also, the deflection equation is known for a square plate with twisting couples uniformly distributed around the edge. These equations are simply quadratic in the space variables x and y and contain the required elastic constants S_{ij} as well as the applied moments and the unknown effective thickness h. In these deflection equations three constants of integration occur and these may be evaluated from knowledge of the locations of the three points of support used for the flexure plate and the location of two points of support and a condition of symmetry for the torsion plate.

The experimental method used to determine the elastic constants (13) is an adaptation of one used by Bergsträsser (11) for isotropic plates and by Hearmon (12) for unstiffened orthotropic plates of constant thickness.

In the bending tests, the equivalent of a uniformly distributed bending moment must be applied to two opposite sides of a plate. In Fig. 3 the schematic arrangement of the plate resting on three supports is shown. Between the supports the assumption, of course, is that the bending moment is distributed uniformly across the plate.

For the twisting tests, the equivalent of a uniformly distributed twisting couple around the entire boundary must be provided. This can be obtained (11) as shown schematically in Fig. 3 by supporting the plate on two opposite vertices and loading on the two remaining vertices.

From the theoretical formulation it is clear what measurements must be made to determine the elastic constants. For the case of bending it is sufficient to measure the deflections at the origin of co-ordinates and at a short distance off center, say, along the y-axis shown in Fig. 3. For the determination of the shearing modulus S_{66}, it is clear that only a single deflection is required and this is measured conveniently at the origin of co-ordinates shown in Fig. 3.

For the bending tests one rectangular stiffened plate is fabricated with its long edge parallel to one set of the stiffeners and another rectangular stiffened plate with its long edge parallel to the other set of stiffeners. The two principal directions of stiffness are thereby orthogonal. For the twisting test a square stiffened plate is fabricated with one set of its stiffeners parallel with one edge of the plate. It may be noted that although only one set of parallel stiffeners is used on the plates in the experiments this is no limitation on the method as it is obvious that two principal directions of different stiffnesses exist. The choice is purely one of economy.

The two bending tests provide data for setting up two simultaneous equations for the determination of the elastic constants S_{11}, S_{12}, and S_{22} in terms of the cube of an unknown thickness. The twist test provides data for the determination of the shear constant S_{66} in terms of the cube of the unknown thickness.

For the purpose of studying experimentally the methods proposed in the present paper the types of stiffened plates were selected with proper regard for economy of fabrication. However, it is considered that they provide useful information about the nature of results to be expected in the general case. The types of stiffeners are shown in Figs. 1 and 2. In Fig. 1 are shown thin steel plates, one with grooves and the other with brass-rod stiffeners silver-soldered to the face of the plate. In Fig. 2 is a duralumin plate with milled grooves.

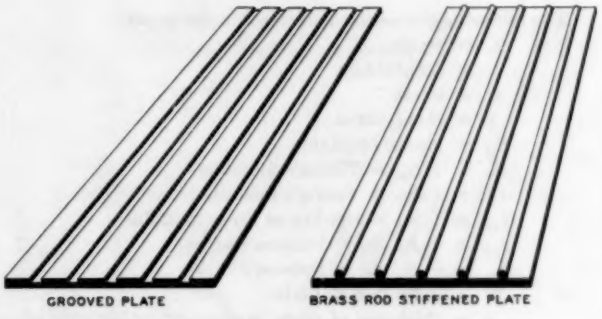

Fig. 1 Stiffened Experimental Plates

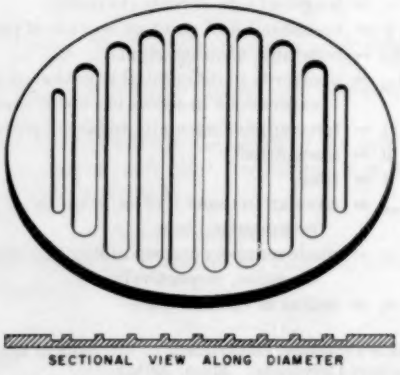

Fig. 2 Stiffened Circular Plate

The test equipment and method of measurement used in these tests are described completely in connection with a paper on homogeneous orthotropic plates of constant thickness without stiffeners presented elsewhere in the literature (13).

As described previously (13) the bending and twisting moments can be expressed in terms of a single force P applied in the tests. As a result the deflection measured at a given point on the plate

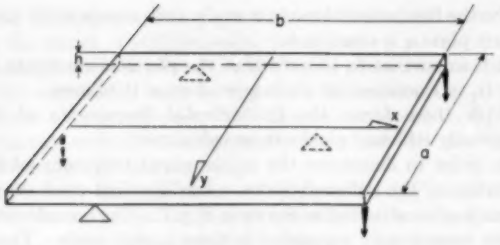

FIG. 3(a) BENDING PLATE

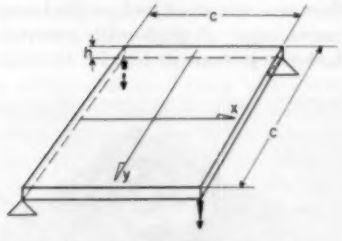

FIG. 3(b) TWISTING PLATE

varies nearly in a linear fashion with P. As a result it is easy to plot a curve of variation of deflection W with force P. It is the slope of this curve that is actually used in computing the elastic constants (13). An example of such a curve for bending is shown in Fig. 4. Results for a twisting test are shown in Fig. 5.

The orthotropic elastic constants determined for the stiffened plates under discussion are given in Table 1.

TABLE 1 ORTHOTROPIC ELASTIC CONSTANTS

Type of stiffener	Elastic constants $\frac{S_{11}}{h^3} \times 10^6$	$\frac{S_{12}}{h^3} \times 10^6$	$\frac{S_{21}}{h^3} \times 10^6$	$\frac{S_{22}}{h^3} \times 10^6$	$\frac{S_{66}}{h^3} \times 10^6$
Brass-rod stiffener.....	9.7	0.06	—4.9	13.9	49.5
Grooved steel.....	24.5	—8.55	—9.3	33.5	82
Groved duralumin...	90	—12.8	—39.2	612	670

One may note that S_{12} is not equal to S_{21} as assumed in the theory. However, it is considered that the plate deflections are not sensitive to this constant and that an average value of S_{12} and S_{21} is quite acceptable. It is further considered that this averaging procedure is superior to the custom of putting it equal to zero or so devising a theory that it is ignored entirely. It turns out in the calculations on the simultaneous algebraic equations for S_{ij} that the S_{12} and S_{21} are determined by small differences between two large quantities whereas the S_{11} and S_{22} are determined from sums of large quantities.

Table 1 also shows that the selection of test plates provides reasonably large differences for the stiffness factors in two orthogonal directions of any one plate for testing the proposed method.

STATIC BENDING OF STIFFENED PLATES

Once the elastic moduli for an equivalent orthotropic plate are determined by test, they may be used in calculating deflections for plates having identical stiffened construction but with any given boundary conditions.

As an illustration consider an orthogonally stiffened circular plate, as shown in Fig. 2, with clamped edge and uniform lateral load. The differential equation for this case is Equation [2] with

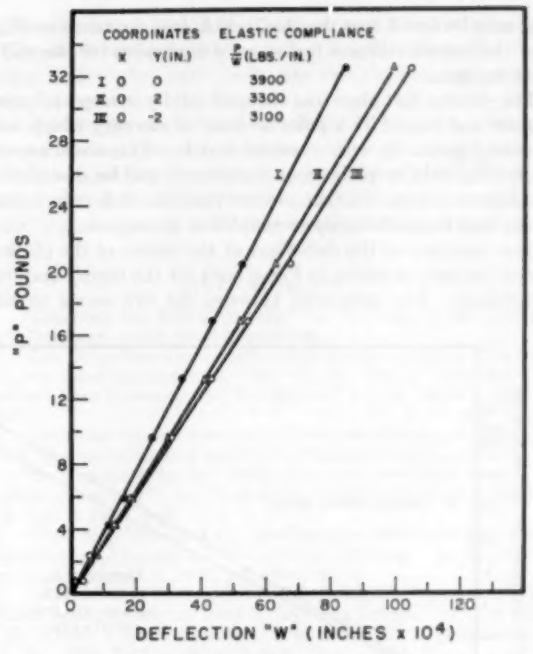

FIG. 4 BENDING TEST OF STEEL PLATE WITH TRANSVERSE GROOVES IN UP POSITION

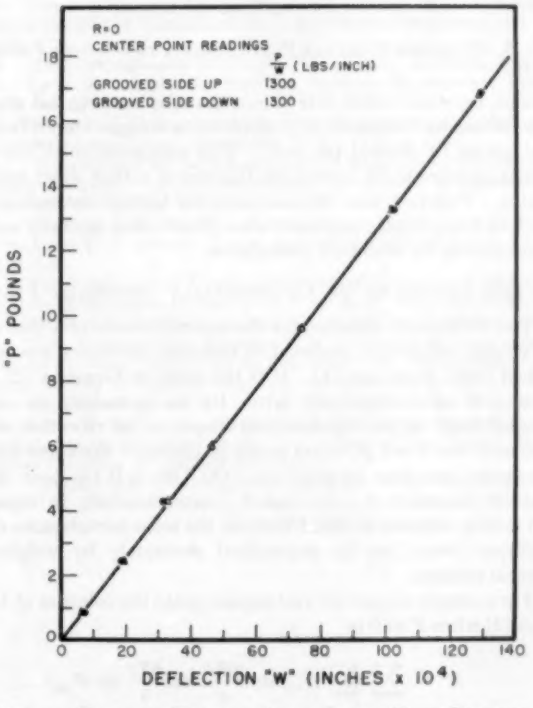

FIG. 5 TWISTING TEST OF STEEL PLATE WITH GROOVES

the acceleration term zero and $F(x, y, t)$ taken as a constant F_0.

A solution for this case is readily seen to be

$$W = W_0(r_0^2 - x^2 - y^2)^2 \quad [3]$$

where r_0 is the radius of the boundary and W_0 is a constant in terms of the elastic constants.

It may be noted that the thickness h does not occur in W_0, but only the known stiffness factors or compliances for the stiffened plate material.

The circular test plate was clamped solidly in a special pressure capsule and loaded by a pressure head of mercury which was increased gradually with a special device. This novel apparatus for testing circular plates and membranes will be described in a subsequent paper. For the present purposes it is only necessary to say that it satisfactorily accomplishes its purpose.

The variation of the deflection at the center of the plate with lateral pressure is shown in Fig. 6 both for the theory and for the experiment. The agreement between the two seems to be excellent, especially when it is known that the bending-test apparatus for elastic constants (11) appears to exaggerate stiffness of test plates by several per cent. This exaggeration of the constants appears to be caused by the use of rather short bending plates. This fact was demonstrated by test of isotropic plates for which the elastic constants were determined carefully and independently by standard procedures.

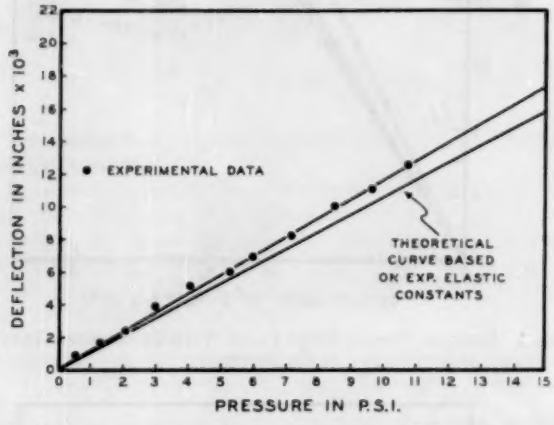

FIG. 6 STIFFENED CIRCULAR PLATE SUBJECT TO UNIFORM PRESSURE

FREE VIBRATIONS OF ORTHOGONALLY STIFFENED PLATES

The differential equation for the free vibrations of a thin plate of elastic orthotropic material of constant thickness was established many years ago (1). It is the same as Equation [2] with $F(x, y, t)$ taken identically zero. Its use in making an experimental study of the fundamental frequency of vibration of unstiffened wood and plywood plates of constant thickness was investigated less than 10 years ago (14). Since it has been shown how to determine A_x, A_y, and A_{xy} experimentally in Equation [2] it only remains to recall that ρh, the mass per unit area of the stiffened plate, can be determined accurately by weighing a typical portion.

For a simply supported rectangular plate the solution of Equation [2] when $F \equiv 0$ is

$$W = \sum \sum A_{mn} \sin \frac{m\pi x}{a} \sin \frac{n\pi y}{b} \sin P_{mn} t \ldots\ldots [4]$$

Substitution of Equation [4] into [2] with $F \equiv 0$ gives the equation for the circular frequencies P_{mn} as follows

$$P_{mn} = \frac{\pi^2}{\sqrt{\rho h}} \sqrt{D_x \frac{m^4}{a^4} + 2H \frac{m^2 n^2}{a^2 b^2} + D_y \frac{n^4}{b^4}} \ldots\ldots [5]$$

The quantities D_x, H, and D_y are in terms of the known stiffness factors.

For the fundamental mode m and n each equals unity and for a square plate a is equal to b.

It is important to observe that the physical constants D_x, H, and D_y in Equation [5] are independent of thickness.

With these facts, the fundamental frequencies of the orthogonally stiffened plate can be calculated.

In order to determine the fundamental frequency of flexural vibration of the stiffened plates, a boxlike rigid steel supporting frame was constructed as shown in Fig. 7. The boundaries of the plates were simply supported in these experiments. They were devised in a manner explained at length in another paper (15). Briefly, each plate for about $^3/_8$ in. from its edge was ground flat and a 90-deg V-notch groove of depth equal to about 80 per cent of the plate thickness was machined at the innermost boundary of the flat ground edge. A plate with grooved edge is shown fastened in the holding frame in Fig. 7. Outside the V-notched groove the flat edge of the plate is held rigidly on all four sides. It has been amply demonstrated (15) that this boundary condition is essentially that of a hinged or simply supported plate.

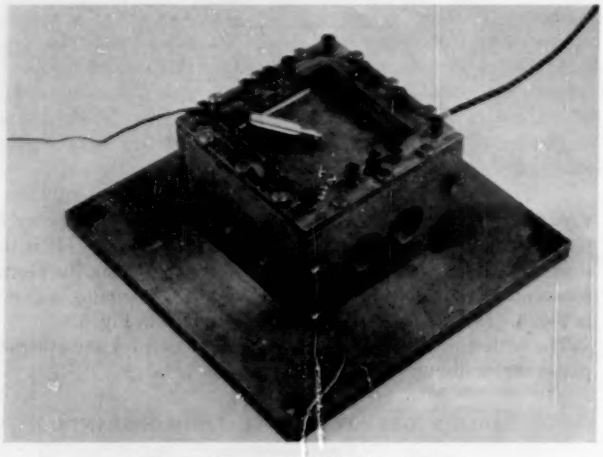

FIG. 7 VIBRATION-TEST APPARATUS

Vibrations were excited in the mounted plate by an electromagnet solidly mounted just below the center of the plate. The magnet was driven by a Hewlett-Packard audio oscillator directly, with frequency being increased slowly until the first resonance condition could be detected. The resonance peak could be detected approximately acoustically by ear but in the experiments it was determined precisely with a crystal-type phonograph pickup gently touching the plate. The output from the pickup was fed to a cathode-ray oscilloscope where the resonance peak could be observed readily.

A comparison of the calculated and observed frequencies is shown in Table 2. Data for an unstiffened plate which is practically isotropic are included also. This plate was ground to a thickness of 0.108 in. It was a plate of this thickness which was grooved according to a definite pattern to produce one type of stiffened plate and had brass rods silver-soldered to it to produce the other type of stiffened plate.

TABLE 2 FUNDAMENTAL FREQUENCY OF PLATE, CYCLES PER SEC

Test plate	Calculated	Observed
Isotropic (unstiffened)	1050	1050
Grooved pattern	980	960
Brass-rod stiffeners	1120	1060

DISCUSSION AND CONCLUSIONS

In view of results obtained, the combination of theory and ex-

periment developed in this paper is recommended for consideration in the design of stiffened-plate structures.

Nowadays with the advent of fabricated plates with stiffeners integrally attached it may be especially appropriate for manufacturers to give consideration to this combination of theory and experimental method for supplying stiffness data for use in designs involving stiffened plates.

It is desirable to experiment with plates having larger stiffeners than those used in the present investigation but the dictates of economy necessarily limited the scope of the present tests. Notwithstanding this fact, the chosen types of stiffeners seem to illustrate clearly the major point of the investigation; that is, the bending and twisting tests give reliable elastic constants for calculating flexural behavior of orthogonally stiffened plates under various loads and with various boundary conditions.

The agreement between the theoretical and experimental deflections of the stiffened circular plate with clamped edge appears quite satisfactory. This is especially significant when it is considered that the stiffness factor in one principal direction is approximately 7 times that in the other principal direction.

At variance with the practice of ignoring the Poisson-type ratios, an averaging procedure has been used to obtain approximate cross-contraction ratios. This procedure is recommended on the basis of results.

The bending data for the brass-rod stiffened plates are not so consistent as those for the plates with machined grooves as might be expected. The silver-soldering process used on the brass-rod stiffeners has some of the same uncontrollable features as the electric-welding process used in the fabrication of built-up structures. As a result the brass-rod stiffened plates were somewhat warped. Averaging deflection measurements from test with the stiffeners up and from test with the stiffeners down, however, appears to minimize the effects caused by this deviation of the plate from a plane.

As noted in the paper, the product of mass density and thickness of plate occurring in the differential equation of motion can be determined directly as mass per unit area of plate by actually weighing a typical section of the plate and dividing by its area. Also, the proposed method for the determination of the effective elastic constants of the stiffened plate make it unnecessary to determine a thickness for the plate explicitly. These two facts combine to provide a straightforward method for the determination of the dynamical response of a stiffened plate. Experiments with plates having larger stiffeners than those used in the present investigation will show the extent to which rotatory inertia must be taken into account.

Acknowledgment

The sponsorship of the Mechanics Branch, Office of Naval Research, is gratefully acknowledged.

The assistance of Mr. R. S. Buxbaum and Mr. Joshua Greenspon, graduate students in Mechanical Engineering at the Johns Hopkins University, with both the calculations and tests, is greatly appreciated.

The opportunity provided by the Johns Hopkins University to construct the equipment for pressure tests of circular plates is gratefully acknowledged. Also, the permission of Mr. E. Kusterer, a graduate student at Hopkins, to publish data on the stiffened circular plate obtained with this equipment is greatly appreciated.

BIBLIOGRAPHY

1 "Lehrbuch der Kristallphysik," by W. Voigt, B. G. Teubner, Berlin, Germany, 1910, pp. 675 and 698.

2 "Die Grundlagen einer rationellen Berechnung der Kruezwise bewehrten Eisenbetonplatten," by M. T. Huber, *Zeitschrift des Oesterreichischen Ingenieur und Architekten-Vereines*, vol. 66, 1914, pp. 557–564.

3 "Probleme der statik technish Wichtiger orthotropen Platten," by M. T. Huber, Gebethner and Wolff, Warsaw, Poland, 1929.

4 "Beitrag zur Frage des Ausbeulens von versteiften Platten bei Schubbeanspruchung," by E. Seydel, *Luftfahrtforschung*, band 8, heft 3, July 2, 1930, p. 71.

5 "Über das Ausbeulen von rechteckigen, isotropen oder orthogonalanistropen Platten bei Schubbeanspruchung," by E. Seydel, *Ingenieur-Archiv*, vol. 4, 1933, pp. 169–191.

6 "Methods and Formulas for Calculating the Strength of Plate and Shell Constructions as Used in Airplane Design," by O. S. Heck and H. Ebner, *Luftfahrtforschung*, vol. 11, 1935. Translation in T. M. No. 785, NACA, Washington, D. C., 1936.

7 "Application of Orthotropic Plate Theory to Ship Bottom Structure," by H. A. Schade, Fifth International Congress of Applied Mechanics, Cambridge, Mass., 1938, p. 140.

8 "Bending Theory of Ship Bottom Structure," by H. A. Schade, Trans. of Society of Naval Architects and Marine Engineers, vol. 46, 1938, p. 176.

9 "The Orthogonally Stiffened Plate Under Uniform Lateral Load," by H. A. Schade, JOURNAL OF APPLIED MECHANICS, Trans. ASME, vol. 62, 1940, p. A-143.

10 "Theory of Plates and Shells," by S. Timoshenko, McGraw-Hill Book Company, Inc., New York, N. Y., 1940, p. 188.

11 "Bestimmung der beiden elastischen Konstanten von plattenformigen Korpern," by M. Bergsträsser, *Zeitschrift der Technische Physik*, vol. 8, 1927, p. 355.

12 "Bending and Twisting of Anisotropic Plates," by R. F. S. Hearmon and E. H. Adams, *British Journal of Applied Physics*, vol. 3, 1952, p. 150.

13 "Determination of Elastic Constants of Orthotropic Materials With Special Reference to Laminates," by R. K. Witt, W. H. Hoppmann, 2nd, and R. S. Buxbaum, Bulletin of ASTM, December, 1953.

14 "The Fundamental Frequency of Vibration of Rectangular Wood and Plywood Plates," by R. F. S. Hearmon, Proceedings of the Physical Society of London, England, vol. 58, 1946, p. 78.

15 "An Experimental Device for Obtaining Elastic Rotational Constraint on Boundary of a Plate," by W. H. Hoppmann, 2nd, and J. Greenspon, to be published in the Proceedings of the Second U. S. National Congress of Applied Mechanics.

16 "Orthogonally Stiffened Circular Plate With Clamped Edge Subjected to Uniform Lateral Pressure," by E. Kusterer, Master's Essay to be submitted to the Johns Hopkins University, 1954.

Buckling of Continuous Columns

By H. C. PERKINS,[1] ITHACA, N. Y.

The following brief note describes an interesting procedure for setting up the characteristic equation of a continuous column, using the method of superposition.

A continuous column, after buckling, is, in effect, a beam of stiffness EI and length L, simply supported at each end, bent (1) by end thrust P regarded as given, and (2) by undetermined reactions consisting of forces Q at intermediate supports and couples M_0 and M_r when left and right ends are clamped. Slopes θ_0 and θ_r at clamps and deflections y at intermediate supports vanish. Their expressions being linear in the reactions can be derived by superposition.[2]

The determinant of the resulting linear homogeneous equations vanishes, thus providing a characteristic equation, each root of which determines a critical load and buckling mode for the column.

Slopes and deflections[2] before superposition are expressed conveniently by Equations [1] to [10] with $K^2 = P/EI$ and further notation as indicated in Fig. 1

$$y/L = \frac{Q}{P \sin KL}\left[\frac{\sin Ka \sin Kz}{KL} - \frac{az \sin KL}{L^2}\right] \text{ valid if } a \leq x \quad \ldots\ldots [1]$$

$$y/L = \frac{Q}{P \sin KL}\left[\frac{\sin Kc \sin Kx}{KL} - \frac{cx}{L^2} \sin KL\right] \text{valid if } a \geq x \quad \ldots\ldots [2]$$

$$y/L = \frac{M_r}{PL \sin KL}\left[\sin Kx - \frac{x}{L} \sin KL\right] \ldots\ldots [3]$$

$$y/L = \frac{M_0}{PL \sin KL}\left[\sin Kz - \frac{z}{L} \sin KL\right] \ldots\ldots [4]$$

$$\theta_0 = \frac{Q}{P \sin KL}\left[\sin Kc - \frac{c}{L} \sin KL\right] \ldots\ldots [5]$$

$$\theta_0 = \frac{M_r}{PL \sin KL}[KL - \sin KL] \ldots\ldots [6]$$

$$\theta_0 = \frac{M_0}{PL \sin KL}[\sin KL - KL \cos KL] \ldots\ldots [7]$$

$$\theta_r = \frac{Q}{P \sin KL}\left[\frac{a}{L} \sin KL - \sin Ka\right] \ldots\ldots [8]$$

$$\theta_r = \frac{M_r}{PL \sin LK}[KL \cos KL - \sin KL] \ldots\ldots [9]$$

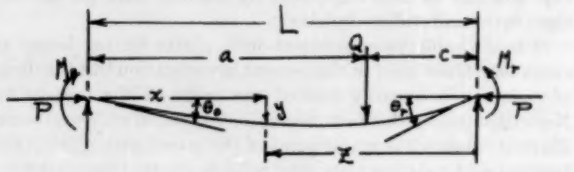

FIG. 1

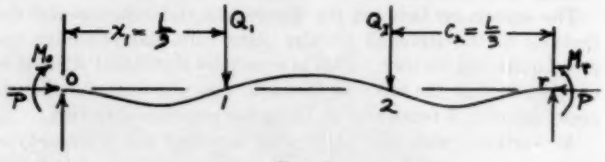

FIG. 2

$$\theta_r = \frac{M_0}{PL \sin KL}[\sin KL - KL] \ldots\ldots [10]$$

It is convenient to number the $r + 1$ supports 0, 1, 2, ...r from left to right as in Fig. 2 and use these numbers as subscripts in Equations [1] to [10] to identify (i) slope or deflection (θ_i, y_i, x_i, z_i) and (j) reactive force or couple (M_j, Q_j, a_j, c_j).

Let $M_j/(PL \sin KL) = m_j$, $Q_j/(P \sin KL) = q_j$ and let b_{ij} represent the corresponding bracketed factor in Equations [1] to [10] (i refers to slope or deflection, j to reaction).

In Fig. 2, where the ends are clamped, the deflection y_1 due to reaction Q_2 can be expressed in the compact form $y_1/L = q_2 b_{12}$. Here $i = 1 < j = 2$ so $x < a$, indicating that Equation [2] is valid and b_{12} is the bracket in Equation [2] with $c = c_2 = L/3$ and $x = x_1 = L/3$. Now the complete y_1/L by superposition, using Equations [4], [1], [2], [3], has the form

$$y_1/L = m_0 b_{10} + q_1 b_{11} + q_2 b_{12} + m_r b_{1r} = 0 \ldots\ldots [11]$$

All four equations (for θ_0, y_1, y_2, θ_r) are linear and homogeneous in m_0, q_1, q_2, m_r so the determinant of coefficients b_{ij} vanishes

$$D = \begin{vmatrix} b_{00} & b_{01} & b_{02} & b_{0r} \\ b_{10} & b_{11} & b_{12} & b_{1r} \\ b_{20} & b_{21} & b_{22} & b_{2r} \\ b_{r0} & b_{r1} & b_{r2} & b_{rr} \end{vmatrix} = 0 \ldots\ldots [12]$$

Since each b_{ij} is finite for all values of K, D plots as a finite ordinate for any positive abscissa K, so graphical evaluation of the fundamental root K_{cr} (and higher roots if desired) is a matter of elementary though somewhat tedious calculation when numerical data are given. For each root the corresponding buckling load is $P_{cr} = EIK^2_{cr}$.

Conclusion

In conclusion, it may be observed that the constraining reactions, after buckling in a given mode, are indeterminate until one reaction has been given an arbitrary value. Thus given a K_{cr} and assuming one reaction, say, $Q_1 = 1$, r of the $r + 1$ equations such as Equation [11], can be solved for the remaining r constraining reactions of that mode. Deflections may then be computed for several values of x using Equations [1] to [10] or similar equations[2] and superposed to obtain the elastic curve for buckling in a given mode.

---

[1] Professor of Mechanics, Cornell University. Mem. ASME.

[2] "Strength of Materials," by S. Timoshenko, part II, article 4, D. Van Nostrand Company, Inc., New York, N. Y., 1941.

Contributed by the Applied Mechanics Division and presented at the Annual Meeting, New York, N. Y., November 28–December 3, 1954, of The American Society of Mechanical Engineers.

Discussion of this paper should be addressed to the Secretary, ASME, 29 West 39th Street, New York, N. Y., and will be accepted until July 11, 1955, for publication at a later date. Discussion received after the closing date will be returned.

Note: Statements and opinions advanced in papers are to be understood as individual expressions of their authors and not those of the Society. Manuscript received by ASME Applied Mechanics Division, October 19, 1953. Paper No. 54—A-32.

Brief Notes*

On the recommendations of the Executive Committee of the ASME Applied Mechanics Division, it has been decided to initiate a section devoted to brief notes on technical matters in mechanics. These notes must not be longer than 750 words (about 2½ double-spaced typewritten pages, including figures) and will be subject to the usual review procedure prior to publication. After approval such notes will be published in the next issue of the Journal. The notes should be submitted to the Secretary of the ASME Applied Mechanics Division.

Representation of Three-Dimensional Stress Distributions by Mohr Circles

By G. A. ZIZICAS,[1] LOS ANGELES, CALIF.

O. Mohr[2,3,4] has developed a diagram representing the normal stress component $s_{nn} = \sigma_n$ and the total shearing stress component τ_n on an element of surface of any prescribed orientation with respect to the directions of the principal stresses. His procedure, however, does not give the orientation of the shearing stress τ_n within the element or, which is equivalent, the components of this shearing stress in a plane co-ordinate system within the element under consideration. An extension of the Mohr method that overcomes this limitation is presented in this note.

CONSIDER the equilibrium of the prismatical element indicated in Fig. 1 with three of its surfaces along the co-ordinate planes of a Cartesian system $Oxyz$. On the inclined surface a co-ordinate system $O'x'nt$ is introduced. It is obtained by rotating the system $O'x'y'z'$, parallel to $Oxyz$ through the surface centroid O', around the x'-axis by an angle θ until the axis $O'y'$ becomes perpendicular to the surface. If the lengths Δx, Δy, Δz are sufficiently small, the stresses on the sides of the prism can be assumed uniformly distributed so that their resultant forces are applied at the corresponding centroids. A summation of forces along the x-, y-, and z-axes gives

$$s_{nx} = s_{yx} \cos\theta + s_{zx} \sin\theta \quad \ldots\ldots [1]$$

$$s_{nn} \cos\theta - s_{nt} \sin\theta = s_{yy} \cos\theta + s_{zy} \sin\theta \quad \ldots\ldots [2]$$

$$s_{nn} \sin\theta + s_{nt} \cos\theta = s_{zz} \sin\theta + s_{yz} \cos\theta \quad \ldots\ldots [3]$$

while a summation of moments around the axes x', y', and z' results in

$$s_{xy} = s_{yx}, \qquad s_{xz} = s_{zx}, \qquad s_{yz} = s_{zy} \quad \ldots\ldots [4]$$

Equations [4] are the well-known reciprocity relations. Equation [1] is a generalization of them.

The important feature of the previous analysis is that the remaining two Equations [2] and [3] give exactly the relations existing in case of two-dimensional stress distributions.[5,6] Therefore a rotation of the inclined surface of the prism around the x-axis results in a standard two-dimensional behavior of the stress-components s_{nn} and s_{nt}, even in case the x-direction is not one of a principal stress. The variation of the component s_{nx} is given by Equation [1]. It follows that the usual two-dimensional Mohr circle representation[5,6] is applicable to the variation of the components s_{nn} and s_{nt}. The resulting extremal normal stresses may

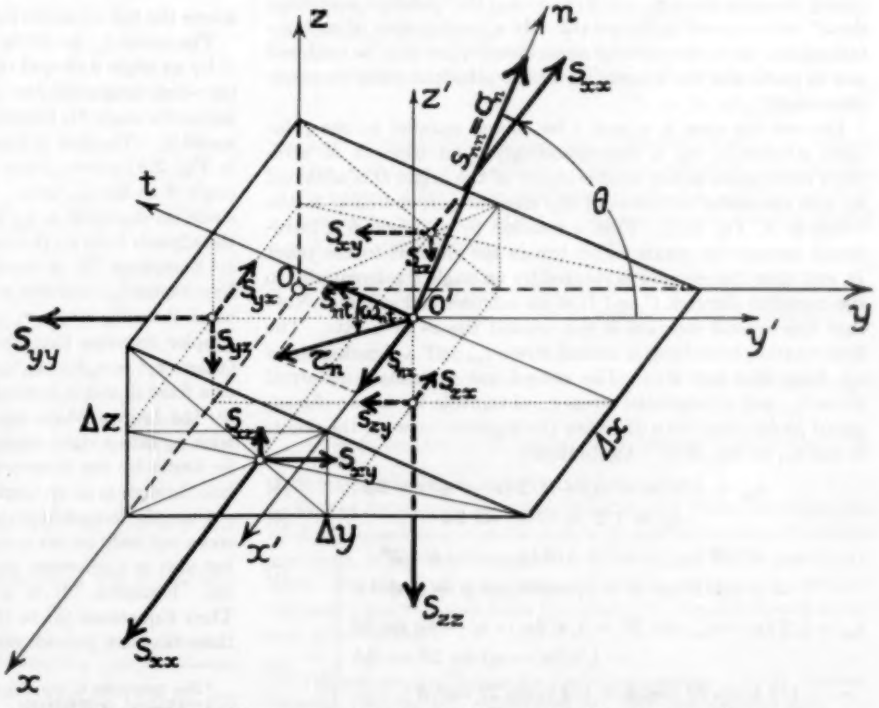

FIG. 1 STRESS COMPONENTS ON A THREE-DIMENSIONAL PRISMATICAL ELEMENT

[1] Assistant Professor of Engineering, University of California.

[2] "Über die Darstellung des Spannungszustandes und des Desformationszustandes eines Körperelementes," by O. Mohr, *Zivilingenieur*, 1882, p. 113.

[3] "Welche Umstände bedingen die Elastizitätsgrenze und den Bruch eines Materiales?" by O. Mohr, *Zeitschrift des Vereines deutscher Ingenieure*, vol. 44, 1900, pp. 1524–1530; pp. 1572–1577.

[4] "Abhandlungen aus dem Gebiete der technischen Mechanik," by O. Mohr, W. Ernst und Sohn, Berlin, Germany, second edition, 1914, pp. 192–202, 235.

* Discussion of papers in Brief Notes should be addressed to the Secretary, ASME, 29 West 39th Street, New York, N. Y., and will be accepted until July 11, 1955, for publication at a later date. Discussion received after the closing date will be returned.

NOTE: Statements and opinions advanced in papers are to be understood as individual expressions of their authors and not those of the Society. Manuscript received by ASME Applied Mechanics Division, November 3, 1954.

[5] "Elements of Strength of Materials," by S. Timoshenko and G. H. MacCullough, D. Van Nostrand Company, Inc., New York, N. Y., third edition, 1949, pp. 72–74. (Note difference in assumption of positive shear.)

[6] "Theory of Flow and Fracture of Solids," by A. Nadai, McGraw-Hill Book Company, Inc., New York, N. Y., vol. 1, second edition, 1950, pp. 94–95.

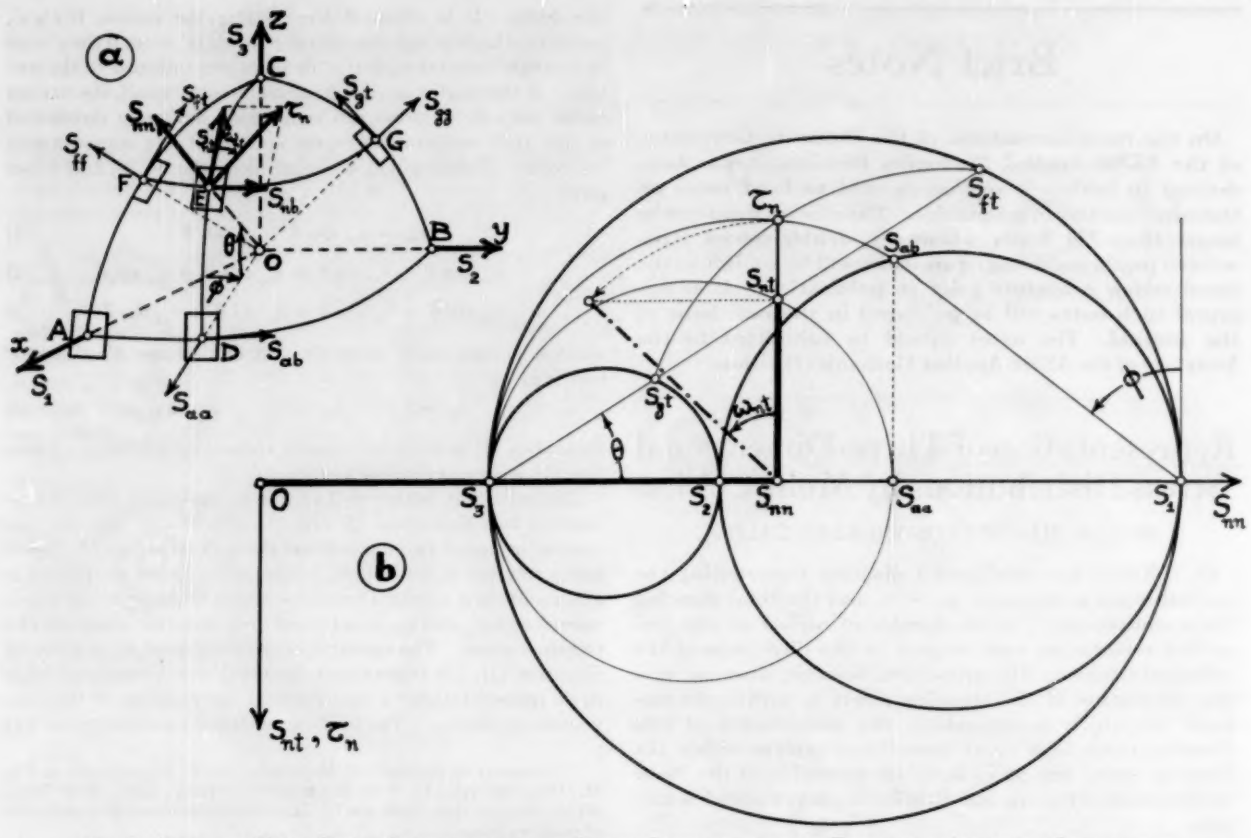

FIG. 2 COMPLETE MOHR CIRCLE REPRESENTATION OF STRESS COMPONENTS ON AN ELEMENT OF ARBITRARY ORIENTATION

be called "relative principal stresses," s_{2x} and s_{3x}, and the extremal shearing stress $\tau_{1x} = 1/2\,(s_{3x} - s_{2x})$ the "relative maximum shear" with respect to the x-axis. By a combination of such rotations any three-dimensional stress distribution may be analyzed and in particular the orientation of the principal stress elements determined.

Let now the axes x, y, and z be chosen parallel to the principal stresses s_1, s_2, s_3 correspondingly. An element of arbitrary orientation in the neighborhood of the origin O is obtained by two successive rotations of the element perpendicular to the x-axis at A, Fig. 2(a). First a rotation by an angle ϕ is introduced around the z-axis which brings the element to the point D, and then the element is rotated by an angle θ tangentially to the meridian through C and D of an infinitesimal sphere. Note that this second rotation is not around the x- or y-axis. The first rotation introduces a normal stress s_{aa} and a shearing stress s_{ab}, Figs. 2(a) and 2(b). The second one introduces a normal stress s_{nn} and a tangential stress s_{nt} obtainable by a two-dimensional Mohr circle with diameter the segment between the points s_2 and s_{aa} of Fig. 2(b). Algebraically

$$s_{aa} = 1/2\,(s_1 + s_2) + 1/2\,(s_1 - s_2)\cos 2\phi \quad \ldots\ldots [5]$$

$$s_{ab} = 1/2\,(s_2 - s_1)\sin 2\phi \quad \ldots\ldots [6]$$

$$\left.\begin{aligned} s_{nn} &= 1/2\,(s_{aa} + s_3) + 1/2\,(s_{aa} - s_3)\cos 2\theta \\ &= s_1\cos^2\theta\cos^2\phi + s_2\cos^2\theta\sin^2\phi + s_3\sin^2\theta \end{aligned}\right\} \ldots [7]$$

$$\left.\begin{aligned} s_{nt} &= 1/2\,(s_3 - s_{aa})\sin 2\theta = 1/4(2s_3 - s_1 - s_2)\sin 2\theta \\ &\quad - 1/4\,(s_1 - s_2)\sin 2\theta\cos 2\phi \\ &= -1/2\,s_1\sin 2\theta\cos^2\phi - 1/2\,s_2\sin 2\theta\sin^2\phi \\ &\quad + 1/2\,s_3\sin 2\theta \end{aligned}\right\} \ldots [8]$$

$$s_{nb} = s_{ab}\cos\theta = 1/2\,(s_2 - s_1)\cos\theta\sin 2\phi \ldots\ldots [9]$$

where the last equation follows from Equations [1] and [6].

The stress s_{aa} is obtained also by first rotating the element at A by an angle θ around the y-axis and then by an angle ϕ around the z-axis tangentially to a parallel circle. During this second rotation the angle θ is kept constant while s_{aa} obtains values between s_1 and s_2. The first of Equations [8] shows then that the point s_{nt} in Fig. 2(b) moves along a straight line through the point s_2 at an angle θ to the s_{nn}-axis. The intersection of this line with the circle on diameter $s_3\,s_{aa}$ locates the point s_{nt} and the normal to the s_{nn}-axis from s_{nt} the point s_{nn}. The component s_{nb} according to Equations [9] is equal to one side of a right triangle with hypotenuse s_{ab} and one angle θ. Together s_{nt} and s_{nb} define the total shearing stress τ_n and the angle ω_{nt}. Nevertheless it is simpler to note that the point with co-ordinates s_{aa} and τ_n (where $\tau_n^2 = s_{nt}^2 + s_{nb}^2$) moves along a circle either for a fixed θ or a fixed ϕ and is located at the intersection of these two circles by the known Mohr procedure.[7,8] A combination then of τ_n with s_{nt} into a right triangle gives ω_{nt}. In such a case s_{nt} could be found by the intersection of the line $s_{aa}\tau_n$ with the straight line through s_3 at an angle θ.

Once the foregoing graphical representation is established it can serve not only for an evaluation of stresses from a scale drawing but also as a reference graph for writing down Equations [5] to [8]. Equation [9] is a direct consequence of Equation [1]. Then Equations [5] to [9] may be used for analytical calculations that can provide the desired accuracy.

---

[7] See footnote 6, pp. 96–99.

[8] "Theory of Elasticity and Plasticity," by H. M. Westergaard, John Wiley & Sons, Inc., New York, N. Y., 1952, pp. 61–64.

On the basis of the mathematical analogy of their equations of transformation to the ones for stresses, the cases of small strains, moments of inertia, etc., and, in general, of symmetrical tensors of the second order lend themselves readily to the foregoing analysis.

Analysis of Some Circular Plates on Elastic Foundations and the Flexural Vibration of Some Circular Plates

By H. D. CONWAY,[1] ITHACA, N. Y.

PROBLEMS involving the analysis of circular plates of variable thickness supported by elastic foundations and the flexural vibrations of circular plates of variable thickness, are occasionally encountered in engineering practice. An example of the former is the structural footing and of the latter the turbine disk.

The following analysis will be confined to axially symmetrical loading and vibrations, and the flexural rigidity D of the plates (proportional to the cube of the thickness) taken as varying with the radius r according to the equation $D = D_0 r^m$, where D_0 and m are constants. By taking arbitrary values of D_0 and m, a great variety of variations of thickness could be obtained, but unfortunately they usually lead to great analytical difficulty. However, it has been found that for certain relationships between the parameter m and Poisson's ratio, analytical treatment is reasonably simple, and this leads to certain solutions of practical interest. Since the form $D = D_0 r^m$ implies zero thickness at the center of the plate for positive m, the following analysis is concerned with ring plates.

The differential equation for a circular plate of variable thickness resting on an elastic foundation of modulus k is,[2] with the usual notation

$$D\frac{d}{dr}\left(\frac{d\phi}{dr}+\frac{\phi}{r}\right)+\frac{dD}{dr}\left(\frac{d\phi}{dr}+\nu\frac{\phi}{r}\right)=-\frac{1}{r}\int_{ri}^{r}(q-kw)\,r\,dr \quad \ldots\ldots [1]$$

Assuming a flexural-rigidity variation of the form $D = D_0 r^m$, we obtain, after simplification

$$r^4\frac{d^4w}{dr^4}+r^3(2m+2)\frac{d^3w}{dr^3}+r^2(m+\nu m-1+m^2)\frac{d^2w}{dr^2}+r(1+\nu m^2-\nu m-m)\frac{dw}{dr}+\frac{k}{D_0}r^{(4-m)}w=\frac{q}{D_0}r^{(4-m)} \quad \ldots [2]$$

The complementary solution of this equation will first be considered. If it can be found, the particular solutions may always be obtained by such methods as "variations of parameters."

For $m = 4$, Equation [2] is homogeneous and making the change of variable $r = e^z$ the complementary solution satisfies the ordinary linear differential equation

$$\frac{d^4w}{dz^4}+4\frac{d^3w}{dz^3}+4\nu\frac{d^2w}{dz^2}-8(1-\nu)\frac{dw}{dz}+\frac{k}{D_0}w=0 \quad \ldots [3]$$

The solution of this equation is elementary and will not be considered further here.

[1] Professor of Mechanics, Cornell University. Staff Member, General Electric Company Advanced Electronics Center, Ithaca, N. Y.

[2] "Theory of Plates and Shells," by S. Timoshenko, McGraw-Hill Book Company, Inc., New York, N. Y., 1940, p. 283.

The solution of the equation

$$r^4\frac{d^4w}{dr^4}+A_3r^3\frac{d^3w}{dr^3}+A_2r^2\frac{d^2w}{dr^2}+A_1r\frac{dw}{dr}+A_0w=0 \quad \ldots [4]$$

where

$$A_3 = 6-4a-4c$$
$$A_2 = 2(a^2-\mu^2c^2)+4(a+c-1)^2+4(a-1)(c-1)-1$$
$$A_1 = [2(\mu^2c^2-a^2)-(2a-1)(2c-1)](2a+2c-1)$$
$$A_0 = (a^2-\mu^2c^2)(a^2+4ac+4c^2-\mu^2c^2)-b^4c^4r^{4c}$$

is given by Nielsen[3] as

$$w = r^a[C_1J_\mu(u)+C_2Y_\mu(u)+C_3I_\mu(u)+C_4K_\mu(u)],\ u = {}^cbr^c \quad \ldots [5]$$

where J_μ, Y_μ, I_μ, and K_μ are Bessel functions.

From a comparison of Equations [2] and [4] it is seen that they are of similar form if either $(a^2-\mu^2c^2) = 0$ or $(a^2+4ac+4c^2-\mu^2c^2) = 0$. From the first of these and writing $a = -m/4$, $c = (4-m)/4$, $\mu = -m/(4-m)$, the complementary solution of Equation [2] is

$$w = r^{-m/4}[C_1J_\mu(br^ci^{1/2})+C_2Y_\mu(br^ci^{1/2})+C_3I_\mu(br^ci^{1/2})+C_4K_\mu(br^ci^{1/2})] \quad \ldots [6]$$

where $b^4 = 256k/D_0(4-m)^4$, $i = \sqrt{-1}$ and if Poisson's ratio $\nu = m/4$. This equation may be written in the more convenient form

$$w = r^{-m/4}[B_1\,\mathrm{ber}_\mu(br^c)+B_2\,\mathrm{bei}_\mu(br^c)+B_3\,\mathrm{ker}_\mu(br^c)+B_4\,\mathrm{kei}_\mu(br^c)] \quad \ldots [7]$$

If, for example, $m = 4/3$ and $\nu = 1/3$, $m/(m-4) = -1/2$ and the solution may be written in closed form. It must be remembered that Poisson's ratio lies between zero and 1/2 for all materials and the solution has only application from $m = 0$ to $m = 2$.

For $(a^2+4ac+4c^2-\mu^2c^2) = 0$ and writing $a = -m/4$, $c = (4-m)/4$, $\mu = (8-3m)/(4-m)$, the complementary solution of Equation [2] is again

$$w = r^{-m/4}[B_1\,\mathrm{ber}_\mu(br^c)+B_2\,\mathrm{bei}_\mu(br^c)+B_3\,\mathrm{ker}_\mu(br^c)+B_4\,\mathrm{kei}_\mu(br^c)] \quad \ldots [8]$$

where $b^4 = 256k/D_0(4-m)^4$, and if Poisson's ratio $\nu = -(3m^2-24m+32)/4m$. This solution has rather limited value because of the nature of the connection between ν and m, and the fact that ν must lie between zero and 1/2. As an example, for $m = 6$ and $\nu = 1/6$, the solution is

$$w = r^{-3/2}[B_1\,\mathrm{ber}_3(br^{-1/2})+B_2\,\mathrm{bei}_3(br^{-1/2})+B_3\,\mathrm{ker}_3(br^{-1/2})+B_4\,\mathrm{kei}_3(br^{-1/2})]$$

where $b^4 = 16k/D_0$.

For a constant-thickness plate we write $m = 0$ and obtain the solution

$$w = B_1\,\mathrm{ber}(br)+B_2\,\mathrm{bei}(br)+B_3\,\mathrm{ker}(br)+B_4\,\mathrm{kei}(br) \quad \ldots [9]$$

This latter solution is valid for all values of ν.

Similar differential equations are obtained when investigations of the frequencies and mode shapes of disks of variable thickness are made. Only axially symmetrical vibrations will be considered here. For the axially symmetrical bending vibrations of a plate of variable thickness and from Equation [1], the differential equation to be solved is

[3] "Handbuch der Theorie der Cylinderfunktionen," by N. Nielsen, Leipzig, 1904, p. 138, reproduced in "Differentialgleichungen," by E. Kamke, Leipzig, vol. 1, 1943, p. 534.

$$D\frac{\partial}{\partial r}\left(\frac{\partial \phi}{\partial r}+\frac{\phi}{r}\right)+\frac{\partial D}{\partial r}\left(\frac{\partial \phi}{\partial r}+\nu\frac{\phi}{r}\right)=-\frac{1}{r}\int_{r_i}^{r}\rho h\,\frac{\partial^2 w}{\partial t^2}\,r\,dr \quad \ldots [10]$$

where ρ is the density of the material and h is the variable thickness of the plate. Writing $D = D_0 r^m$ where $D_0 = Eh_0^3/12(1-\nu^2)$, the differential Equation [10] becomes, after simplification

$$r^4\frac{\partial^4 w}{\partial r^4}+r^3(2m+2)\frac{\partial^3 w}{\partial r^3}+r^2(m+\nu m-1+m^2)\frac{\partial^2 w}{\partial r^2}+r(1+\nu m^2-\nu m-m)\frac{\partial w}{\partial r}=\frac{-12\rho(1-\nu^2)}{Eh_0^2}r^{(12-2m)/3}\frac{\partial^2 w}{\partial t^2} \quad \ldots [11]$$

Writing the deflection w in the product form

$$w = f(r)e^{ipt} \quad \ldots [12]$$

it follows that

$$r^4\frac{d^4 f}{dr^4}+r^3(2m+2)\frac{d^3 f}{dr^3}+r^2(m+\nu m-1+m^2)\frac{d^2 f}{dr^2}+r(1+\nu m^2-\nu m-m)\frac{df}{dr}-\frac{12\rho p^2(1-\nu^2)}{Eh_0^2}r^{(12-2m)/3}f=0 \quad \ldots [13]$$

This equation must be solved before the frequencies and mode shapes may be determined in the usual manner for the required boundary conditions.

If $m = 6$, Equation [13] is homogeneous and its solution is elementary and will not be considered further here. Referring to Equation [4] with $(a^2-\mu^2c^2)=0$ and with $a=-m/3$, $c=(6-m)/6$, $\mu=2m/(m-6)$, the solution of Equation [13] is

$$f = r^{-m/3}[B_1J_\mu(br^c)+B_2Y_\mu(br^c)+B_3I_\mu(br^c)+b_4K_\mu(br^c)] \quad \ldots [14]$$

where $b^4 = 12\rho p^2(1-\nu^2)/Eh_0^2(1-m/6)^4$ and if Poisson's ratio $\nu=(2m-3)/9$. An interesting special case is when $m=3$ (linear variation of thickness) for which $\nu=1/3$, which is a good value for several materials. If, as another example, $m=18/7$, the Poisson's ratio necessary is $5/21$ and, since $2m/(m-6)=-3/2$, the solution may be written in closed form.

From Equation [4] with $(a^2+4ac+4c^2-\mu^2c^2)=0$ and with $a=-m/3$, $c=(6-m)/6$, $\mu=4(m-3)/(m-6)$, the solution of Equation [13] is again

$$f = r^{-m/3}[B_1J_\mu(br^c)+B_2Y_\mu(br^c)+B_3I_\mu(br^c)+B_4K_\mu(br^c)] \quad \ldots [15]$$

where $b^4 = 12\rho p^2(1-\nu^2)/Eh_0^2(1-m/6)^4$ and if Poisson's ratio $\nu=-(4m^2-45m+72)/9m$. As in the case of the plate on an elastic foundation, this solution is of limited value because of the nature of the connection between ν and m, and because ν must lie between zero and $1/2$. Solutions of possible interest are when $m=8$, $\nu=4/9$ and $m=9$, $\nu=1/9$ and those between these ranges of m and ν.

For the constant-thickness plate, $m=0$ and

$$f = [B_1J_0(br)+B_2Y_0(br)+B_3I_0(br)+B_4K_0(br)] \quad \ldots [16]$$

where $b^4 = 12\rho p^2(1-\nu^2)/Eh^2$. This solution is valid for all values of Poisson's ratio.

Discussion

Experimental Measurement of Mechanical Impedance or Mobility[1]

M. C. JUNGER.[2] In this paper, the mobilities of several systems, as observed by means of an impedance-measuring device, are plotted as a function of frequency. The most striking feature of these results is the fundamental difference between the response of the plate and that of the free-free beam. For the latter, the mean value of mobility decreases approximately inversely as the square root of frequency. For the plate, the mean mobility first decreases and then rises, and possibly levels out at high frequencies (the measurements do not extend to sufficiently high frequencies to afford certainty on this last point). The author notes that the general trend of the mobility curve above 700 cycles per sec (cps) seems to follow a line of constant compliance. The explanation offered is that this behavior is a result of "the local response of the base plate at these frequencies, which seems to be relatively independent of lateral dimensions." In other words, boundary conditions are unimportant if the frequency is sufficiently high. The input impedance of the plate to a transverse force therefore may be taken approximately equal to the input impedance of an infinite plate. This impedance is stated by Cremer[3] as follows

$$Z = \frac{4}{\sqrt{3}} \sqrt{E\rho}\, h^2 \ldots\ldots\ldots\ldots [1]$$

where E is the Young's modulus, ρ the density of the plate material, and h the plate thickness. The impedance is purely resistive and frequency-independent. The latter trait is most surprising because flexural waves in beams are strongly frequency-dispersive. In addition, even propagation phenomena which are nondispersive in one and three dimensions, viz., phenomena governed by the wave equation, are dispersive in two dimensions (for example, waves propagating in a string are nondispersive, but dispersive in a membrane). This unexpected result stated in Equation [1] is relatively little known, even though it had already been found by Boussinesq.[4]

When $1/Z$ is plotted as a function of frequency, one obtains, of course, a horizontal line. Measuring the thickness of the plate from the sketch in Fig. 7 of the paper one finds $h = 0.42$ in. (apparently the note "1/4 scale" applies to the original drawing, and not to Fig. 7). The corresponding expression for the mobility is, from Equation [1]

$$\frac{1}{Z} = 0.0167 \frac{\text{in/sec.}}{\text{lb}} \ldots\ldots\ldots\ldots [1a]$$

The equivalent average thickness, computed from the total weight of the base plate including ribs, is found to be $h = 0.48$ in. The corresponding mobility is

$$\frac{1}{Z} = 0.0127 \frac{\text{in/sec.}}{\text{lb}} \ldots\ldots\ldots\ldots [1b]$$

The two values of mobility thus calculated are of the order of the mean value of the mobility curve in Fig. 2 of this discussion. The general trend of the observed mobility probably would follow Equation [1] of this discussion more closely if the plate did not have stiffening ribs. In particular, at low frequencies the mobility seems to vary as $f^{-1/2}$ (where f is the frequency)—a behavior which was found to be characteristic of a beam. This similarity

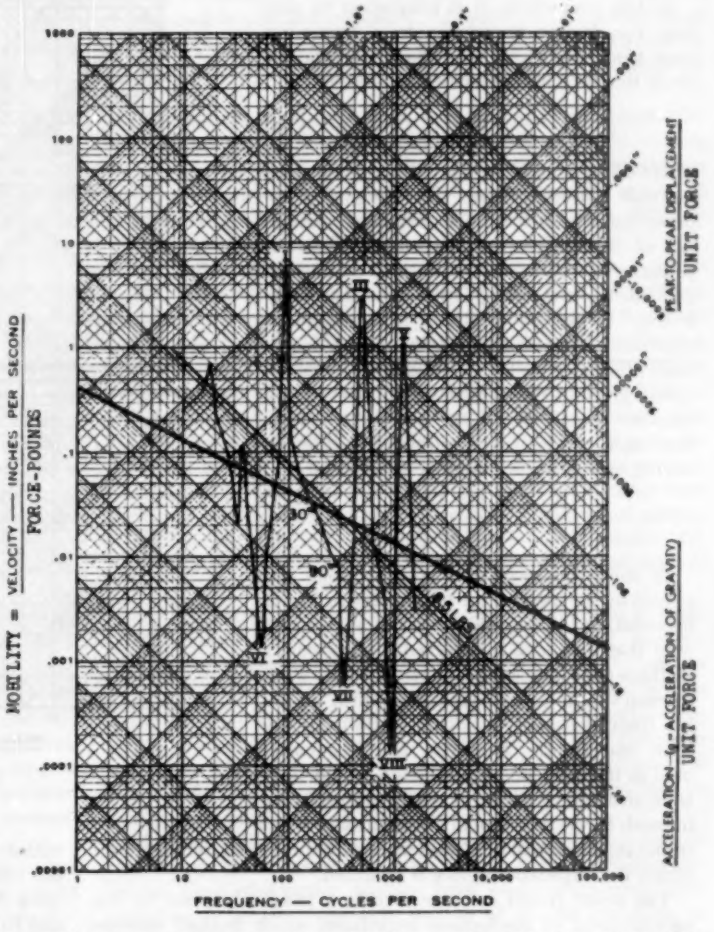

FIG. 1 MOBILITY OF CENTER OF 48-IN. × 2-IN. × 1-IN. FREE-FREE STEEL BAR (Fig. 4 of the paper.)

[1] By R. Plunkett, published in the September, 1954, issue of the JOURNAL OF APPLIED MECHANICS, Trans. ASME, vol. 76, pp. 250–256.

[2] Acoustics Research Laboratory, Harvard University, Cambridge, Mass. Assoc. Mem. ASME.

[3] "The Propagation of Structure-Borne Sound," by L. Cremer, Department of Scientific and Industrial Research, London, England, Sponsored Research (Germany) no. 1, series B, 1948, chapter II.

[4] "Application des Potentiels a l'Etude de l'Equilibre et du Mouvement des Solides Elastiques," by J. Boussinesq, Mémoires de la Société des Sciences de Lille, Imprimerie L. Danel, Lille, 1885, Note II, § III.21.

between plate and beam may result from the fact that the plate is excited through the intermediary of the rib to which the measuring device is attached; as a result, the outgoing waves are not truly two-dimensional, as in a uniform plate, but rather one-dimensional, as in a beam.

In this connection, it is interesting to note that the driving impedance to a transverse force applied to a very long beam displays precisely this type of frequency dependence[5]

$$Z = 4\sqrt{\pi}(EI)^{1/4} m^{3/4} \sqrt{f}\, e^{j\frac{\pi}{2}} \ldots\ldots [2]$$

where EI is the bending rigidity, and m the mass per unit length of beam. The frequency dependence results from the dispersive character of flexural waves in beams. The impedance has a resistive as well as an inertial component, even though friction has been neglected. It may be of interest to note that the expression for mobility obtained from Equation [2] yields a fair approximation to the values given in Fig. 1 of this discussion for the free-free beam. When the parameters of the test beam are used in Equation [2], the following expression for mobility is obtained

$$\frac{1}{|Z|} = \frac{0.404}{\sqrt{f}} \frac{\text{in/sec.}}{\text{lb}} \ldots\ldots [2a]$$

In connection with the positive slope displayed by the mean value of mobility in Fig. 2, herewith, in the range above 700 cps, one may note that extended elastic media do present a stiffness-type reactance at all frequencies when Poisson's ratio is less than one third, and at low frequencies only when this ratio is greater than one third.[5] However, the frequencies used in the tests under discussion would have to be increased by several orders of magnitude for such three-dimensional phenomena to occur in the small volume of elastic material represented by the rib on which the impedance device is mounted.

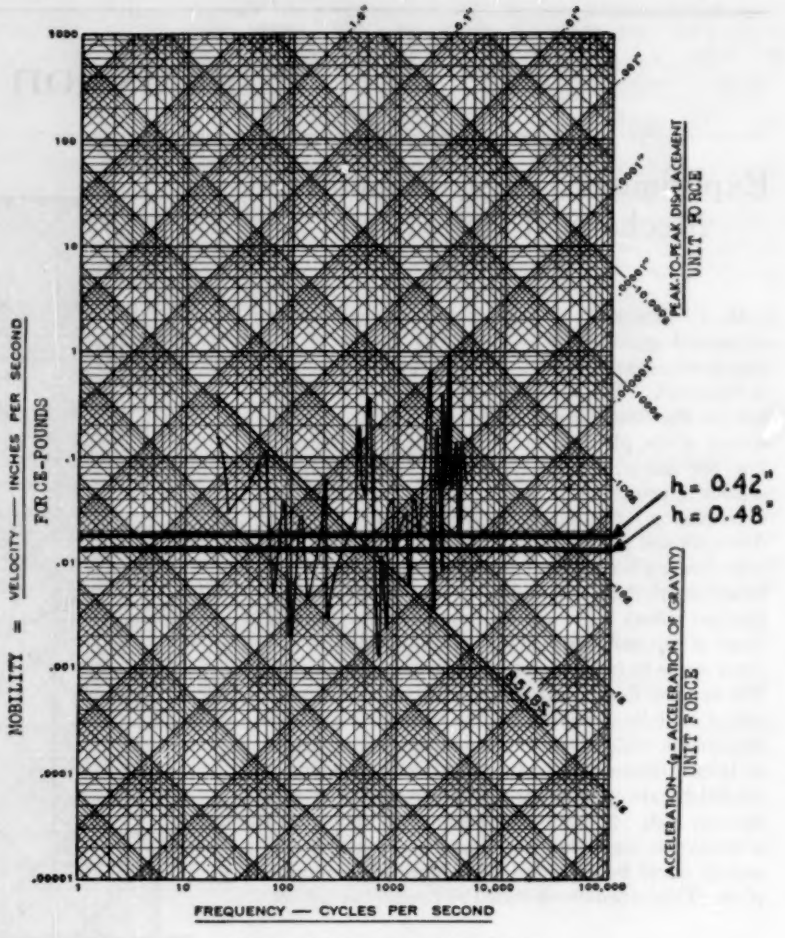

FIG. 2 MOBILITY OF BASE PLATE
(Fig. 8 of the paper.)

The writer would call attention to a practical device for the measurement of mechanical impedance which worked successfully on a purely electrodynamic principle, as described in a paper by Subra.[6]

Mechanism of Fretting Corrosion[1]

DOUGLAS GODFREY.[2] The author has presented a critical analysis of the factors involved in the scraping off of regenerative oxide films from mild steel. Several observations, however, can be considered from another viewpoint. Although a chemical-reaction product is formed, the fretting phenomenon should not be termed "truly one of corrosion." To cite an analogy—a milling operation is not truly corrosion because the chips, the tool, or even the metal oxidizes; milling still remains a cutting process. I believe fretting is caused by mechanical wear from reciprocating slip of low amplitude. The author's chemical term does not exist without the mechanical factors of plowing. The occurrence and the effect of a chemical-reaction product is entirely dependent upon the medium. Fretting occurs in vacuum and inert media, and to unreactive materials which shows that fretting damage is independent of corrosion. But even with a reactive material and a corrosive medium, weight loss by fretting is not necessarily high. Consider a medium of a gas or liquid, such as sulphur or chlorine compound, which would react with mild steel to form a low shear-strength film, such as iron sulphide or iron chloride. Under these conditions weight loss would be low because the chemical-reaction product would lubricate the surface.

The term "fretting damage" should not be used synonymously with "weight loss." For example, the first fact cited in the introduction, "fretting damage is reduced in vacuum or inert atmosphere," should be "weight loss is reduced in vacuum or inert atmosphere." The surfaces probably suffered extensive damage by cold welding and metal transfer or galling.

The model shown might be over-idealized because it does not have one of the features which is well established in friction and wear research. This feature is the existence of a rough surface from which asperities are broken off by a moving element. Inasmuch as in these fretting experiments the metal surfaces are separated completely by compacted oxides, the moving element is most likely an oxide particle or a partly oxidized metal fragment.

The general applicability of the author's equation is not clear.

[5] "Spherical Wave Propagation in Solid Media," by F. G. Blake, Jr., *Journal of the Acoustical Society of America*, vol. 29, 1952, pp. 211–215.

[6] "Le Vibromètre," by H. Subra, *Revue Générale de l'Electricité*, vol. 31, 1932, pp. 371–376.

[1] By H. H. Uhlig, published in December, 1954, issue of the JOURNAL OF APPLIED MECHANICS, Trans. ASME, vol. 76, pp. 401–407.

[2] National Advisory Committee for Aeronautics, Lewis Flight Propulsion Laboratory, Cleveland, Ohio.

In particular, do the values of the constants k_0, k_1, and k_2 apply only to the conditions of these experiments?

Table 1 of the paper shows that chemical wear is greater than 50 per cent only in 4 out of 18 cases. One of these is at the greatest load and greatest slip, another at the greatest load and medium frequency; and in another, the percentages are approximately equal. Therefore, the writer believes there is little justification for the statement, "the chemical factor of fretting damage predominates for small values of load, slip, and frequency."

The rigid exclusion of air and other substances does not appear to be a good remedial measure for fretting damage. To encourage metal-to-metal contact by exclusion of all substances in the presence of reciprocating slip, is asking for serious surface damage by galling, plowing, and metal transfer which could be worse than damage by fretting in air.

Author's Closure

Mr. Godfrey's first comments focus on some of our present definitions and their inherent weaknesses. The definition of corrosion, to the contrary, is now well established. Hence, looking at the initial steel and the ultimate composition of the fretting-damage debris in air, there is no question that corrosion has occurred, whatever the mechanism one assumes. The definition of corrosion, in other words, fits the situation of a chemical reaction between a metal and its environment resulting in chemical-reaction products. Where damage occurs in absence of chemical reaction, this obviously is not corrosion. Hence wear of two metals in contact and moving with respect to each other is a physical degradation process which in absence of a reactive environment is sometimes defined as galling or simply as wear, and is also sometimes called fretting. It is not properly called fretting corrosion.

With this distinction in mind, the present papers discuss fretting corrosion. The accompanying mechanical damage, which seems always to be part of fretting damage, is also included. The latter damage may be, and probably is, the same kind of damage as that which occurs without formation of corrosion products when metals are rubbed against each other in vacuum or in an inert atmosphere.

Our results show clearly that metal lost by fretting is less extensive in nitrogen than in air, which confirms results that have been published previously by others. We have indicated that weight loss in nitrogen, although appreciably less than in air, is not zero and that metal is transferred from one surface to the other. The calculated mechanical component of weight loss when steel is fretted in air is greater than the observed weight loss which results from mechanical damage in nitrogen, because less or no metal transfer occurs when oxide is present at the interface. The surface of steel in nitrogen suffers severe cold work, which is properly termed a form of damage, but it is doubtful that real damage of this kind is at any time as serious as occurs in air. Marked pitting, for example, is not observed in a nitrogen atmosphere, and hence fatigue crack nuclei are not generated to the same extent as in air where pitting is common.

I believe that weight loss is a good quantitative measure of fretting damage for most situations where damage of this kind is observed in test or in practice. Admittedly, it may not be a satisfactory criterion for some specific applications where surface cold work or metal transfer is an important consideration. It is a far better criterion of fretting damage than the usual visual estimate of damage typical of many older investigations reported in the past. On the basis of weight loss, our results truly show that fretting damage is reduced in nitrogen and would presumably be reduced similarly in vacuum or in any other inert atmosphere. Many practical measures for reducing fretting damage bear out this conclusion and hence support the presently described laboratory results based on weight-loss measurements.

It is true that oxide particles present at fretted surfaces have a greater probability of rubbing against the metal surface after fretting corrosion starts than do metal particles. This situation is described in the first complete paragraph on the second page of the paper, and is mentioned again in describing the model for fretting action. The described theory takes this situation into account.

The constants k_0, k_1, and k_2 apply to any situation where mild steel is fretted against itself in air, and where the motion is essentially sinusoidal. For other metals the mechanical-wear term containing k_2 differs, as do k_0 and k_1, the latter being altered by a different oxidation rate constant k/τ and by a different yield pressure term p_m.

The chemical evidence of fretting damage, taken as a whole and including secondary fretting action, by far predominates over the mechanical evidence for all the test conditions described in the present paper. This is illustrated by the fact that fretting debris is almost all Fe_2O_3, and only a small portion consists of metallic iron. As discussed in the paper, the observed amount of metallic residue is evidence of secondary fretting action between oxide and metal particles; the latter, according to the described theory, having been dislodged from the metal surface, originally in greater amount, by the factor of mechanical wear accompanying chemical reaction induced by mechanical activation. Primary fretting action, as Table 1 and Equation [14] show, becomes increasingly chemical in nature for conditions of low load, slip, or frequency.

The rigid exclusion of air is found to be advantageous in practice for some metal structures that suffer fretting damage, and the prediction of this advantage is contained in the present data and theory. However, exclusion of air alone may not be adequate for other structures or machines operating under more severe conditions where major damage results from galling or wear, and where the chemical component of fretting damage is less important. These conditions, according to theory, include heavy loads, large slip, and high frequencies.

Mr. Godfrey's discussion provides the opportunity to point out that many of the present misconceptions and misleading intuitive ideas of fretting damage have arisen from qualitative experiments without adequate control of all the variables, or from visual observations of service performance where again all the factors were not known. Quantitative data, which until recently were almost nonexistent, promise much more in achieving the ultimate understanding of fretting corrosion helpful to a practical solution of the problem. The empirical, hit-or-miss approach has reached the stage of diminishing returns—the scientific approach is the only one that remains, and in this respect much more needs to be done.

Existence and Stability of Ultraharmonics and Subharmonics in Forced Nonlinear Oscillations[1]

H. Norman Abramson.[2] The method of analysis used by the author appears to be a variation of the well-known method of

[1] By T. K. Caughey, published in the December, 1954, issue of the Journal of Applied Mechanics, Trans. ASME, vol. 76, pp. 327–335.

[2] Associate Professor of Aeronautical Engineering, The Agricultural and Mechanical College of Texas, College Station, Texas. Assoc. Mem. ASME.

Kryloff and Bogoliuboff, and as such this writer believes that two points concerning the analysis are worthy of discussion.

The author's somewhat brief presentation may confuse some readers at the outset because of his failure to explain why the terms $-KA(d\phi/dt)$ and $K(dA/dt)$ do not appear in his Equations [4] and [5] For small nonlinearity and for $P \ll \omega^2$, one attempts to find a solution similar in form to the solution of the corresponding linear problem, viz

$$y = A \cos(\Omega t + \phi) \quad [1]$$

$$\dot{y} = -A\Omega \sin(\Omega t + \phi) \quad [2]$$

Allowing both A and ϕ to be functions of time in the nonlinear problem, however, introduces somewhat too much variability into the problem and therefore the additional restriction that

$$\frac{dA}{dt} \cos(\Omega t + \phi) - A \frac{d\phi}{dt} \sin(\Omega t + \phi) = 0 \quad [3]$$

may be employed, in correspondence with the form of Equation [2] of this discussion. The procedure is essentially the method of variation of parameters, well known in ordinary differential equation theory.

The writer wonders why the author did not choose the use to complete Kryloff-Bogoliuboff procedure which involves solving for $\dot{A}$ and $\dot{\phi}$ and then "smoothing out" these periodic functions by integration over one period. This would lead to equations of the same form as the author's Equations [7] and [8].

The second point that the writer would like to discuss is the following: The Kryloff-Bogoliuboff method is essentially a "resonance analysis" in that one must assume at the outset that $\omega \simeq \Omega$ (considering here only harmonic solutions of period $2\pi/\Omega$—the author explicitly states the assumption of a resonance analysis only for the cases of superharmonics and subharmonics, Equations [21] and [46]). Therefore, in the vicinity of the peaks of the response curves (point P of author's Fig. 1) reliable results may not always be obtained. This may explain certain differences between results of the author and of the writer. According to Equation [10] of the paper, the steady-state phase angle is $\pi/2$ on the upper locus of vertical tangents, while the writer has shown by a different method[3] that the phase angle has the value $\pi/2$ at the point where the response curve crosses the curve for free undamped oscillations, this curve lying somewhat to the side of lower frequency of the upper locus curve.

The writer believes that the method of analysis presented in the paper would not be satisfactory for a similar discussion of a system with $\mu < 0$, because of the nature of the "resonance analysis" just mentioned. In the case of a softening system ($\mu < 0$), the response curves are quite different than in the case of the hardening system[4] and appear to lead to stability questions of very complex nature. For that problem the region of interest is given by $\Omega \ll \omega$. The question of subharmonics in this region may very well be amendable to treatment by the method of the present paper.

JOHN C. BURGESS.[5] In his interesting article on forced nonlinear oscillations, the author has shown some diagrams not previously published. By coincidence, the writer has written his

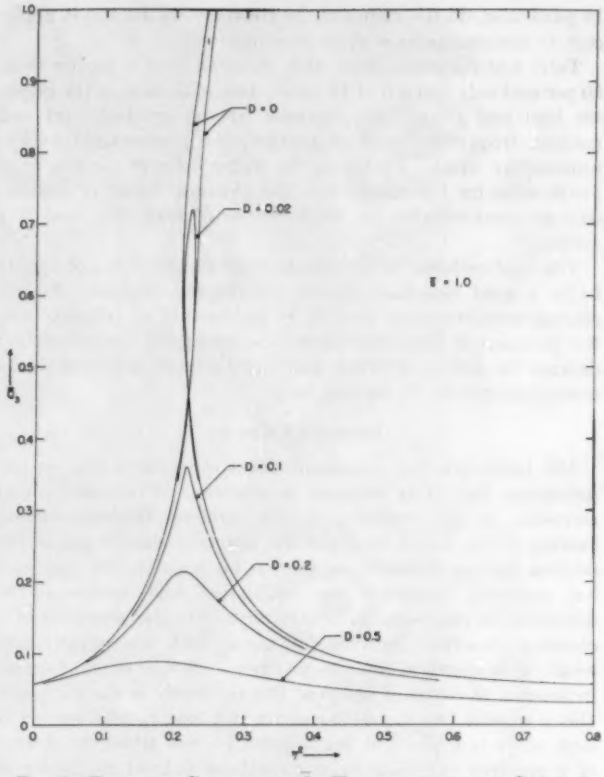

FIG. 1 RESPONSE CURVES FOR Q_3, ULTRAHARMONIC OF ORDER 3

dissertation[6] at Stanford University on precisely the same phenomena described by the author, with the same differential equation treated by the author, and with a method (the Ritz method[7]) which amounts to that used by the author. The principal differences appear to be that the author concentrated on the effects of initial conditions and on stability of the various motions while keeping his algebra as simple as possible; the writer concentrated on solving the complete algebraic equations, leaving the considerations of initial conditions and stability to later times or to other writers. The author also limits his considerations to small values of the nonlinearity (i.e., to quasilinear systems) and to small values of the amplitude of the forcing function.

The writer's curves are drawn for a moderately high value of the amplitude of the forcing function, and he believes that his results are not limited to small values of the nonlinearity. Another difference is that the author's curves are qualitative, the writer's are quantitative. The general characteristics of the amplitude-frequency response curves shown by the author agree with those found by the writer with the exception of that for ultraharmonic motion.[8] The writer, basing his conclusions on the exact solution of the algebraic equations resulting from the use of an approximation containing all the features of the author's Equation [20], found the response curves for ultraharmonic motion to be those shown in Fig. 1 of this discussion. The jump region is shown in more detail in Fig. 2.

It is obvious that the ultraharmonic response indicated by these

[3] "Resonance Amplitudes in Systems With a Single Degree of Freedom," by H. Norman Abramson, *Product Engineering*, August, 1954, pp. 179–182 (also, MS thesis, Stanford University, May, 1951).

[4] "Remarks on Response Curves for a Single Mass System With a Softening Restoring Force," by H. Norman Abramson, JOURNAL OF APPLIED MECHANICS, to be published.

[5] Mechanical Engineer, Department of Physics, Stanford Research Institute, Stanford, Calif.

[6] "Harmonic, Superharmonic and Subharmonic Response for Single Degree of Freedom Systems of the Duffing Type," by J. C. Burgess, PhD thesis, School of Engineering, Stanford University, Stanford, Calif., September, 1954.

[7] "Nonlinear Vibration Problems Treated by the Averaging Method of W. Ritz," by K. Klotter, Proceedings of the First U. S. National Congress of Applied Mechanics, THE AMERICAN SOCIETY OF MECHANICAL ENGINEERS, New York, N. Y., 1952, pp. 125–131.

[8] Also called superharmonic motion.

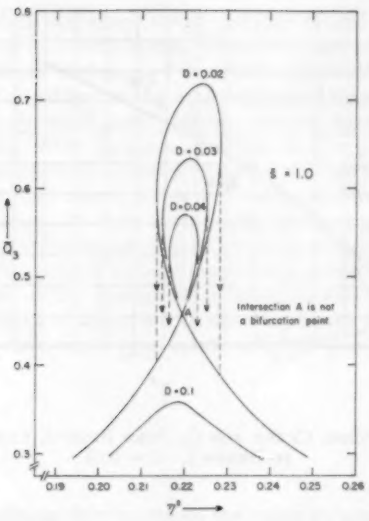

FIG. 2 RESPONSE CURVES FOR $\bar{Q}_3$, JUMP REGION, ULTRAHARMONIC OF ORDER 3

curves is distinctly different from that indicated by the author's curve. For interpreting the writer's curves in terms of the author's notation, the following dimensionless identities may be observed

$$\bar{Q}_{1/3} \equiv S_0 \frac{1}{\omega} \sqrt{\frac{3}{4}\mu}$$

$$\bar{Q}_1 \equiv A_0 \frac{1}{\omega} \sqrt{\frac{3}{4}\mu}$$

$$\bar{Q}_3 \equiv U_3 \frac{1}{\omega} \sqrt{\frac{3}{4}\mu}$$

$$\bar{s} \equiv P \frac{1}{\omega^3} \sqrt{\frac{3}{4}\mu}$$

$$D \equiv \frac{K}{2\omega}$$

$$\eta \equiv \frac{\Omega}{\omega}$$

The co-ordinate systems are seen to be qualitatively similar. With respect to damping, the parameter D represents the ratio of the actual damping to the critical damping of the system.

In deriving his response relations [29] for steady-state ultraharmonic motion, the author has made some assumptions which result in a considerable simplification of the process of solving the simultaneous nonlinear algebraic equations. In the writer's opinion, there are cases for which these assumptions constitute oversimplification, the author's results being an example. The author has tried to show, Equations [27] and [28], that the phase angle α may be taken to be zero and that the amplitude of the fundamental harmonic may be taken as that for the corresponding linear oscillation. It is not clear whether or not he used also the condition [21], that $\Omega' \doteq \omega$. In Figs. 3 and 4 of this discussion are shown the writer's response curves for α and $\bar{Q}_1$. These curves indicate that as the damping coefficient becomes smaller, the assumptions made by the author become more questionable. It should be noted that the author specifically restricts his equation to vanishingly small damping coefficients.

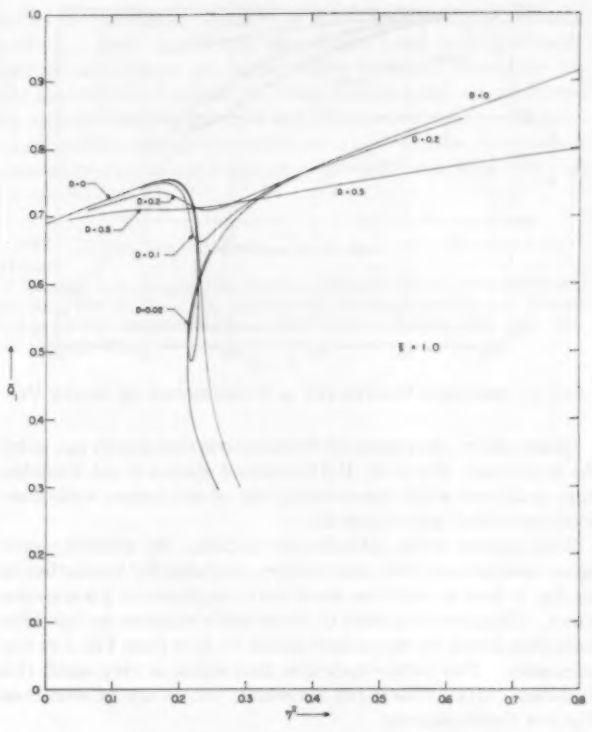

FIG. 3 RESPONSE CURVES FOR $\bar{Q}_1$, ULTRAHARMONIC OF ORDER 3

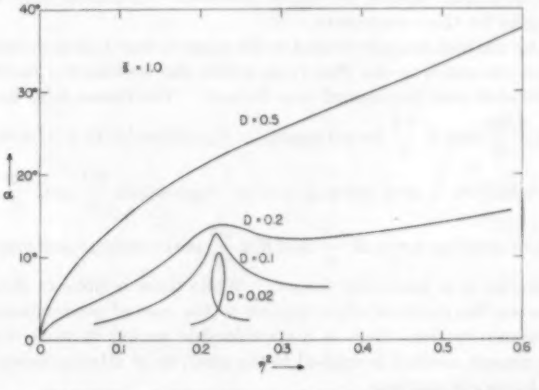

FIG. 4 RESPONSE CURVES FOR α, ULTRAHARMONIC OF ORDER 3

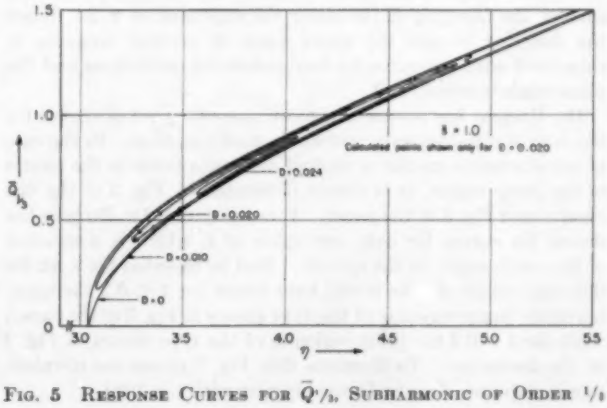

FIG. 5 RESPONSE CURVES FOR $\bar{Q}_{1/3}$, SUBHARMONIC OF ORDER $^1/_3$

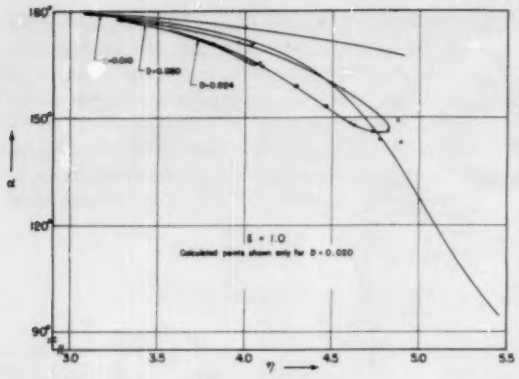

FIG. 6 RESPONSE CURVES FOR α, SUBHARMONIC OF ORDER $^1/_3$

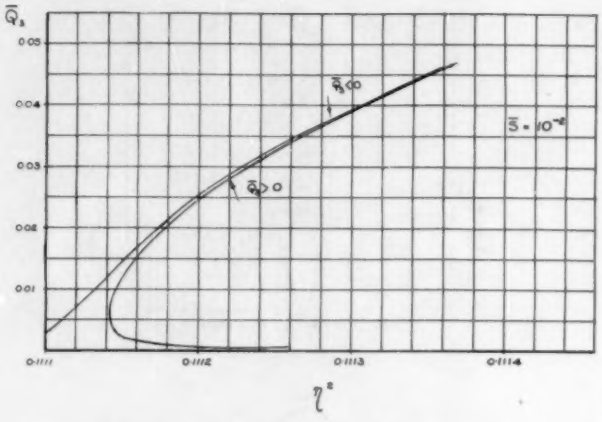

FIG. 7 RESPONSE CURVE FOR $\bar{Q}_3$, JUMP REGION, ULTRAHARMONIC OF ORDER 3. $\bar{\delta} = 0.01$

Qualitatively, the reason for retaining α is that energy can enter the system only if $\alpha \neq 0$. If β is retained while α is not, a mechanism is allowed which takes energy out of the system while none is allowed which puts energy in.

With respect to the subharmonic solution, the writer's results agree qualitatively with the relation presented by the author in his Fig. 5, that is, with the closed curve character of his response curve. The exact character of the writer's response curves differ from that shown by the author, as can be seen from Fig. 5 of this discussion. The author indicates that sin α is very small (his Equation [51]). This is not necessarily so, as can be seen from Fig. 6 of this discussion.

AUTHOR'S CLOSURE

The author wishes to thank Professor Abramson and Dr. Burgess for their comments.

The method of analysis used in the paper is based on the work of Appleton and Van der Pol, from which the well-known method of Kryloff and Bogoliuboff was derived. The reason why terms $-KA\dfrac{d\phi}{dt}$ and $K\dfrac{dA}{dt}$ do not appear in Equations [4] and [5] is that, by definition K is of order μ, and by supposition $\dfrac{dA}{dt}$ and $\dfrac{d\phi}{dt}$ are also of order μ; hence $K\dfrac{dA}{dt}$ and $KA\dfrac{d\phi}{dt}$ are of order μ^2 and may be neglected in a first-order theory. While there is little to choose between the methods when applied to the case of predominantly harmonic motion, there is a considerable saving in work when the present method is applied to the analysis of ultraharmonic or subharmonic motions.

It will be observed from Equation [10] that on the upper locus of vertical tangency the phase angle is approximately $\pi/2$, the smaller the damping K the closer the approach to $\pi/2$. When the damping is zero the upper locus of vertical tangency is coincident with the curve for free undamped oscillations and the phase angle is exactly $\pi/2$.

Dr. Burgess has produced a most interesting set of curves for the case of ultraharmonic and subharmonic motion. In the case of ultraharmonic motion a marked difference exists in the nature of the jump region, as is clearly illustrated by Fig. 2 of the discussion and Fig. 3 of the paper. It is a pity that Dr. Burgess has drawn his curves for only one value of $\bar{\delta}$, which is a measure of the nonlinearity in the system. Had he repeated his work for differing values of $\bar{\delta}$ he would have found for $\bar{\delta} < 0.2$ the ultraharmonic jump region is of the type shown in Fig. 3 of the paper, while for $\bar{\delta} > 0.2$ the jump region is of the type shown in Fig. 2 of the discussion. To illustrate this, Fig. 7 shows the ultraharmonic response of an undamped system with $\bar{\delta} = 10^{-2}$.

Since the original paper was concerned with quasilinear systems the ultraharmonic response will be as shown in Fig. 3 of the paper.

Similar comments may be made about the subharmonic response and its dependence on the magnitude of the nonlinearity.

It may be of some interest to mention that when the ultraharmonic jump phenomena were first predicted late in 1952, a small analog computer was built to verify these predictions. It was observed that for small nonlinearities or small exciting forces the ultraharmonic jump behavior was of the Caughey type but for large nonlinearities or large exciting forces the behavior was of the Burgess type.

Torsional Vibrations of Beams of Thin-Walled Open Section[1]

J. E. GOLDBERG.[2] Approximately a year ago the writer published[3] a solution to the major problem discussed by the author—that of the torsional oscillations of a simply supported I-type beam. Except for minor differences in notation, the writer's formula for the natural frequencies is essentially the same as the author's Equation [14]. Whereas the author used Timoshenko's equation for the statical twisting of an I-beam as his starting point, the writer used the Lagrange procedure to obtain the system of dynamical equations of the beam.

In view of the fact that the writer's prior publication in the same journal confirms the major result obtained subsequently by the author, it is quite surprising that no reference was made by the author to this earlier work, particularly since this earlier work was called to the author's attention at the time[4] the paper was presented.

AUTHOR'S CLOSURE

The author's paper was concerned with the general problem of the free torsional vibrations of bars of thin-walled open

[1] By J. M. Gere, published in the December, 1954, issue of the JOURNAL OF APPLIED MECHANICS, Trans. ASME, vol. 76, pp. 381–387.

[2] Associate Professor of Structural Engineering, School of Civil Engineering, Purdue University, Lafayette, Ind.

[3] "Note on Torsional Oscillation of I-Type Beams," by J. E. Goldberg, JOURNAL OF APPLIED MECHANICS, Trans. ASME, vol. 75, 1953, pp. 567–568.

[4] At the West Coast Conference of the Applied Mechanics Division, Berkeley, Calif., June 21–23, 1954.

section for which the shear center and the centroid coincide. These sections include I-beams, Z-sections, and other more complicated shapes such as used in aircraft construction. Mode shapes and principal frequencies were determined for six different sets of end conditions, including simple supports, fixed ends, and cantilevers. The effect on the mode shapes and frequencies of a variation in the physical constants of the bar was also shown.

For the particular case of an I-beam, and for the case of simple supports, Equation [14] of the author's paper reduces to the equation derived by Professor Goldberg. This can be seen by substituting into Equation [14] the value of the warping constant C_w for an I-section. The author apologizes for being unaware of the discusser's note until it was called to his attention at the time of presentation, which was several months after the paper had been sent to the publisher. To have included a reference to Professor Goldberg's note would not necessarily have been pertinent, however, since there are earlier works in which essentially the same material can be found.[5,6] These earlier works are concerned with coupled bending and torsional vibrations of simply supported beams, and the authors arrived at the expression for the principal torsional frequencies of a simply supported beam Equation [14] as a special case.

---

[5] "Thin Walled Elastic Rods," by V. Z. Vlasov (Russian), 1940, p. 266.

[6] "Eigenschwingungen von geraden Stäben mit dünnwandigen und offenen Querschnitten," K. Federhofer, Sitzungsberichte der Wiener Akademie der Wissenschaften, *Math.-natur. Klasse*, vol. 156, abt. IIa. 1947, p. 405.

Book Reviews

Energy Transfer in Hot Gases

ENERGY TRANSFER IN HOT GASES. Proceedings of the NBS Semicentennial Symposium on Energy in Hot Gases, held at the National Bureau of Standards on Sept. 17 and 18, 1951. National Bureau of Standards Circular 523, issued March 10, 1954, Washington, D. C. Cloth, 6 × 9 in., iv and 126 pp., figs. For sale by the Superintendent of Documents, U. S. Government Printing Office, Washington 25, D. C. Buckram $1.50.

REVIEWED BY T. P. TORDA[1]

THE bulletin of 126 pages contains a foreword by A. V. Astin, Director of NBS, and the following 16 papers:

"Processes of Electronic Excitation in Relation to Flame Spectra," by A. G. Gaydon; "Studies of Some Polyatomic Flame Bands," by George A. Hornbeck and Robert C. Herman; "Emission Spectra of Polyatomic Free Radicals," by P. J. Dyne; "Distributions of OH Rotational Intensities in Flames," by Herbert P. Broida; "Spectroscopic Studies of Low-Pressure Combustion Flames," by S. S. Penner, M. Gilbert, and D. Weber; "Studies of Emission and Absorption in Flames," by G. H. Dieke and H. M. Crosswhite; "Energy Distribution of CO Molecules in CO-O_2 Flames," by Shirleigh Silverman; "High-Resolution Spectra of Hydrocarbon Flames in the Infrared," by W. S. Benedict and Earle K. Plyler; "Infrared Emissivity of Diatomic Gases," by S. S. Penner; "Infrared Spectra of Thermally Excited Gases," by Richard H. Tourin; "Present Position of the Theory of Flames," by Bernard Lewis; "Detailed Mechanism of Elementary Reactions: Production of OH($^2\Sigma^+$) in the H_2-O_2 Flame" (Abstract), by Kurt E. Shuler; "Some Reactions of Atomic Hydrogen in Flames," by J. R. Arthur and D. T. A. Townend; "Temperature of the Hydrogen-Fluorine Flame," by R. H. Wilson, Jr., J. B. Conway, A. Engelbrecht, and A. V. Grosse; "Effect of Flame-Generated Turbulence on Heat Transfer From Combustion Gases," by Bela Karlovitz; "Astrophysicist's Concept of Temperature," by Hari K. Sen.

It is thought that a volume containing such varied material can be reviewed best by giving, where possible, summaries or conclusions of the authors themselves.

A. G. Gaydon gives the following summary of his paper: Observations of flame spectra and most optical methods of temperature measurement depend on electronic excitation which occurs by collision with molecules carrying energy as internal vibrational energy. The spectrum-line reversal method of temperature measurement gives basically the electronic excitation temperature; if equilibrium is not established this is likely to be closer to the vibrational than to the translational temperature of the gas. It is suggested that observations of predissociation of band systems such as CH in flames may serve as a sensitive test for the existence, or otherwise, of thermal equilibrium.

G. A. Hornbeck and R. C. Herman present the results of investigations of some polyatomic flame bands carried out with a low-temperature burner. Hydrocarbon flame bands, the alpha bands of ammonia, and CO flame bands have been studied. Their work indicates the importance of using low-temperature high-intensity sources for the study of polyatomic flame spectra. The suppression of diatomic spectra and the higher resolution possible because of lower temperature and higher intensity have revealed many hitherto obscure features in polyatomic flame bands.

P. J. Dyne discusses the apparatus for study of emission spectra of polyatomic free radicals, and some particular experiments conducted, with reference to previous experimental and theoretical results.

H. P. Broida gives the following abstract of his paper: Intensity distributions of rotational lines in the (0,0) band of the $^2\Sigma \rightarrow {}^2\Pi$ electronic transition of OH in a variety of flames have been obtained with a high-resolution grating monochromator. Various parts of the flames have been observed. These spectra have been used to investigate thermal equilibrium in the hot gases and to measure rotational "temperatures." Flames of stoichiometric mixtures of various fuels with oxygen have been studied systematically. Preliminary investigations of flames using up to 90 per cent diluent have been made. Hydrocarbon flames burning in a slot burner with a long observable path through the reaction gave an abnormal distribution of OH rotational intensities similar to that obtained in a discharge through water vapor.

S. S. Penner, M. Gilbert, and D. Weber describe the improved apparatus which has been used for the spectrographic study of two-dimensional, low-pressure combustion flames. They state that excellent spatial resolution is obtained at the expense of loss of light intensity, but that this can be compensated for by long exposures. Several emission spectra from the luminous zone of a propane-oxygen flame burning at a 5-mm pressure have been obtained. Also, a preliminary rotational analysis of the CH spectrum shows a reasonably normal rotational distribution, in agreement with the work of Gaydon and Wolfhard.

G. H. Dieke and H. M. Crosswhite present and discuss the results of new studies of emission and absorption in flames.

S. Silverman gives the following abstract of his paper: The energy distribution in CO-O_2 flames has been studied in the CO harmonic region at 2.3, under moderately high resolution (slip width ~ 0.8 cm^{-1}). "Temperature profiles" were obtained for an essentially two-dimensional flame. In the cooler regions near the orifice, the rotational and vibrational temperatures are equal. The vibrational temperature seems to correspond to thermochemical values throughout the flame profile. On the other hand, in the outer cone rotational temperatures are higher than the adiabatic flame temperatures. Introduction of CO_2 or N_2 as a diluent into the fuel system is effective in establishing vibration-rotation equilibrium, with CO_2 being especially effective.

W. S. Benedict and E. K. Plyler give the following abstract of their paper: In this paper is presented a summary of recent work in which the spectra of hydrocarbon flames have been studied between 1 and 2.6 microns with considerably higher resolution than has hitherto been possible. (For the strongest regions of emission, resolution of 0.2 cm^{-1} has been achieved.) The improvement in resolution has resulted from the use of lead-sulphide photoconductive cells, which are sensitive detectors in that region, together with a 15,000 lines-per-in. grating spectrometer of high optical quality. The results for the most part have been presented in greater detail elsewhere; the emphasis of the present paper will be to point out the similarities and the differences between flame spectra in the near-infrared and in the more familiar visible and near-ultraviolet regions.

[1] Professor of Aeronautical Engineering, University of Illinois, Urbana, Ill.

S. S. Penner gives the following abstract of his paper: An outline is presented of the basic theoretical relations which are used to calculate the infrared emissivity of diatomic gases. Next, the measurement of absolute values for the integrated absorption, together with the determination of rotational half-widths resulting from collision broadening, is described. The experimental results are useful for the calculation of the infrared emissivity of diatomic gases at low pressures, where overlapping between rotational lines may be neglected, and at very high pressures, where complete overlapping occurs. Calculations at elevated pressures are believed to yield reasonable approximations for the conditions existing in rocket combustion chambers. The theoretical calculations have been found to be in satisfactory agreement with available empirical emissivity data for CO.

R. H. Tourin gives the following abstract of his paper: Instrumentation has been developed for the measurement of infrared emission and absorption spectra of gases heated under controlled conditions of temperature, pressure, and composition. The setup now in use consists of a specially made quartz gas cell heated by a tube furnace, and an optical system which illuminates the entrance slit of a monochromator with radiation from the gas sample or the globar source. Spectra are measured with a modified Perkin-Elmer Infrared Spectrometer. Some preliminary results have been obtained on carbon dioxide in both emission and absorption.

B. Lewis discusses and evaluates the present state of knowledge of the macro and microstructure of flames.

Only an abstract of K. E. Shuler's paper is printed.

J. R. Arthur and D. T. A. Townend give the following abstract of their paper: Methods of detecting the presence of atoms in flames are summarized. Particular attention is given to the chemiluminescence observed when hydrogen flames are brought into contact with certain promoted oxides. Proof that this luminescence is due to the recombination of hydrogen atoms is furnished by experiments with the oxides in a hydrogen discharge. The influence of various gaseous additives in extinguishing the chemiluminescence induced by hydrogen flames is examined and the suppression of the sodium *D* lines is observed at the same additive concentration. An apparent expansion of flames which occurs when sodium salts are added to them is also described, the expansion depending on the fuel, the mode of combustion, and the nature of the sodium salt. It is suggested that additives suppress the chemiluminescence by inducing the recombination of hydrogen atoms and that these atoms are mainly responsible for the formation of sodium atoms ($NaX + H \rightarrow Na + HX$) when sodium salts are present in flames. The latter process also appears to provide a basis for explaining the expansion phenomena.

R. H. Wilson, Jr., J. B. Conway, A. Engelbrecht, and A. V. Grosse give the following abstract of their paper: The high exothermicity of the combination of hydrogen with fluorine combined with the excellent stability of the reaction product results in a very high flame temperature. The maximum theoretical flame temperature is calculated to be 4300 deg K at one atm pressure. After preliminary experiments indicated that this maximum temperature must be higher than that of any man-made radiator, a new technique was developed using the sun as a comparison source. The actual flame temperature, measured by means of the line-reversal method using the lithium line is 4300 deg K $\pm$ 150 deg.

B. Karlovitz presents a simple analysis of the turbulence generated by a turbulent flame. He states that at flow velocities up to a few hundred feet per second the flame-generated turbulence by far outweighs the turbulence of the approach flow. It has decisive influence on the turbulent flame propagation and on every mixing and heat-transport phenomenon behind the flame.

H. K. Sen gives the following abstract of his paper: The paper gives an account of deviations from thermodynamic equilibrium in stars, which have made the astrophysicist revise his concept of temperature. Temperature of the solar and stellar atmospheres is now an "operational" concept, critically dependent on the method used to obtain it. Theoretical extensions of thermodynamic concepts designed to meet the non-thermodynamic cases are discussed, together with a recent investigation (unpublished) by the author on the effect of the non-Maxwellian electron velocity distribution in a shock front on certain apparent temperature anomalies in giant stars and in the solar chromosphere.

High-Speed Aerodynamics

GENERAL THEORY OF HIGH SPEED AERODYNAMICS. Edited by W. R. Sears. Vol. 6 of "High Speed Aerodynamics and Jet Propulsion." Princeton University Press, Princeton, N. J., 1954. Cloth, 6 × 9½ in., xiv and 758 pp., 3 pages of plates, figs., references, index, $15.

REVIEWED BY ASCHER H. SHAPIRO[2]

THIS is one of the first volumes of the long-heralded twelve-volume Princeton series on high-speed aerodynamics and jet propulsion to reach publication. Conceived in the spirit of the twenty-year-old six-volume series on aerodynamic theory edited by W. F. Durand, the Princeton series has as its objective the consolidation of the prodigious literature which has arisen since 1940 on the diverse phases of aeronautical science which have contributed to the remarkable advances in high-speed flight in the past decade and a half. How broad is the present conception of the term *aeronautical science* may be gathered from a reading of the titles of the twelve volumes, covering as they do thermodynamics, combustion, gas dynamics, laminar and turbulent flows, aerodynamics, high-speed aircraft, physical measurements, aerodynamics of machinery, gas-turbine power plants, and jet-propulsion engines. If the volume reviewed here is typical of the series, we may expect the entire work to be not only a monumental record of what has been accomplished, but a classic reference source and a spur to further research for years to come.

In any case the present volume is by itself an outstanding addition to the literature on high-speed aerodynamics. Addressed primarily to the aerodynamic problems of high-speed aircraft, it has been written by men who have, themselves, made notable contributions to theoretical high-speed aerodynamics. Perhaps the greatest pitfall in a large volume like this having seven different authors is that the work will lack integration in spirit, style, and subject matter. Although there are some inevitable remnants of loose bonds between the several parts, Prof. W. R. Sears (the volume editor) has been on the whole remarkably successful in infusing the book with a sense of uniformity and connectedness. A brief outline of the different sections of the book follows:

(*a*) "On the Foundations of High-Speed Aerodynamics," by Th. von Karman, 27 pages. A survey of the basic physical concepts and mathematical methods which have been fruitful, written in the Olympian style of Dr. von Karman, and forming a preview of what follows in the remainder of the book.

(*b*) "Mathematical Aspects of Flow Problems of Hyperbolic Type," by K. O. Friedrichs, 30 pages. A study of certain mathematical phases of supersonic flows, extending from notions

[2] Professor of Mechanical Engineering, Massachusetts Institute of Technology, Cambridge, Mass. Mem. ASME.

of uniqueness to those of appropriate initial data, and comprising *in toto* the foundations of the method of characteristics.

(*c*) "Small Perturbation Theory," by W. R. Sears, 61 pages. A presentation of the fundamental ideas of small perturbation theory, based on the acoustic approximation, and applied to problems of subsonic aerodynamics.

(*d*) "Supersonic and Transonic Small Perturbation Theory," by Max A. Heaslet and Harvard Lomax, 223 pages. A unified exposition of the whole subject of linearized supersonic theory. A small volume in itself, the subjects covered include methods of solution of the wave equation, two-dimensional supersonic steady flow, three-dimensional supersonic steady flow, axisymmetric supersonic steady flow, slender airplane theory, unsteady lift, reciprocity relations and reverse-flow theorems, and small perturbation theories of transonic and hypersonic flow.

(*e*) "Higher Approximations," by M. J. Lighthill, 145 pages. This is a notable synthesis of the nonlinear approximations to compressible flow, and constitutes as well a critique and appraisal of the first-order perturbation methods. Much more than a conglomeration of the principal techniques to be found in the technical literature, this section places a tremendous variety of ideas within a common framework.

(*f*) "Plane Subsonic and Transonic Potential Flows," by Y. H. Kuo and W. R. Sears, 93 pages. A discussion of the hodograph method as applied to subsonic and to mixed subsonic-supersonic flows.

(*g*) "The Method of Characteristics," by Antonio Ferri, 87 pages. A detailed presentation of the application of the method of characteristics to supersonic flows. The text covers two-dimensional and axisymmetric potential flows, two-dimensional and axisymmetric rotational flows, characteristics methods for three independent variables, and linearized characteristics methods.

(*h*) "Supersonic Flows With Shock Waves," by Antonio Ferri, 79 pages. A survey of theoretical considerations concerning the difficult subject of flows containing shocks, including supersonic and transonic flows of plane and axisymmetric character, and flow past cones.

The production and appearance of the book are both excellent. The reviewer takes no risk in predicting a long and esteemed life for this volume.

Fluid Mechanics and Computing

TRANSACTIONS OF THE SYMPOSIUM ON FLUID MECHANICS AND COMPUTING—Held at New York University, April 23–24, 1953. Edited by G. Birkhoff, K. O. Friedrichs, and T. E. Sterne. Interscience Publishers, Inc., New York, N. Y., 1954. Cloth, 7 × 10 in., 243 pp., figs., tables, $5.

REVIEWED BY ASCHER H. SHAPIRO[3]

THIS volume contains.....the papers delivered at the first symposium in applied mathematics sponsored by the American Mathematical Society and the Office of Ordnance Research, U. S. Army...in April, 1953... The scientific fields explored at the symposium are many and diverse. They include broad areas in mathematics, fluid mechanics, mathematical physics, and computer techniques. British, French, German, and American scientists co-operated to make the symposium of significant international interest.....Each paper presented represents in a sense a critical point in the continuing frontal attack on the general problem of the understanding and control of the physical world."

[3] Professor of Mechanical Engineering, Massachusetts Institute of Technology, Cambridge, Mass. Mem. ASME.

The foregoing introduction launches a miscellany of 14 papers on the general theme of the mathematical foundations of fluid dynamics. Most of the papers pertain to compressible flows, and fall into three main categories: (1) Methods of solution of specific types of problems in fluid dynamics, (2) investigations of the mathematical character of several classes of problems, with a concern for uniqueness and existence aspects, and (3) techniques for obtaining numerical solutions with the help of high-speed computing machines. The roster of distinguished names forming the authorship is a warranty of the significance and quality of the work.

Some notion of the scope of the volume is given by the list of authors and titles:

M. J. Lighthill: Mathematical methods in compressible flow theory.

G. F. Carrier: Boundary layer problems in applied mathematics.

Garrett Birkhoff: Fourier synthesis of homogeneous turbulence.

G. S. S. Ludford and M. H. Martin: One-dimensional anisentropic flows.

J. H. Giese: Approximate methods for computing flow fields.

Lipman Bers: Results and conjectures in the mathematical theory of subsonic and transonic gas flow.

Alexander Weinstein: The singular solutions and the Cauchy problem for generalized Tricomi equations.

P. Germain: Remarks on the theory of partial differential equations of mixed type and applications to the study of transonic flow.

R. von Mises: Discussion on transonic flow.

Mark Lotkin: Some problems solvable on computing machines.

Peter D. Lax: Weak solutions of nonlinear hyperbolic equations and their numerical computation.

L. H. Thomas: Computation of one-dimensional compressible flows including shocks.

G. E. Hudson: The deformation of a thin material shell of nonuniform thickness by a detonation wave.

Hubert Schardin: Measurement of spherical shock waves.

The subject matter of most of the papers is of advanced character and will have meaning primarily for individuals struggling with the barriers standing at the frontiers of our knowledge. For these the book will be a valuable reference source.

Aluminum in Iron and Steel

ALUMINUM IN IRON AND STEEL. By Samuel L. Case and Kent R. Van Horn. Engineering Foundation, John Wiley & Sons, Inc., New York, N. Y.; Chapman & Hall, Ltd., London, England, 1953. Cloth, 6 × 9 in., xii and 478 pp., figs., $8.50.

REVIEWED BY P. E. KYLE[4]

THIS is the first volume of the New Series of Alloys of Iron Research Monographs directed and edited by Frank T. Sisco. The purpose of this new series is to revise and complete the partially finished manuscripts on nickel and manganese as addition elements in steel and cast iron and to prepare monographs on selected elements which have recently assumed importance in ferrous metallurgy. This first volume is devoted to one of these elements, aluminum.

The text material is divided into two parts—the first being devoted to aluminum as a deoxidizer, and the second to aluminum as an alloying element.

[4] Vice-President, Lessells and Associates, Inc., Boston, Mass. Mem. ASME.

In part 1 the first chapter is devoted to discussion of the thermodynamics of deoxidation with aluminum, methods of making additions, and the practices for various grades of steels. The other six chapters treat the subjects of oxide, sulphide, and nitride inclusions and the effect of deoxidation on austenitic grain-size control, notch sensitivity, aging, hardenability, spheroidization, and graphitization of iron carbide, and creep.

The first chapter in part 2 covers the consitution of iron-aluminum alloys, iron-rich iron-aluminum-carbon alloys, and other ternary systems. The remaining six chapters are devoted to the manufacture of the simple and complex iron-aluminum alloys, aluminum in heat-resisting and permanent magnet alloys, the function of aluminum in nitriding steels, aluminum coatings on steels, and the use of aluminum in cast irons, transformer steels, tool steels, and nickel-base alloys.

Special features include brief one to two-page chapter summaries, a bibliography of 341 references covering the period 1897 to 1952, a name index, and a well-prepared subject index.

To those familiar with the monographs of the earlier series it will suffice to say that this new volume is of the same high standard of quality. It has been prepared by the authors with the advice and assistance of an able Iron Alloys Committee of the Engineering Foundation, and is highly recommended as a comprehensive review of the literature of the world on this subject. By its nature it is not a textbook but is a valuable reference book for the libraries of engineers and scientists.

Nickel in Iron and Steel

NICKEL IN IRON AND STEEL. By A. M. Hall. Engineering Foundation, John Wiley & Sons, Inc., New York, N. Y.; Chapman & Hall, Ltd., London, England, 1954. Cloth, 6 × 9 in., xii and 595 pp., figs., $10.

REVIEWED BY P. E. KYLE[5]

THIS is the second volume of the New Series of Alloys of Iron Research Monographs directed and edited by Frank T. Sisco, and represents a revision of, and additions to, an earlier manuscript which was partially completed by Frank T. Sisco and John S. Marsh in 1942.

The introductory first chapter is devoted to nickel minerals and the occurrence and refinement of nickel ores. The remaining chapters refer to the cast and wrought steels and cast irons containing nickel. Among the many subjects covered are melting, working, physical properties, metallography, heat-treatment, room-temperature properties, effects of temperature on mechanical properties, corrosion, welding, brazing, soldering, machinability, and wear resistance.

The style of this volume is similar to that of the first volume of this new series which was entitled "Aluminum in Iron and Steel." It contains valuable chapter summaries and a bibliography of 784 references covering the period essentially from 1900 to 1953 with a few selected references between 1858 and 1900. A name index and detailed subject index are also included.

This book is written to the same high standards as other Alloys of Iron Monographs and gives thorough coverage of the effects of nickel as one of the most common alloying elements in steels and cast irons. It is a reference work rather than a textbook and contains some unpublished data as well as a concise review of the essential literature on the subject. It is recommended as a valuable addition for permanent libraries of engineers and scientists, research workers and operating personnel, designers and users of machines and structures.

[5] Vice-President, Lessells and Associates, Inc., Boston, Mass. Mem. ASME.

Residual Stresses in Metals

RESIDUAL STRESSES IN METALS AND METAL CONSTRUCTION. Edited by William R. Osgood. Reinhold Publishing Corporation, New York, N. Y., 1954. Cloth, 6 1/4 × 9 in., figs., references, index, xii and 363 pp., $10.

REVIEWED BY D. G. RICHARDS[6]

BECAUSE of conflicting opinions concerning the contribution of residual stresses to fractures in welded ships, the Ship Structure Committee recognized a need for a critical examination and appraisal of contemporary knowledge of residual stresses and the conditions under which their effects become significant. Accordingly, they requested the Committee on Residual Stresses of the National Academy of Sciences—National Research Council to prepare this monograph.

The Ship Structure Committee is composed of five member agencies: The Bureau of Ships, the Military Sea Transportation Service, the United States Coast Guard, the Maritime Administration, and the American Bureau of Shipping. The Committee on Residual Stresses is a seven-man committee, headed by Dr. John T. Norton.

The monograph is made up of 21 papers prepared by 23 contributors: Thirteen from the United States, five from England, three from Belgium, one from Germany, and one from Scotland. The representation from industry and from the academic institutions is about equal. A 22-page summary, presented at the end of the book, was written by the editor and the Committee on Residual Stresses.

It was intended that the monograph should summarize and assess the present state of knowledge on the effects of residual stresses upon the performance of various kinds of structures, with particular emphasis on possible contributions of these stresses to fracture. The scope was to be broad and not limited to the welded-ship fracture problem. It was hoped that this survey would enable formulation of generally applicable principles describing the modification of structural behavior which could be expected as a result of the presence of residual stresses.

A publication of this nature is quite welcome since considerable information has been published on methods of measurement, origin, and magnitude of residual stresses, but relatively little has been published on the significance of these stresses.

The first seven papers deal chiefly with examples of fractures in large structures and welded ships, typical stresses in welded ships, and welding stresses. The next nine papers cover the significance and influence of residual stresses, a theoretical discussion of shakedown, and a discussion of microstresses originated by gas inclusions. The last five papers include a discussion of the assumptions and principles which underlie the application of mechanical methods of measuring residual stresses, two papers on x-ray measurements of strain, and two papers on specific measurement techniques.

The summary is based on the papers in the monograph, the literature, and the experience of the members of the Committee on Residual Stresses. It is divided into nine sections: Superposition, flow, and fracture; microstresses; latent energy; buckling; variation of temperature; fatigue; measurement of residual stresses; ships; and recommendations for research.

The majority of the papers contribute to the main object of the monograph and are of interest. A paper by MacGregor on the significance of residual stresses aims directly at the object and is "recommended reading." This paper and the summary clearly define the present state of knowledge. Several of the authors

[6] Chief, Vibration and Mechanical Metallurgy, Hamilton Standard Division, United Aircraft Corporation, Windsor Locks, Connecticut. Mem. ASME.

discuss the subject of macrostresses versus microstresses and considerable emphasis is given to the probable importance of microstresses. A paper by Greenough, another by Hyler and Jackson, and a section in the summary, bear on this subject. Rosenthal contributes a good discussion on measurement of residual stress in a paper in which he seeks an answer to the question: "What is actually being measured?" The results of several series of fatigue tests on large shafts and axles involving different states of residual stress are presented in a paper by Horger and Neifert. The summary is well written, thorough, and explicit.

It is clear from the evidence now available that engineers should give careful consideration to the subject of residual stresses. This monograph should serve as a useful guide to practicing engineers and it should serve to stimulate those working on the fundamental aspects of residual-stress problems. It is evident that the book was carefully edited and the text is very easy to read.

Failure of Structural Units

TECHNICAL REPORT, New Series, vol. 2, September, 1954, British Engine Boiler & Electrical Insurance Co., Ltd., Manchester, England. Paper, 9½ × 7 in., 21 figs., 256 pp., 12s. 6d.

REVIEWED BY JOHN M. LESSELLS[7]

FURTHER information on the failure of structural units is given in volume 2 of the New Series of Technical Reports issued by the British Engine Boiler & Electrical Insurance Co., Ltd. Such kind of knowledge, as mentioned in the review of volume 1 published in the JOURNAL OF APPLIED MECHANICS for September, 1953, page 451, is of extreme importance to all engineers concerned with the design and operation of structural parts.

The present volume devotes the first section to a historical review of a century's progress in the organized inspection of engineering plants. It is interesting to learn that in 1854 boiler explosions were generally regarded as fortuitous, and it was not until the efforts of such engineering giants as Fairbairn, Whitworth, Longridge, and others that a more rational approach was made to the design and operation of pressure vessels. Some interesting remarks are made on the contribution of the competent inspection provided by such insurance companies as the British Engine Boiler & Electrical Insurance Company in assisting to avert such failures by the dissemination of technical knowledge regarding particular failures. All engineers will agree with the statement in the report regarding the future possibilities which lie open before the engineer: "There is no doubt that mankind stands on the threshold of an era that is likely to surpass in technological development the ones that preceded it. It may be that in a hundred years the basic prime movers of today may join the beam engine and the Haystack boiler as museum curiosities."

The next section is devoted to a discussion of failure of a variety of units such as steam boilers, pipe flanges, turbine bearings, and the like. Interesting descriptions are given of several crankshaft failures. These indicate the influence of bad welding technique on such failures. Other cases are cited which show the possible influence of chromium plating in reducing the fatigue strength unless proper attention is given to the chromium-plating technique. All of these are problems of current engineering significance.

Not the least of the interesting features of this and the previous report are the excellent macrographs and micrographs which have been used with competent metallurgical knowledge as an aid to the engineer in uncovering the causes of failure.

The latter part of the report is devoted to a review by the Company's Research Engineer, G. A. Cottell, of the knowledge of fatigue phenomena. This includes a discussion of crack formation and growth on which more knowledge is still required by the engineer. An interesting bibliography draws attention to the pertinent literature of the subject.

[7] President, Lessells and Associates, Inc., Boston, Mass.; Associate Professor of Mechanical Engineering, Emeritus, Massachusetts Institute of Technology, Cambridge, Mass. Hon. Mem. ASME.

Strength of Materials

STRENGTH OF MATERIALS. By Joseph Marin and John A. Sauer. The Macmillan Company, New York, N. Y., second edition, 1954. Cloth, 9 × 6 in., xvii and 518 pp., figs., $6.75.

REVIEWED BY T. A. HEWSON[8]

THE book under review by Joseph Marin and John A. Sauer is a noteworthy contribution to American college undergraduate texts on this important subject. The second edition, like the first, combines the mechanics of each stress system discussed with a brief treatment of the corresponding mechanical properties of materials. Simple stresses are presented in a lucid manner in part 1. Part 2 takes up statically indeterminate stresses including deformation methods of analysis and energy analytic methods. Combined stresses are presented in part 3. Special topics are discussed in part 4. These include riveted and welded joints, special problems on bending of beams, members subjected to fatigue and impact loads, temperature and creep, and experimental stress analysis. In fact, a principal feature of the book is the correlation of stress analysis, mechanical properties, and design. This correlation should prepare students more adequately for the study of machine, structural, and aircraft design. The book is exceptionally well written and illustrated.

[8] Chief Engineer, Lessells and Associates, Inc., Boston, Mass.

Third U. S. National Congress of Applied Mechanics
Preliminary Announcement

The Third U. S. National Congress of Applied Mechanics will be held at Brown University, Providence, Rhode Island, during June 11–14, 1958. It is hoped that the scheduling of conflicting meetings can be avoided by this early announcement of the date chosen for the Congress. Further announcements concerning the preparation of papers will be made as the Congress draws nearer.

Inquiries regarding the Congress should be addressed to one of the following members of the Organizing Committee at Brown University, Providence, R. I.:

Professor D. C. Drucker, *Secretary*
Professor E. H. Lee, *Treasurer*
Professor W. Prager, *Chairman*

NOW AVAILABLE . . .

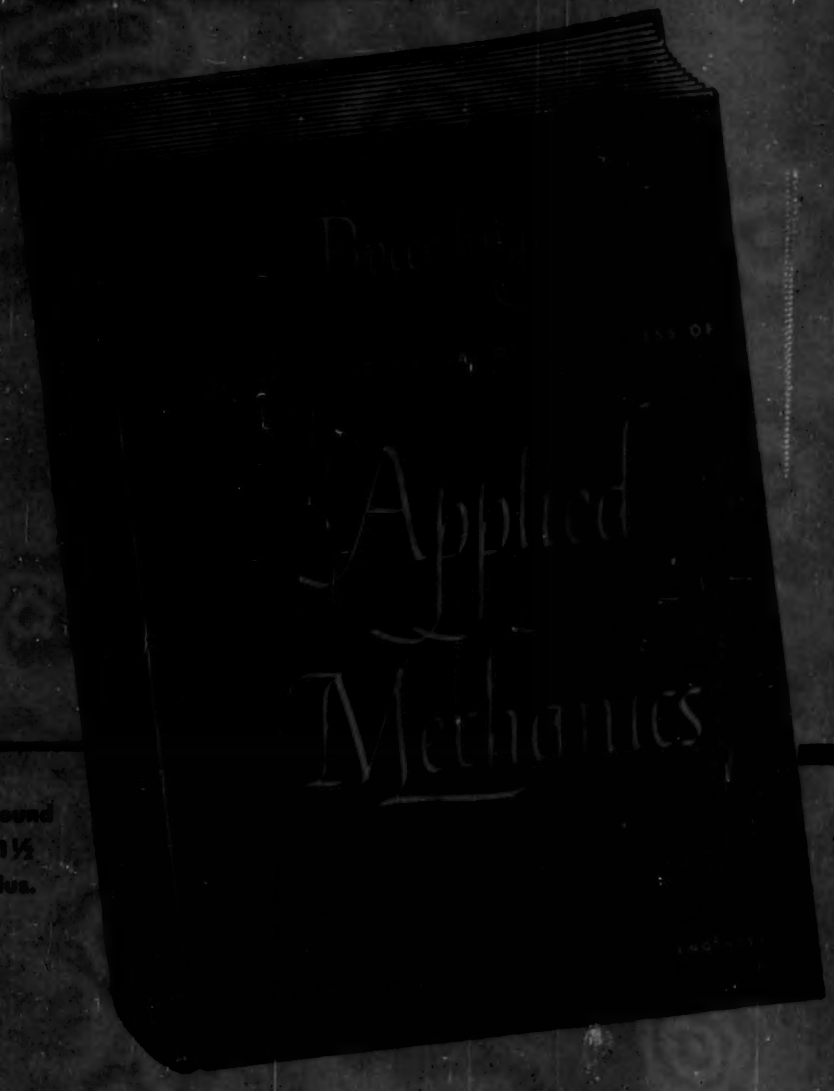

Cloth Bound
8½ x 11½
825 Illus.

$9.00
to members
and
nonmembers

. . . offering a unique collection of data, calculations, procedures, and solutions for attacking problems associated with

DYNAMICS VIBRATION WAVE MOTION
ELASTICITY SHELLS PLATES ELASTIC INSTABILITY STRUCTURES
PLASTICITY VISCOELASTIC FLOW FAILURE BEHAVIOR OF MATERIALS
FLUID FLOW AERODYNAMICS HEAT TRANSFER

This information is provided through ninety-five technical papers, each of which constitutes an original research; four general lectures; hundreds of tables, diagrams, and equations; and bibliographies keyed to many of the articles.

In brief, this 825-page volume gives you access to an unequaled amount of reference material, original viewpoints of recognized authorities of the field, and information on significant advances and on the use of new analytical tools and procedures.

Send for a copy today—you will be glad you did.

THE AMERICAN SOCIETY OF MECHANICAL ENGINEERS, 29 W. 39th St., New York 18, N. Y.